

Investigating the molecular basis of human NLRP1 inflammasome activation

Jonas Möcking

ORCID ID:
0000-0001-5914-1359

from Kamp-Lintfort, Germany

Submitted in total fulfilment of the requirements of the joint degree of

Doctor of Philosophy (PhD) of

The Medical Faculty,

The Rheinische Friedrich-Wilhelms-Universität Bonn

and

The Department of Medical Biology,

The University of Melbourne

Bonn/Melbourne, 2020

Performed and approved by The Medical Faculty of The Rheinische Friedrich-
Wilhelms-Universität Bonn and The University of Melbourne

1. Supervisor: Prof. Matthias Geyer
2. Supervisor: Associate Prof. Seth Masters

Date of submission: September 2019

Date of oral examination: January 2020

Institute of Structural Biology (Bonn), Director:
Prof. Matthias Geyer

Table of Contents

Table of Contents	I
Abbreviations	VI
List of Tables	XII
List of Figures.....	XIII
Abstract	XV
Declaration	XVII
Preface	XVIII
Acknowledgements	XXI
List of Publications	XXIV
1. Introduction	1
1.1 The innate immune system	1
1.2 Pattern recognition receptors (PRRs)	2
1.2.1 Transmembrane PRRs.....	3
1.2.1.1 C-type lectin receptors (CLRs)	3
1.2.1.2 Toll-like receptors (TLRs)	5
1.2.2 Cytoplasmic PRRs.....	8
1.2.2.1 RIG-I-like receptors (RLRs).....	8
1.2.2.2 NOD-like receptors (NLRs).....	9
1.2.2.3 Other cytosolic PRRs	12
1.3 The current model of inflammasome activation.....	14
1.3.1 The pro-inflammatory cytokines IL-1 β and IL-18	17
1.3.2 Pyroptosis – an inflammatory form of cell death	19
1.4 ATPases associated with diverse cellular activities (AAA+ ATPase).....	20
1.4.1 What are AAA+ ATPases? Classification of P-loop NTPases	20
1.4.2 The role of self-assembly in AAA+ activity.....	24

1.5	The NLRP1 inflammasome	26
1.5.1	Differences between rodent and human NLRP1	26
1.5.2	Mechanisms of NLRP1 activation	29
1.5.3	NLRP1-associated autoinflammatory diseases	35
1.6	Thesis aims	37
2.	Materials and Methods	38
2.1	Materials	38
2.1.1	Reagents and consumables	38
2.1.2	Cell culture and bacterial culture media	40
2.1.3	Equipment	41
2.1.4	Cell lines and bacterial strains	43
2.1.5	Buffers for protein purification	43
2.2	Methods – Molecular Biology	46
2.2.1	Polymerase Chain Reaction (PCR)	46
2.2.2	Agarose gel electrophoresis	46
2.2.3	Restriction digest	47
2.2.4	Ligation	47
2.2.5	Transformation of bacteria	48
2.2.6	Sequencing	48
2.2.7	Preparation of amplified plasmids from <i>E. coli</i>	49
2.2.8	Isolation of baculovirus shuttle vector (Bacmid)	49
2.3	Methods – Cell Biology	51
2.3.1	<i>Sf9</i> and <i>Sf21</i> cell culture	51
2.3.2	Transfection of <i>Sf9</i> and <i>Sf21</i> cells	51
2.3.3	Virus amplification (V_1 and V_2)	52
2.3.4	Cell culture of human cell lines	53
2.3.5	Transfection of HEK293T cells	53
2.3.6	ASC speck formation assay	54
2.3.7	Immunoprecipitation	57
2.3.8	Enzyme-linked Immunosorbent Assay (ELISA)	57

2.4	Methods – Protein biochemistry	59
2.4.1	Expression of recombinant protein in bacteria.....	59
2.4.2	Expression of recombinant protein in <i>Sf9</i> or <i>Sf21</i> cells	59
2.4.3	Cell lysis – Sonication.....	60
2.4.4	Protein purification – Affinity chromatography	60
2.4.5	Concentration of protein samples	61
2.4.6	Determination of protein sample concentration	62
2.4.7	Tobacco Etch Virus (TEV) protease digestion	62
2.4.8	Protein purification – Size exclusion chromatography (SEC).....	62
2.4.9	Sodium dodecyl sulphate polyacrylamide gel electrophoresis (SDS-PAGE).....	63
2.4.10	Western blot	64
2.4.11	Mass spectrometry	65
2.4.12	Small-angle X-Ray scattering (SAXS)	66
2.4.13	Reversed-Phase High-Performance Liquid Chromatography (RP-HPLC) based hydrolysis assay	66
3.	Biochemical and structural characterisation of recombinant NLRP1	69
3.1	Introduction	69
3.2	Results	72
3.2.1	Sequence based analysis of NLRP1 domain architecture.....	72
3.2.2	Purification and characterization of NLRP1 PYD.....	75
3.2.3	Purification and characterization of NLRP1 LRR.....	79
3.2.4	Analysis of potential intramolecular interactions in NLRP1.....	83
3.2.5	Recombinant full-length MBP-NLRP1 forms oligomers	90
3.2.6	SEC-SAXS analysis suggests MBP-NLRP1 assembles into a hexamer.....	95
3.3	Discussion	102

4.	The role of nucleotides in regulating NLRP1 activity	106
4.1	Introduction	106
4.2	Results	109
4.2.1	MBP-NLRP1 exhibits ATP hydrolysis activity	109
4.2.2	Identification of conserved nucleotide binding motifs in NLRP1	113
4.2.3	Structural model of the NLRP1 NACHT domain	117
4.2.4	Effect of mutations in the nucleotide binding site of MBP-NLRP1 on its hydrolysis activity.....	121
4.2.5	Nucleotide binding site variants exhibit increased NLRP1 activation.....	124
4.2.6	Clones of THP1s harbouring the E414Q Walker B mutation show no significant spontaneous activation.....	127
4.2.7	Mutations of the nucleotide binding site do not affect FIIND cleavage or the interaction of N- and C-terminal fragments.....	130
4.3	Discussion	132
5.	NLRP1 inflammasome activity is tightly regulated through diverse molecular mechanisms	137
5.1	Introduction	137
5.2	Results	141
5.2.1	Computational analysis of the NLRP1 polymorphism M1184V..	141
5.2.2	Effect of increased FIIND cleavage on NLRP1 activation.....	145
5.2.3	Investigation of a potential phosphorylation site in NLRP1 CARD	152
5.3	Discussion	160
6.	Overall Discussion	168
6.1	Key findings.....	168
6.2	Physiological implications of NLRP1 self-assembly.....	170

6.3	The role of ATP hydrolysis in NLRP1 oligomerisation	171
6.4	The mechanisms and role of PTMs and DPP9 in NLRP1 regulation.....	173
6.5	Model of NLRP1 activation.....	175
6.3	Future directions.....	179
Bibliography		182
Curriculum Vitae.....		225
Appendix		227

Abbreviations

A

Å	Angstrom (10 ⁻¹⁰ m)
AAA+ ATPase	ATPases associated with diverse cellular activities
AD	Acidic transactivation domain
ADP	Adenosine diphosphate
AF-F08	VHH nanobody specific for NLRP1 PYD
AFC	Affinity chromatography
AIM2	Absent in melanoma 2
AMP	Adenosine monophosphate
ASC	Apoptosis-associated speck-like protein containing a CARD
ATP	Adenosine triphosphate

B

β-ME	β-mercaptoethanol
BIR	Baculo-virus inhibitor of apoptosis repeat
BMDM	Bone marrow derived macrophages
bp	Base pair

C

CARD	Caspase activation and recruitment domain
CDN	Cyclic dinucleotide
cGAMP	Cyclic GMP-AMP
cGAS	Cyclic GMP-AMP synthase
CIITA	Class II, major histocompatibility complex, transactivator
CLR	C-lectin type receptor
CRD	Carbohydrate-recognition domain
CRISPR	Clustered, Regularly Interspersed, Small, Palindromic Repeat
CTLD	C-type lectin-like domain
CV	Column volume

D

DAMP	Damage-associated molecular patter
dATP	Deoxyadenosine triphosphate
DC	Dendritic cell
DD	Death domain
DMEM	Dulbecco's Modified Eagle Medium
DMSO	Dimethyl sulfoxide
DNA	Deoxyribonucleic acid
DPBS	Dulbecco's Phosphate Buffer Saline
dsRNA	Double-stranded ribonucleic acid

E

<i>E. coli</i>	<i>Escherichia coli</i>
EDTA	ethylenediaminetetraacetic acid
EF	oedema factor
ELISA	Enzyme-Linked Immunosorbent Assay

F

FACS	Fluorescence-Activated Cell Sorting
FBS	foetal bovine serum
FcR γ	fragment crystallizable receptor
FIIND	domain with function to find

G

GFP	Green fluorescent protein
GSDMD	Gasdermin D
GSH	Glutathione
GST	Glutathione S-transferase

VIII

H

h	Hours
HAMP	Homeostasis-associated molecular patter
HD	Helical domain
HEK	Human embryonic kidney
HEPES	4-(2-hydroxyethyl)-1-piperazineethanesulfonic acid
HPLC	High performance liquid chromatography
HPV	Human papillomavirus
HRP	Horseradish peroxidase

I

IFN	Interferon
IL	Interleukin
IPTG	Isopropyl- β -D-thiogalactopyranoside
IRF	Interferon-regulatory factor
ISG	Interferon stimulated genes
ITAM	Immunoreceptor tyrosine-based activation motifs

K

K_{av}	Partition coefficient (SEC)
K_d	Dissociation constant
kDa	Kilodalton

L

LB	Luria Bertani medium
LeTx	Lethal Toxin
LF	Lethal factor
LGP2	Laboratory of Genetics and Physiology 2
LPS	Lipopolysaccharide
LRR	Leucine-rich repeat

M

mA	Milliampere
MAPK	Mitogen-Activated Protein Kinase
MAVS	Mitochondrial antiviral signalling
M-CSF	Macrophage Colony Stimulating Factor
MDA5	Melanoma Differentiation Associated gene 5
MDP	Muramyl dipeptide
MES	2-(N-morpholino)ethane sulfonic acid
min	Minutes
mL	Millilitre
MSPC	Multiple Self-healing Palmoplantar Carcinoma
MW	Molecular weight
MyD88	Myeloid Differentiation primary response gene 88

N

NAIP	Neuronal apoptosis inhibitory protein
NEB	New England Biolabs
NF- κ B	Nuclear Factor kappa-light-chain-enhancer of activated B cells
ng	Nanogram
NLR	Nod-like receptor
NLRA	Nod-like receptor containing an acidic transactivation domain
NLRB	Nod-like receptor containing an BIR domain
NLRC	Nod-like receptor containing an CARD
NLRP	NOD-like receptor containing a PYD
NLRP1-A	Construct for full-length NLRP1
NLRP1-B	Construct for NLRP1 LRR (791-990)
NLRP1-C	Construct for NLRP1 FIIND-CARD (1084-1467)
NLRP1-D	Construct for NLRP1 CARD (1372-1467)
NLRP1-E	Construct for NLRP1 FIIND (1084-1376)
NLRP1-F	Construct for NLRP1 PYD (1-93)

NOD	Nucleotide-binding oligomerization domain
NP-40	Nonidet P-40
NR100	NH2-terminal domain of rodent Nlrp1 proteins, approximately 100 amino acids
O	
o/n	Over night
OD _{600nm}	Optical density at 600 nm
P	
PA	Protective antigen
Pam ₃ CSK ₄	N- α -Palmitoyl-S-[2,3-bis(palmitoyloxy)-(2RS)-propyl] - Cysteine, Serine, Lysine(4)
PAMP	Pathogen-associated molecular pattern
PBS	Phosphate-buffered saline
PBS-T	Phosphate-buffered saline + Tween 20
PCR	Polymerase Chain Reaction
PMSF	Phenylmethylsulfonylfluorid
PRR	Pattern recognition receptor
PTM	Posttranslational modification
PVDF	Polyvinylidenfluoride
PYD	Pyrin domain
Q	
Q2-G06	VHH nanobody specific for NLRP1 CARD
R	
RIG-I	Retinoic acid Inducible Gene I
RLR	RIG-I-like receptor
RNA	Ribonucleic acid
RT	Room temperature
RU	Response units

S

s	Seconds
SDS	Sodium Dodecyl Sulphate
SEC	Size exclusion chromatography
SEM	Standard Error of the Mean
Sf9/Sf21	Spodoptera frugiperda 9/21 cells (immortalized insect cell lines)
SOB	Super Optimal Broth
STAND	Signal transduction ATPases with numerous domains
STING	Stimulator of interferon genes
SYK	Spleen tyrosine kinase

T

TAE	Tris Acetate-EDTA
TCEP	Tris-(2-carboxyethyl)phosphine
TEV	Tobacco etch virus protease
TIR	Toll/interleukin-1 receptor
TLR	Toll-like receptor
TNF	Tumour Necrosis Factor
TRAM	TRIF-related adaptor molecule
TRIF	TIR-domain-containing adaptor inducing IFN β
Tris	Tris(hydroxymethyl)-aminomethane (THAM)

V

V	Volt
v/v	volume per volume

W

w/v	weight per volume
WHD	Winged helix domain
WT	Wild-type

List of Tables

Table 2.1: Protein molecular weight and DNA marker.....	38
Table 2.2: Kits.....	38
Table 2.3: Primer sequences.....	39
Table 2.4: Cell culture and bacterial culture media.....	41
Table 2.5: Equipment.....	41
Table 2.6: Cell lines.....	43
Table 2.7: Buffers for protein purification (affinity chromatography).....	43
Table 2.8: Buffers for protein purification (size exclusion chromatography).....	44
Table 5.1: Disease associated with the M1184V polymorphism.....	163

List of Figures

Figure 1.1:	Current model of inflammasome activation.....	16
Figure 1.2:	Classification of P-loop NTPases and structural characteristics of the nucleotide binding site	22
Figure 1.3:	Comparison of the human and murine NLRP1 proteins	28
Figure 2.1:	Gating strategy used in ASC speck assay.....	55
Figure 3.1:	Domain and construct boundaries determined for NLRP1.....	73
Figure 3.2:	Biochemical and computational characterization of NLRP1 PYD.....	77
Figure 3.3:	Biochemical characterization and crystal structure determination of NLRP1 LRR.....	81
Figure 3.4:	Interaction studies of NLRP1 PYD with other domains of NLRP1	84
Figure 3.5:	Interaction studies with NLRP1-specific nanobodies	88
Figure 3.6:	Purification and negative stain EM of MBP-NLRP1	91
Figure 3.7:	Modification of MBP-NLRP1 purification protocol leads to improved elution behaviour.....	93
Figure 3.8:	SEC-SAXS analysis of MBP-NLRP1 Peak 2 reveals an oligomeric state of the protein particle	96
Figure 3.9:	<i>Ab initio</i> model and molecular envelope of the MBP-NLRP1 oligomer determined from SAXS data	100
Figure 4.1:	MBP-NLRP1 exhibits ATP hydrolysis activity	110
Figure 4.2:	MBP-NLRP1 exhibits adenylate kinase activity	112
Figure 4.3:	Sequence alignment of human NLRP proteins and NOD1 and NOD2 reveals conserved nucleotide binding site motifs.....	115
Figure 4.4:	Homology model of NLRP1 NACHT domain	119
Figure 4.5:	Effect of mutations in the nucleotide binding site on ATP hydrolysis.....	123
Figure 4.6:	Effect of mutations in the nucleotide binding site on NLRP1 activation.....	125

Figure 4.7:	THP1 clones harbouring E414Q exhibit no spontaneous activation.....	129
Figure 4.8:	Effect of nucleotide binding site variants on FIIND cleavage ...	131
Figure 5.1:	Computational analysis of the human NLRP1 FIIND domain ..	143
Figure 5.2:	Effect of M1184V on NLRP1 activation by destabilization of the N-terminus	146
Figure 5.3:	Activation of NLRP1 by Talabostat is delayed by M1184V	148
Figure 5.4:	P1214R induces NLRP1 activation similar to Talabostat.....	150
Figure 5.5:	Substitution of Y1413 impairs NLRP1 activity.....	153
Figure 5.6:	Structural analysis of Y1413 in NLRP1 CARD.....	157
Figure 5.7:	Screening for tyrosine kinase inhibitors of NLRP1 activity	159
Figure 6.1:	Sequence of molecular events required for NLRP1 activation.....	177
Figure A1:	Sequence alignment of PYDs of all NLRPs and ASC.....	227
Figure A2:	Mass spectrometry analysis of MBP-NLRP1	228
Figure A3:	Representative FACS plots of ASC speck assay (Fig 4.6)	229
Figure A4:	Effect of Talabostat on NLRP1 A66V and P1214R variants	230
Figure A5:	Uncropped blots (Fig. 4.8)	231
Figure A6:	Representative FACS plots of ASC speck assay (Fig 5.2)	232
Figure A7:	Representative FACS plots of ASC speck assay (Fig 5.3)	234
Figure A8:	Effect of Talabostat on NLRP1 A66V and P1214R variants	235
Figure A9:	Representative FACS plots of ASC speck assay (Fig 5.5)	236
Figure A10:	Uncropped blots (Fig. 5.5)	237
Figure A11:	Representative FACS plots of ASC speck assay (Fig. 5.7)	238

Abstract

Cytosolic sensor proteins like NLRP1 (NOD-like receptor containing a pyrin domain 1) play a fundamental role in mediating innate immunity. Upon activation they form signalling hubs that recruit the adaptor protein ASC (apoptosis-associated speck-like protein containing a CARD) and procaspase-1 to form an inflammasome. Procaspase-1 is in turn activated and processes the cytokines pro-IL-1 β and pro-IL-18 as well as the pore-forming protein GSDMD (Gasdermin D) into their mature forms, resulting in inflammation and pyroptosis. When dysregulated, inflammasomes are often involved in the development of autoinflammatory diseases. Therefore, it is of major interest to understand the molecular mechanisms underlying the regulation of inflammasome sensors.

A biochemical approach was taken to investigate the structural basis of inflammasome formation. Producing and characterizing recombinant protein of separate domains of NLRP1 demonstrated that NLRP1 autoinhibition is not mediated by direct intramolecular interaction of the N-terminal PYD with other domains. Additionally, the full-length NLRP1 protein was characterized by biochemical and structural means. Size exclusion chromatography indicated that recombinant NLRP1 forms oligomers in solution. Small-angle X-ray scattering confirmed this observation and further allowed the calculation of a molecular envelope of the NLRP1 oligomer. The oligomeric state of the protein was estimated to be hexameric, based on the particle volume derived from the molecular envelope.

Furthermore, a highly sensitive reversed-phase HPLC assay was employed to measure the ATP hydrolysis activity of recombinant full-length NLRP1. In contrast to previous reports, we found that NLRP1 hydrolyses ATP at a low rate. The physiological relevance of this activity was investigated by taking a mutational approach in functional assays in cells measuring inflammasome activation. Substitution of residues identified by computational analysis of the nucleotide binding site suggested that ATP hydrolysis is involved in maintaining NLRP1 in an autoinhibited state.

A similar approach was taken to investigate the involvement of direct modifications of the NLRP1 protein in regulating inflammasome activity. Functional effects of a single nucleotide polymorphism, which leads to the amino acid substitution M1184V in the NLRP1 protein and is described to increase autoproteolysis in the NLRP1 FIIND domain, were investigated. The results showed that increased cleavage can amplify or inhibited activation of NLRP1 in the context of different stimuli. Moreover, a potential phosphorylation within the CARD domain was identified as another essential modification regulating the activity of NLRP1.

Overall, this work provides new insights into the role of structural mechanisms, ATP as a cofactor and posttranslational modifications in regulating NLRP1 inflammasome activity.

Declaration

The work that is presented in this thesis was conducted at The Rheinische Friedrich-Wilhelms-Universität Bonn and The University of Melbourne in the laboratories of Professor Matthias Geyer (Institute of Structural Biology, Bonn) and Associate Professor Seth L. Masters (Walter and Eliza Hall Institute, Melbourne). The research work was funded by the Bo&MeRanG Graduate School.

This is to certify that

- (i) the thesis comprises only my original work towards the PhD except where indicated in the Preface,
- (ii) due acknowledgement has been made in the text to all other material used,
- (iii) the thesis is less than 100,000 words in length, exclusive of tables, maps, bibliographies and appendices.

Jonas Möcking

Preface

Chapter 3:

Part of the introduction of this chapter is based on the section “NLRP1 domain organization” from “Mechanisms of NLRP1-Mediated Autoinflammatory Disease in Humans and Mice” published in the Journal of Molecular Biology (Yu *et al.*, 2018). I contributed significantly in writing this section and I am the second author of this publication.

Crystallization trials, X-ray diffraction measurements as well as subsequent molecular replacement were performed by Dr. Kanchan Anand from the Institute of Structural Biology (University of Bonn).

The SPR measurement shown in Figure 3.5D was carried out by Dr. Karl Gatterdam from the Institute of Structural Biology (University of Bonn). I provided the purified proteins used in these measurements.

Plasmids for the nanobodies were provided by Dr. Florian I. Schmidt from the Institute of Innate Immunity (University of Bonn).

Electron microscopy was carried out by Dr. Heide Behrmann from the Institute of Structural Biology (University of Bonn).

Prof. James M. Murphy from the Walter and Eliza Hall Institute (Melbourne) assisted in SEC-SAXS experiments and gave valuable advice on how to analyse the recorded SAXS data.

Mass spectrometry was performed by Dr. Jarrod Sandow from the mass spectrometry facility of the Walter and Eliza Hall Institute (Melbourne). I prepared the samples for the mass spectrometry measurements myself.

Chapter 4:

Some data in this chapter were kindly generated with the help of members from the laboratories of Prof. Matthias Geyer (Bonn) and Prof. Seth L. Masters (Melbourne).

Melanie Specht from the Institute of Structural Biology (Bonn) cloned plasmid constructs for the expression of mutant MBP-NLRP1. Dr. David Fußhöller from the Institute of Structural Biology (Bonn) expressed and purified all nucleotide variants shown in Figure 4.4. Furthermore, he measured ATP-hydrolysis activity of those variants and repeated the WT measurement.

The THP1 single cell clones were generated by Dale Calleja from the Walter and Eliza Hall Institute (Melbourne) and the according experiments and measurements shown in Figure 4.6 were carried out by Pawat Laohamonthonkul from the Walter and Eliza Hall Institute (Melbourne).

All other data shown in this chapter were generated by myself.

Chapter 5:

Some data in this chapter was kindly generated with the help of members from the laboratories of Matthias Geyer (Bonn) and Seth L. Masters (Melbourne).

Dr. Alan Chien-Hsiung Yu from the Walter and Elisa Hall Institute (Melbourne) performed initial experiments with WT, A66V and M1184V variants of NLRP1.

The ASC speck assay with WT NLRP1 and the P1214R mutant as well as the according western blot shown in Figure 5.4 were carried out by Pawat Laohamonthonkul from the Walter and Elisa Hall Institute (Melbourne).

Tyrosine kinase inhibitors were kindly provided by the Drug Discovery Centre of the Walter and Elisa Hall Institute (Melbourne).

All other data shown in this chapter was generated by myself.

Overview of contributions:

Chapter	Figure	Contribution (Contributor)
3	3.3	Crystallization, Calculation of structure (Dr. Kanchan Anand)
3	3.5D	SPR measurement (Dr. Karl Gatterdam)
3	3.5, 3.7	Provided expression constructs for VHHs (Dr. Florian I. Schmidt)
3	3.8, 3.9	Assistance in SAXS experiment, Advice for data analysis (Prof. James Murphy)
3	A2	Measurement and analysis of mass spectrometry (Dr. Jarrod Sandow)
4		Cloning of expression plasmids (Melanie Specht)
4	4.4	Protein purification, ATP-hydrolysis measurement, data analysis (Dr. David Fußhöller)
4	4.6	Generation of THP KO/mutant cell lines (Dale Calleja) THP1 experiments and data analysis (Pawat Laohamonthonkul)
5		Initial experiments on NLRP1 M1184V variant (Dr. Alan Chien-Hsiung Yu)
5	5.4	ASC-speck-assays, Western blot (Pawat Laohamonthonkul)

Acknowledgements

During the course of my PhD many people contributed by supporting me in many different ways. To everyone who helped by giving advice, assisting in experiments or simply listening to me – THANK YOU!

First and foremost I would like to thank my primary supervisors, Matthias Geyer and Seth Masters.

Matthias, your enthusiasms for structural biology is truly contagious. Thanks so much for giving me the chance to get infected. Thank you also for the freedom you gave me during my candidature to pursue my own ideas in the lab.

Seth, you are incredibly good communicating science. I really feel I learned how to efficiently deliver a scientific message to an audience from you. Thanks for welcoming me in your lab and teaching me so much about the biology of inflammasomes – and how to investigate it.

I am incredibly appreciative of the support that I experienced from both of you during the last three and a half years. Especially, since you both agreed to taking part in the Bo&MeRanG program and thereby gave me the chance to learn and work in two different laboratories across the world. It certainly was a formidable experience that I will value for the rest of my life.

Prof. Dr. Eicke Latz and Prof. Dr. Oliver Fackler, thank you for joining my PhD committee in Bonn. Eicke, I would also like to thank you for inviting me to retreats with the entire Institute of Innate Immunity.

Further, I want to thank my PhD committee in Melbourne, A. Prof. Sandra Nicholson, A. Prof. Chris Tonkin and A. Prof. James Murphy. I am very thankful for the advice and support I had from all three of you. I am particularly thankful to James for giving valuable advice and helping me with the structural work I did in Melbourne.

Thanks also to my Co-Supervisor in Melbourne, Alan. It was always fun to work with you. Thank you for being patient with me and always answering my questions.

David, thank you for continuing my project while I was in Melbourne. I sincerely appreciate all your effort, help and advice during my PhD. And even more for always being fun and down to earth.

This brings me to thanking every former and current member from the laboratories of Matthias and Seth. So many of you helped me with so many things. So many that I might not remember all of it. But believe me, I am incredibly thankful to all of you. Ann Katrin for introducing me to protein purification procedures. Melanie for helping out with cloning. Heide and Inga for your work on the electron microscope. Robert, Sebastian, Rebecca, Inga, Rubi, Ines, Anja, Sofia, Sophie, Michael, Karl – thank you all for listening, for giving advice and for fruitful discussions on scientific and non-scientific matters.

From the laboratory in Melbourne, thank you to Dale, Anni, Dom, Kate, Sophia, Cass, Pawat, Emira, Heather, Paul and Fiona (and Daniel) for making me feel so welcome at WEHI and always being supportive. Special thanks to Dale for including me from the start and teaching me how to behave properly in Australia. Special thanks also to Anni for joining me in complaining about the PhD life while doing cell culture and for always being kind and supportive.

Apart from everyone in the labs I worked in, the people around those labs (Toni's lab at the Caesar in Bonn, The Inflammation Division at WEHI) were always great in helping out with advice, reagents or a chat over a beer after work.

Thank you to my collaborators at WEHI. Alex Uboldi for teaching me a lot about *Toxoplasma* and also being very kind, patient and understanding. Thanks to Cheree, Alexandra and Lung Yu for showing me the insect cell facility at WEHI and helping me with my purifications.

I am also very grateful to Prof. Christian Kurts and Sammy Bedoui, for initiating a program like the IRTG 2168, allowing me to spend one year in Melbourne and doing research in two different labs during my PhD. As mentioned above, it was an experience that I will never forget. Saying (writing) this, I am also thankful for the support I received from the organization team, Lucie Delforge and Marie Greyer. You really made my life a lot easier during the PhD.

Most importantly I want to say a huge THANK YOU to my family and friends, who were always understanding and supportive. Undertaking a PhD was not an easy task and I could not have done it without your constant support. From the bottom of my heart: Thank you all so much! I am deeply grateful to have all of you in my life!! Ganz besonderen Dank an meine Eltern und meine Brüder, die immer zu mir halten und mich in allem unterstützen. Und zwar auch dann, wenn ich ein Jahr im ca. 16000 km entfernten Australien verbracht habe (schon wieder). Ich bin dankbar und froh eine so tolle Familie zu haben. Ihr seid die Besten!

Last but definitely not least, I would like to thank my mustache for giving me strength when I needed it!

List of Publications

1. Yu C-H, **Moecking J**, Geyer M, Masters SL. Mechanisms of NLRP1-Mediated Autoinflammatory Disease in Humans and Mice. *J Mol Biol* 2018;430:142–152

1. Introduction

1.1 The innate immune system

Multicellular organisms have developed a multitude of mechanisms to defend themselves against infectious pathogens - the immune system. The immune system of vertebrates is commonly divided into the innate immune system and the adaptive immune system (Medzhitov and Janeway, 1997; Tosi, 2005). The innate immune system has developed earlier than the adaptive immune system and can therefore be regarded as phylogenetically primitive compared to the adaptive immune system. Nevertheless, the innate immune system plays an important role in defending the host against pathogens as it is required to trigger an immune response rapidly after infection. Furthermore, it is described to be involved in inducing adaptive immunity (Beutler, 2004; Tosi, 2005; Kumar *et al.*, 2011).

Anatomical barriers like the skin, mucosal membranes and epithelial tissue form a first line of defence and are parts of the innate immune system (Carrillo *et al.*, 2017). Pathogens that have passed this first line of defence and have invaded the host, can be detected and cleared by humoral and cellular mechanisms. Apart from pathogen-derived material, cell debris derived from damaged tissue can also be recognised and cleared by these mechanisms (Carrillo *et al.*, 2017). Humoral components of the innate immune system include molecules that can sense and eliminate pathogens, like the complement proteins secreted in the liver and by local macrophages and monocytes (Ricklin *et al.*, 2010). This humoral response can act cell-independent. However, it is often mediated in cooperation with a cellular innate immune response (Beutler, 2004; Bottazzi *et al.*, 2010; Ricklin *et al.*, 2010). Different cell types are part of the innate immune system and are typically derived of myeloid precursors. These cell types include granulocytes (eosinophils, neutrophils, basophils, mast cells), monocytes, macrophages and dendritic cells (DCs). These cell types commonly mediate an immune response through phagocytosis of pathogen- or damage-derived material and the secretion of chemokines and cytokines to attract and stimulate other immune cells (Lacy,

2015). Some lymphoid cells, such as natural killer cells (NK), natural killer T-cells (NKT) and innate lymphoid cells (ILCs) have roles in innate immunity as well (Carrillo *et al.*, 2017). On a molecular level, germline-encoded receptors, termed pattern recognition receptors (PRR), are expressed on the surface or in the cytosol of these and other cells to facilitate the specific recognition of a broad range of pathogens. Thus, these receptors play an essential role in inducing an inflammatory innate immune response (Takeuchi and Akira, 2010; Kumar *et al.*, 2011). Taken together, the main goals of the innate immune system are to prevent infection through physical barriers, to sense and inhibit the spread of and eventually clear an infection or damaged tissue via a humoral and cellular immune response and to induce adaptive immunity by cytokine release and antigen presentation to T- and B-cells (Carrillo *et al.*, 2017).

In contrast to the innate immune system, adaptive immunity essentially relies on receptors that are generated in somatic mechanisms upon antigen presentation and thus possess a more diverse range of pathogen-specificity. This is because the specificity is not predetermined but evolved during the somatic maturation process according to the target (antigen) presented and can therefore be different for each individual organism. A consequence of somatic maturation of these receptors is a delayed response of the adaptive immune system compared to the innate immune system (Medzhitov and Janeway, 1997; Tosi, 2005). Out of the different innate immune cell types, DCs are specialised in antigen-presentation and therefore form an important link between innate and adaptive immunity. As mentioned above, innate immune cells, like DCs, take up antigen by phagocytosis upon activation. Activated DCs can then migrate to lymph nodes to present antigen to T- and B-cells and induce adaptive immunity (Merad *et al.*, 2013).

1.2 Pattern recognition receptors (PRRs)

Innate immune receptors have evolved to recognise conserved pathogenic patterns, also called pathogen-associated molecular patterns (PAMPs). These receptors are therefore referred to as pattern recognition receptors (PRRs). Apart

from PAMPs, PRRs are also reported to recognise molecular parts of cell debris derived from damaged tissue, which has been termed damage-associated molecular patterns (DAMPs) (Medzhitov and Janeway, 1997; Polly Matzinger, 2002). More recently, it has been proposed that homeostasis-altering molecular processes (HAMPs) pose another pattern that can be recognised by the innate immune system (Liston and Masters, 2017). In the case of HAMPs, the innate immune receptor responds to an alteration in cellular homeostasis rather than a certain molecule or parts of a molecule.

PRRs can be distinguished in regards to their cellular localization. C-type lectin receptors (CLRs) and Toll-like receptors (TLRs) reside in the cellular or in endolysosomal membranes. Retinoic acid inducible gene I (RIG-I) -like receptors (RLRs) and nucleotide-binding oligomerization domain-containing (NOD) -like receptors (NLRs) are localized in the cytoplasm of the cell (Takeuchi and Akira, 2010). PRRs are typically expressed in innate immune cells like macrophages and DCs, but also in non-immune cells (Takeuchi and Akira, 2010; Carrillo *et al.*, 2017). Together, this broad range of receptors is able to detect a large and diverse set of molecular patterns and therefore form an essential part of the innate immune system (Bardoel and Van Strijp, 2011). Upon activation these receptors mainly induce the expression of key molecules such as tumour necrosis factor (TNF), interleukin-6 (IL-6), interleukin-1 β (IL-1 β), and type 1 interferons (e.g. INF α , INF β), which in turn mediate an antimicrobial and inflammatory immune response (Takeuchi and Akira, 2010).

1.2.1 Transmembrane PRRs

1.2.1.1 C-type lectin receptors (CLRs)

CLRs are part of the C-type lectin-like domain (CTLD) protein superfamily, which constitutes a diverse group of membrane proteins in multicellular organisms. CTLD proteins have been reported to have diverse functions (Zelensky and Gready, 2005). The term “C-type lectin” originates from the distinction between calcium dependent (C-type) and calcium independent carbohydrate binding

proteins (lectin) (Zelensky and Gready, 2005). CLRs are ubiquitously expressed and found in a diverse set of organisms like humans and sponges (Gundacker *et al.*, 2001; Zelensky and Gready, 2005).

Typically, CLRs are composed of an extracellular domain involved in carbohydrate binding, a transmembrane domain, and in some cases an intracellular domain involved in mediating downstream signalling (Kingeter and Lin, 2012). The extracellular domain consists of a stalk and a carbohydrate-recognition domain (CRD). Structurally, the CRD is formed by two loops, which are stabilized through disulphide-bonds formed by highly conserved cysteines (Zelensky and Gready, 2005). Other conserved residues form the hydrophobic core of the domain fold and constitute the Ca^{2+} binding site (Drickamer and Taylor, 2015).

The family of CLRs can be grouped into two distinct clusters, the Dectin-1 cluster and the Dectin-2 cluster. This clustering is based on differences in the functionality of the extracellular and cytoplasmic domains and downstream signalling pathways (Kanazawa *et al.*, 2004; Kanazawa, 2007; Huysamen and Brown, 2008; Graham and Brown, 2009). While members of the Dectin-1 cluster are described to bind mainly β -glucans with their CRD, members of the Dectin-2 cluster are reported to bind α -mannans (Brown and Gordon, 2001; Brown *et al.*, 2002; McGreal *et al.*, 2006). Dectin-1 molecules further contain a cytoplasmic signal transduction domain, harbouring immunoreceptor tyrosine-based activation motifs (ITAMs) or inhibitory motifs. Depending on the nature of the signal transduction motifs, ligand binding to the receptor results in activation or inhibition of transcription factors (Kingeter and Lin, 2012). A main difference between Dectin-1 and Dectin-2 molecules is that Dectin-2 molecules only contain a very short cytoplasmic domain incapable of mediating signal transduction. To facilitate signal transduction, Dectin-2 receptors form heterodimers with the FcR γ chain (Cao *et al.*, 2007; Yamasaki *et al.*, 2008). Binding of the two molecules is facilitated through a positively charged residue in the transmembrane domain of the Dectin-2 type receptor (Kingeter and Lin, 2012). Binding of pathogen carbohydrates has been shown to be dependent on homo-oligomer formation of

the CLRs. Hetero-oligomer formation as for the Dectin-2/FcR γ chain dimer, adds to the complexity of CLR mediated signalling (Drickamer and Taylor, 2015).

The involvement of CLRs in inducing an immune response has been discussed extensively in the literature. In this context they have been described to induce endocytosis, phagocytosis, anti-microbial as well as inflammatory and anti-inflammatory responses (Hoving *et al.*, 2014). Their ability to recognize different fungi is well characterized. However, CLRs are also described to recognise viruses, bacteria and parasites and have further been shown to be involved in autoimmunity, homeostasis and the recognition of dead and cancerous cells (Hoving *et al.*, 2014; Dambuza and Brown, 2015).

A key mediator in many downstream signalling pathways of Dectin-1 type and Dectin-2 type CLRs is spleen tyrosine kinase (SYK). SYK binds to the cytoplasmic signal transduction domains of the CLR or its interaction partner and orchestrates the formation of a complex of CARD9, B cell lymphoma 10 (Bcl10) and mucosa-associated lymphoid tissue lymphoma translocation protein 1 (Malt1), ultimately resulting in activation of NF- κ B and the expression of inflammatory cytokines (Kingeter and Lin, 2012; Hoving *et al.*, 2014). Another common feature of PRR signalling is the cross-talk between different PRR pathways. For instance, functionality of the inflammasome adaptor protein apoptosis associated speck-like protein-containing a CARD (ASC) depends on tyrosine phosphorylation in a SYK dependent manner. As described above, SYK can be activated through CLRs, while ASC is an important factor in NLR signalling (Hara *et al.*, 2013; Hoving *et al.*, 2014). Moreover, the recognition and subsequent immune response to zymosan, a part of fungal cell wall components, has been shown to depend on the interplay of CLRs and TLRs (Gantner *et al.*, 2003).

1.2.1.2 Toll-like receptors (TLRs)

Out of the different groups of PRRs, TLRs are the most ancient ones and have the widest range of pathogen recognition (Nie *et al.*, 2018). The term “Toll-like” was coined in accordance with the first Toll-gene identified in *Drosophila*

melanogaster. In 1985 Christiane Nüsslein-Volhard, a scientist at the Max Planck Institute in Tübingen (Germany), found that a mutation in this gene resulted in deformed fly larvae. When she first made this discovery she exclaimed “Das ist ja toll!” translating to “That’s great!” (Hansson and Edfeldt, 2005). It took 10 more years until the involvement of the Toll-gene in the immune response was identified (Hoffmann *et al.*, 1996).

Since then, 10 members of the Toll-like receptor family have been identified in humans and 13 members have been identified in mice (Kawai and Akira, 2007). TLRs are expressed in different cells like innate immune cells (e.g. macrophages, dendritic cells) or non-immune cells (e.g. fibroblasts, epithelial cells) and can be distinguished by their cellular localization. Some TLRs locate to the cell surface, like TLR1, TLR2, TLR4, TLR5, TLR6 and TLR10, while others are located in the endosome including TLR3, TLR7, TLR8, TLR9, TLR11, TLR12 and TLR13 (Kawasaki and Kawai, 2014).

Structurally, all TLRs share a similar modular domain architecture with an extracellular domain, a transmembrane domain and an intracellular domain. The extracellular portion of TLRs is comprised of 16-28 leucine-rich repeats (LRRs) (Matsushima *et al.*, 2007). One LRR is comprised of about 24 amino acids in length and folds into a secondary structure element consisting of a short β -strand, a turn and a more variable region (Park *et al.*, 2015). Multiple consecutive LRRs typically fold into a bent, horseshoe-like shape. Conserved hydrophobic amino acid residues within the β -sheet of each repeat form the concave inner core of the overall fold (Gay and Gangloff, 2007). In TLRs, the above mentioned more variable region of the LRR forms parallel 3_{10} helices, which comprise the convex outer surface of the overall LRR fold (Jin and Lee, 2008). The transmembrane domain of TLRs is comprised of a single α -helix. The amino acid sequence of this helix does not show obvious sequence conservation between TLRs apart from hydrophobicity. Nevertheless, the transmembrane region as well as a small portion of the intracellular part of the protein, the juxtamembrane sequence, are thought to be critically involved in receptor activation (Jin and Lee, 2008). The intracellular domain shares significant homology with that of interleukin-1 receptors and is therefore also referred to as Toll/interleukin-1 receptor (TIR)

domain. The cytoplasmic domain adapts an overall β/α -fold. Its core is comprised of a parallel β -sheet composed of five β -strands. This β -core is surrounded by five α -helices (Akira and Hemmi, 2003; Jin and Lee, 2008).

Functionally, the extracellular LRR is required for the recognition of PAMPs or DAMPS by direct binding of pathogen or damage-derived molecules. The variable residues in the inner concave surface of the LRR determine the specificity of the corresponding receptor (Gay and Gangloff, 2007). Thus, not only the number of LRRs but also and more importantly the variable residues present in the β -sheet of each repeat can be varied and combined in sheer endless ways. This enables the formation of highly diverse receptors with specificity for different pathogenic molecules. Ligands of TLRs include bacterial lipopolysaccharide (LPS), glycolipids or lipoproteins (TLR1/TLR2/TLR4), fungal zymosan (TLR2), double stranded RNA (TLR3) or viral and bacterial DNA (TLR9), to only name a few (Akira and Hemmi, 2003). The cytoplasmic domain of TLRs is, similar to CLR, involved in signal transduction via various pathways. Also similar to CLR and receptor tyrosine kinases, efficient signalling through TLRs requires the dimerization or oligomerization after ligand recognition. This oligomerization is facilitated through the cytoplasmic TIRs and mainly mediated by electrostatic interaction between these domains (Gay and Gangloff, 2007; Jin and Lee, 2008).

After oligomerization, TLR signalling is facilitated by a set of adapter proteins containing a TIR domain including MyD88 (Myeloid differentiation primary response 88), TRIF and TRAM. MyD88 signalling is utilised by all TLRs, except TLR3 which signals through TRIF and TLR4, which can signal through MyD88 and TRIF (Medzhitov *et al.*, 1998; Kawai and Akira, 2007). Ultimately, TLR signalling leads to the activation of the transcription factors NF- κ B and AP-1 and mitogen-activated protein kinase (MAPK) pathways (Kawai and Akira, 2007; Lim *et al.*, 2007; Kawasaki and Kawai, 2014). Activation of these pathways induces the expression of inflammatory cytokine genes. TRIF is an adaptor recruited by TLR3 and TLR4 to activate IRF3, NF- κ B and MAPKs through an alternative pathway, again resulting in the induction of inflammatory cytokine genes and also type 1 interferon (IFN) genes (Kawasaki and Kawai, 2014).

1.2.2 Cytoplasmic PRRs

1.2.2.1 RIG-I-like receptors (RLRs)

RLRs were named after the retinoic-acid inducible gene I (RIG-I), the most extensively studied receptor in this group. Apart from RIG-I itself, the mammalian RLR family includes the receptors MDA5 (melanoma differentiation associated factor 5) and LGP2 (laboratory of genetics and physiology 2) (Loo and Gale, 2011). RLRs are cytoplasmic DExD/H-box containing helicases, which detect patterns in viral RNA (Yoneyama *et al.*, 2004; Loo and Gale, 2011).

The modular domain architecture is similar for all three members of the RLR family and is typically composed of two N-terminal caspase activation and recruitment domains (CARD), central helicase domains (Hel1 and Hel2) and an insertion domain in helicase domain 2 (Hel2i), a bridging/pincer domain and a C-terminal domain (CTD) (Loo and Gale, 2011; Yoneyama *et al.*, 2015). CARDS are a subfamily of the death domain superfamily. These death domains typically form a six-helix bundle fold and are commonly involved in mediating protein-protein interactions (Park, Lo, *et al.*, 2007). Of note, LGP2 lacks both N-terminal CARD domains.

The helicase domains Hel1, Hel2 as well as the helicase insertion domain in Hel2 and the CTD are involved in the recognition and binding of viral dsRNA. For RIG-I, a structure of the ligand-bound state showed that these domains completely surround the dsRNA. This fold is supported by a complex network of interactions. The elbow-shaped bridging domain is composed of an α -helix and constitutes an important mechanical connection between Hel1, Hel2, and the CTD (Luo *et al.*, 2011; Kolakofsky *et al.*, 2012). In the ligand-free state, Hel2i is involved in keeping the protein in an autoinhibited state by binding to one of the N-terminal CARD domains via hydrophobic and electrostatic interactions (Kolakofsky *et al.*, 2012). Moreover, an ATP binding site is formed at the interface of Hel1 and Hel2 of RIG-I. Especially Hel1 harbours typical nucleotide binding and hydrolysis motifs like the Walker A and Walker B motifs (also see chapter

1.4) (Kolakofsky *et al.*, 2012; Lässig *et al.*, 2015). Nucleotide hydrolysis has been shown to determine dsRNA specificity of the receptor, preventing the recognition of self-RNA (Lässig *et al.*, 2015; Baek *et al.*, 2016).

As mentioned above, RLRs are important factors in inducing an immune response to viral infections by sensing dsRNA of viral origin. Both, RIG-I and MDA5, have been described to differentially recognize and bind viral nucleic acids that are different in length and originate from different viruses. Thus, these receptors have evolved to detect a broad range of RNA and DNA viruses, like Paramyxoviridae, Picornaviridae and Flaviviridae (Kato *et al.*, 2008; Loo and Gale, 2011). Upon binding of viral RNA, RIG-I and MDA5 recruit the adaptor protein mitochondrial antiviral signalling (MAVS) via CARD-CARD interactions. In turn, MAVS orchestrates the assembly of a large signalling complex, also referred to as the signalosome. This complex signals via multiple pathways to stimulate the expression of type I and type III IFN as well as ISGs (interferon stimulated genes). Expression of these genes ultimately results in an inflammatory immune response to control and eventually clear the viral infection (Loo and Gale, 2011; Yoneyama *et al.*, 2015).

1.2.2.2 NOD-like receptors (NLRs)

The nucleotide-binding oligomerization domain (NOD) -like receptor family is comprised of 23 proteins in humans and at least 34 proteins in mice (Franchi *et al.*, 2009). The common denominator of NLRs is the central NACHT (domain present in NAIP, CIITA, HET-E and TP-1) domain, also termed NOD/NBD (nucleotide-binding oligomerization domain). Most NLRs present with a tripartite domain architecture, with an effector domain located N-terminally of the NACHT domain and an LRR domain on the C-terminus (Shaw *et al.*, 2008).

The family of NLRs can be further divided into four subfamilies according to their N-terminal effector domain: NLRAs, NLRBs, NLRCs and NLRPs (Meunier and Broz, 2017). CIITA (class II, major histocompatibility complex, transactivator), belongs to the subfamily of NLRAs, which contain an N-terminal CARD domain and an acidic transactivation (AD) domain. NLRBs harbour a

baculo-virus inhibitor of apoptosis repeat (BIR)-like domain as their effector domain and are commonly referred to as NAIPs (neuronal apoptosis inhibitory proteins). While humans only have a single NAIP gene, mice have a total of seven NAIPs (Franchi *et al.*, 2009). The subfamily of NLRCs includes NOD1, NOD2, NOD3, NLRC4, NLRC5 and NLRX1. Most NLRCs feature an N-terminal CARD domain as their effector domain (Meunier and Broz, 2017). The fourth subfamily, the NLRPs, is comprised of 14 proteins (NLRP1 - NLRP14), which all contain a pyrin domain (PYD) at their N-terminus (Tschopp *et al.*, 2003). As CARD domains, PYD domains belong to the death domain superfamily, which commonly assemble into a six helix bundle fold and mediate protein-protein interactions via homotypic PYD-PYD or CARD-CARD interactions (Park, Lo, *et al.*, 2007; Meunier and Broz, 2017).

NLRs as well as other NACHT domain containing proteins are described to adapt an autorepressed, closed conformation in the cytoplasm of the cell. Upon ligand binding, a conformational change is induced, resulting in a transition to an open, active conformation and finally oligomerization of the protein. NLR oligomerization is described to be mainly facilitated by the NACHT domain (Danot *et al.*, 2009). The NACHT domain can be divided into four subdomains, the nucleotide binding domain, two helical domains (HD1, HD2) and a so called winged helix domain (WHD), which is located in between the two helical domains. The NBD harbours conserved motifs for nucleotide binding, the Walker A and Walker B motifs. Other motifs involved in nucleotide binding and hydrolysis, the sensor 1 and sensor 2 motifs, are located in the HD1 and WHD subdomains (Macdonald *et al.*, 2013). Containing these features, NLRs can be categorized as members of the STAND (signal transduction ATPases with numerous domains) clade of AAA+ ATPases (ATPases associated with various cellular activities) (Macdonald *et al.*, 2013). The superfamily of AAA+ ATPases and the role of protein oligomerization in mediating activity will be described in more detail in Chapter 1.4.

For mouse NLRC4, it has been shown by crystallographic structure analysis of the NACHT-LRR domains that in the closed, ADP-bound conformation, the LRR domain folds over the NACHT domain. Thereby, the LRR covers one side

of the NACHT domain, blocking oligomerization and keeping the protein in an autoinhibited state (Hu *et al.*, 2013; Hu and Chai, 2016). However, a crystal structure of the rabbit NOD2 NACHT and LRR domains in the closed ADP-bound state revealed that NOD2 LRR is pointed outwards and therefore not blocking the NACHT domain. This shows that despite high similarities in their modular domain architecture, regulation of NLR activity is likely to be achieved through different mechanisms for different NLRs (Maekawa *et al.*, 2016).

LRR domains are commonly described to be involved in ligand recognition and binding for TLRs (see above) and also NLRs. For instance, murine NAIP5 directly recognizes and binds bacterial flagellin with parts of its LRR domain and also parts of the helical domain 2, a subdomain of the NACHT domain (Meunier and Broz, 2017; Tenthorey *et al.*, 2017). Furthermore the LRR has been shown to aid in oligomer formation for NLRC4 (Moghaddas *et al.*, 2018). The key domain for oligomerization and self-assembly however is the NACHT domain (Proell *et al.*, 2008; Maharana *et al.*, 2018).

As mentioned above, signalling occurs through the N-terminal effector domains and results in the activation of a multitude of pathways. Similar to TLRs, some NLRs, like NOD1 and NOD2, signal through pathways amounting in the induction of NF- κ B and MAPK pathways, ultimately resulting in the expression of antimicrobial and inflammatory mediators like TNF, IL-6 and IL-1 β (Chen *et al.*, 2009; Franchi *et al.*, 2009). In contrast, another group of NLRs differs significantly from other PRRs in regards to their signalling and downstream targets. Among others, NLRP1, NLRP3 and NLRC4 are described to form large signalling platforms, termed inflammasomes (Martinon *et al.*, 2002). In this signalling pathway the active, oligomerized NLR recruits the adaptor protein ASC through either PYD-PYD or CARD-CARD interactions. In turn, ASC assembles into large oligomeric filaments, so called specks, and recruits procaspase-1 (Dick *et al.*, 2016). Procaspase-1 is the inactive precursor of caspase-1 and needs to be proteolytically cleaved to become active. Through the accumulation of procaspase-1 molecules on ASC specks, procaspase-1 dimers are formed to allow intermolecular cleavage of the two associated molecules, finally resulting in the release of active caspase-1 (Elliott *et al.*, 2009). Active caspase-1 is a key

inflammatory protein as it directly cleaves the inactive pro-forms of the inflammatory cytokines IL-1 β and IL-18 into their mature forms and also cleaves gasdermin D (GSDMD). Cleaved GSDMD possesses pore-forming activity, and can induce a rapid form of cell-death, which was termed pyroptosis (Martinon and Tschopp, 2005; Place and Kanneganti, 2018). Interestingly, cleavage of IL-1 β and IL-18 links NLR signalling to pathways similar to TLR signalling, since the respective transmembrane receptors for both cytokines (IL-1R, IL-18R) harbour an intracellular TIR domain, which upon ligand (i.e. cytokine) binding can recruit MyD88, ultimately resulting in the induction of NF- κ B (Martinon and Tschopp, 2005).

1.2.2.3 Other cytosolic PRRs

Other important intracellular PRRs that are not classified as RLRs or NLRs are AIM2 (absent in melanoma 2), Pyrin (encoded by the gene MEFV – Mediterranean fever), cGAS (cyclic GMP-AMP synthase) and STING (stimulator of interferon genes). Both, AIM2 and Pyrin, are reported to form inflammasomes similar to some NLRs (Guo *et al.*, 2015).

AIM2 has been shown to be involved in sensing pathogen-derived DNA or self-DNA released into the cytosol from a disintegrated nucleus or mitochondria (Man *et al.*, 2016). It consists of an N-terminal PYD and a C-terminal HIN (hematopoietic expression, interferon-inducible nature, and nuclear localization) domain. The HIN domain is involved in directly binding DNA, while the PYD is involved in inflammasome formation by facilitating protein-protein interactions with the adaptor protein ASC (Lugrin and Martinon, 2018). As for other (NLR) inflammasomes, binding of ASC induces speck formation and subsequent procaspase-1 activation, resulting in the cleavage of the proinflammatory cytokines pro-IL-1 β and pro-IL-18 and the pore-forming protein GSDMD (Hornung *et al.*, 2009; Fernandes-Alnemri *et al.*, 2009; Liu *et al.*, 2016). AIM2 has been shown to play a role in autoinflammatory diseases in the context of self-DNA recognition (Jakobs *et al.*, 2015). However, no gain-of-function mutations have been identified for AIM2 itself (Lugrin and Martinon, 2018).

Similar to AIM2, Pypin is also described to form an inflammasome. The modular domain architecture of Pypin presents with an N-terminal PYD, a central Bbox and coiled-coil domain and a C-terminal B30.2 domain. Interestingly, its domain architecture resembles that of E3 ligases, with the typical ring domain in ligases being switched for the PYD (Heilig and Broz, 2018). As for AIM2 and other NLR inflammasomes, the PYD is involved in ASC binding and inflammasome formation. While different functions have been proposed, the role of the B30.2 domain has not been completely clarified yet (Heilig and Broz, 2018). Pypin is described to indirectly sense pathogen-derived toxins that modulate the activity of the small GTPase RhoA (Ras homolog family member A) (Park *et al.*, 2016). Inhibition of RhoA by bacterial toxins results in loss of PKN1/2 (protein kinase N) activity. These kinases directly phosphorylate pypin, which is required to maintain pypin autoinhibition. More precisely, phosphorylation mediates binding of 14-3-3 proteins that keep pypin in an autoinhibited conformation (Park *et al.*, 2016; Masters *et al.*, 2016). Activation of Pypin results in inflammasome formation and release of mature IL-1 β and IL-18 as well as GSDMD cleavage and pyroptosis (Broz and Dixit, 2016; Heilig and Broz, 2018). Multiple gain-of-function mutations have been reported for Pypin, causing autoinflammatory diseases. Some of these mutations are reported to disrupt 14-3-3 binding, resulting in autoactivation of the protein and a disease pypin-associated autoinflammation with neutrophilic dermatosis (PAAND) (Masters *et al.*, 2016; Moghaddas *et al.*, 2017). The mechanisms of other mutations involved in causing familial mediterranean fever (FMF) are not yet understood (Alghamdi, 2017).

As AIM2, the cGAS protein has been shown to directly sense cytosolic dsDNA longer than 30 bp. cGAS consists of a poorly conserved and unstructured N-terminus and a highly conserved C-terminus. The C-terminus is composed of an NTase (nucleotidyltransferase) core domain and a Mab21 domain. The Mab21 domain further contains a zinc-ribbon domain (Wu *et al.*, 2014). The NTase domain has enzymatic activity to synthesize the cyclic di-nucleotide (CDN) cyclic-GMP-AMP (cGAMP). CDNs like cAMP can also be of direct pathogenic origin as they are secreted by certain pathogens like bacteria (e.g. *Listeria monocytogenes*) (Woodward *et al.*, 2010; Lam *et al.*, 2014). One CDN molecule,

which is either generated upon sensing of cytosolic dsDNA by cGAS or of pathogenic origin, can induce a complex trafficking event by directly binding to two molecules of STING (Gao *et al.*, 2013; Gao *et al.*, 2014). STING is anchored in the membrane of the endoplasmic reticulum with several transmembrane regions. The cyclic di-nucleotide binding site is located in the cytoplasm and is formed by a STING dimer (Wu *et al.*, 2014). Binding of CDNs induces a structural change of the STING dimer, allowing for an interaction with TANK binding kinase 1 (TBK1) (Ishikawa *et al.*, 2009). The complex of STING and TBK1 is trafficked to the perinuclear Golgi via processes that resemble autophagy, relocating the complex to endolysosomal compartments of the cell (Ishikawa *et al.*, 2009). Here, TBK1 activates the transcription factors IRF3 and NF- κ B. Activation of these transcription factors induces the expression of cytokines and proteins belonging to the type-1 INF family, resulting in an inflammatory immune response (Shu *et al.*, 2014; Barber, 2015). In the cGAS/STING pathway, two different sensing mechanisms converge. cGAS can induce an immune response through STING upon dsDNA binding, which can be self-DNA or pathogen-derived DNA. As mentioned above, STING can further sense CDNs directly derived from pathogens. Interestingly, the cGAS/STING pathway is described to be independent of other PRRs activated by dsDNA, like TLR9 and AIM2 (Barber, 2015). This highlights the diversity of mechanisms used by the innate immune system to recognize PAMPs and DAMPs. As for other innate immune sensors, dysregulation of cGAS/STING leads to autoinflammatory disease. For instance, activating variants of STING are reported to cause an autoinflammatory disease called STING-associated vasculopathy with onset in infancy (SAVI) (Liu *et al.*, 2014).

1.3 The current model of inflammasome activation

Inflammasomes are large signalling platforms comprised of oligomerized PRRs, the adaptor protein ASC and caspase-1. NLR proteins (NLRP1, NLRP2, NLRP3, NLRP6, NLRP12, NLRC4) as well as non-NLR proteins (AIM2, IFI16, Pyrin) have been shown to be involved in the formation of these signalling complexes

(Rathinam *et al.*, 2012; Walsh *et al.*, 2014). The common model of how inflammasome activation occurs is described as a two-checkpoint mechanism (Figure 1.1). In a first step, also referred to as signal 1 or priming, microbial TLR ligands induce the activation of NF- κ B, resulting in the transcription and translation of the cytokine pro-IL-1 β and the inflammasome sensor itself (Bauernfeind *et al.*, 2010; Walsh *et al.*, 2014). The second step, termed signal 2, refers to the specific recognition of PAMPs, DAMPs or HAMPs through the respective inflammasome sensor molecule (Walsh *et al.*, 2014). Activation by signal 2 results in oligomerization of the sensor molecule, providing a recruitment hub for the adaptor protein ASC and finally procaspase-1 (Martinon and Tschopp, 2005). Active caspase-1 is described to induce an inflammatory immune response by processing pro-IL-1 β and pro-IL-18 into their active forms by proteolytic cleavage. Moreover, caspase-1 cleaves GSDMD, which can in turn induce pyroptosis, a rapid inflammatory form of cell death (Sollberger *et al.*, 2014; Liu *et al.*, 2016).

The ability of inflammasomes to trigger the release of cytokines also links this pathway to other parts of the immune system. For instance, IL-1 β has a role in tumor metastasis and blood vessel formation. Furthermore, it potently induces IL-6 production, which is directly involved in linking innate and adaptive immunity. IL-18 can act on different cells of the immune system, namely Th1 and Th2 cells, depending on the presence or absence of other cytokines, particularly IL-12 (Dinarello, 2009).

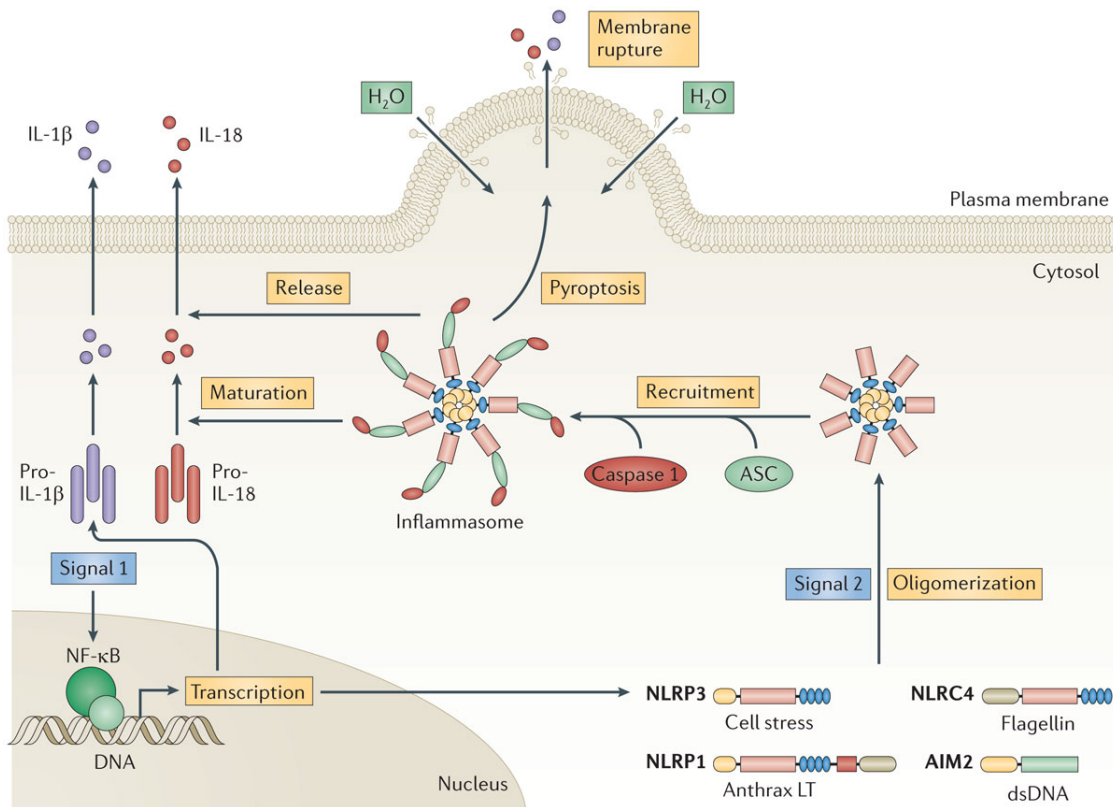


Figure 1.1: Current model of inflammasome activation

Schematic depiction of the current model of inflammasome activation. Upon activation of TLR signalling, which can be induced by pathogen-derived stimuli like bacterial LPS (Signal 1), NF- κ B induces the expression of inflammasome sensor molecules (e.g. NLRP1, NLRP3, NLRC4, AIM2) and the pro-forms of IL-1 β and IL-18. The sensor molecules are localized in the cytosol as autoinhibited monomers. A conformational change is induced by a sensor-specific stimulus (e.g. bacterial flagellin for NLRC4), allowing the sensor molecules to oligomerize (Signal 2). The oligomerized sensors provide a platform to recruit the adapter protein ASC and procaspase-1 and form the inflammasome complex. In this complex, procaspase-1 becomes active through proteolytic cleavage. Active caspase-1 can process pro-IL-1 β and pro-IL-18 into their mature forms. Furthermore, GSDMD is cleaved, resulting in the release of the pore-forming N-terminus of the protein, inducing pyroptosis. Pyroptosis and the release of mature IL-1 β and IL-18 stimulate an inflammatory immune response. Note the depicted stimulus for NLRP1, anthrax lethal toxin (LT), only activates certain variants of rodent but not human NLRP1. Adapted from Walsh *et al.* 2014.

In recent years, a different mechanism, termed the non-canonical inflammasome pathway, was described to induce pyroptosis and NLRP3 inflammasome formation. In this pathway, the human inflammatory caspases 4 and 5 as well as murine caspase-11 directly sense pathogen-derived cytosolic LPS, resulting in the cleavage of GSDMD and pyroptosis (Shi *et al.*, 2014; Russo *et al.*, 2018). Another effect of activation by LPS is activation of the NLRP3 inflammasome, again leading to activation of caspase-1 and the release of IL-1 β and IL-18 (Russo *et al.*, 2018).

1.3.1 The pro-inflammatory cytokines IL-1 β and IL-18

The family of IL-1 ligands includes a total of eleven molecules. Seven of these have receptor agonist activity, including IL-1 β and IL-18, three have receptor antagonist activity and one, IL-37, is an anti-inflammatory cytokine (Dinarello, 2009; Garlanda *et al.*, 2013). Sensing of these cytokines is facilitated through IL-1 receptors (IL-1R). The IL-1R family also consists of 11 members. These receptors are commonly composed of an extracellular domain consisting of three immunoglobulin (Ig)-like domains. Only the receptors TIR8 and IL-18BP (IL-18 binding protein) have just one extracellular Ig-like domain. Similar to TLRs, an intracellular TIR domain is responsible for downstream signalling by binding the MyD88 adaptor. A functional receptor is formed by dimerization of two molecules of the IL-1R family. The IL-1 receptor is formed by the molecules IL1-R1 and IL-1RAcP (IL-1 receptor accessory protein). The IL-18 receptor is formed by IL-18R α and IL-18R β (Garlanda *et al.*, 2013).

IL-1 β is produced mainly by monocytes, macrophages and dendritic cells. As described above, expression of the inactive precursor pro-IL-1 β is potently induced upon activation of TLRs by bacterial LPS. However, active IL-1 β can also stimulate the expression of more pro-IL-1 β by binding to its receptor. Stimulation of expression by IL-1 β itself is significantly prolonged compared to stimulation through products like bacterial LPS (Schindler *et al.*, 1990; Dinarello, 2009; Dinarello, 2018). To unfold its inflammatory functions, IL-1 β needs to be cleaved

by caspase-1. One mechanism by which IL-1 β induces an inflammatory immune response, is to induce the expression of cyclooxygenase type 2 (COX-2) and inducible nitric oxide synthase (iNOS). These enzymes catalyse the production of prostaglandins and nitric oxide, inducing classic inflammatory symptoms like fever, vasodilatation and hypotension. Furthermore, secreted IL-1 β induces the expression of chemokines and adhesion molecules which are both important for the infiltration of immune cells into the inflamed tissue (Dinarello, 2009).

IL-18 was initially found in the serum of mice and named “IFN γ - inducing factor”. In many ways IL-18 is similar to IL-1 β . IL-18 is synthesized as an inactive precursor protein, pro-IL-18, which needs to be cleaved by caspase-1 to become active. Moreover, it shares significant structural similarities with IL-1 β , despite having only 15 % sequence identity (Okamura *et al.*, 1995; Dinarello, 1999). Nevertheless, the biology of these two cytokines is different. IL-18 is constitutively present in monocytes, macrophages and DCs of healthy individuals, which are the primary source for the production of this cytokine. It contains less mRNA destabilizing elements compared to other cytokines, resulting in a stable expression. Transcription of IL-18 is induced by NF- κ B upon TLR stimulation. Interestingly, IL-18 is constitutively expressed in endothelial cells, keratinocytes and intestinal epithelial cells (Kaplanski, 2018). Similar to IL-1 β , active IL-18 induces inflammation by inducing the production of adhesion molecules, chemokines and nitric oxide. However, significantly higher concentrations of IL-18 are required to induce an inflammatory response in cells compared to IL-1 β (Kaplanski, 2018). IL-18 is well-described to also act cooperatively with other cytokines. Together with either IL-12 or IL-15 it can induce expression of IFN γ (Dinarello *et al.*, 2013). The activity of IL-18 can be regulated by the soluble single Ig-like domain containing protein IL-18BP (IL-18 binding protein). It has an extraordinarily high affinity to IL-18 and can therefore inhibit its function (Dinarello *et al.*, 2013). Apart from their pro-inflammatory functions both, IL-1 β and IL-18, play a key role in the differentiation of innate and adaptive lymphoid cells (Garlanda *et al.*, 2013). For instance, IL-18 is directly involved in regulating the immune response by Th1 and Th2 cells (Nakanishi *et al.*, 2001).

Dysregulation of IL-1 β and IL-18 has been described to be the cause of or involved in the development of several autoinflammatory diseases, such as rheumatoid arthritis, neurodegenerative diseases including Alzheimer's and Parkinson's, type 2 diabetes and multiple sclerosis. Discovery of the involvement of these two cytokines in multiple autoinflammatory diseases has led to the development of drugs that specifically inhibit the signalling pathways triggered by them. For instance, IL-1R blockade has become a successful treatment for type 2 diabetes (Volin and Koch, 2011; Lukens *et al.*, 2012; Giacomelli *et al.*, 2016).

1.3.2 Pyroptosis – an inflammatory form of cell death

Pyroptosis is a regulated form of cell death, which can be induced by a disturbance of extra- or intracellular homeostasis. It is directly linked to innate immunity and distinct from other forms of regulated cell death, like apoptosis or necroptosis, by certain characteristics such as a specific morphotype (Miao, 2015; Galluzzi *et al.*, 2018). The pyroptotic morphotype shows an atypical form of chromatin condensation and DNA damage. In contrast to apoptosis, the nucleus of cells undergoing pyroptosis remains intact (Fink and Cookson, 2006). Moreover, pyroptotic cell death features rapid swelling and osmotic lysis through ruptures of the plasma membrane (Jorgensen and Miao, 2015). This results in the uncontrolled release of proinflammatory cell contents, which is again different from the packaging of cell contents that occurs during apoptosis (Jorgensen and Miao, 2015; Galluzzi *et al.*, 2018).

The rapidly induced rupture of the cell membrane during pyroptosis is described to be mainly dependent on the pore-forming proteins of the gasdermin (GSDM) family. Members of the gasdermin family include GSDMA, GSDMB, GSDMC, GSDMD, GSDME and Pejvakin (PJVK). Expression of these proteins is tissue dependent in mice and humans. For example, GSDMD is mainly expressed in the skin, oesophagus, stomach and placenta in humans (Feng *et al.*, 2018). With the exception of PJVK, all GSDMs contain an N-terminal domain that has pore-forming activity and can induce pyroptosis-like cell death in overexpression systems (Ding *et al.*, 2016; Feng *et al.*, 2018). GSDMD is

expressed as an autoinhibited precursor protein, in which the pore-forming N-terminus is structurally inhibited by the C-terminus (Liu *et al.*, 2019). After proteolytic cleavage by inflammatory caspases (caspase-1, caspase-4/5 or the mouse homolog of caspase-4, caspase-11) its N-terminal fragment is released from the inhibitory C-terminal fragment and can form membrane pores to induce pyroptosis (He *et al.*, 2015; Shi *et al.*, 2015). However, pyroptosis has been shown to be not solely dependent on GSDMD. This was demonstrated by stimulating BMDMs lacking the GSDMD gene with canonical inflammasome activators. These cells were still able to undergo pyroptosis, even though the process was significantly delayed (Kayagaki *et al.*, 2015).

Different mutations in members of the gasdermin family have been shown to be the cause of or involved in causing different diseases like alopecia, asthma or gastric cancer (Feng *et al.*, 2018). Thus, gasdermin proteins have become a focus in research to better understand the mechanistic basis of their function and enable the design of drugs specifically inhibiting their pore-forming activity and consequently the induction of pyroptosis (Hu *et al.*, 2018; Pandeya *et al.*, 2019).

1.4 ATPases associated with diverse cellular activities (AAA+ ATPase)

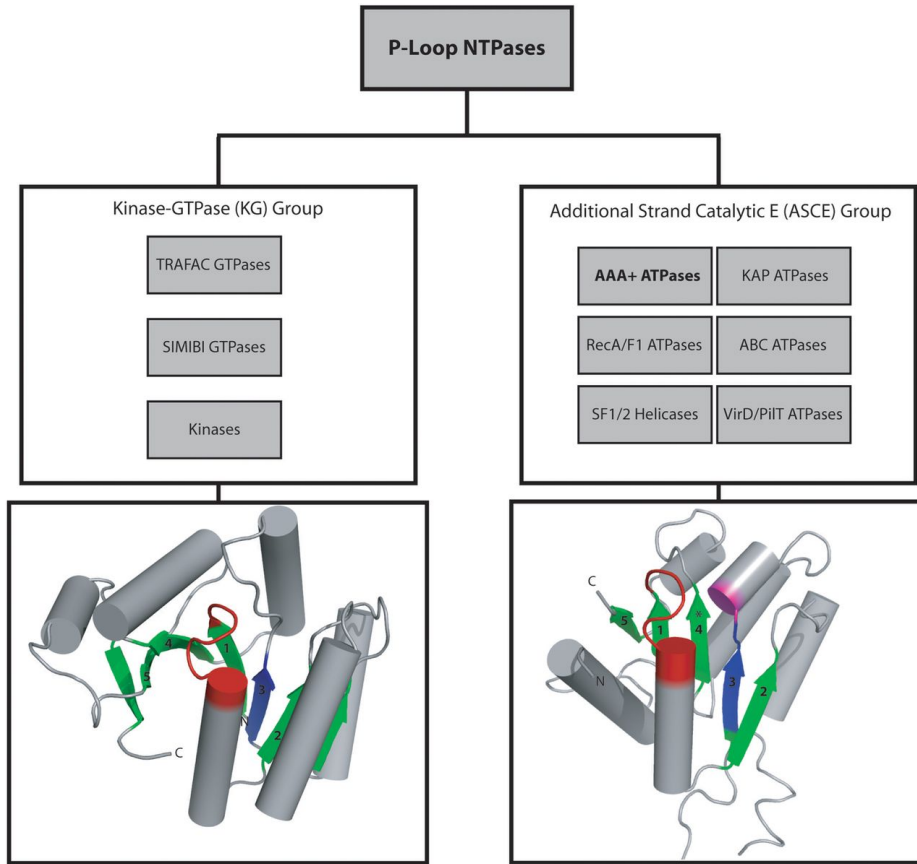
1.4.1 What are AAA+ ATPases? Classification of P-loop NTPases

A common approach to understanding the nature of how the biology of different organisms works on a molecular level, is to organise molecules with similarities in their sequences, their structure or their function into different classes. Finding these similarities (and differences) as part of this classification, helps to find patterns in regards to their functionality and therefore improves the understanding of yet to be characterised members of these classes. This further enables the prediction of the function a protein might have (to a limited extent) and allows for the design of targeted experiments. A very good example of such a classification is the organisation of the class of P-loop NTPases, which comprises an estimated 5-10 % of the (in 2004) fully sequenced genomes of prokaryotic and eukaryotic genomes (Koonin *et al.*, 2004; Snider and Houry, 2008). These proteins contain

a shared $\alpha\beta\alpha$ core domain with a parallel β -sheet centred between two sets of α -helices (James Milner-White *et al.*, 1991). On the sequence level, P-loop proteins commonly contain conserved motifs, the Walker A and Walker B motif. These motifs were named after John E. Walker, who first described these conserved sequences (Walker *et al.*, 1982). The Walker A motif was initially identified to contain a set of conserved residues following the pattern GxxxxGK(T)xxxxxxI/V (x denotes any of the proteinogenic amino acids). The Walker B motif was described to be located downstream of the Walker A motif and was described to follow the pattern R/KxxxGxxxLhhhhD (h denotes any hydrophobic amino acid) (Walker *et al.*, 1982). Originally, the Walker A motif was referred to as the phosphate-binding loop or P-loop, hence the name P-loop NTPases (Saraste *et al.*, 1990). Both, the Walker A and Walker B motifs, play an important role in protein function, as they contain conserved residues involved in nucleotide binding and hydrolysis (Walker *et al.*, 1982; Saraste *et al.*, 1990).

P-loop NTPases can be further subdivided into two major groups, the kinase-GTPase (KG) group and the additional strand catalytic E (ASCE) group (Figure 1.2A). KG group members present with a strand order of 5-4-1-3-2 in the core β -sheet, with the Walker B strand and the strand connected to the Walker A (P-loop) being adjacent to each other. Indicated by the name, members of the ASCE group contain a strand between the Walker B strand (strand 3, which commonly contains the catalytic glutamate (E)) and the strand connected to Walker A (strand 1), resulting a strand order of 5-1-4-3-2 (Figure 1.2B) (Snider and Houry, 2008). ASCE proteins are again divided into different families of proteins, including the ATPases with diverse cellular activities (AAA+ ATPases) (Figure 1.2A) (Snider and Houry, 2008). The key element that defines ASCE proteins as members of the AAA+ ATPase superfamily is the so called C-domain, an α -helical domain C-terminal of the ATPase domain (Ammelburg *et al.*, 2006).

A



B

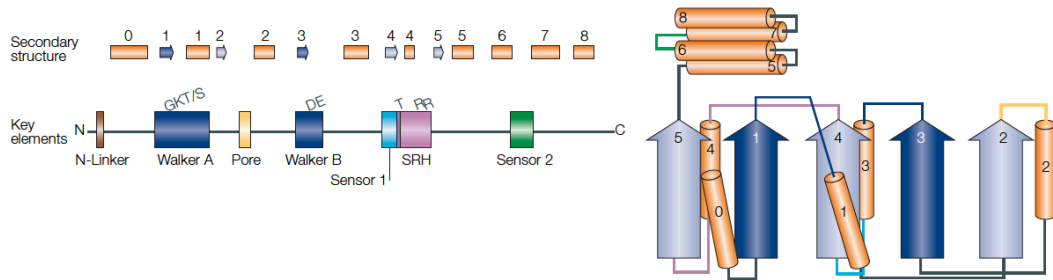


Figure 1.2: Classification of P-loop NTPases and structural characteristics of the nucleotide binding site

(A) Classification of P-loop NTPases into the two major subgroups, the kinase-GTPase (KG) group and the additional strand catalytic E (ASCE) group. Several subfamilies of the KG and ASCE groups are denoted below, including the superfamily of AAA+ ATPases as part of the ASCE group. The structural elements comprising the catalytic domain are depicted. The strand order, which distinguishes the two groups of P-loop NTPases, are noted in the β -strands of the structures. **(B)** Secondary structure elements of the nucleotide binding site of AAA+ ATPases are numbered as they occur according to the primary sequence of the proteins (top left). For the classification of P-loop NTPases the organization of secondary structure elements as they occur in the nucleotide binding site fold is compared (right). The organization of the β -sheet in AAA+ ATPases follows the 5-1-4-3-2 pattern, which is typical for members of the ASCE group. Key elements of AAA+ ATPases involved in nucleotide binding and hydrolysis including the Walker A, Walker B, Sensor 1 and Sensor 2 motif, are denoted in the schematic at the bottom left as they occur in the primary sequence of the proteins. (Adapted from Snider *et al.* 2008; Hanson and Whiteheart 2005).

Some AAA+ proteins such as plant resistance (R) proteins and their human AP ATPase homologs like Apaf-1 (apoptotic protease activating factor 1) and CED-4 (cell death protein 4) were originally classified into a separate subgroup of P-loop NTPases, the signal transduction ATPases with numerous domains (STAND) (Leipe *et al.*, 2004). This subgroup has subsequently been described to be part of the ASCE/AAA+ ATPase superfamily (Ammelburg *et al.*, 2006). As the name implies, AAA+ proteins are involved in a vast number of different cellular functions, including protein unfolding and degradation, fusion and fission of membranes and transcriptional activation (Snider *et al.*, 2008; Sysoeva, 2017). The Walker A and Walker B motifs of AAA+ ATPases were redefined to follow the pattern GxxxxGK(T/S) and hhhhDE, respectively. Furthermore, additional motifs involved in nucleotide binding and hydrolysis were identified, such as the Sensor 1 and Sensor 2 motif (Figure 1.2B) (Hanson and Whiteheart, 2005). Proteins involved in regulating different forms of cell death, like the above mentioned Apaf-1 or inflammasome forming NLRs contain these motifs and are thus consequently categorized as members of the STAND clade of the AAA+ ATPase superfamily (Ogura and Wilkinson, 2001; Leipe *et al.*, 2004; Danot *et al.*, 2009).

1.4.2 The role of self-assembly in AAA+ activity

As mentioned above (Chapter 1.3), oligomerization of the sensor protein is a central event in the assembly of inflammasomes. Members of the AAA+ ATPase superfamily are well-described to form biologically active, ring-like oligomeric complexes (Ogura and Wilkinson, 2001; Hanson and Whiteheart, 2005; Sysoeva, 2017). The oligomeric state is described to range from pentamers to octamers, with hexamers being the most prevalent form among AAA+ proteins. Oligomers can be homooligomers or heterooligomers (Hanson and Whiteheart, 2005; Sysoeva, 2017). A common model described for AAA+ oligomer activity, is that the energy of nucleotide hydrolysis events within the subunits of the oligomer are converted into mechanical energy in form of conformational changes. Consequently, these molecules are known to adapt different conformations in

their active and inactive state (Sysoeva, 2017). Different mechanisms for the sequence of hydrolysis events in the single subunits of one oligomer have been proposed. The concerted hydrolysis model suggests that all hydrolysis events and the coupled conformational changes occur simultaneously. Other hydrolysis models include the rotary, the sequential and the stochastic model, all of which propose different sequences of hydrolysis events (Ogura and Wilkinson, 2001; Sysoeva, 2017).

A well-described example for a functional hexamer is the AAA+ ATPase p97, which is involved in a variety of biological mechanisms like the ubiquitin proteasome system (Meyer *et al.*, 2012). Crystal structures of p97 in the apo state or bound to different nucleotides revealed that ATP binding and hydrolysis induces significant conformational changes in the p97 hexamer (Hänzelmann and Schindelin, 2016). Similar observations were made for the NtrC1 AAA+ ATPase by structural analysis of the heptameric protein in the apo state or bound to different nucleotides (Chen *et al.*, 2010). A conserved arginine residue, also referred to as the arginine finger (Figure 1.2B), is crucial in transmitting conformational changes between the subunits of the oligomeric AAA+ ATPase complex. Typically, this arginine is located at the interface between two subunits of the oligomer and has been shown to participate in formation of the nucleotide binding site of the neighbouring molecule (Hanson and Whiteheart, 2005; Chen *et al.*, 2010; Hänzelmann and Schindelin, 2016). This arginine residue is not found in members of the STAND group of AAA+ ATPases, to which Apaf-1, MalT and also NLRs belong (Leipe *et al.*, 2004). Interestingly, in the model of activation for Apaf-1 and MalT these proteins are monomeric in their inactive conformation and only oligomerize upon activation (Danot *et al.*, 2009). Structural data for both proteins in their monomeric and oligomeric forms supports this model. For MalT, binding of its ligand maltotriose and ATP as a cofactor was required to induce oligomerization of the protein (Acehan *et al.*, 2004; Larquet *et al.*, 2004). However, ATP hydrolysis was not required for oligomerization, as the non-hydrolysable AMP-PNP was sufficient to induce oligomerization in combination with maltotriose (Larquet *et al.*, 2004). In contrast, Apaf-1 needs both ATP binding

and hydrolysis upon activation by binding of mitochondrial Cytochrome C to form an active apoptosome (Kim *et al.*, 2005).

A similar activation model is described for inflammasome forming NLRs. For the NLRC4 inflammasome this model is supported by high resolution structural information on the active and inactive conformation. A crystal structure of an ADP-bound murine NLRC4 construct including its NACHT and LRR domain revealed the monomeric, autoinhibited conformation of NLRC4 (Hu *et al.*, 2013). More recent studies unveiled the structure of the active NLRC4 oligomer, which requires a NAIP molecule as nucleation factor. A single NAIP molecule is described to undergo conformational changes upon binding of its ligand, bacterial flagellin. Subsequently it can recruit an NLRC4 molecule and thereby induce NLRC4 oligomerization (Diebolder *et al.*, 2015; Zhang *et al.*, 2015; Tentorey *et al.*, 2017). The role of nucleotides in NLRC4 inflammasome activity has not yet been clarified.

Negative-stain electron microscopy of full-length NLRP1 showed monomers as well as pentameric and heptameric oligomers (Faustin *et al.*, 2007). However, no high resolution structural information for active or inactive NLRP1 is available yet. Thus, the mechanism of NLRP1 oligomerization, its oligomeric state and the role of nucleotide binding in mediating inflammasome assembly remain to be clarified.

1.5 The NLRP1 inflammasome

1.5.1 Differences between rodent and human NLRP1

Human NLRP1 is encoded by a single gene, located on chromosome 17 (Gene ID: 22861). It encodes 18 exons and is described to be transcribed and translated into seven isoforms produced by alternative splicing. NLRP1 expression was detected in multiple tissues such as heart, thymus spleen and intestine and in different immune cells including macrophages and neutrophils (Kummer *et al.*, 2007). The protein described as canonical isoform 1 in the protein database UniProt contains 1473 amino acids and has a calculated molecular weight of 166

kDa (UniProt ID: Q9C000). In contrast, there are three paralogs described for murine NLRP1, namely NLRP1a, NLRP1b and NLRP1c, which are likely the result of evolutionary gene duplication events (Chavarria-Smith and Vance, 2015). Furthermore, the existence of five highly polymorphic alleles is reported for the NLRP1b paralog (Boyden and Dietrich, 2006).

Human and murine NLRP1 further differ on the protein level in regards to their modular domain architecture (Figure 1.3) (Yu *et al.*, 2018). Human NLRP1 is composed of an N-terminal PYD, a central NACHT and LRR domain, followed by a FIIND (domain with “function to find”) domain and a C-terminal CARD. Both the PYD and the CARD domain belong to the family of death domains. Members of this family are typically involved in mediating protein-protein interaction via homotypic interactions (Weber and Vincenz, 2001). While the PYD of NLRP1 is involved in keeping the protein in an autoinhibited conformation, the C-terminal CARD domain is the effector domain required for downstream signalling (Finger *et al.*, 2012; Zhong *et al.*, 2016). NACHT domains are described to be involved in nucleotide binding and oligomerization of NLR proteins (Proell *et al.*, 2008). The FIIND domain consists of a ZU5-UPA domain tandem also present in non-NLR proteins like PIDD and Unc5b (Tinel *et al.*, 2007; Wang *et al.*, 2009). It is described to undergo autolytic cleavage, which is required but not sufficient for NLRP1 activation (D’Osualdo *et al.*, 2011; Finger *et al.*, 2012).

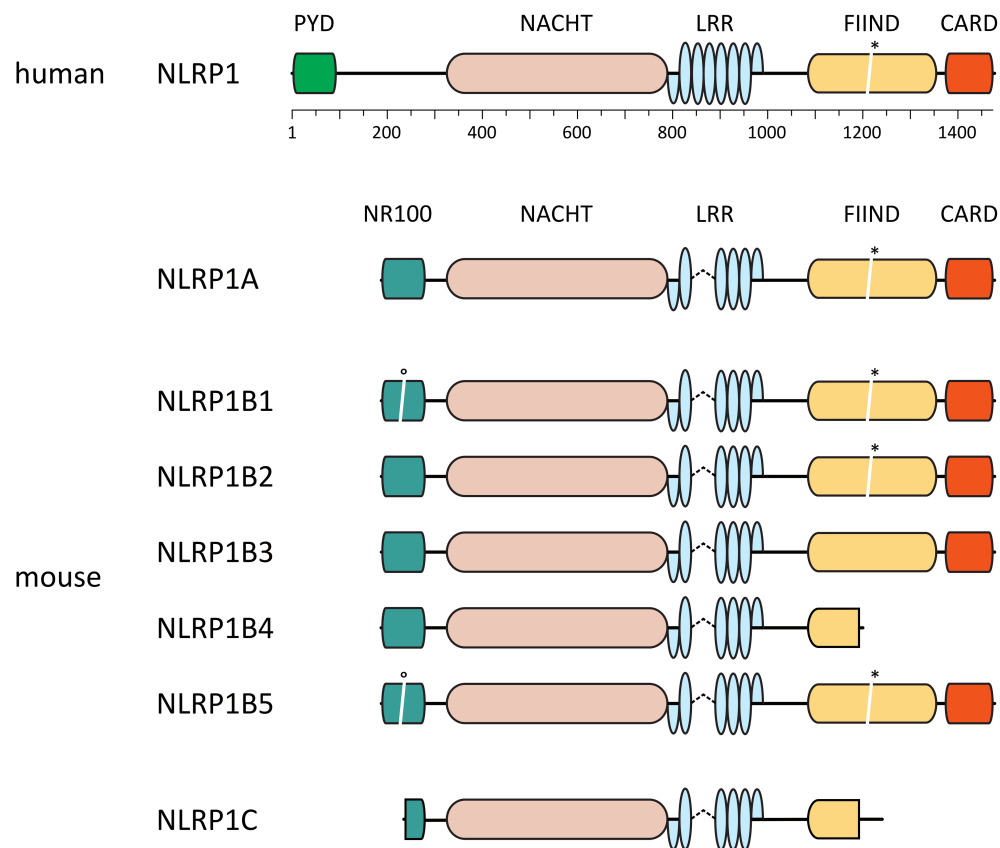


Figure 1.3: Comparison of the human and murine NLRP1 proteins

Modular domain architecture of human and murine NLRP1 proteins. Human NLRP1 contains an N-terminal PYD, a central NACHT and LRR domain, a FIIND and C-terminal CARD. The domain boundaries and positions are drawn to scale (based on the human NLRP1 protein). Murine NLRP1 contains an NR100 domain instead of the PYD found in human NLRP1 and a significantly shorter linker between the N-terminal NR100 domain and the NACHT domain. Furthermore, a truncation of the second and third LRR is found in murine NLRP1 compared to human NLRP1. Autolytic cleavage within the FIIND is depicted with a star (*) and proteolytic cleavage by anthrax lethal toxin in the murine NR100 domain with a circle (°). Protein sequences were obtained from the UniProt database and from NCBI. Accession codes were as follows: for NLRP1 human, Q9C000; NLRP1A mouse, Q2LKU9; NLRP1B1 mouse, Q2LKW6; NLRP1B2 mouse, A1Z198; NLRP1B3 mouse, Q2LKV5; NLRP1B4 mouse, Q2LKV2; NLRP1B5 mouse, Q0GKD5; NLRP1C mouse, AAI41385.1. (Adapted from Yu, Moecking *et al.* 2018).

All mouse NLRP1 paralogs lack the N-terminal PYD and instead contain a region of roughly 100 amino acids, which was termed NR100 domain (Figure 1.3) (Moayeri *et al.*, 2012). Moreover, the linker connecting the N-terminal domain and the NACHT domain in human NLRP1 is missing in the mouse variants (Yu *et al.*, 2018). Mouse NLRP1b allele 1 and 5 are described to be susceptible to cleavage by anthrax lethal toxin, resulting in inflammasome activation. The cleavage site is located in the NR100 domain. Neither human NLRP1 nor mouse NLRP1a, NLRP1b allele 2, 3 and 4 or NLRP1c contain this cleavage site (also see chapter 1.5.2) (Yu *et al.*, 2018). NLRP1b allele 3 is further not cleaved within its FIIND domain, rendering this variant inactive. NLRP1b allele 4 and NLRP1c lack the entire C-terminal CARD domain and part of the FIIND domain and are therefore also completely inactive variants. NLRP1c further lacks part of the NR100 domain (Yu *et al.*, 2018). The physiological role of the constitutively inactive mouse variants of NLRP1 has not yet been elucidated.

The human genome further encodes a protein called CARD8, which is composed only of a FIIND and a CARD domain. According to the UniProt database 5 isoforms of CARD8 exist, which are produced by alternative splicing. Canonical isoform 1 consists of 431 amino acids and has a molecular weight of 49 kDa (UniProt ID: Q9Y2G2). In a pairwise sequence alignment CARD8 showed 38 % sequence identity and 53 % sequence similarity to the NLRP1 FIIND and CARD domains (amino acids 991-1473; Clustal Needle Tool, default settings). As for NLRP1, the CARD8 FIIND domain is reported to undergo autoproteolysis (D’Oswaldo *et al.*, 2011). The mouse genome does not encode a CARD8 protein.

1.5.2 Mechanisms of NLRP1 activation

Although no pathogenic ligand is described that directly binds to and activates NLRP1 (as bacterial flagellin for NLRC4), several pathogenic and non-pathogenic stimuli have been reported to specifically induce NLRP1 inflammasome formation (Tenthorey *et al.*, 2017). Some of these stimuli activate both human and rodent NLRP1, while others are specific for certain rodent NLRP1 variants.

In particular, anthrax toxin from *Bacillus anthracis* is shown to only activate a few variants of NLRP1 in mice and certain rat strains (Yu *et al.*, 2018). Anthrax toxin is an exotoxin composed of the three proteins protective antigen (PA), oedema factor (EF), and lethal factor (LF) (Smith and Keppie, 1954; Turk, 2007). PA facilitates the entry of EF and LF into the cytosol of host cells via endosomes. Inside the cell, EF and LF act on intracellular signalling pathways to disrupt and inhibit an efficient immune response. The combination of PA and LF is also referred to as LeTx (lethal toxin). LF is a metalloproteinase that directly cleaves mitogen-activated protein kinase kinases (MKKs), ultimately resulting in the down-regulation of the MAPK pathway and an impaired immune response (Dong *et al.*, 2002; Turk, 2007). The first connection between anthrax toxin and NLRP1 was made when LeTx susceptibility of mouse macrophages was shown to be dependent on NLRP1b (Boyden and Dietrich, 2006; Liao and Mogridge, 2009). However, only macrophages of certain mouse strains tested in these studies showed susceptibility to LeTx, which was attributed to the highly polymorphic nature of the NLRP1b paralog (Boyden and Dietrich, 2006). Further studies showed that LF directly cleaves the murine NLRP1b protein (allele 1 and allele 5) as well as the NLRP1 protein of certain rat strains within the N-terminal NR100 domain (Hellmich *et al.*, 2012; Levinsohn *et al.*, 2012). This cleavage event was later on confirmed to be sufficient to induce NLRP1 inflammasome activation (Chavarría-Smith and Vance, 2013).

Human NLRP1 and other murine and rat NLRP1 variants (e.g. murine NLRP1a) are not direct substrates of LF and thus not activated when exposed to this protease. Nevertheless, proteolytic cleavage within the linker region connecting the N-terminal PYD or NR100 domain to the NACHT domain was shown to induce inflammasome activation in a reconstituted overexpression system in HEK293T cells. Proteolytic cleavage was achieved by introducing a TEV cleavage site in the aforementioned linker region and treating the cells with TEV protease (Chavarría-Smith *et al.*, 2016). Interestingly, when the N-terminal PYD was replaced by a GFP (green fluorescent protein) molecule, NLRP1 retained its autoinhibited conformation and could still be activated by TEV cleavage. Thus, it was concluded that the autoinhibitory effect of NLRP1 PYD is

mediated through steric hindrance rather than a specific intramolecular interaction (Chavarría-Smith *et al.*, 2016).

Consistent with the above mentioned finding that cleavage of the N-terminal PYD (or NR100 domain in rodents) results in activation of NLRP1, a deletion variant of NLRP1 lacking the N-terminal PYD was found to be constitutively active in overexpression system in 293T cells (Zhong *et al.*, 2016). Similarly, deletion of the LRR domain leads to constitutive activation of the NLRP1 inflammasome in both humans and mice (Liao and Mogridge, 2009; Chavarría-Smith *et al.*, 2016). Thus, the PYD and LRR of human NLRP1 are assumed to be involved in keeping the protein in an autoinhibited conformation. An activating effect of LRR deletion mutants has been reported for other NLR family members like NLRC4 and NOD2 (Ogura *et al.*, 2001; Kofoed and Vance, 2011). In contrast, an activating effect of a PYD deletion mutant has only been reported in the context of NLRP1. In other NLRP proteins, such as NLRP3, the N-terminal PYD is required for binding of the adaptor protein ASC and therefore essential in downstream signalling (Vajjhala *et al.*, 2012; Swanson *et al.*, 2019).

Toxoplasma gondii is a parasitic pathogen shown to induce NLRP1-dependent pyroptosis and IL-1 β release in rodents. As for LeTx, sensitivity to *Toxoplasma gondii* is highly variable for different mouse and rat strains carrying different NLRP1 variants (Cavaillès *et al.*, 2006; Ewald *et al.*, 2014; Cirelli *et al.*, 2014; Cavaillès *et al.*, 2014). For instance, rat strains carrying allele 1 or 2 of NLRP1 are significantly more sensitive to *T. gondii* infection compared to rat strains carrying allele 5. Consistent with this finding, rat macrophages infected with *T. gondii* exhibited reduced pyroptosis and IL-1 β release when carrying allele 1 or 2 of NLRP1 compared to macrophages carrying allele 5 (Ewald *et al.*, 2014; Cirelli *et al.*, 2014). Similarly, BMDMs expressing NLRP1a or NLRP1b allele 2 undergo *T. gondii* induced pyroptosis. In contrast to LeTx, activation of murine NLRP1 variants was shown to be independent of a cleavage event in the N-terminus of the protein, suggesting a different underlying activation mechanism (Ewald *et al.*, 2014). In another study the role of NLRP1 in resistance to *T. gondii* was confirmed, as NLRP1^{-/-} mice exhibited increased parasite load (Gorfu *et al.*, 2014). Three dense granule proteins were identified to be required to induce

pyroptosis in rat macrophages (Wang *et al.*, 2019). However, the exact mechanism by which *T. gondii* activates NLRP1 in mice and rats is still unknown. NLRP1 might also play a role mediating resistance to *T. gondii* infection in humans, as polymorphisms in NLRP1 are linked to increased susceptibility to congenital toxoplasmosis (Witola *et al.*, 2011). Furthermore, human innate immunity to *T. gondii* was shown to depend on ASC and caspase-1, as treatment with a caspase-1 inhibitor reduced IL-1 β release of monocytes. This was confirmed by performing shRNA knockdown experiments of caspase-1 and ASC (Gov *et al.*, 2013). However, the direct involvement of NLRP1 in sensing *T. gondii* and the underlying mechanisms have yet to be elucidated.

Apart from LeTx and *T. gondii*, other pathogens, namely the bacteria *Shigella flexneri* and *Listeria monocytogenes*, have recently been demonstrated to activate the NLRP1b inflammasome in mice (Neiman-Zenevich *et al.*, 2017). However, the molecular basis of inflammasome activation by these bacteria has not been clarified.

Another mechanism described to induce NLRP1 activation in mice and humans is inhibition of dipeptidyl peptidase 9 (DPP9) (Okondo *et al.*, 2018; Zhong *et al.*, 2018; de Vasconcelos *et al.*, 2019). Dipeptidyl peptidases are involved in multiple physiological processes and associated with immune pathologies (Waumans *et al.*, 2015). For instance, DPP9 has been reported to regulate the protein turnover of spleen tyrosine kinase (SYK) by directly cleaving a dipeptide at its N-terminus and thereby directing it to the N-end rule pathway (Justa-Schuch *et al.*, 2016). DPP9 forms functional dimers and specifically cleaves off dipeptides from proteins with a proline in the second position from the N-terminus (Zhang *et al.*, 2013; Ross *et al.*, 2018). It shares 77 % sequence similarity and 57 % sequence identity to DPP8, increasing to 100 % and 90 %, respectively, when only taking the catalytic domain into account (Van Goethem *et al.*, 2011). Inhibition of DPP8/9 was first shown to activate NLRP1b in mice by treating cells with the DPP8/9 inhibitor Talabostat. Interestingly, this activation mechanism was reported to be independent of the adaptor protein ASC (Okondo *et al.*, 2018). Inflammasome activation independent of ASC was previously reported for other stimuli of murine NLRP1b, for instance, when activated by LeTx, but not for

human NLRP1 (Van Opdenbosch *et al.*, 2014). Consistent with these findings, human NLRP1 activation by inhibition of DPP9 was shown to be dependent on ASC in immortalized keratinocytes (Zhong *et al.*, 2018). Furthermore, experiments in BMDMs revealed that ASC amplifies signalling of the active inflammasome, as measured by release of IL-1 β (Zhong *et al.*, 2018). The inhibitory mechanism of DPP9 was identified to be mediated by direct binding of DPP9 to the FIIND domain of NLRP1 by immunoprecipitation experiments with DPP9 and NLRP1 overexpressed in HEK293T cells. Treatment with Talabostat impairs binding of DPP9 to NLRP1, resulting in inflammasome activation. Furthermore, DPP9 requires its catalytic activity to unfold its inhibitory effect on NLRP1, as a catalytically inactive mutant (DPP9 S759A) was still able to bind NLRP1 but unable to rescue ASC speck formation in DPP8/9 double KO 293T cells (Zhong *et al.*, 2018). In contrast to LeTx, DPP8/9 inhibition induces inflammasome activation for all functional rodent NLRP1 variants. Moreover, comparing the activation pattern of DPP8/9 inhibition with that of *T. gondii* showed that both stimulate rodent NLRP1 variants in a very similar pattern. Thus, it was concluded that *T. gondii* activation mimics DPP8/9 inhibition, or at least activates NLRP1 by a similar mechanism (Gai *et al.*, 2019). Importantly, DPP8/9 inhibition was also reported to induce pyroptosis by activating the CARD8 protein in two human NLRP1^{-/-} cell lines. It was therefore suggested that depending on the cell type DPP8/9 inhibitor induced pyroptosis can be independent of NLRP1 (Johnson *et al.*, 2018). This has to be considered when using DPP8/9 inhibitors as activating stimuli for NLRP1.

Very recently, two independent studies described a mechanism that could serve as universal model for NLRP1 activation (Chui *et al.*, 2019; Sandstrom *et al.*, 2019). One study identified genes required for NLRP1b dependent pyroptosis in a genome-wide CRISPR-Cas9 knockout screen. Several components of the N-end rule pathway were identified in this screen, like Ubr2, Ubr4 or Uba6 (Chui *et al.*, 2019). Indeed, NLRP1b activation by LT or Talabostat induced degradation of the N-terminal cleavage fragment of NLRP1, which was shown by western blot. Double knockout of Ubr2/Ubr4 completely abrogated LT induced pyroptosis and NLRP1b degradation, as measured by LDH release or western blot analysis,

respectively (Chui *et al.*, 2019). Moreover, inhibitors of the N-end rule degradation pathway and proteasome inhibitors efficiently rescued cells from LT or Talabostat induced pyroptosis (Chui *et al.*, 2019). Specific degradation of the NLRP1b N-terminal cleavage fragment upon cleavage by LT and the rescuing effect of proteasome inhibitors were confirmed in another study (Sandstrom *et al.*, 2019). Furthermore, the C-terminal cleavage fragment of NLRP1b was shown to be sufficient to oligomerize and form a functional inflammasome. The *Shigella flexneri* E3 ubiquitin ligase IpaH7.8 was demonstrated to directly activate NLRP1 by ubiquitination of the NLRP1 N-terminal fragment (Sandstrom *et al.*, 2019). Ubiquitination is commonly described to direct proteins to proteasomal degradation (Ciechanover, 1994). The proposed model for inflammasome activation derived from these results suggests that NLRP1b poses an integrated decoy target to pathogen enzymes. These enzymes induce degradation of the N-terminal cleavage fragment containing the NR100, NACHT, LRR and part of the FIIND domain of NLRP1b. Consequently, the C-terminal cleavage fragment, composed of part of the FIIND domain and the CARD domain, would be released and could assemble into an active inflammasome (Chui *et al.*, 2019; Sandstrom *et al.*, 2019). Similar mechanisms were previously described for the NLR-related plant resistance proteins (Jones *et al.*, 2016).

Bacterial muramyl dipeptide (MDP) was initially described to enhance NLRP1 inflammasome activation in a cell-free system and was considered a direct pathogen-derived ligand for NLRP1 (Faustin *et al.*, 2007; Bruey *et al.*, 2007). MDP is part of the bacterial cell wall of gram negative and gram positive bacteria. Later studies found that MDP does not directly bind the NLRP1 LRR or NACHT-LRR domains in an *in vitro* cell-free system (Reubold *et al.*, 2014; Martino *et al.*, 2016). Moreover, BMDMs from NLRP1b^{-/-} mice exhibited unchanged IL-1 β levels when activated with MDP (Kovarova *et al.*, 2012). Other studies reported that MDP is a direct ligand of NOD2 and NLRP3 (Inohara *et al.*, 2003; Girardin *et al.*, 2003; Martinon *et al.*, 2004). Thus, it has to be concluded that MDP is not a direct activator of the NLRP1 inflammasome.

Another controversy regarding mechanisms underlying NLRP1 activation is the role of ATP. As for MDP, ATP was described to enhance NLRP1

oligomerization in a cell-free system (Faustin *et al.*, 2007). In this context, the proteins Bcl-2 and Bcl-X_L were reported to inhibit NLRP1 activation by blocking ATP binding and thereby prevent NLRP1 oligomerization (Bruey *et al.*, 2007; Faustin *et al.*, 2009). Both proteins belong to the group of Bcl-2 family proteins, which is known to be involved in regulating cell death (Kale *et al.*, 2018). However, in another study it was found that a reduction of cytosolic ATP resulted in specific activation of NLRP1b (Liao and Mogridge, 2013). Additionally, Walker A mutation variants of mouse NLRP1b or human NLRP1 are shown to exhibit increased or constitutive inflammasome activity, respectively (Liao and Mogridge, 2013; Chavarría-Smith *et al.*, 2016). Walker A mutations typically impair nucleotide binding, which has been shown for recombinant human NLRP1 in a Scintillation Proximity Assay with radiolabelled, non-hydrolysable [³⁵S]- γ -ATP (Harris *et al.*, 2015). Moreover, screening for ATP-competitive inhibitors did not lead to the identification of a specific inhibitor for NLRP1, however assays for NLRP1 activation were not well developed at this time (Harris *et al.*, 2015). A recombinant protein construct containing the NACHT and LRR domains of NLRP1 was shown to be constitutively bound to ATP in an open, active though monomeric conformation. However, no hydrolysis activity was detected when incubating this protein with ATP and Mg²⁺ (Martino *et al.*, 2016). Taken together, NLRP1 does bind ATP, however oligomerization and inflammasome activity do not seem to depend on ATP binding. Thus, the role of nucleotide binding in the NACHT domain for regulating NLRP1 activity remains to be elucidated.

1.5.3 NLRP1-associated autoinflammatory diseases

A number of missense mutations in the NLRP1 gene locus have been identified to directly cause constitutive inflammasome activation, resulting in autoinflammatory disease. These mutations are located within different domains of NLRP1 and contributed in the understanding of the molecular mechanisms governing NLRP1 regulation. Mutations found in the PYD (A54T, A66V, M77T) were described induce dyskeratosis and multiple self-healing palmoplantar carcinoma (MSPC) in patients (Soler *et al.*, 2013; Zhong *et al.*, 2016).

Mechanistically, these mutations disrupt the fold of the PYD since they disturb the hydrophobic core of the domain (Soler *et al.*, 2013; Zhong *et al.*, 2016). These mutations confirmed the identification of the NLRP1 PYD as an autoinhibitory rather than an effector domain. A homozygous mutation in the HD2-LRR transition region (R726W) and a *de novo* mutation in the FIIND domain of NLRP1 were reported to induce an autoinflammatory phenotype with arthritis and dyskeratosis (NAIAD - NLRP1-associated autoinflammation with arthritis and dyskeratosis) (Grandemange *et al.*, 2017). A deletion of exon five (amino acids F787-R843) was shown to cause familial keratosis lichenoides chronica (FKLC) in patients (Zhong *et al.*, 2016). Interestingly, all mutations reported for NLRP1 to cause the systemic autoinflammatory syndromes MSPC, FKLC and NAIAD, are associated with skin inflammation. This is consistent with the finding that NLRP1 is strongly expressed in keratinocytes and epithelial cells. In addition to the above mentioned mutations, a rare genetic variant within the NACHT domain of NLRP1 (G578S) was found to be potentially involved in the development of sporadic multiple sclerosis and concomitant malignant melanoma (Maver *et al.*, 2017).

Multiple common single nucleotide polymorphisms (SNPs) are described for NLRP1 that are associated with autoinflammatory diseases. Different SNPs in NLRP1 are reported to be involved in vitiligo and associated autoimmunity by causing increased IL-1 β processing (Y. Jin *et al.*, 2007; Levandowski *et al.*, 2013). Other autoinflammatory disorders associated with NLRP1 polymorphisms include type 1 diabetes, diabetic kidney disease, asthma and Crohn's disease (Cummings *et al.*, 2010; Leal *et al.*, 2018; Soares *et al.*, 2018; Sun *et al.*, 2019). NLRP1 variants are also described to increase susceptibility for congenital toxoplasmosis, bacterial meningitis, HPV infection and associated cervical cancer, infection with the malaria parasite *Plasmodium vivax* and *Trypanosoma cruzi* associated Chagas cardiomyopathy (Witola *et al.*, 2011; Geldhoff *et al.*, 2013; Santos *et al.*, 2016; Pontillo *et al.*, 2016; Clipman *et al.*, 2018). Furthermore, NLRP1 was identified as a potential risk locus for the development of breast cancer (Gao *et al.*, 2012).

1.6 Thesis aims

The increasing number of autoinflammatory diseases associated with or directly linked to a dysregulated NLRP1 inflammasome, made it a conceivable drug development target. As mentioned above, a screening for ATP competitive inhibitors did not reveal specific NLRP1 inhibitors (Harris *et al.*, 2015). Apart from that, no other drugs or screenings for drugs directly inhibiting the NLRP1 inflammasome have been reported yet. Identification of the activation mechanism by N-terminal degradation demonstrated that proteasome and N-end rule pathway inhibitors could pose a new treatment strategy for NLRP1 related diseases (Chui *et al.*, 2019; Sandstrom *et al.*, 2019). Indeed, proteasome inhibitors like Bortezomib are already clinically used in the therapy of multiple myeloma. However, the proteasome is involved in regulating protein turnover of many proteins and inhibition can therefore have adverse effects in patients (Curran and McKeage, 2009). Thus, more specific inhibitors for NLRP1 would greatly improve disease management options in patients suffering from NLRP1-associated autoinflammatory disease. A better understanding of the molecular mechanisms would aid in the development of assays for NLRP1 specific drug screenings. Therefore, the aims of this thesis were defined to:

1. Improve the understanding of NLRP1 autoinhibition and activation by biochemical analysis and generating structural data.
2. Gain insight into the mechanisms underlying nucleotide binding and the requirement of nucleotides for NLRP1 activation.
3. Identify and understand molecular mechanisms regulating NLRP1 activity.

To achieve these aims, a combination of a computational analysis of sequence and structural features of NLRP1, biochemical and structural experimental approaches and *in vitro* cell culture assays measuring inflammasome activation were used. This work was focused entirely on the human NLRP1 inflammasome.

2. Materials and Methods

2.1 Materials

2.1.1 Reagents and consumables

Table 2.1: DNA and Protein molecular weight marker

Marker	Supplier
DNA Ladder 1 kb	CarlRoth, Karlsruhe, Germany
DNA Ladder 100 bp	CarlRoth, Karlsruhe, Germany
Gel filtration standard	Bio-Rad, Munich, Germany
Low molecular weight (LMW) marker	GE Healthcare (Munich, Germany)
Page Ruler Prestained Plus	Thermo Fisher Scientific, Waltham, USA
Precision Plus Protein™ All Blue Prestained Protein Standards	Bio-Rad, Munich, Germany

Table 2.2: Kits

Kit	Supplier
ExtractMe Plasmid Mini Kit	Blirt, Gdańsk, Poland
ExtractMe DNA Clean-Up & Gel-Out Kit	Blirt, Gdańsk, Poland
GeneJET Plasmid Maxiprep Kit	Thermo Fisher Scientific, Waltham, USA
QuikChange Mutagenesis PCR	Agilent, Santa Clara, USA

Table 2.3: Primer sequences

Construct/Mutation	Sequence (5'-3')
Amplification	
NLRP1-A fwd	CATGCCATGGCTGGTGGTGCTTGGG
NLRP1-A rev	CGGAATTCAGGAGGACAGGGGCAGCAGG
NLRP1-B fwd	CATGCCATGGGACCCGTGACCGACGCTTACTGGC
NLRP1-B rev	CGGAATTCAGGAGGGCTTGCGACGGCTG
NLRP1-C fwd	CGCGGATCCGGTCCCGTGGCTACTGAGGTGG
NLRP1-C rev	CGGAATTCAGCCCTTCTTGAACCCTTCTCCCAC
NLRP1-D fwd	CGCGGATCCCCTCTGGACGCTCCTCAGCTG
NLRP1-D rev	CGGAATTCAGCCCTTCTTGAACCCTTCTCCCAC
NLRP1-E fwd	CGCGGATCCGGTCCCGTGGCTACTGAGGTGG
NLRP1-E rev	CGGAATTCAAGGAGCGTCCAGAGGAGAGGGC
NLRP1-F fwd	CATGCCATGGCTGGTGGTGCTTGGG
NLRP1-F rev	CGGAATTCAGGAGTGACCAGCACCCCTCTTGAGC
Mutagenesis	
	Template pCIG2-NLRP1
K340A fwd	GCTGGAATTGGGGCGTCAACACTGGC
K340A rev	GCCAGTGTTGACGCCCAATTCCAGC
S341A fwd	GGAATTGGGAAGGCAACACTGGCCAGG
S341A rev	CCTGGCCAGTGTTGCCTTCCCAATTCC
E414Q fwd	GATGGTGTAGATCAGCCAGGATGGGTC
E414Q rev	GACCCATCCTGGCTGATCTACACCATC
T389A fwd	GCCGGAGTGGCTGCCCATCTTTTCCG
T389A rev	CGGAAAAGATGGGGCAGCCACTCCGGC
H623A fwd	GCTACAGCTTCATTGCCCTCTGTTTCCAAG
H623A rev	CTTGAAACAGAGGGCAATGAAGCTGTAGC

P1214R fwd	GAGGACTCCCAAGGTCTAGAAGCTGGGGTTTTCCAGA ACTATGT
P1214R rev	ACATAGTTCTGGAAAACCCCAGCTTCTAGACCTTGGA GTCCTC
Y1413F fwd	GCTGAGCCAGGAGCAGTTCGAGAGGGT
Y1413F rev	ACCCTCTCGAACTGCTCCTGGCTCAGC
Y1413E fwd	GCCAGCACCTCTCTTCTGCTCCTGGCTCA
Y1413E rev	TGAGCCAGGAGCAGGAAGAGAGGGTGCTGGC
Y1413Q fwd	TGAGCCAGGAGCAGCAAGAGAGGGTGCTGGC
Y1413Q rev	GCCAGCACCTCTCTTGCTGCTCCTGGCTCA
Mutagenesis	Template pACE-Bac1-MBPtev-NLRP1
M1184V fwd	CTGTTCCAGGTGGCTCACTTCAAGGAAGAG
M1184V rev	GAAGTGAGCCACCTGGAACAGGGAGGTGTC
S1213A fwd	GAACCCCTCCTTCGCCCCCTGGGTGTC
S1213A rev	GACACCCAGGGGGGCGAAGGAGGGGTTC
K340A fwd	GTATCGGCGCGTCCACCCTGGCTCGTCAAG
K340A rev	CAGGGTGGACGCGCCGATACCAGCAGCAC

Primers were purchased from Metabion International AG (Bonn) or from Integrated DNA Technologies (Melbourne). (fwd: forward; rev: reverse)

2.1.2 Cell culture and bacterial culture media

All cell culture and bacterial culture media were prepared and used under sterile conditions. Bacterial culture media was prepared from powder with Milli-Q® water (Bonn, Germany) or supplied by the WEHI media kitchen (Melbourne, Australia). Foetal Bovine Serum (FBS) for mammalian cell culture was heat inactivated at 55 °C for 30 min before adding it to cell culture media.

Table 2.4: Cell culture and bacterial culture media

Chemical/Reagent	Supplier
Dulbecco's Modified Eagle's Medium (DMEM)	Thermo Fisher Scientific, Waltham, USA
Foetal Bovine Serum (FBS)	Sigma-Aldrich, USA
Insect-XPRESS™	Lonza, Basel, Switzerland
Luria Broth (LB)	CarlRoth, Karlsruhe, Germany/ WEHI Media Kitchen, Melbourne, Australia
OptiMEM	Thermo Fisher Scientific, Waltham, USA
Roswell Park Memorial Institute medium 1640 (RPMI)	WEHI Media Kitchen
Sf-900™ III SFM 1x	Invitrogen, Karlsruhe, Germany
Super-Optimal Broth (SOB)	WEHI Media Kitchen, Melbourne, Australia

2.1.3 Equipment

Table 2.5: Equipment

Device	Supplier
Agarose gel chamber, DNA-SUB-Cell	Bio-Rad, Munich, Germany
Autoclave 5075 EL	Systec, Linden, Germany
Biophotometer	Eppendorf, Munich, Germany
Centrifuge, Avanti J265 XP	Beckman and Coulter, Brea, California, USA
Centrifuge, Eppendorf 5810	Eppendorf, Munich, Germany
Centrifuge, Eppendorf 5810R	Eppendorf, Munich, Germany
ChemiDoc™ Touch Imaging System	Bio-Rad, Munich, Germany

Electroporator, Eporator	Eppendorf, Munich, Germany
FPLC-System Äkta micro	GE Healthcare, Munich, Germany
FPLC-System Äkta prime plus	GE Healthcare, Munich, Germany
FPLC-System Äkta Pure	GE Healthcare, Munich, Germany
FPLC-System Äkta Start	GE Healthcare, Munich, Germany
Freezer (-80 °C)	Thermo Scientific, Corston, UK
HPLC system, Agilent 1260 Infinity II	Agilent, Stevens Creek, USA
Incubator Heratherm	Thermo Scientific, Waltham, USA
Incubator Innova 40	New Brunswick Scientific, Jersey, USA
Incubator Multitron pro	Infors HAT, Bottmingen, Switzerland
Incubator, Heraeus CO2 Auto zero	Heraeus Instruments, Hanau, Germany
LSR Fortessa X-20	BD, Australia
Magnetic stirrer MR 2000	Heidolph, Schwabach, Germany
Mastercycler nexus SX1	Eppendorf, Munich, Germany
Microbalance CPA324S	Sartorius, Göttingen, Germany
Microscope Axiolab	Carl Zeiss, Jena, Germany
Mini protean Tetra Cell	Bio-Rad, Munich, Germany
Nanodrop 2000/c UV-Spectrometer	Thermo Scientific, Waltham, USA
Odyssey, gel documentation system	Li-Cor Biosciences, Bad Homburg, Germany
pH meter lab 850	Schott Instruments, Mainz, Germany
Sonifier Vibra cell	Sonics, Newton, USA
Sonifier W-250	Branson, Danbury, USA
Tabletop centrifuge Eppendorf 3424	Eppendorf, Munich, Germany
Thermomixer comfort	Eppendorf, Munich, Germany
Vortexer Vortex Genie 2	Bender & Hobein, Bruchsal, Germany
Water bath Julabo 5	Julabo, Seelbach, Germany

2.1.4 Cell lines and bacterial strains

Table 2.6: Cell lines

Cell line	Supplier
Sf9 insect cells (clonal isolates derived from <i>Spodoptera frugiperda</i> cell line IPLB-Sf21-AE)	Thermo Fisher Scientific, Waltham, USA
Sf21 insect cells (clonal isolates derived from <i>Spodoptera frugiperda</i> cell line IPLB-Sf21-AE)	Thermo Fisher Scientific, Waltham, USA
Human embryonic kidney (HEK) 293T cells	ATCC Australia
Human embryonic kidney (HEK) 293T cells (ASC-RFP)	Dr. Dominic De Nardo

2.1.5 Buffers for protein purification

Table 2.7: Buffers for protein purification (affinity chromatography)

Construct	Buffer/Application	Composition
NLRP1-A	Lysis/Wash buffer	20 mM Tris/HCl (pH 8.0), 150 mM NaCl, 5 mM β -ME
	Elution buffer	20 mM Tris/HCl (pH 8.0), 150 mM NaCl, 10 mM maltose, 5 mM β -ME,
NLRP1-C NLRP1-D NLRP1-E	Lysis buffer	20 mM Tris/HCl (pH 7.0), 150 mM NaCl, 5 mM β -ME
	Wash buffer	20 mM Tris/HCl (pH 7.0), 500 mM NaCl, 5 mM β -ME

NLRP1-B	Elution buffer	20 mM Tris/HCl (pH 7.0), 150 mM NaCl, 10 mM maltose, 5 mM β -ME
	Lysis buffer	50 mM MES/NaOH (pH 6.5), 500 mM NaCl, 1 % (v/v) NP-40, 5 mM β -ME
	Wash buffer	50 mM MES/NaOH (pH 6.5), 100 mM NaCl, 5 mM β -ME
	Elution buffer (GST)	50 mM MES/NaOH (pH 6.5), 500 mM NaCl, 30 mM GSH (reduced), 5 mM β -ME
	Elution buffer (IEC)	50 mM MES/NaOH (pH 6.5), 1000 mM NaCl, 5 mM β -ME
NLRP1-F	Lysis buffer	20 mM Tris/HCl (pH 7.0), 150 mM NaCl, 5 mM β -ME
	Wash buffer	20 mM Tris/HCl (pH 7.0), 500 mM NaCl, 5 mM β -ME
	Elution buffer	20 mM Tris/HCl (pH 7.0), 150 mM NaCl, 30 mM GSH (reduced), 5 mM β -ME

Table 2.8: Buffers for protein purification (size exclusion chromatography)

Construct/Application	Composition
NLRP1-A	20 mM HEPES/NaOH (pH 8.0), 150 mM NaCl, 1 mM TCEP
NLRP1-B	50 mM MES/NaOH (pH 6.5), 100 mM NaCl, 1 mM TCEP

NLRP1-C NLRP1-D NLRP1-E NLRP1-F	20 mM HEPES/NaOH (pH 7.2), 100 mM NaCl, 1 mM TCEP
Analytical SEC	20 mM HEPES/NaOH (pH 7.2), 100 mM NaCl, 1 mM TCEP

2.2 Methods – Molecular Biology

2.2.1 Polymerase Chain Reaction (PCR)

PCR was used to specifically amplify fragments from a DNA template or to mutate a gene of interest into a DNA plasmid. Furthermore, a PCR was carried out on cell lysates (e.g. from HEK293T cells) to test these cells for contamination with mycobacteria.

For the amplification of DNA fragments for cloning, either a Phusion Polymerase or Q5 Polymerase (New England Biolabs), was used. In these reactions, the annealing temperature and elongation time were adjusted to the primer melting temperatures and length of the DNA fragment as recommended by the manufacturer. Mutagenesis PCR was carried out using the QuikChange Lightning Site-Directed Mutagenesis Kit (Agilent) following the instructions described in the manual of the manufacturer.

To test cell lysates for contamination with mycobacteria by PCR, a GoTaq-Mix was used. 1×10^6 cells were spun down and resuspended in 100 μ L tail lysis buffer (Viagen) supplemented with 1 x Proteinase K (Sigma Aldrich) to degrade DNases. Lysis was performed at 55 °C o/n. Afterwards, Proteinase K was heat inactivated by incubating at 80 °C for 10 min. 1 μ L of the lysate served as template in the PCR reaction. A set of primers designed to identify a contamination was applied, resulting in a DNA fragment of about 350 bp for contaminated samples. A positive and negative control were run alongside the samples.

2.2.2 Agarose gel electrophoresis

DNA fragments from PCR reactions were separated according to their size by running them on a 1 % agarose gel in 1 x TAE buffer (40 mM Tris base, 20 mM acetic acid, 1 mM EDTA sodium salt dihydrate). Gels were typically run at 100 V for at least 30 min. Before applying samples to a gel, the appropriate amount of 6 x loading buffer was added to each sample. Additionally, a DNA marker was run on the gel, to confirm the size of the fragments produced by PCR. If the DNA

fragments were to be used in cloning procedures afterwards, they were purified from the gel using the ExtractMe DNA Clean-Up & Gel-Out Kit (Blirt) following the instructions of the supplied manual.

2.2.3 Restriction digest

Restriction endonucleases are a class of enzymes described to be responsible for the sequence-specific recognition and cleavage of foreign double stranded DNA. Prokaryotes distinguish foreign from self-DNA, by making use of a specific methylation pattern. Type II restriction endonucleases recognize both asymmetric or symmetric patterns, so called palindromic, DNA sequence motifs and cleave the covalent phosphodiester bond within these sequences producing a break in the DNA strand. The resulting either sticky or blunt ends can be further ligated according to the cohesive ends.

Restriction enzymes were primarily utilized to produce compatible overhangs (sticky ends) on DNA fragments produced in PCR and target vectors, making them accessible to ligation. All restriction enzymes were purchased from New England Biolabs and reactions were set up as recommended by the manufacturer. Digested fragments and vectors were purified by gel extraction (ExtractMe DNA Clean-Up & Gel-Out Kit, Blirt) to remove enzymes and unneeded fragments resulting from the digest. Analytical restriction digest was performed after ligation (Chapter 2.2.4) and transformation (Chapter 2.2.5), to confirm that the vector contains the correct insert. In these reactions 0.2 μL per enzyme were used in a total reaction volume of 20 μL .

2.2.4 Ligation

To insert a DNA fragment into a vector with compatible sticky ends, T4 DNA ligase (New England Biolabs) was used. Reactions were set up to contain 50 ng of digested and purified vector DNA and three times as much digested and purified insert DNA (molar ratio). The total reaction volume of a ligation was 20

μL , containing 1 μL of ligase and 2 μL of 10 x T4-DNA Ligase Buffer (New England Biolabs). Reactions were incubated for 2 h at RT or o/n at 4 °C.

2.2.5 Transformation of bacteria

A volume of 50 μL of chemically competent *E. coli* DH10 β was mixed with 100 ng plasmid DNA or 10 μL of a ligation and incubated on ice for 15 min. Transformation was carried out by applying a heat shock (42 °C, 30 s). Subsequently, the bacteria were recovered by immediately placing them on ice for 2 min. Afterwards 900 μL of Super-Optimal Broth (SOB) medium were added and the transformed bacteria were incubated at 37 °C for at least 1 h. Transformed and recovered bacteria were streaked out on an LB-agarose plate containing the appropriate antibiotics. Typically, Ampicillin (100 $\mu\text{g}/\text{mL}$), Kanamycin (50 $\mu\text{g}/\text{mL}$), Gentamycin or Tetracyclin (both 10 $\mu\text{g}/\text{mL}$) served as selection antibiotics.

For the production of Bacmids (Chapter 2.2.8), 25 μL of *E. coli* DH10 MultiBac^{Turbo} (electrocompetent or chemically competent) were mixed with 100 ng of the according plasmid and transformed in a cuvette by electroporation (2 kV) or by applying a heat shock (42 °C, 30 s). Immediately after electroporation, 900 μL of SOB medium were added. The transformed cells were incubated at 37 °C for at least 3 h and then streaked on an LB-agarose plate containing Ampicillin, Kanamycin, Tetracyclin and Gentamycin at the concentrations described above. Additionally, these plates contained IPTG (40 $\mu\text{g}/\text{mL}$) and BlueGal (100 $\mu\text{g}/\text{mL}$) to enable a blue-white screening. In this screening, positive clones (containing the insert) appear white while negative clones (not containing the insert) appear blue.

2.2.6 Sequencing

Plasmids identified to contain the desired insert after ligation or purified from *E. coli* after mutagenesis, were analysed by Sanger sequencing. Sequencing was carried out by external services (GATC/Bonn; AGRF/Melbourne). Sequencing

samples were prepared according to the requirements of the respective sequencing service supplier. Sequencing results were analysed using ApE and Serial Cloner (2-6-1) software.

2.2.7 Preparation of amplified plasmids from *E. coli*

To amplify ligated plasmids or plasmids that had the correct sequence insert or mutation, 100 ng of the according plasmid DNA were transformed into *E. coli* as described in 2.2.5. From the transformation plates a single colony was picked with a pipette tip, which was then dropped into LB media containing the appropriate antibiotics. For a large-scale plasmid purification (Maxiprep), 300 mL of LB were used. Plasmids intended for use in human cell lines were always purified by Maxiprep to ensure the removal of endotoxins. The GeneJET Plasmid Maxiprep Kit (Thermo Fisher Scientific) was used and the Maxiprep performed following the instructions given in the manual. For a small-scale purification (Miniprep), 4 mL of LB were inoculated with a single colony of transformed bacteria as described above. The purification was carried out with the ExtractMe Miniprep Kit (Blirt) or the Promega™ Wizard™ PlusSV Minipreps DNA Purification System (Promega) according to the manufacturer's protocol. In both, Mini- and Maxipreps, nuclease-free water was used instead of the provided elution buffer to elute the purified DNA from the columns. The concentration of the eluted DNA was determined by measuring the absorbance at 260 nm using a Nanodrop spectrophotometer. The 260/230 nm and 260/280 nm ratios were recorded to check for potential contaminants like proteins.

2.2.8 Isolation of baculovirus shuttle vector (Bacmid)

Bacmids are large shuttle vectors used to generate recombinant baculoviruses. Due to their size they cannot be purified using a Miniprep Kit, since the shearing forces caused by spinning the DNA onto DNA-binding columns could potentially damage the Bacmid.

From the blue-white screening plates (Chapter 2.2.5) a single white colony was picked with a pipette-tip and transferred to 4 mL LB media containing Ampicillin, Kanamycin, Gentamycin and Tetracycline at the concentrations previously described (2.2.5). The bacteria were grown at 37 °C for 48 h and harvested according to the protocol of the Miniprep Kit mentioned above. The protocol was followed up to the step where the lysate is clarified by centrifugation. The cleared lysate was then transferred to a fresh tube containing 800 µL of ice-cold isopropanol to precipitate the bacmid. Precipitated bacmids were spun down at maximum speed in a microcentrifuge at 4 °C for 30 min. After removing the supernatant, 800 µL of ice-cold 70 % ethanol were added to wash the bacmid pellet followed by another centrifugation step (4 °C, 15 min). The washing step with cold ethanol was repeated twice. Before removing the ethanol after the second wash, the tube was placed in a class 2 biosafety cabinet. After removing the ethanol, the lid of tube was left open to air-dry any residual ethanol for about 15 min. Afterwards, the bacmid was resuspended in 22 µL nuclease-free water and immediately used for transfection of *Sf9* or *Sf21* cells as described in Chapter 2.3.2.

2.3 Methods – Cell Biology

Work with cells (insect or human) was conducted within a class 2 biosafety cabinet. Materials used inside the biosafety cabinet were sterilized using 80 % ethanol before placing them in the biosafety cabinet. If cells were removed from the biosafety cabinet to transfer them to an incubator or for centrifugation, they were kept in a sealed, sterile container (e.g. cell culture flask, falcon tube).

2.3.1 *Sf9* and *Sf21* cell culture

Generally, *Sf9* cells (Bonn, Germany) were cultured in Sf-900™ SFM III (Invitrogen) in a shaking incubator at 27 °C. *Sf21* cells (Melbourne, Australia) were grown in Insect-XPRESS™ media (Lonza) under the same conditions. Culture growth and cell size was monitored every third day to ensure a cell density not exceeding 5×10^6 cells per mL. For cell counting and size measurements an automatic cell counter (EVE™ Automated Cell Counter, NanoEnTek) was used. Cells were mixed 1:1 with 0.4 % trypan blue to stain dead cells. 10 µL of the mix were applied to a counting slide. Viability and size of uninfected cells was typically between 90-99 % and between 11-13 µM, respectively. Infected cells increased in size to about 14-15 µM and had a viability of at least 80 %.

2.3.2 Transfection of *Sf9* and *Sf21* cells

Recombinant baculovirus is used as a vector for heterologous gene expression in *Sf9* and *Sf21* cells. For recombinant virus production, bacmids purified as described in Chapter 2.2.8 need to be transfected into the insect cells.

A culture of *Sf9* or *Sf21* cells was diluted to a cell density of 0.7×10^6 cells per mL and 2 mL of the suspension were transferred to each well of a 6 well cell culture plate. Cells were allowed to settle for 30 min at RT inside the biosafety cabinet. Purified bacmids were resuspended in nuclease-free water as described in 2.2.8. Additionally, 100 µL medium were added to each bacmid. In a different

tube, 8 μL of Cellfectin™ II Reagent (Thermo Fisher Scientific) and 100 μL of insect cell media were mixed. To achieve transfection of the insect cells by lipofection, the Cellfectin™ mix was added to the bacmids and incubated at RT for 15-30 min. Subsequently, 200 μL of the bacmids incubated with Cellfectin™ was added to the according well. As a negative control, only Cellfectin™ and medium were used. Cells were incubated with the transfection mix for 5 h at 27 °C. Afterwards, the supernatant was removed and 3 mL of fresh medium were added to each well following further incubation for 72 h at 27 °C. Transfection plates were kept in a humidified stationary incubator to prevent the cells from drying out. The produced virus (V_0) was harvested by collecting the supernatant. To ensure the supernatant was sterile and did not contain any residual insect cells or debris, it was passed through a 0.22 μm sterile filter. The filtered V_0 was used for further virus amplification and excess of virus was stored at 4 °C.

2.3.3 Virus amplification (V_1 and V_2)

For a large-scale culture used for recombinant protein expression in insect cells, a high titre virus stock is needed to efficiently infect a large number of cells. Therefore, the V_0 virus was expanded in two steps. First, a small culture (25-50 mL, 0.6×10^6 cells/mL) of *Sf9* or *Sf21* cells was infected with 3 mL of V_0 . Cell growth was monitored every day using a cell counter and the cell density was adjusted to 0.6×10^6 cells/mL until the cells stopped growing. Then the culture was collected in a 50 mL falcon tube and spun down at 45 x g for 20 min. The supernatant was filtered through a 0.22 μm sterile filter and the virus stock (V_1) was stored at 4 °C. For the second step of virus amplification, a culture of 100-250 mL at 1×10^6 cells/mL was infected with 1 % (v/v) of V_1 . As for the first virus amplification, cell growth was monitored every day and the cell density adjusted to 1×10^6 cells/mL until the cells stopped dividing. The culture was collected as described for V_1 and the resulting viral stock (V_2) stored at 4 °C until it was used to infect cultures for protein expression (Chapter 2.4.2).

2.3.4 Cell culture of human cell lines

HEK293T cells were cultured in complete Dulbecco's Modified Eagle's Medium (DMEM) containing 100 U/mL Penicillin and 0.1 % (w/v) Streptomycin (supplied by WEHI Media Kitchen, Melbourne) supplemented with 10 % foetal bovine serum (FBS). A continuous culture was monitored every second or third day. Cells were harvested and counted using a haemocytometer. To harvest the cells, all medium was taken off and the cells were washed once with 10 mL 1 x DPBS at RT. Then 5 mL of Trypsin/ethylenediaminetetraacetic acid (EDTA) were added to the cells, followed by 5 min of incubation at 37 °C. After adding 5 mL of DMEM the cells were resuspended and counted. A continuous culture was prepared at a 1:10 dilution.

Murine primary bone marrow was cultured in complete DMEM containing Penicillin and Streptomycin at the concentrations described above and supplemented with 10 % FBS. Macrophages were differentiated from murine bone marrow by supplementation with 10 % L292 conditioned media (L292 contains Macrophage Colony Stimulating Factor (M-CSF), WEHI Media Kitchen) for 6 days. Apart from that, isolation and differentiation of murine primary bone marrow was carried out as described previously (Gloria *et al.*, 2018). All cells were cultured at 37 °C and 10 % CO₂ in a stationary incubator.

2.3.5 Transfection of HEK293T cells

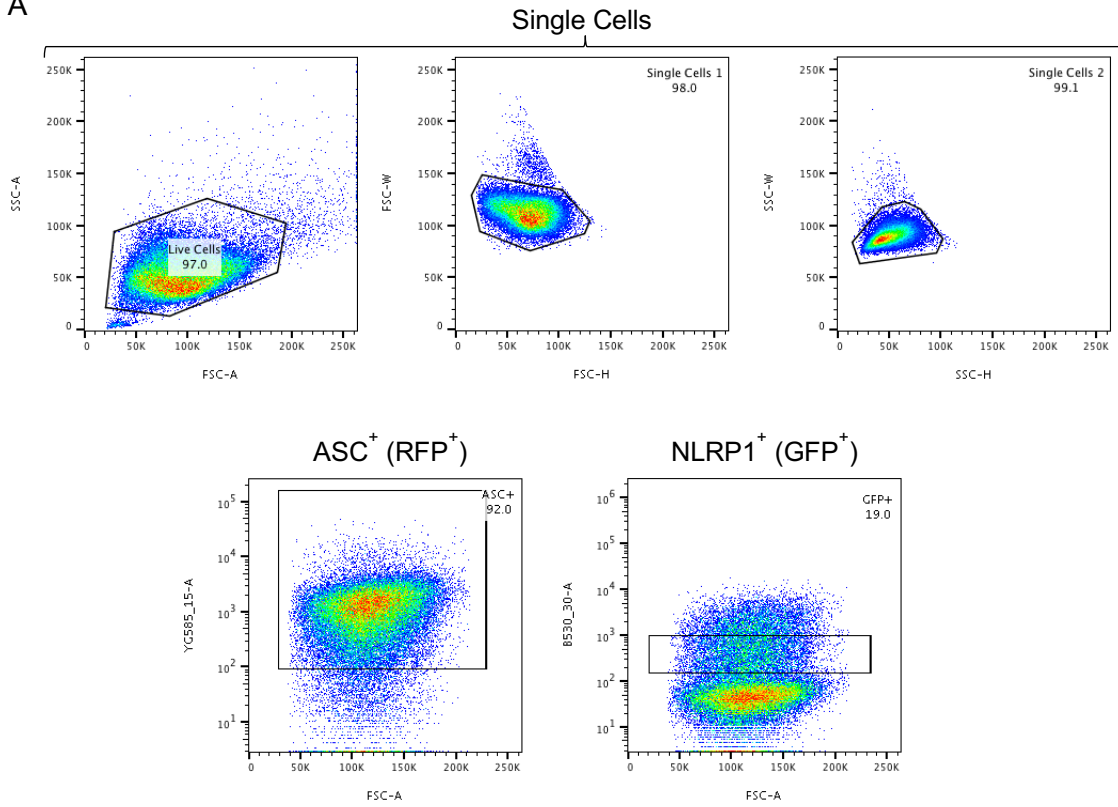
A culture of HEK293T cells was harvested and counted as described in Chapter 2.3.4. For an ASC speck (Chapter 2.3.6) assay, 0.5×10^6 cells per well were seeded in a 24 well plate. For immunoprecipitation and western blot experiments, 2.5×10^6 cells per well were seeded in a 6 well plate. Cells were incubated at 37 °C and 10 % CO₂ for 24 h before transfection. For the transfection, two separate tubes were prepared. In one tube an appropriate amount of OptiMEM was mixed with the required amount of DNA (50 ng/well for a 24 well plate, 2.5 µg/well for a 6-well plate). The other tube contained OptiMEM and the required amount of Lipofectamine transfection reagent (1 µL/well for a 24 well plate, 3.25 µL/well for

a 6-well plate). Both, the DNA and Lipofectamine solutions, were incubated separately for 5 min at RT and then mixed and incubated for another 25 min at RT. This transfection mix was added to each well of the according plate and incubated with the cells for 18 h at 37 °C and 10 % CO₂.

2.3.6 ASC speck formation assay

This assay was performed according to a technique described previously by Sester and colleagues (Sester *et al.*, 2015). It was used to quantitatively determine ASC speck formation, which can be used as a measure for inflammasome activation. HEK293T cells stably expressing an ASC protein fused to a red fluorescent protein (RFP) were transfected with either a plasmid encoding for human NLRP1 or a DNA control vector. The plasmid also encoded for a green fluorescent protein (GFP), which was expressed from an internal ribosomal entry site to enable gating for cells that are positive for NLRP1. The assay was performed in a 24 well plate and the transfection was carried out as described in Chapter 2.3.5. 50 ng of plasmid DNA were used per transfection per well. If the cells were to be treated with Talabostat, the medium was replaced with fresh medium containing 2 µM Talabostat or an equivalent amount of DMSO as a control, 18 h after transfection. After incubation for an additional 6 h (first time point) or 24 h (second time point) the cells were harvested for FACS analysis. To this end, the medium was removed from the cells and the cells washed once with 1 x DPBS. Afterwards 100 µL Trypsin/EDTA was added to each well of the plate and the cells were incubated for 5 min at 37 °C. After adding 100 µL of DMEM to each well, cells were resuspended and transferred to a round bottom 96 well plate and then centrifuged for 5 min at 400 x g. The supernatant was discarded and the cells resuspended in 100 µL FACS buffer. FACS measurements were carried out with a Fortessa X20 (BD) using a High Throughput System. 80 µL of each well were analysed at a flow rate of 3 µL/s. The gating strategy used for FACS analysis and a representative fluorescence microscopy image of HEK293T cells with and without specks is visualized in Figure 2.1.

A



B

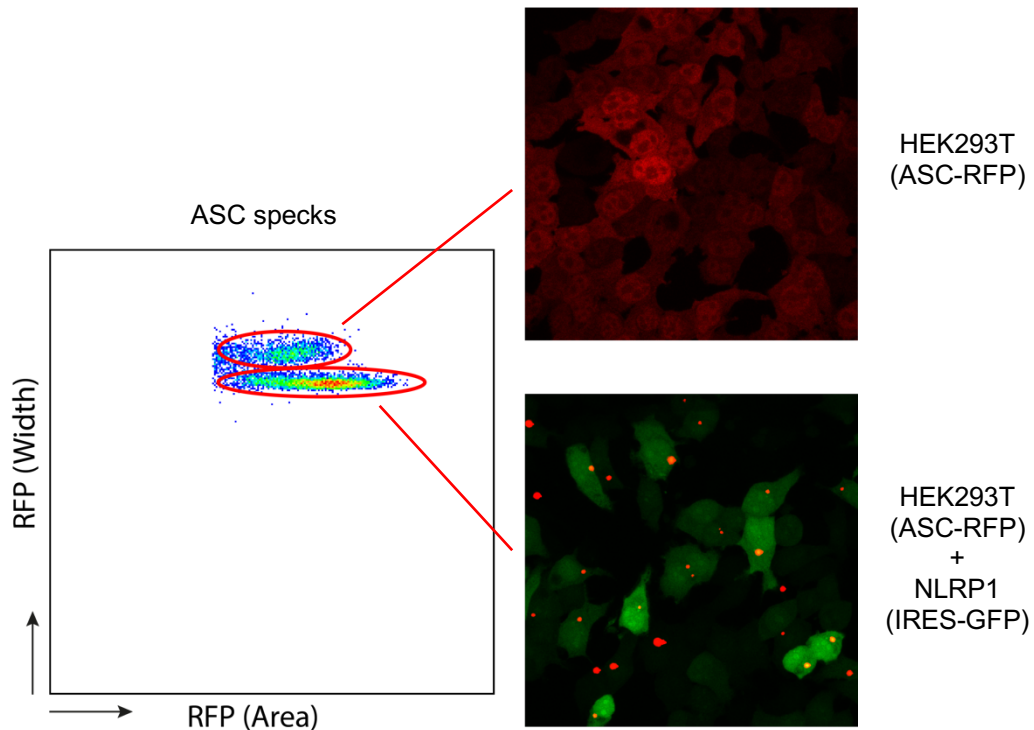


Figure 2.1: Gating strategy used in ASC speck assay

(A) Representative dot plots and gating strategy of an ASC speck assay. In the first three graphs, the gating for single cells is displayed. The last two graphs show the gating for ASC⁺ cells (i.e. RFP⁺) and the gating for NLRP1⁺ cells (i.e. GFP⁺). Note that the cells were gated for low expression levels of GFP to reduce the influence of background activation from NLRP1 activated by high levels overexpression. **(B)** Dot plot representing the gating strategy to distinguish cells containing ASC specks from cells not containing ASC specks. Included are representative images of untransfected cells not showing any specks and cells transfected with NLRP1 and subsequently activated and thus showing ASC specks. Fluorescence microscopy was performed in assistance with Dr. Dominic de Nardo (Abbreviations: SSC: Side Scatter; FSC: Forward Scatter; A: Area; H: Height; W: Width; YG585_15: Filter for RFP; B530_30: Filter for GFP).

2.3.7 Immunoprecipitation

For immunoprecipitation experiments, HEK293T cells were transfected with a plasmid encoding for NLRP1 or with an empty vector as a control. Immunoprecipitation was performed in a 6 well plate and the transfection carried out as described in Chapter 2.3.5. Cells were harvested 24 h after transfection by removing the media, washing the cells with 1 mL cold DPBS per well and adding 500 μ L of cold NP-40 lysis buffer (1 % NP40 (v/v), 10 % Glycerol (v/v), 20 mM Tris-HCl, 150 mM NaCl, 1 mM EGTA, 10 mM NaPPi, 5 mM NaF, 1 mM Na₃VO₄, 1 mM PMSF) supplemented with 1 x protease inhibitor cocktail. The cells were incubated in lysis buffer for 30 min on ice, transferred to a 1.5 mL Eppendorf tube and spun down in a microcentrifuge at 4 °C and maximum speed for 15 min. 60 μ L of the supernatant were added to a fresh tube containing 20 μ L 4 x SDS sample buffer (240 mM Tris pH 6.8, 8 % (w/v) SDS, 40 % (v/v) glycerol, 0.04 % (w/v) bromophenol blue, 5% (v/v) β -ME) serving as whole cell lysate control samples. The remaining supernatant was then added to 40 μ L of 50 % Anti-FLAG M2[®] beads, which were previously washed twice in NP-40 lysis buffer. After incubation o/n at 4 °C under rotation, the beads were spun down in a microcentrifuge at 4 °C and maximum speed for 20 s and the supernatant was removed using a vacuum pump. The beads were washed three times in lysis buffer, resuspended in 30 μ L SDS sample buffer and boiled at 96 °C for 5 min. Afterwards the samples were centrifuged at maximum speed for 5 min and immediately loaded onto a polyacrylamide gel or stored at -20 °C. In these experiments, 15 μ L of the immunoprecipitation samples and 30 μ L of the whole cell lysate samples were loaded onto a gel. SDS-PAGE and western blot analysis were performed as described in Chapter 2.4.9 and Chapter 2.4.10, respectively.

2.3.8 Enzyme-linked Immunosorbent Assay (ELISA)

Enzyme-linked Immunosorbent Assay (ELISA) was used to determine cytokine levels in supernatants of BMDM cultures. Culture supernatants were used neat or diluted 1 in 4 if required. A commercial ELISA kit was used to detect mouse or

human IL-1 β (R&D Systems). ELISA plates were washed 4 times with 1 x PBS supplemented with 0.05 % Tween 20 between the single steps and developed using a 3,3',5,5'-Tetramethylbenzidine (TMB) peroxidase substrate kit (VWR) and the reaction was stopped using 1 M H₂SO₄ (Thermo Fisher Scientific).

2.4 Methods – Protein biochemistry

2.4.1 Expression of recombinant protein in bacteria

For the expression of recombinant proteins in bacteria, *E. coli* BL21 (DE3) pLysS were used. After transformation of chemically competent *E. coli* BL21 with the plasmid containing the gene encoding the protein of interest, pre-cultures were grown in a shaking incubator o/n at 37 °C in 100 mL LB media supplemented with the appropriate antibiotics. Optical density of the pre-culture was determined the next day by measurement of the absorbance at 600 nm (OD_{600nm}). An amount of pre-culture was used to inoculate the expression culture to reach a final OD_{600nm} of 0.1. Expression cultures were grown at 37 °C and at a shaking frequency of 110 rpm in 5 L flasks with baffles. OD_{600nm} was determined every hour until the culture reached an optical density of 0.4-0.6. Protein expression was induced by adding isopropyl-β-D-thiogalactopyranoside (IPTG) at a final concentration of 0.3 mM and the cultures were incubated for another 4 h at 30 °C or o/n at 20 °C.

Cultures were harvested in 1 L buckets by centrifugation at 6229 x g at 4 °C for 20 min. The supernatant was discarded and the cell pellets were washed once in 1 x PBS and then transferred to 50 mL Falcon tubes. After another centrifugation step at 4501 x g and at 4 °C for 15 min, the cell pellets were either snap-frozen in liquid nitrogen and then stored at -20 °C or directly subjected to cell lysis and protein purification procedures.

2.4.2 Expression of recombinant protein in Sf9 or Sf21 cells

A culture of insect cells was diluted to a density of 1.5 x 10⁶ cells/mL and then 5 % (v/v) of V₂ were added. The infected insect cells were grown in Fernbach flasks (max. culture volume 750 mL) or in 5 L Erlenmeyer flasks (max. culture volume 1.5 L) at 27 °C. After 72 h the culture was checked for growth, vitality and average cell diameter using the EVE™ cell counter. If all of the parameters were as expected (decreased cell growth; viability > 80 %; average diameter > 13 μM) the culture was harvested at 1125 x g in 1 L buckets at 4 °C for 20 min. Afterwards,

the cell pellets were washed once in 1 x PBS, centrifuged again at 1125 x g at 4 °C for 20 min and then snap-frozen in liquid nitrogen and stored at -20 °C or subjected to lysis and subsequent protein purification procedures.

2.4.3 Cell lysis – Sonication

Both, bacterial and insect cells, were lysed by sonication. The pellets were resuspended in 3 mL lysis buffer per gram cell pellet using a magnetic stirrer. The lysis buffer was supplemented with fresh phenylmethylsulfonylfluorid (PMFS) to a final concentration of 1 mM. The completely resuspended cell-suspension was sonicated with an amplitude of 30 % on ice. Bacterial cells were sonicated on ice 4 x for 30 s with a break of 30 s between each sonication step. Insect cells were sonicated on ice 4 x for 15 s with a break of 15 s between each sonication step. Lysates were clarified by centrifugation in an Avanti J-26S XP centrifuge (Beckman Coulter) with a JA 25.50 rotor at 75481 x g at 4 °C for 30 min (bacterial lysates) or 1 h (insect cell lysates). Clarified lysates were further processed through a 0.45 µm filter to remove residual cell debris. Finally, the filtered lysates were used for affinity chromatography. For affinity chromatography performed according to the batch protocol, lysates were used unfiltered.

2.4.4 Protein purification – Affinity chromatography

Affinity chromatography is used to separate the protein of interest from contaminations like other proteins and nucleic acids present in the cell lysate. This is achieved by expressing the protein of interest as a fusion with an affinity tag. The tags used in this project include a Histidine₆ tag (His₆-tag), a glutathione S-transferase tag (GST-tag) and a maltose binding protein tag (MBP-tag). The affinity tags can specifically bind to ligands immobilized on a stationary phase, contaminants can be washed away and subsequently the protein of interest can be eluted from the stationary phase. The separation was carried out using either His-Trap FF, GSTrap FF or MBPTrap HP columns (GE Healthcare) attached to an FPLC (Äkta prime plus, GE Healthcare) or in a “batch” procedure using

Amylose Resin (New England Biolabs, for MBP-tagged proteins) or cComplete His-Tag Purification Resin (Roche). All purification steps were carried out on ice or at 4 °C.

FPLCs were run at a flow rate of 1 mL/min when applying the lysate to the column. To reduce the amount of non-specifically bound protein, columns were washed with at least 10 column volumes (CV) of buffer. Afterwards another washing step was carried out with 5 CV lysis buffer to reduce the salt concentration. In purifications with His-tagged proteins only one wash step with at least 10 CV lysis buffer was carried out. All washing steps were carried out using a flow rate of 3 mL/min. Finally, the specifically bound protein was eluted at a flow rate of 1 mL/min using a buffer containing 250 mM Imidazole, 30 mM reduced glutathione, or 10 mM maltose for His₆-tagged, GST-tagged or MBP-tagged proteins, respectively. Eluate was collected by an automated fractionator.

For the batch protocol, clarified lysates were incubated with the according resin in 50 mL falcon tubes for at least 2 h at 4 °C under constant rotation. Washing steps were carried out similar to the FPLC protocol with the resin incubating in 10 x resin volume of wash buffer for 10 min. The washing procedure was repeated three times. Elution was carried out by incubating the resin with 1 x resin volume elution buffer for 30 min at 4 °C. Elution procedure was repeated three times. In between wash and elution steps the beads were collected by centrifugation at 405 x g. During all purification steps the flow-through and wash fractions were collected and analysed by SDS-PAGE.

2.4.5 Concentration of protein samples

Protein samples were concentrated using Amicon Ultra Centrifugal Filter Units (Merck Millipore). In this application protein solution is filtered through an Ultracel[®] regenerated cellulose membrane. Proteins of larger size than the pore size of the membrane are retained, while the buffer and proteins of smaller size than the pore size pass through the membrane. Thereby, a concentration of the purified protein can be achieved. Filtration was carried out by centrifugation at 4 °C until the desired volume or protein concentration was reached.

2.4.6 Determination of protein sample concentration

A Nanodrop spectrophotometer was used to determine the protein concentration by measuring absorbance at 280 nm. Absorption at 260 nm was measured to monitor potential nucleic acid contaminations. The protein concentration was calculated according to the Beer–Lambert law, using the molecular weight and specific absorption coefficient determined with the ExPASy ProtParam tool (<https://web.expasy.org/protparam>).

2.4.7 Tobacco Etch Virus (TEV) protease digestion

For most constructs, the affinity-tag was fused N-terminally to the protein of interest and a TEV-protease cleavage site (amino acid sequence: ENLYVQGS) was inserted between the protein of interest and the affinity tag. The cleavage site was inserted to enable specific removal of the tag by proteolytic cleavage after affinity chromatography. To cleave off the affinity tag, TEV protease was added to the concentrated fusion protein at a ratio of 1/100 (mg TEV/mg protein). The protein was incubated with TEV at 4 °C o/n. Afterwards, size exclusion chromatography was performed to separate the TEV protease from the protein of interest. If the TEV protease was too similar in size to be separated by size exclusion chromatography, an additional affinity step was carried out to remove His₆-tagged TEV protease. TEV protease was produced at the laboratory in Bonn (Germany).

2.4.8 Protein purification – Size exclusion chromatography (SEC)

In SEC, proteins are separated by size by applying them to a column containing a porous matrix with various pore sizes. Larger proteins elute earlier as they cannot enter smaller pores and therefore take less time to pass through the column. The opposite is the case for small proteins. Different columns were used for proteins of different molecular weight. A Superdex75, a Superdex200 or a

Superose6 (GE Healthcare) connected to an FPLC (Äkta Primer or Äkta Pure, GE Healthcare) were used in this work. After equilibrating the column in at least one CV of the according SEC buffer, protein samples were applied by injecting them into a loop connected to the FLPC. The flow-through was collected by an automated fractionator in fraction volumes of 0.5-2 mL. Small samples of each fraction were taken to be analysed by SDS PAGE. Fractions containing the protein of interest were pooled and concentrated as described in Chapter 2.4.5 and then used for further analysis or snap-frozen in liquid nitrogen and stored at -80 °C.

For the calculation of molecular weight estimates from analytical SEC elution profiles, the following formula was applied to calculate the K_{av} value:

$$\frac{V_e - V_0}{V_c - V_0} = K_{av}$$

Here, V_e , V_c and V_0 denote the elution volume of the analyte, the volume of the entire column and the void volume of the column, respectively. K_{av} is the partition coefficient and can be described as the proportion of pores available to the analyte. Since there is a linear relationship between the K_{av} of a molecule and the logarithm of its molecular weight, a calibration curve can be generated by running a molecular weight standard. This makes it possible to calculate an estimate of the molecular weight from the elution volume of a protein. Proteins of molecular weight standards eluting outside the separation range of a column were excluded from the calibration curve.

2.4.9 Sodium dodecyl sulphate polyacrylamide gel electrophoresis (SDS-PAGE)

Monitoring of protein purity and molecular weight was carried out by analysing chromatography fractions and concentrated protein samples by SDS-PAGE and subsequent Coomassie-staining. In SDS-PAGE the proteins are denatured by diluting them in Laemmli sample buffer containing sodium dodecyl sulphate

(SDS) and boiling the samples at 96 °C for 5-10 min. The SDS is negatively charged and therefore masks the charge of the protein itself. Because proteins are denatured and negatively charged, they are separated only according to their relative molecular weight when run on a polyacrylamide gel. Gels that were run to be stained with Coomassie were poured using the BioRad miniPROTEAN system. Different percentages of acrylamide (12-20 %) were used in separation gels to ensure sufficient protein separation. Electrophoresis was performed at a constant current of 30 mA in the BioRad miniPROTEAN system. Coomassie-staining was performed by incubating gels in 0.1 % (w/v) Coomassie R250 diluted in 40 % (v/v) ethanol and 10 % (v/v) acetic acid for 1 h. Afterwards, gels were destained in 10 % (v/v) ethanol and 5 % (v/v) acetic acid 2-3 times for 1 h or o/n. Commercial 4-12 % gradient gels with a thickness of 1.5 mm (NuPAGE® Novex™, Thermo Fisher Scientific) were used if the samples were further analysed by western blotting. Gradient gels were run at a constant voltage of 120 V. Protein transfer and western blot analysis are described in detail in Chapter 2.4.10. Commercial Novex™ SimplyBlue SafeStain solution (Thermo Fisher Scientific) was used for staining and Milli-Q® water was used for destaining of SDS gels run for mass spectrometric analysis of proteins.

2.4.10 Western blot

For analysis by western blot, protein samples were first separated according to their size by SDS-PAGE as described in Chapter 2.4.9. Afterwards the protein was transferred from the gel onto a Polyvinylidenfluoride (PVDF) membrane. For the transfer, the gel was placed on two layers of filter paper and a sponge previously soaked in 1 x western transfer buffer. The PVDF membrane was activated in 100 % methanol before it was positioned directly on the gel and covered with two more layers of soaked filter paper and a sponge. The transfer was carried out at a constant voltage of 100 V at 4 °C for 90 min. Subsequently, the membrane was stained with Ponceau S solution to confirm the successful transfer of proteins. Then the membranes were destained in PBS supplemented with 1 % Tween 20 (PBS-T) and blocked for 1 h at RT in 5 % skim milk in PBS-

T. The membranes were incubated with primary antibody o/n at 4 °C. Primary antibody incubation was followed by 3 washing steps in PBS-T for 10 min each and incubation with secondary antibody conjugated to horseradish peroxidase (HRP) at RT for 1 h. After incubation with secondary antibody the membranes were washed 3 times for 30 min in PBS-T. The membranes were then incubated with a solution containing substrate for HRP and directly exposed. Images were taken using a ChemiDoc™ Touch Imaging System (Bio-Rad). Antibodies: α NLRP1: AL176 (AdipoGen); α FLAG: 9H1 (WEHI protein facility); α Actin: β -Actin.

2.4.11 Mass spectrometry

To confirm the identity of recombinant proteins, several samples were analysed by peptide mass fingerprint. In this mass spectrometry approach, proteins are first digested using a protease (e.g. trypsin) and the resulting peptides are purified and applied to mass spectrometry. The peptide masses can then be compared to a database of peptides to identify the proteins that were subjected to enzymatic digestion.

Protein that was intended to be analysed by mass spectrometry was separated by SDS-PAGE as described in Chapter 2.4.9 and then stained with SimplyBlue SafeStain (Thermo Fisher Scientific). Bands of interest were excised from the gel and transferred to a clean 1.5 mL polypropylene tube. Gel pieces were centrifuged to the bottom of the tube and then destained for 15 min at 37 °C while shaking in 100 μ L of a 50 mM ammonium bicarbonate and 50 % acetonitrile solution. Destaining solution was removed by vacuum and the destaining step repeated until the gel pieces appeared clear. After removing the destaining solution 100 μ L of 100 % acetonitrile were added, followed by 15 min incubation at RT. Proteins were then reduced in 10 mM dithiothreitol in 100 mM ammonium bicarbonate for 30 min at 37 °C while shaking. Excess DTT was removed using vacuum suction. Subsequently, proteins were alkylated in 100 μ L of 55 mM iodoacetamide in 100 mM ammonium bicarbonate for 30 min at 37 °C (protected from light). Then the alkylation solution was removed, the gel slices washed twice

in destaining solution and dehydrated in 100 μ L of 100 % acetonitrile for 15 min. After removing the acetonitrile, the gel slices were air dried and then rehydrated in 40 μ L of trypsin solution (15 ng/ μ L) for 45 min on ice. When the slices were completely rehydrated, the trypsin solution was removed, the gel pieces covered in 40 μ L of 25 mM ammonium bicarbonate and the samples wrapped in parafilm and incubated o/n at 37 °C. The next day samples were centrifuged before adding 60 μ L of extraction buffer (0.1 % formic acid in 60 % acetonitrile) to each tube. Samples were incubated for 30 min at RT with extraction buffer and the extracted peptides then transferred to a labelled microvial. The extraction procedure was repeated once. Samples were acidified by adding formic acid to a final concentration of 1 % (v/v). Prior to analysis samples were lyophilized to dryness and stored at -80 °C. Samples were reconstituted in 20 μ L of 0.1 % formic acid and 2 % acetonitrile before measurements. Mass spectrometry samples were run and analysed by Dr. Jarred Sandow at the proteomics facility of the Walter and Eliza Hall Institute (Melbourne, Australia).

2.4.12 Small-angle X-Ray scattering (SAXS)

Protein of the second peak (Chapter 3.3.5 and 3.3.6) of a full length MBP-NLRP1 (WT) purification was pooled and concentrated to the indicated concentrations. 100 μ L of protein sample was loaded onto a Superose 6 increase (5/150) column. The SEC run was performed at a flow rate of 0.4 mL/min. The column was connected to the SAXS capillary, ensuring that the protein enters the capillary directly after eluting from the SEC column. SAXS measurement was carried out at the Australian Synchrotron in Melbourne in assistance with Prof. James Murphy from the Walter and Eliza Hall Institute.

2.4.13 Reversed-Phase High-Performance Liquid Chromatography (RP-HPLC) based hydrolysis assay

High-performance liquid chromatography (HPLC) is a technique used in analytical chemistry to separate, identify and quantify different chemicals

contained in a mixture. In Reversed-Phase (RP) applications of HPLC the stationary phase of the chromatography column is inverted compared to Normal-Phase chromatography, as it is hydrophobic. This gave rise to the name Reversed-Phase Chromatography. RP-HPLC poses a highly sensitive technique to separate analytes. Adding ion pair reagent to the HPLC buffer, further allows the separation of partly ionized analytes. The nucleotides ATP, ADP and AMP all carry negative charges (ATP: 4⁻, ADP: 3⁻, AMP: 2⁻) at neutral pH and only differ slightly in size. Using ion pair RP-HPLC the three nucleotides can be separated. By determination of the area of the elution peaks in the according chromatogram, a quantification of the nucleotides is possible. With these properties ion pair RP-HPLC is a suitable and highly sensitive technique to measure and characterise ATP hydrolysis reactions and was therefore used to determine the hydrolysis activity of MBP-NLRP1.

Nucleotides were separated using a Chromolith Performance RP-18 100-4.6 HPLC column and the corresponding guard cartridge Chromolith RP-18 (Merck, Darmstadt, Germany). The measurement was performed using an Agilent 1260 infinity PSS bio-inert HPLC System (Agilent Technologies, Inc., Santa Clara, USA). The mobile phase was composed of 10 mM TBA-Br, 30 mM K₂HPO₄, 70 mM KH₂PO₄, 0.2 mM sodium-azide, and 4 % acetonitrile. The pH of the mobile phase was adjusted to 6.5 and afterwards it was filtered through a 0.22 µm filter. Acetonitrile was added after adjusting the pH and filtering the mobile phase to avoid foaming during the filtration step. Reactions were set up to contain 3 µM MBP-NLRP1 Peak 1 protein and 100 µM ATP (or a different nucleotide as indicated) in a 10 x buffer containing 20 mM HEPES (pH 8.0), 150 mM sodium chloride and 5 mM MgCl₂. Nucleotides were added last and reactions were placed in the autosampler of the HPLC immediately after addition of the nucleotides. Reactions were incubated and run at 25 °C and at a flow rate of 1 mL/min. A sample was taken by the autosampler at the start of the measurement and every 10 minutes afterwards. Nucleotide elution was monitored at 254 nm and protein elution was monitored at 280 nm. Peaks were manually identified and automatically integrated. The sum of the peak integrals of one measurement was

normalized to 100 % to allow quantification and comparison of the nucleotide content in the reaction.

3. Biochemical and structural characterisation of recombinant NLRP1

3.1 Introduction

Seven isoforms of human NLRP1 are reported in the UniProt database (Accession Code: Q9C000). Isoform 1 of the human NLRP1 protein consists of 1473 amino acids and has a theoretical molecular weight (MW) of 165.86 kDa. As other members of the NLRP protein family it harbours an N-terminal PYD (pyrin domain) and a central NACHT domain (found in NAIP, CIITA, HET-E and TEP1) followed by a domain composed of leucine rich repeats (LRR). Additionally, NLRP1 contains a FIIND (domain with “function to find”) located C-terminal in respect to the LRR and a CARD (caspase activation and recruitment domain) on the very C-terminus. This unique feature makes NLRP1 stand out in the family of NLRP inflammasome proteins. Furthermore, with about 240 amino acids in length the linker region connecting the PYD and NACHT domain is by far the longest compared to that of other NLRPs. For instance, in the NLRP3 protein this linker region is comprised only of about 130 amino acids.

Both, the PYD and the CARD domain, belong to the superfamily of death domains (DD), typically adapting a six helix bundle fold (Park, Lo, *et al.*, 2007). Their 3D structures have been determined by solution NMR and X-ray crystallography, respectively (Hiller *et al.*, 2003; Jin *et al.*, 2013). Interestingly, the NMR structure of the NLRP1 PYD revealed a lack of alpha helix 3 ($\alpha 3$) and instead a flexible, unstructured loop between $\alpha 2$ and $\alpha 4$. Recent findings showed that for NLRP1 the PYD has an autoinhibitory function (Zhong *et al.*, 2016). This is different compared to other NLRP proteins like NLRP3, where the PYD is directly involved in the activation of Caspase-1 by binding the adaptor protein apoptosis-associated speck-like protein containing a CARD (ASC) (Vajjhala *et al.*, 2012). Furthermore, NMR studies of the PYD showed that a destabilization of the hydrophobic core by introducing point mutations results in autoactivation of the NLRP1 inflammasome (Zhong *et al.*, 2016). The lack of $\alpha 3$ might explain

the difference in function of the NLRP1 PYD compared to other NLRP proteins. However, this aspect has never been investigated in depth.

The NLRP1 CARD structure (PDB: 3KAT) presents as a typical six helix bundle fold. Since NLRP1 harbours a CARD domain, it was hypothesized that it could interact directly with Caspase-1 CARD. Electrostatic surface charge analysis of the NLRP1 CARD crystal structure and a Caspase-1 CARD homology model unveiled complementary charged surfaces, which could promote an interaction between the two domains (Jin *et al.*, 2013). Indeed, it has been shown that under some conditions mouse NLRP1 variants can activate Caspase-1 independent of ASC (Masters *et al.*, 2012; Van Opdenbosch *et al.*, 2014). However, different functional studies have also shown that the CARD of NLRP1 can engage with the adaptor protein ASC to form a functional inflammasome (Faustin *et al.*, 2007; Zhong *et al.*, 2016).

In addition, the NLRP1 LRR structure has been determined by X-ray crystallography, showing six consecutive repeats with an N-terminal capping helix and an additional C-terminal β -sheet (Reubold *et al.*, 2014). Furthermore, a molecular envelope was calculated from SAXS data recorded for a construct spanning the NACHT and LRR domains. When fitting the closed (inhibited) and open (active) conformation of reported NLRC4 NACHT-LRR structures into this envelope, the open conformation was found to produce the better fit (Martino *et al.*, 2016). Functionally, it was shown that the protein is constitutively active when the LRR is missing, indicating an autoinhibitory function of this domain (Chavarría-Smith *et al.*, 2016).

Using a bioinformatics approach it was found that the FIIND domain has high structural similarity to a ZU5 (initially found in ZO-1 and UNC5) and UPA (conserved in UNC5, PIDD and Ankyrins) domain tandem (D'Osualdo *et al.*, 2011). However, to date there is no high resolution structural information available for the NLRP1 FIIND domain.

NLRPs are described to adopt a closed conformation in an autoinhibited state and undergo conformational changes to an open conformation when activated. After transition to the open, active state NLRPs assemble into oligomers. The N-terminal part of NLRP1 has a similar modular domain architecture as other

NLRPs and would therefore be expected to adapt a similar oligomeric conformation. As mentioned above, NLRP1 has two additional domains (FIIND and CARD) compared to other NLRP proteins. Therefore, it is likely that its overall oligomeric fold is extended compared to other NLRP oligomers. The only structural information available on full-length NLRP1 is a negative stain electron microscopy (EM) study on recombinant protein purified from Sf9 cells. The EM analysis showed a mix of monomers and oligomers, where most oligomers presented as pentamers or heptamers (Faustin *et al.*, 2007).

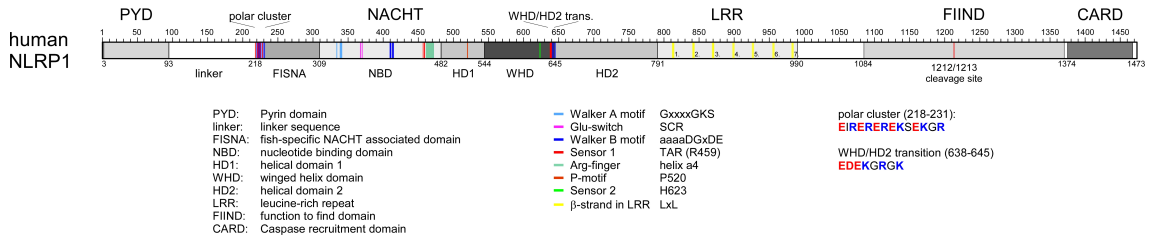
Further structural information on the NLRP1 protein is of great interest to gain a better understanding of the molecular mechanisms underlying regulation and activation of this inflammasome.

3.2 Results

3.2.1 Sequence based analysis of NLRP1 domain architecture

Improving the understanding of the molecular basis of NLRP1 inflammasome regulation and activation by gaining structural information was approached in two different ways. The gene encoding full-length human NLRP1 was cloned into a vector as an N-terminal maltose binding protein (MBP) fusion (full-length approach). Apart from that several constructs of separate domains of NLRP1 were designed (domain-based approach). Analysis of the primary amino acid sequence of the canonical isoform 1 of human NLRP1 was performed, to get an understanding of its domain architecture. This is crucial to determine boundaries for constructs for recombinant protein expression. For a thorough analysis, a combination of sequence alignments with the known structures described in Chapter 3.1 and sequence analysis tools were applied. A detailed analysis of the primary sequence of the NLRP1 protein revealed several subdomains and conserved motifs and repeats. This analysis further allowed determination of domain boundaries, which are depicted in Figure 3.1A. For the PYD (1-93), NACHT-LRR (230-990), LRR (791-990) and CARD (1372-1467) domain containing constructs, the boundaries were mainly determined based on alignments with the sequence of the according published structures. Since there was no structure available for the FIIND domain, an alignment with a similar domain that has been structurally determined was performed. The protein Unc5b harbours a ZU5-UPA tandem as well, of which the structure has been determined by X-ray crystallography (PDB: 3G5B). Based on an alignment of the NLRP1 FIIND with the ZU5-UPA sequence of Unc5b (Figure 3.1B) and considering the boundaries of the flanking domains, the FIIND domain containing construct was determined to span residues 1084-1376. A biochemical characterization and in-depth structural analysis of selected constructs including the full-length NLRP1 protein will be described in the following chapters.

A



B

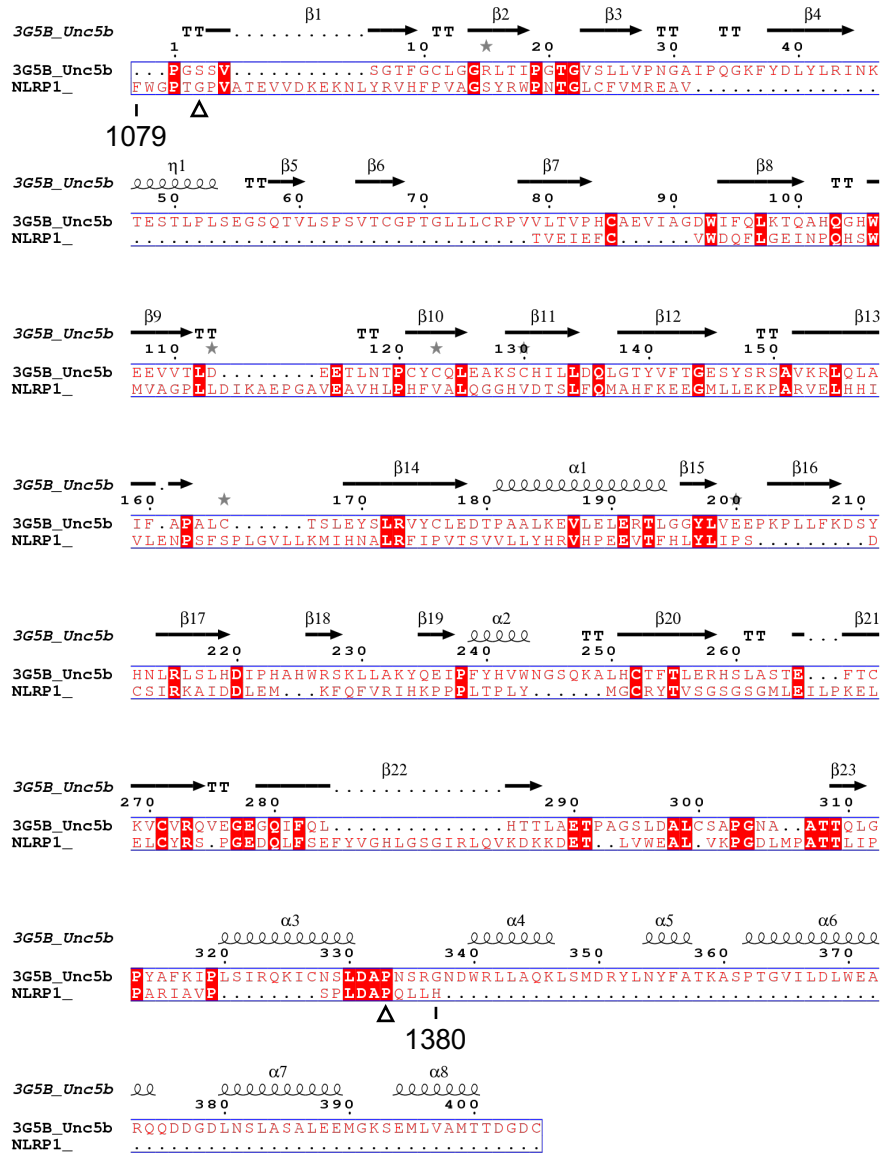


Figure 3.1: Domain and construct boundaries determined for NLRP1

(A) Schematic diagram of the modular domain architecture of human NLRP1. Numbers indicate amino acid number according to the primary amino acid sequence. Numbers below the schematic represent domain boundaries determined from the primary amino acid sequence and used for the design of constructs for recombinant protein expression. Subdomains are depicted below the bar diagram. Conserved motifs and sequence elements are highlighted in different colours. **(B)** Sequence alignment of the sequence of the UNC5b cytoplasmic domain (taken from PDB: 3G5B) with NLRP1-FIIND domain (amino acid 1079-1380). Alignment: Clustal Omega (Madeira *et al.*, 2019); Secondary structure assignment: ESPrit 3.0 (Robert and Gouet, 2014); Explanation of symbols: squiggles: helix, arrows: β -sheet, TT: β -turn, black empty arrows indicate domain boundaries chosen for FIIND domain construct.

3.2.2 Purification and characterization of NLRP1 PYD

NLRP1-PYD was expressed in *E. coli* BL21 cells as an N-terminal GST-fusion protein (Figure 3.2A). It was purified to homogeneity as shown by analytical SEC and SDS-PAGE analysis (Figure 3.2B and C). Analytical SEC after removing the GST-tag by TEV cleavage showed that the PYD behaves as a monomer in solution. NLRP1 PYD elutes as a single peak with an apparent MW of 15.96 kDa as determined from the SEC elution profile. This is slightly higher than the calculated molecular weight of 10.37 kDa, based on the amino acid sequence. In SDS-PAGE analysis the PYD runs at the expected molecular weight below the 14.4 kDa band of the marker.

The structure of NLRP1 PYD has been determined previously by NMR spectroscopy (PDB: 1PN5) (Hiller *et al.*, 2003). A computational structure function analysis was carried out, aiming to understand the difference in function between NLRP1 PYD and other PYDs in the NLRP protein family. In the NMR study the lack of $\alpha 3$ was already identified. This is a major difference to other PYDs. A sequence alignment with the NLRP3 PYD showed that NLRP1 has a proline (P45) residue in the centre of the region where $\alpha 3$ would be expected to form (Figure 3.2D). Proline residues are known to disrupt α -helices (Li *et al.*, 2005). Alignment of the sequence of the first 120 amino acids (containing the PYD) of all NLRP proteins revealed that only NLRP1 harbours a proline in this position (Appendix, Figure A1). Thus, the presence of a proline residue in this position could prevent $\alpha 3$ formation in NLRP1 PYD. However, a comparison of the structure of NLRP1 and NLRP3 PYD showed that a lack of $\alpha 3$ in NLRP1 does not disrupt the overall fold (Figure 3.2E). In fact, it is comparable to NLRP3 PYD with some helices ($\alpha 4$, $\alpha 5$, $\alpha 6$) showing slightly different orientations. So far it is not clear, whether the lack of $\alpha 3$ is the reason for NLRP1 PYD being autoinhibitory rather than the effector domain and binding ASC like NLRP3 PYD. To further assess this, the surfaces of NLRP3 PYD required for its interaction with ASC PYD were investigated regarding conservation in NLRP1 PYD. In an NMR study two main interfaces were identified to facilitate the interaction of NLRP3 and ASC PYD (Oroz *et al.*, 2016). The according residues identified in these

interfaces are highlighted in Figure 3.2D. Interface 1 is mainly formed by $\alpha 1$ and $\alpha 2$. Residues Y12, E14 and L21 are identical to NLRP3 in regards to their relative positions. Residues E20 and E52 are charge conserved between NLRP3 and NLRP1. Interface 2 is located mainly in $\alpha 5$ and residues G62 and W67 are identical with NLRP3 PYD. L71 is hydrophobic in interface 2 of NLRP3 PYD and H92 is charge conserved between the two PYDs. For NLRP3, none of the residues directly involved in the interaction with ASC are located within $\alpha 3$. Thus, the structural difference of NLRP1 PYD compared to NLRP3 PYD does not directly indicate the difference in their function. Nevertheless, the $\alpha 3$ helix has been described to play an essential role in self-association and the formation of filaments for both ASC and NLRP3 PYD (Oroz *et al.*, 2016). As such an important mediator of homotypic interactions between PYDs, $\alpha 3$ might still affect interactions of heterotypic interactions of PYDs of different proteins by allowing homotypic interactions.

Figure 3.2: Biochemical and computational characterization of NLRP1 PYD

(A) Schematic representation of the GST-PYD expression construct. **(B)** Analytical SEC of NLRP1 PYD (TEV cleaved). The protein sample was run on a Superdex 75 (3.2/300) column at a flow rate of 0.04 mL/min. **(C)** Coomassie-stained SDS-PAGE of TEV-cleaved, purified NLRP1 PYD. 4 μ g of the protein sample were run on a 20 % acrylamide gel. **(D)** Sequence alignment of NLRP3 and NLRP1 PYD sequences. The position of Proline 45 of NLRP1 PYD located within the region where α 3 would be expected is highlighted in blue. Alignment: Multalin Tool (Corpet, 1988); Secondary structure assignment: ESPrit 3.0 (Robert and Gouet, 2014); Explanation of symbols: squiggles: helix, filled arrows: residues identified for interface 1 required for ASC interaction of NLRP3 PYD, empty arrows: residues identified for interface 2 required for ASC interaction of NLRP3 PYD. **(E)** Structures of NLRP3 PYD (PDB: 2NAQ) and NLRP1 PYD (PDB: 1PN5). Secondary structure elements are shown in cartoon representation. Proline 45 of NLRP1 PYD is shown in stick representation. Images were generated with PyMOL.

3.2.3 Purification and characterization of NLRP1 LRR

The construct for recombinant protein expression of the NLRP1 LRR domain was designed as an N-terminal GST-fusion protein as shown in Figure 3.3A. It was expressed in *E. coli* BL21 cells and purity and homogeneity of the final TEV cleaved protein product were analysed by analytical SEC and SDS-PAGE. On the Coomassie-stained SDS-gel only minor impurities can be observed. NLRP1 LRR, with a calculated molecular weight of 22.61 kDa, runs at the expected height just below the 25 kDa band of the marker (Figure 3.3B). In analytical SEC the TEV cleaved LRR elutes as a single peak species with an elution volume corresponding to an apparent molecular weight of 55 kDa (Figure 3.3C). Interestingly, this is more than twice as much as calculated for monomeric NLRP1 LRR (22.61 kDa) from the amino acid sequence. This suggests that the LRR might form a dimer in solution. To further analyse the LRR, the protein was crystallized (Figure 3.3D) and the structure of the LRR determined to a resolution of 2.1 Å (Protein crystallization, X-ray diffraction measurement, density calculation and model building was performed by Dr. Kanchan Anand). The structure of one asymmetric unit is visualized in Figure 3.3E. Since there were two molecules per asymmetric unit and analysis by analytical SEC indicated a dimer, the structure was analysed for a potential interface that facilitates an interaction between LRR molecules. Only one potential interaction site was found located near the C-terminus of one molecule and the N-terminus of the other molecule within the asymmetric unit. Residues that are in close proximity at this site are shown in stick representation in Figure 3.3E. Distance measurements in PyMOL reveal that these residues are close enough to interact by ionic interactions or to form hydrogen bonds. However, no obvious complementary charges, hydrogen bond donors or acceptors or hydrophobic patches between the residues of the two molecules can be observed. Therefore, the dimer formation of the purified LRR is more likely to be an artefact of the purification or crystallization procedure and might not be of physiological relevance.

The previously published structure of NLRP1 LRR was crystallized with one molecule per asymmetric unit (Reubold *et al.*, 2014). An overlay of the structure

solved in this work and the published structure is shown in Figure 3.3F. Both structures display six consecutive repeats with an N-terminal capping helix and a C-terminal β -sheet. On the outside of both structures the α -helices form a convex surface and on the inside the β -sheets form a concave surface. The structures are well fitted with all α -helices and β -sheets adapting very similar orientations. The root-mean-square deviation (RMSD) calculated by PyMol was 0.622, further indicating a good fit of the two structures.

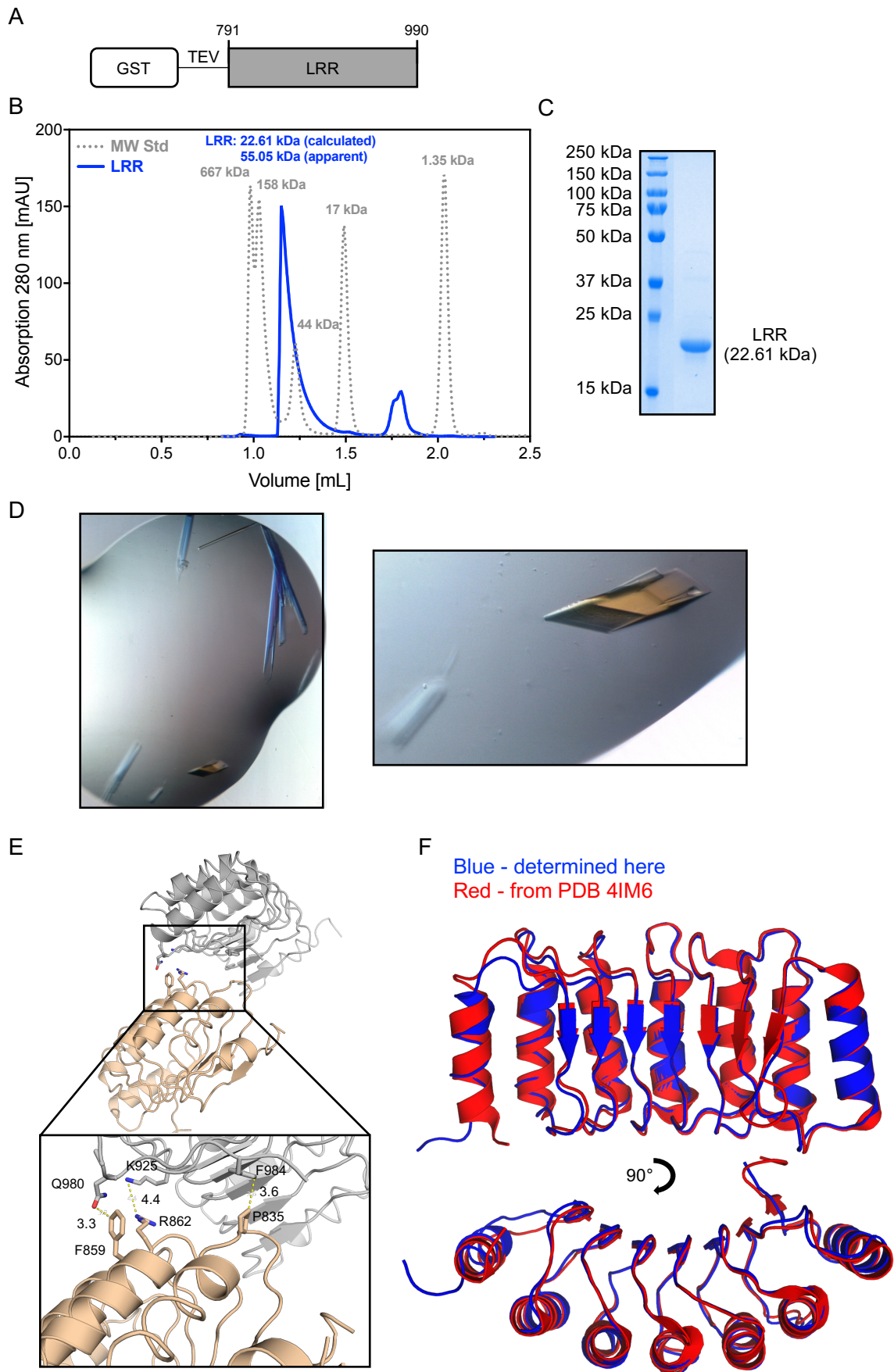


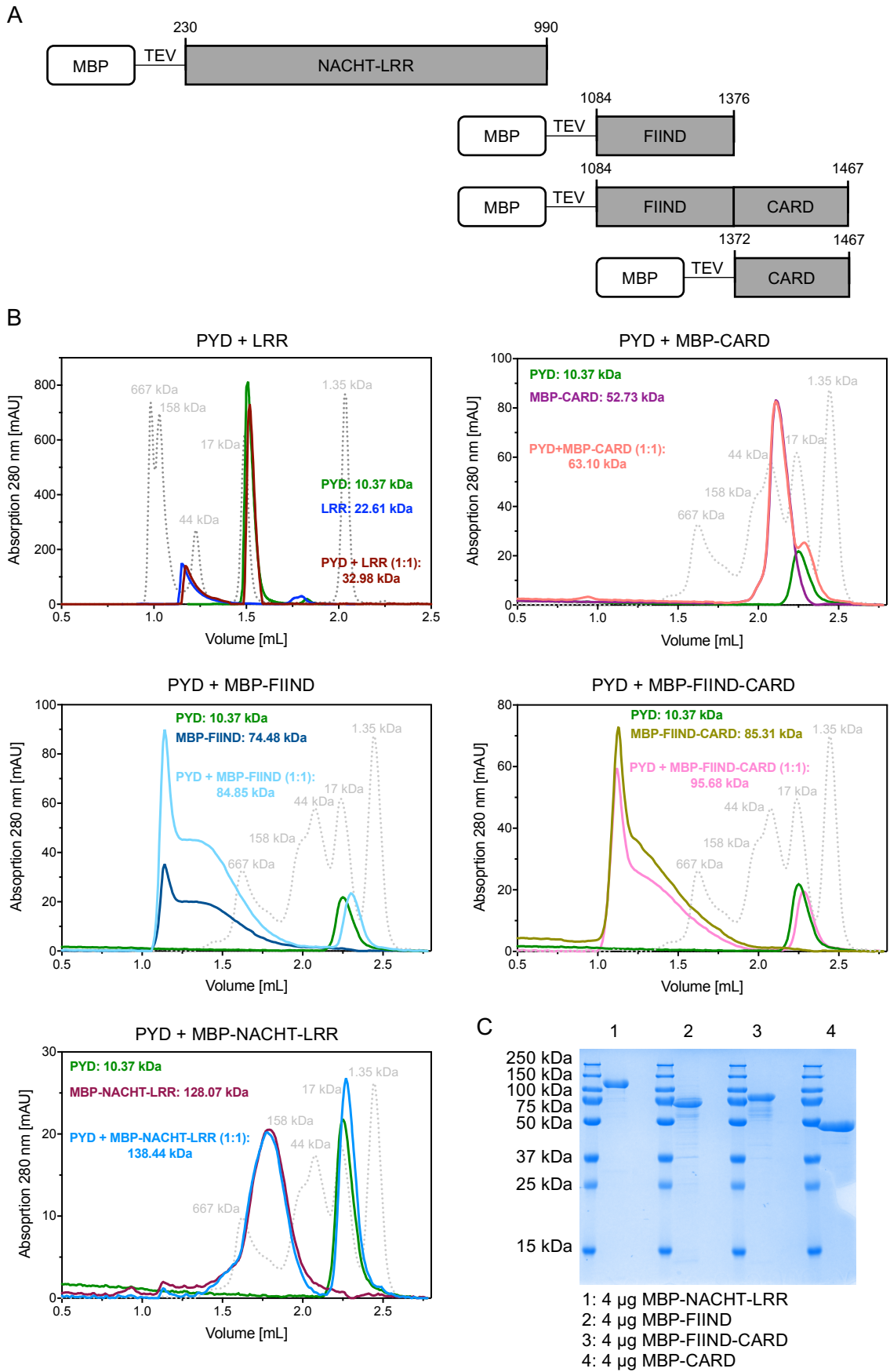
Figure 3.3: Biochemical characterization and crystal structure determination of NLRP1 LRR

(A) Schematic representation of the GST-LRR expression construct. **(B)** Analytical SEC of NLRP1 LRR (TEV cleaved). The protein sample was run on a Superdex 75 (3.2/300) column at a flow rate of 0.04 mL/min. **(C)** Coomassie-stained SDS-PAGE of purified NLRP1 PYD (TEV cleaved). 4 μ g of the protein sample were run on a 15 % acrylamide gel. **(D)** Images of crystals of TEV cleaved NLRP1 LRR protein. **(E)** Crystal structure of NLRP1 LRR with two molecules (molecule one: grey, molecule two: wheat) in the asymmetric unit. Residues potentially involved in an interaction between LRR molecules are shown in stick representation and labelled with the respective one-letter code and number in the NLRP1 amino acid sequence. Numbers between residues depict distances (in \AA) measured between atoms connected by dashed yellow line. **(F)** Overlay of the NLRP1 LRR structure determined in this work (blue) with the structure previously published for NLRP1 LRR (red, PDB: 4IM6) revealed an RMSD of 0.622. Images and distance measurements in E and F were generated with PyMOL.

3.2.4 Analysis of potential intramolecular interactions in NLRP1

Since the domain architecture as well as the function of the PYD of NLRP1 differs from that of other members of the NLRP protein family, its overall conformation is likely to be different as well. NLRP1 PYD might fold back onto another domain, thereby keeping the protein in an autoinhibited conformation. To investigate if intramolecular interactions are involved in keeping the protein in an autoinhibited conformation, analytical SEC of different constructs spanning one or multiple domains of NLRP1 was performed. The constructs for NLRP1 PYD and LRR were the same as described in Chapters 3.2.2 and 3.2.3. Constructs spanning the NACHT-LRR domain as well as the FIIND, CARD or both the FIIND and CARD domains were designed as N-terminal MBP-fusion proteins (Figure 3.4A). All of the MBP-tagged constructs were purified to high purity and homogeneity as shown by SDS-PAGE analysis (Figure 3.4C) and used without the tag being cleaved off. Cleavage of the MBP led to aggregation and precipitation of the proteins, making them unusable for further experiments.

In Figure 3.4B, analytical SEC elution profiles of the interaction studies are displayed. In analytical SEC runs, the MBP-CARD construct behaved as a monomer, eluting as a single peak at a volume corresponding to a molecular weight of 35.65 kDa. This is significantly lower than the expected molecular weight of 52.73 kDa, indicating that the MBP-CARD protein is tightly packed. Both constructs harbouring the FIIND domain eluted as a tailing peak in the void volume of the column. This indicates either a high degree of oligomerization or aggregation of the protein. The molecular weight of these constructs was therefore not determined. The MBP-NACHT-LRR construct eluted as a single peak at a volume corresponding to a molecular weight of 239.64 kDa. This is almost twice as much as the molecular weight calculated for the monomeric MBP-NACHT-LRR construct of 126.68 kDa, indicating the possibility of dimer formation.



Results

Figure 3.4: Interaction studies of NLRP1 PYD with other domains of NLRP1

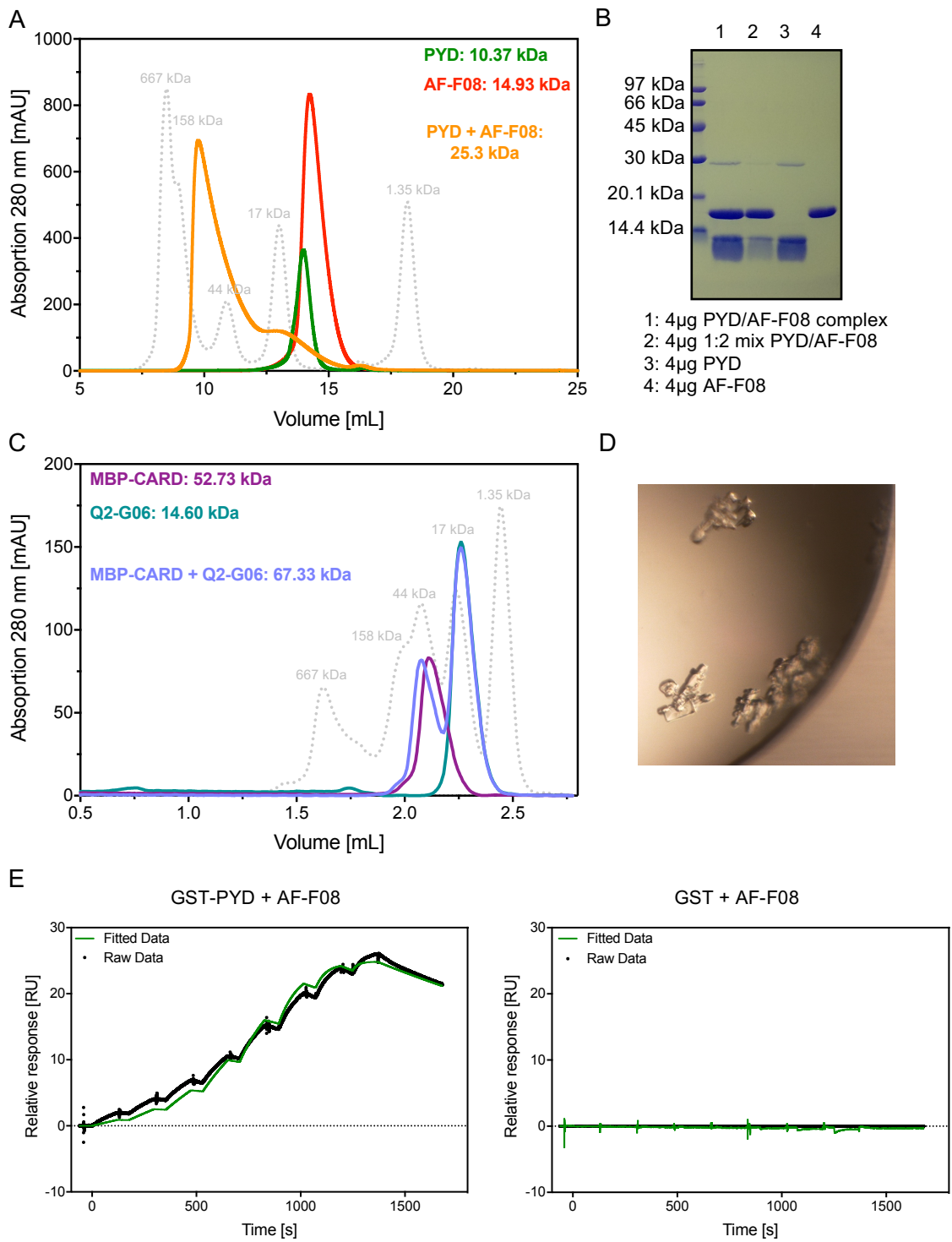
(A) Schematic representation of the expression constructs for the FIIND, FIIND-CARD and NACHT-LRR domains used in interaction studies. **(B)** Analytical SEC of NLRP1 PYD with other domains of NLRP1. Proteins were mixed in a 1:1 molar ratio at a concentration of 10 μ M in a total volume of 50 μ L. The protein mix was incubated at RT for 30 min before loading into a 20 μ L loop connected to an ÄKTA micro device. The PYD and LRR samples were run on a Superdex 75 (3.2/300) column. The PYD and MBP-NACHT-LRR, MBP-FIIND, MBP-FIIND-CARD and MBP-CARD samples were run on a Superose 6 (3.2/300) column. All SEC samples were run at a flow rate of 0.04 mL/min. Peaks of the molecular weight standard are 667 kDa, 158 kDa, 44 kDa, 17 kDa and 1.35 kDa (left to right). **(C)** Coomassie-stained SDS-PAGE of purified MBP-NACHT-LRR, MBP-FIIND, MBP-FIIND-CARD and MBP-CARD. 4 μ g of the protein samples were run on a 15 % acrylamide gel.

Whether NLRP1 PYD interacts intramolecularly with any of the other domains of NLRP1 was investigated by mixing TEV-cleaved NLRP1 PYD in a 1:1 molar ratio with one of the other domains. The protein mixture was incubated at RT for 30 min before applying the sample to a SEC column. If the PYD would interact with any of the other domains, a new peak species eluting at a higher molecular weight than the peaks of the domains by themselves would be expected to appear in the according elution profile. However, no peaks corresponding to a complex formed between the PYD and another domain was found in these experiments (Figure 3.4B). These results indicate that the NLRP1 PYD does not strongly interact with any of these domains under the experimental conditions tested. Nevertheless, this does not exclude the possibility of intramolecular interactions in the context of the full-length protein.

As a positive control for the analytical SEC experiments, nanobodies specific for the NLRP1 PYD and CARD domain were applied (expression plasmids for nanobodies provided by Dr. Florian I. Schmidt). Nanobodies were purified to homogeneity as shown by SDS-PAGE and preparative (AF-F08, PYD specific nanobody) or analytical (Q2-G06, CARD-specific nanobody) SEC (Figure 3.5A, B and C). Both nanobodies elute as a single peak species with an apparent molecular weight of 9.42 kDa (AF-F08) and 14.67 kDa (Q2-G06). This is close to their calculated molecular weight of 14.61 kDa and 14.67 kDa, respectively. Interaction of the nanobodies with the respective interacting domain was first analysed by analytical SEC. For NLRP1 PYD and the according nanobody AF-F08, complex formation is clearly visible in the SEC elution profile. A mixture of the two proteins (1:1 molar ratio), which was incubated at RT for 30 min, elutes as a higher molecular weight complex compared to the run of the PYD or the nanobody separately (Figure 3.5A). Samples of a preparative SEC run of the PYD/AF-F08 complex were analysed by SDS-PAGE, showing a 1:1 ratio of the two proteins. A sample containing 1:1 protein complex of PYD/AF-F08 was subjected to crystallization trials (carried out by Dr. Kanchan Anand). The complex grew into rod-shaped crystals (Figure 3.5D). However, when exposed to X-rays these crystals did not diffract. Binding of AF-F08 to NLRP1 PYD was further characterized by SPR (SPR measurement carried out by Dr. Karl

Gatterdam). The nanobody showed good binding to the immobilized GST-PYD in the SPR experiment and the k_D was determined to 52.8 nM.

Elution profiles recorded for the nanobody specific for NLRP1 CARD did not indicate complex formation, since no new peak species could be observed (Figure 3.5C). This implies that in solution, the surface of NLRP1 CARD required for the interaction with the nanobody might be blocked by the MBP-tag. Therefore, results obtained for the investigation of intramolecular interactions with MBP-fusion proteins have to be interpreted with care.



Results

Figure 3.5: Interaction studies with NLRP1-specific nanobodies

(A) Analytical SEC of NLRP1 PYD with a PYD specific nanobody (AF-F08). Nanobody and PYD were run separately and as a complex. For complex formation, proteins were mixed in a 1:2 molar ratio (PYD:nanobody) and incubated at RT for 30 min. All samples were run on a Superdex 75 (10/300 GL) column at a flow rate of 0.4 mL/min. **(B)** SDS-PAGE of PYD/AF-F08 complex after SEC (1), a 1:2 mix before SEC (2) and PYD (3) and AF-F08 (4) separately. Samples were run on a 20 % acrylamide gel. **(C)** Analytical SEC of NLRP1 CARD fused to MBP with a CARD specific nanobody (Q2-G06). Nanobody and Q2-G06 were run separately and as a complex. For complex formation, proteins were mixed in a 1:1 molar ratio (MBP-CARD:nanobody) and incubated at RT for 30 min. All samples were run on a Superose 6 (3.2/300) column at a flow rate of 0.04 mL/min. **(D)** Crystals of the PYD/AF-F08 protein complex. **(E)** SPR measurement of GST-PYD (ligand) and AF-F08 (analyte) as well as of a GST only control. Concentrations: GST-PYD (25 nM); AF-F08 (32, 64, 128, 256, 512, 1024, 2048, 4096 nM).

3.2.5 Recombinant full-length MBP-NLRP1 forms oligomers

Structural information of full-length NLRP1 is required for a more detailed structure-function analysis. A high resolution structure could reveal intramolecular interactions and potential interaction interfaces. This information could further be used to map mutations involved in autoimmune disorders associated with NLRP1 and thus unveil the functional consequences that these mutations might have. Therefore, full-length human NLRP1 was expressed as an N-terminal MBP-fusion protein (Figure 3.6A) in baculo virus infected Sf9 and Sf21 insect cells. The protein was processed to high purity, as shown by SDS-PAGE analysis in Figure 3.6B. In preparative SEC experiments the protein eluted as a single peak in the void volume of the chromatography column (Figure 3.6B). The peak showed a significant tail, running near the void volume. Since the main peak was eluting outside the separation range of the column, no molecular weight estimate could be determined by SEC for MBP-NLRP1. Elution in the void volume corresponds to a higher molecular weight than the column is able to separate. In the case of MBP-NLRP1 this means it elutes much bigger than its monomeric molecular weight of 207 kDa. This indicates that the protein is forming higher order oligomers or protein aggregates.

To investigate this further, samples of the main peak as well as the tail were taken for analysis by negative stain electron microscopy (images recorded by Dr. Heide Behrmann). For the main peak, many large protein particles of different size were observed, showing that the majority of the protein in this sample is comprised of inhomogeneous oligomers and aggregates (Figure 3.6C). Protein samples taken from the tail of the peak looked more homogeneous. Therefore, isolating this part of the protein sample was intended to be achieved by modifying the purification protocol.

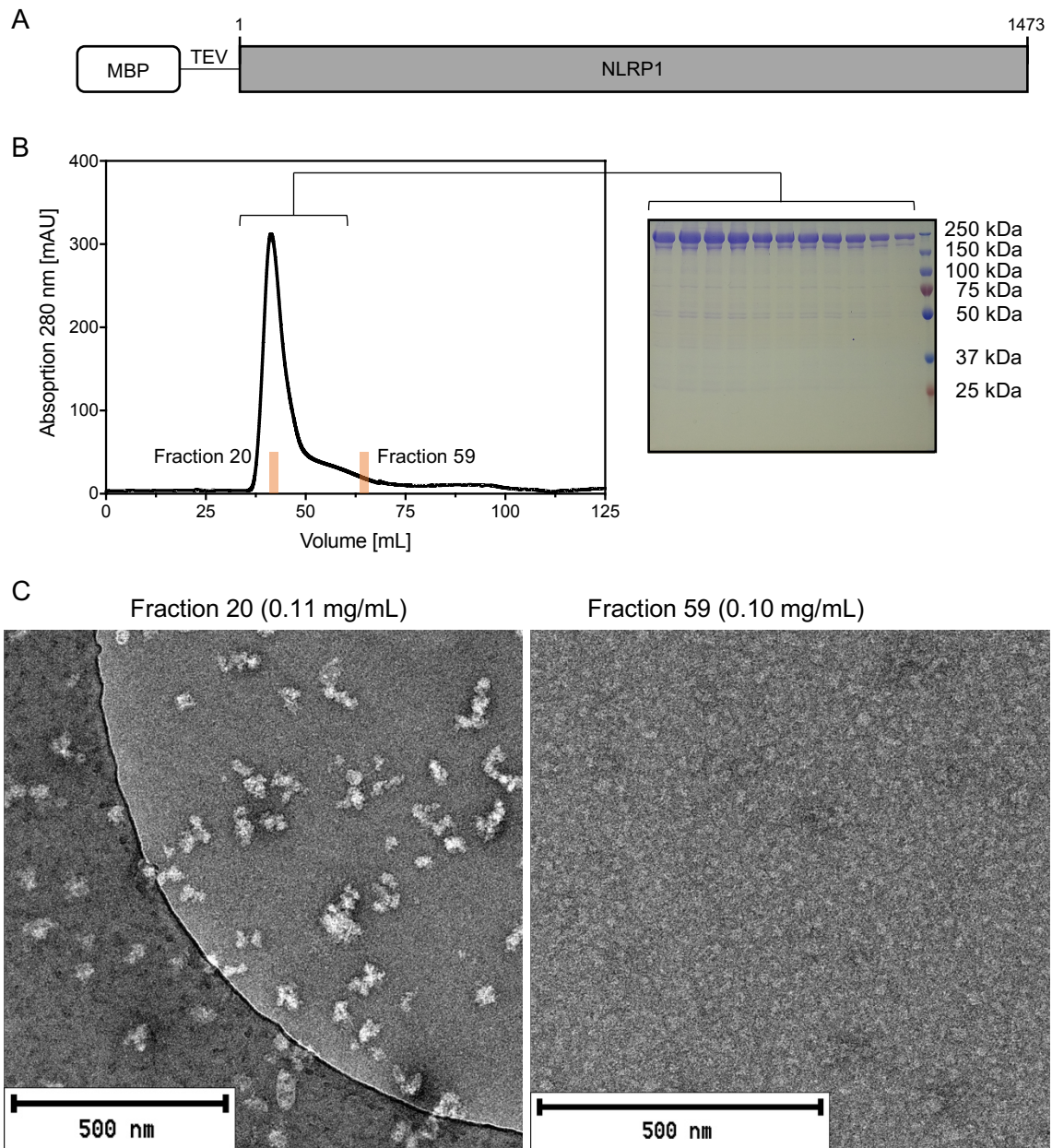


Figure 3.6: Purification and negative stain EM of MBP-NLRP1

(A) Schematic of the MBP-NLRP1 construct. **(B)** Representative elution profile of a preparative SEC and SDS-PAGE analysis of MBP-NLRP1. MBP-NLRP1 was run on a Superose 6 (16/600) column at a flow rate of 0.2 mL/min. 10 μ L of the eluting fractions were taken as samples for SDS-PAGE. The displayed Coomassie-stained gel covers the range of the peaks as marked by the black bracket. SDS samples were run on a 12 % acrylamide gel. **(C)** Negative stain electron microscopy of MBP-NLRP1. Samples were taken directly from fractions 20 and 59 as highlighted in the chromatogram. Fraction 20 was diluted in SEC buffer to a concentration of 0.11 mg/mL. Fraction 59 had a concentration of 0.10 mg/mL and was applied to an EM grid without further processing.

One approach to single out the homogeneous protein and prevent uncontrolled oligomer formation, is to add specific nanobodies that could potentially block interaction interfaces involved in oligomerization. The two nanobodies described in 3.3.5 are appropriate candidates to test in this context. However, in analytical SEC experiments, addition of either of the nanobodies did not result in a significant change in the elution behaviour of MBP-NLRP1 (Figure 3.7A). The main peak of the MBP-NLRP1 protein was slightly shifted towards a higher elution volume. Nevertheless, no new peak species could be observed when the nanobodies were added to MBP-NLRP1 in a 1:1 molar ratio. Thus, an accumulation of the homogeneous protein sample was not achieved.

In addition to utilizing the nanobodies to separate the homogeneous protein from the inhomogeneous protein, alternative purification protocols were developed. One major change in the protocol was the usage of amylose resin following a gravity flow protocol instead of MBPTrap columns connected to an ÄKTA FPLC device. This change in the affinity chromatography step seemed to improve the elution behaviour of MBP-NLRP1. The more gentle batch method changed the elution behaviour of the protein, resulting in two distinct peaks and an accumulation of the homogenous part of the protein sample (Figure 3.7B). SDS-PAGE analysis of the different peaks showed that both, the first and the second peak, contained mainly MBP-NLRP1 (Figure 3.7B). A third peak species visible in the elution profile was shown to contain mainly contaminations or degradation products by SDS-PAGE (Figure 3.7B, SDS-PAGE not shown). Protein of the second peak was further analysed by mass spectrometry. Identity of the protein in the top two bands (Figure 3.7B) was confirmed to contain MBP-NLRP1. Interestingly, the band observed just above the 25 kDa band of the marker, was shown to contain the C-terminal cleavage fragment of NLRP1 (Appendix, Figure A2). Thus, the protein sample is comprised of a mixture of full-length MBP-NLRP1 and MBP-NLRP1 that was autolytically cleaved within the FIIND domain. However, the cleaved protein makes up only a minor portion of the sample. The full-length proteins probably comprises more than 90 % of the protein present in the sample, as estimated from SDS-PAGE analysis.

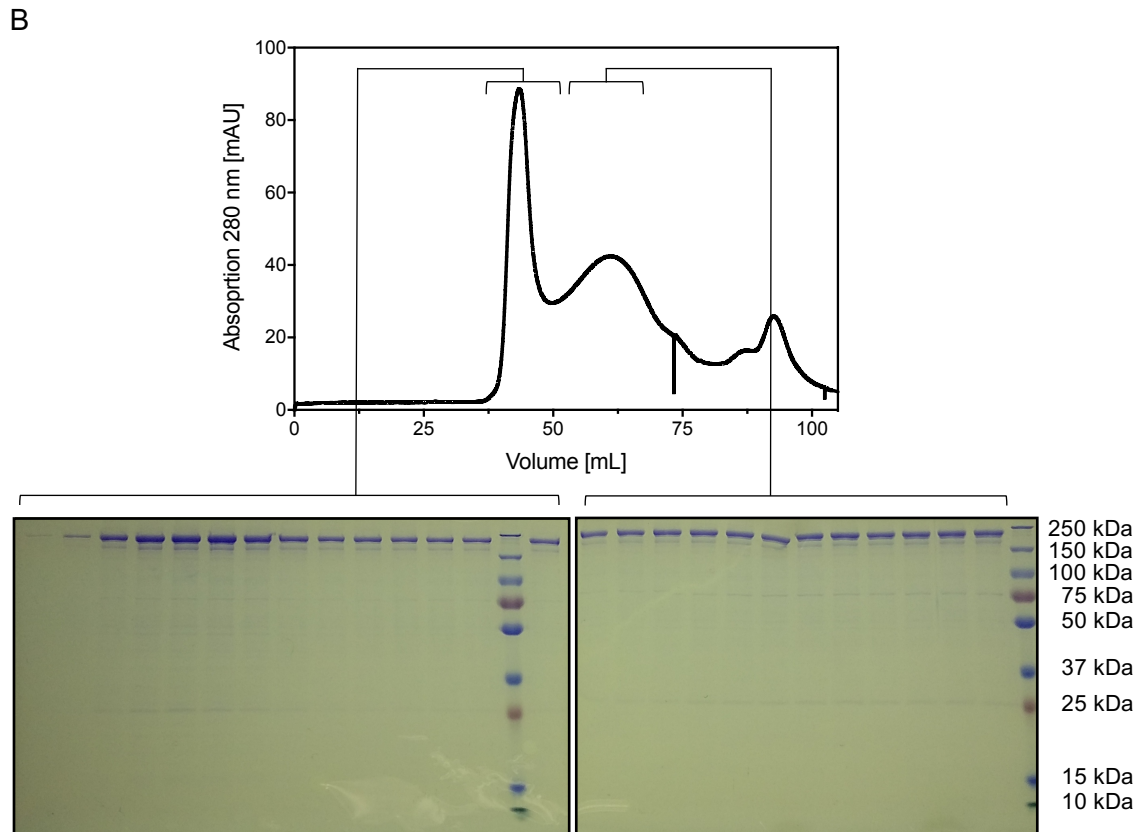
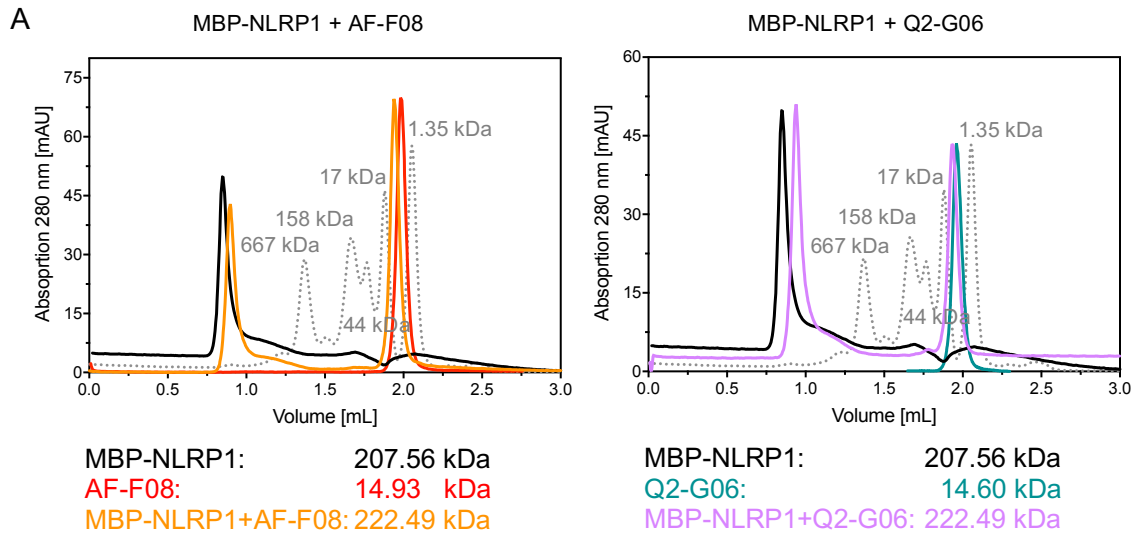


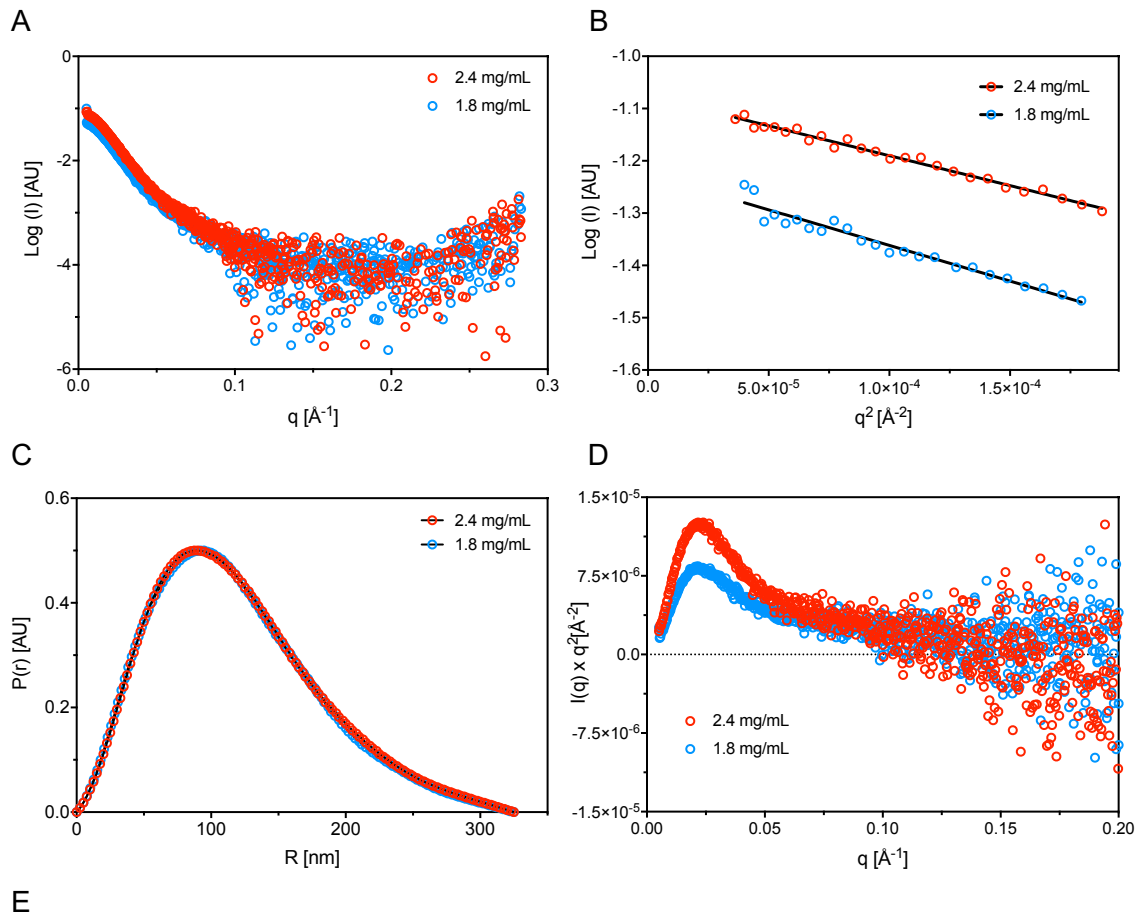
Figure 3.7: Modification of MBP-NLRP1 purification protocol leads to improved elution behaviour

(A) Analytical SEC of MBP-NLRP1 with a PYD-specific (AF-F08) and a CARD-specific (Q2-G06) nanobody. Samples were run on a Superose 6 (3.2/300) column at a flow rate of 0.02 mL/min. Proteins were mixed in a 1:1 molar ratio and incubated at RT for 30 min before loading the samples into a 20 μ L loop connected to an ÄKTA micro. **(B)** Elution profile of a preparative SEC and SDS-PAGE of MBP-NLRP1 purified following the modified purification protocol. MBP-NLRP1 was run on a Superose 6 (16/600) column at a flow rate of 0.2 mL/min. 10 μ L of the eluting fractions were taken as samples for SDS-PAGE. The displayed Coomassie-stained gel covers every second fraction within the range of the peaks as marked by the black bracket. Fractions had a volume of 0.5 mL. SDS samples were run on a 12 % acrylamide gel.

The MBP-NLRP1 peak 2 protein elutes at a volume significantly smaller than the peak corresponding to a molecular weight of 667 kDa of a molecular weight standard provided by the manufacturer of the column. This implies that MBP-NLRP1 peak 2 protein forms an oligomer, as the SEC elution profile indicates a molecular weight significantly higher than the monomeric molecular weight of MBP-NLRP1 (207 kDa). Noteworthy, the second peak containing the homogeneous protein spans a wide range of the column. This might indicate that there are different assemblies of the oligomer present in this peak. The homogeneous sample was isolated by pooling the main fractions of the second peak and the protein was concentrated for further structural analysis.

3.2.6 SEC-SAXS analysis suggests MBP-NLRP1 assembles into a hexamer

Since full-length NLRP1 was unstable without the MBP-tag and only soluble at concentrations up to 3 mg/mL, protein crystallization for the generation of structural information was not feasible. To investigate the overall shape and oligomeric state of the protein we sought to analyse the second peak of MBP-NLRP1 by size exclusion chromatography coupled Small Angle X-ray Scattering (SEC-SAXS). SEC-SAXS data was collected for two samples of MBP-NLRP1 concentrated to 2.4 mg/mL and 1.8 mg/mL before loading the sample on the SEC column. A detailed analysis of recorded data is reported in Figure 3.8. The scattering data was indicative of a well behaved protein and was therefore further analysed for structural parameters (Figure 3.8A). Radius of gyration (R_g) values determined from Guinier analysis were 90.74 Å and 91.89 Å for the sample at 2.4 mg/mL and 1.8 mg/mL, respectively (Figure 3.8B and E). The distance distribution revealed similar values for R_g with 94.46 Å and 93.62 Å (Figure 3.8C and E). The maximum dimension of the particle (D_{max}) derived from the distance distribution function was 325 Å for both samples. Kratky analysis indicated that the sample is comprised of folded protein and has only minor flexible regions (Figure 3.8D).



Concentration	2.4 mg/ml	1.8 mg/ml
R_g (Guinier) [\AA]	90.74 ± 3.04	91.89 ± 5.93
R_g (P(r)) [\AA]	94.46 ± 0.09	93.62 ± 0.06
D_{max} [\AA]	325	325
Porod volume [\AA^3]	2050000	2010000
Molecular mass monomer [kDa]	207	207
Molecular mass ($V_{\text{Porod}}/1.66$) [kDa]	1234.9	1210.8
Molecular mass (SAXSMoW2) [kDa]	1284.3	1269.8
Oligomeric state	6	6

Figure 3.8: SEC-SAXS analysis of MBP-NLRP1 Peak 2 reveals an oligomeric state of the protein particle

(A) Scattering data recorded for samples at two different concentrations (2.4 mg/mL and 1.8 mg/mL) of MBP-NLRP1. **(B)** Linear low- q regions used for the Guinier analysis of the scattering data shown in A. **(C)** Normalized pairwise distance distribution function ($P(r)$) derived from the scattering data shown in A. The distance distribution function revealed a maximum particle dimension of 315 Å. **(D)**: Kratky plot of the scattering data obtained from the two samples of MBP-NLRP1, showing a distinct peak and thus indicating low intrinsic flexibility of the protein particle. **(E)** Overview of the parameters derived from the scattering data recorded for the two concentrations of MBP-NLRP1 including a calculation of the oligomeric state of the protein particle.

Two different methods were used to calculate an estimate for the molecular weight of the protein. One approach was to utilize the approximate Porod volume and divide it by 1.66 (Petoukhov *et al.*, 2012). This approach resulted in a molecular weight of 1228.9 kDa and 1204.8 kDa for the 2.4 mg/mL and 1.8 mg/mL sample, respectively. As a second method for molecular weight estimation, the raw scattering data was submitted for automated analysis by the SAXSMoW2 online tool (<http://saxs.ifsc.usp.br/>) (Fischer *et al.*, 2010; Piiadov *et al.*, 2019). This gave a molecular weight of 1284.3 kDa and 1269.8 kDa for the 2.4 mg/mL and 1.8 mg/mL sample, respectively. Dividing the molecular weight determined from the SAXS data by the molecular weight of the monomeric MBP-NLRP1 resulted in a factor between 5.8 and 6.2. This indicated that one protein particle consists of about six monomers of MBP-NLRP1. Thus, the oligomeric state of the protein was determined to be hexameric.

The distance distribution function derived from the scattering data recorded for the 2.4 mg/mL sample was used to generate an *ab initio* bead model using the DAMMIF and DAMAVER tools of the ATSAS software. The bead model can be displayed as a molecular envelope and provide information about the overall shape of the protein particle. Such a molecular envelope for the MBP-NLRP1 oligomer is visualized in Figure 3.9A. The overall shape can be described as an elongated, disc-like assembly with a triangular geometry. Dimensions of the particle were determined to be 316 Å in width, 342 Å in height and 112 Å in depth using the UCSF Chimera software (Pettersen *et al.*, 2004).

In a next step, a structure of NLRP1 was fitted into the molecular envelope, to investigate the nature of the oligomer assembly. Since there is no structure of full-length NLRP1 or any other full-length NLR protein available, a model of MBP-NLRP1 was generated by submitting the entire amino acid sequence of 1851 amino acids to the RaptorX secondary structure prediction tool (Wang *et al.*, 2016). The resulting model is visualized in Figure 3.9B and the different domains as well as the MBP-tag are depicted separately. A large linker region between the PYD and NACHT domain spanning amino acids 472-614 (corresponding to amino acids 94-236, the PYD-NACHT linker, in human NLRP1) was automatically excluded during the generation of this model. The fold of the overall

protein presented as an elongated molecule with the CARD folding back towards the NACHT domain. Apart from that, no intramolecular interactions and folds were found. It should be noted that the overall fold of the protein is a prediction and may not necessarily represent the true conformation of the full-length NLRP1 protein.

For a size comparison an overlay of the MBP-NLRP1 molecule and the molecular envelope generated from the SAXS data was produced (Figure 3.9C). The elongated model of MBP-NLRP1 fits to the length of the molecular envelope. The width of the particle could potentially fit two MBP-NLRP1 monomers next to each other. Hypothetically, the envelope could fit three dimers or two trimers, which could form a homotrimer or a homodimer, respectively. However, the overall conformation of the oligomer is difficult to predict without a high resolution structure of the oligomer or the monomer.

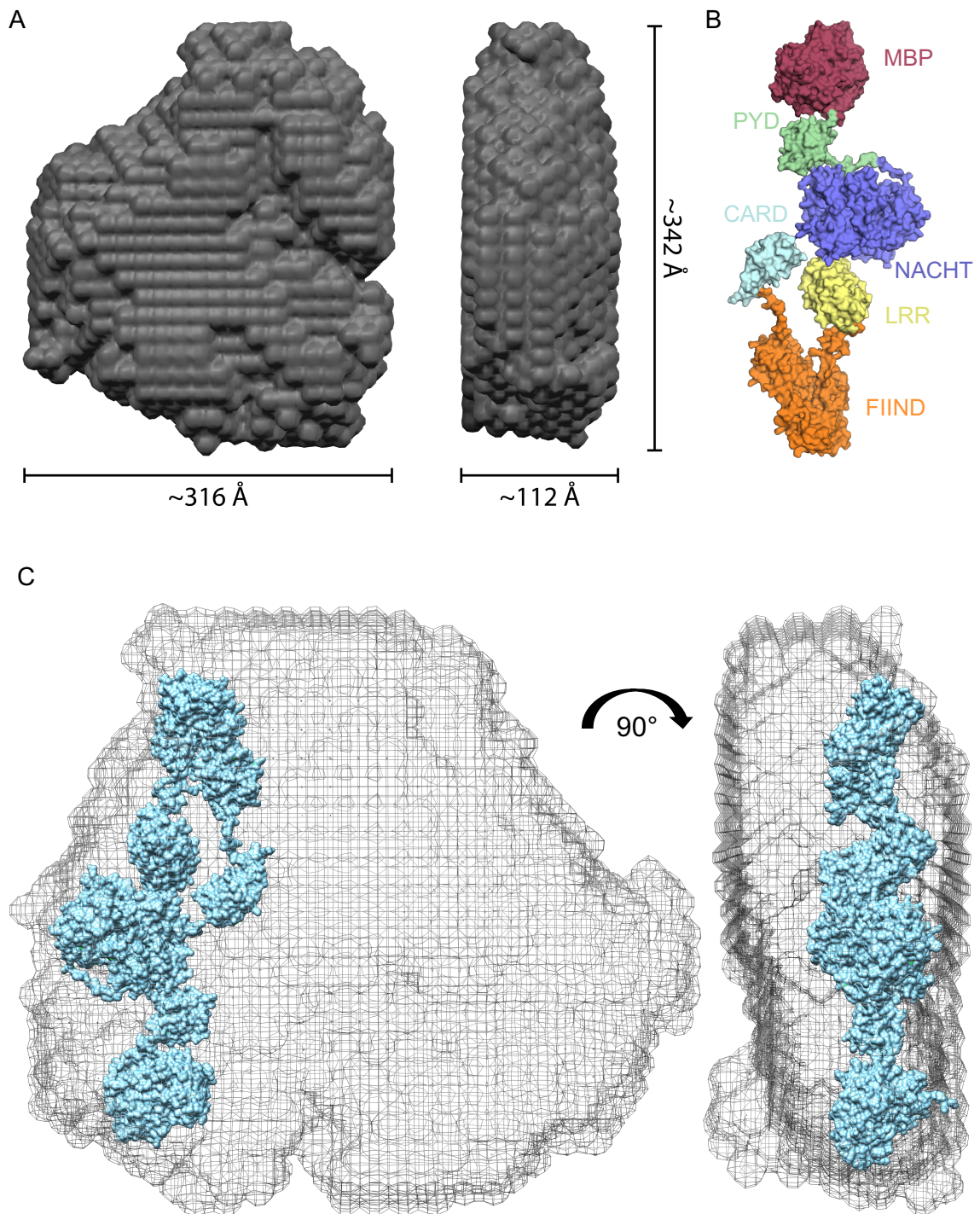


Figure 3.9: *Ab initio* model and molecular envelope of the MBP-NLRP1 oligomer determined from SAXS data

(A) Volume representation of the molecular envelope calculated from the SAXS data obtained for the 2.4 mg/mL sample of the MBP-NLRP1 oligomer. Dimensions were manually measured using Chimera software (Pettersen *et al.*, 2004). **(B)** Model of MBP-NLRP1. Different domains are highlighted and labelled in different colours. The model was generated using the RaptorX structure prediction tool (Wang *et al.*, 2016). **(C)** Overlay of the MBP-NLRP1 model and the molecular envelope calculated from SAXS data shown in A.

3.3 Discussion

Even though NLRP1 is – apart from NLRP3 – the most extensively studied NLR inflammasome, many questions about its mechanism of activation remain elusive. For other inflammasomes like NLRP3 and NLRC4, high resolution structural information has greatly contributed in improving the understanding of how these molecules are regulated (Hu *et al.*, 2013; Diebolder *et al.*, 2015; Zhang *et al.*, 2015; Sharif *et al.*, 2019). These structures helped to understand the mechanism by which certain mutations identified in patients lead to spontaneous activation of the according inflammasome (Sharif *et al.*, 2019). The aim of this study was therefore to generate such structural data for NLRP1. However, problems with aggregation and oligomerization did not allow for the generation of high resolution structural information on the full-length protein. Similar problems with aggregation and degradation of recombinant NLRP1 protein have been reported in the literature previously (Martino *et al.*, 2016). Making use of the MBP-affinity tag helped resolving solubility issues for the NACHT, FIIND and CARD domain containing constructs as well as for the full-length protein. The resulting proteins were soluble and pure and were used for further biophysical characterization. The PYD and LRR constructs were stable without any affinity tag in solution and did not require an MBP-tag for solubilization.

Structural analysis of NLRP1 PYD and LRR was not directly indicative of how these domains are involved in keeping NLRP1 autoinhibited. The absence of $\alpha 3$ in NLRP1 PYD has been discussed previously. It was speculated that this helix cannot form in NLRP1 PYD due to a *cis-trans* isomerisation of a preceding peptide bond or the lack of a conserved lysine residue involved in inducing the formation of $\alpha 3$ (Hiller *et al.*, 2003; Chu *et al.*, 2015). A third reason for the absence of this helix in NLRP1 PYD could be the proline in position 45 (Chapter 3.2.2). As shown by the interface analysis in Chapter 3.2.2, the absence of $\alpha 3$ by itself does not directly explain why NLRP1 PYD is autoinhibitory. Thus, it was hypothesized that the PYD contributes to autoinhibition by folding onto another domain in the full-length protein. No direct interaction between the PYD and the NACHT-LRR, LRR, FIIND, FIIND-CARD or CARD domain could be observed in

analytical SEC experiments. Interestingly, the MBP-CARD protein did also not interact with a nanobody which was supposed to be specific for NLRP1 CARD. Consequently, it is reasonable to consider that the MBP blocks important interfaces. Indeed, by doing so it could actively promote solubility of the fused construct in case of an otherwise exposed oligomerization interface. Recombinant PYD and LRR showed no interaction in an analytical SEC experiment despite not having any N-terminal affinity-tag, implying that these domains do not contribute to autoinhibition by interacting directly with each other intramolecularly. Additional repeats or a different approach to investigate intramolecular interactions of separate domains, like SPR, would be desirable to further support the findings described above.

A biophysical characterization of full-length NLRP1 fused to MBP revealed that this protein forms oligomers in solution. It has to be considered that oligomer formation is induced by the MBP-tag. Nevertheless, oligomer formation is a well-known feature of AAA+ ATPases and NACHT domain containing proteins and has been demonstrated previously by cryoelectron microscopy for the NLRC4 inflammasome or the Apaf-1 apoptosome (Diebolder *et al.*, 2015; Zhang *et al.*, 2015). In the case of NLRC4, one additional sensor molecule called NAIP (Neuronal Apoptosis Inhibitory Protein) is needed for the induction of oligomer formation. After induction by the NAIP protein, between nine and eleven NLRC4 monomers assemble into a disk-like oligomer (Zhang *et al.*, 2015). For NLRP1 no nucleation factor, like NAIP for NLRC4, has been reported yet. In this study, the MBP-NLRP1 oligomer was found to be hexameric as calculated from the SAXS data. Since the domain architecture of the NLRC4 and NLRP1 proteins is considerably different (NLRC4 has an N-terminal CARD, a NACHT and an LRR domain), the oligomeric state of these two proteins might as well be different. Negative stain electron microscopy of full-length NLRP1 was found to also contain monomers and different oligomeric assemblies, the majority the oligomers being pentamers or heptamers (Faustin *et al.*, 2007). Since the SAXS data is the result of the average of the scattering pattern of the protein particle in solution, the observations from the electron microscopy study do not directly support our finding that full-length MBP-NLRP1 may form a hexamer in solution

(Jacques and Trewella, 2010). Technically, if heptamers were present in the sample analysed by SAXS, they should dominate in the scattering pattern, as they would be expected to form larger particles than hexamers. However, depending on the apparent fold of the oligomer and the required hydration radius, this must not necessarily be the case. Furthermore, the oligomeric state was determined by approximation of the molecular weight or more precisely the Porod volume. This approximation might have an intrinsic error, which could explain the difference between the present study and the previously reported insights into the NLRP1 oligomer (Faustin *et al.*, 2007). Moreover, the manual fitting of an MBP-NLRP1 model showed that the molecular envelope calculated from the SAXS data could fit seven monomers of MBP-NLRP1.

The overall shape of the particle could also be interpreted as a triangle. For a triangular shape, a hexameric assembly would be more likely than a pentameric or a heptameric assembly. From a mathematical point of view, the geometrical space of a triangle could be filled by a hexamer composed of three dimers (Figure 3.9C) or two trimers. Other AAA+ ATPases have been shown to form hexameric assemblies as well, supporting our finding of a hexameric oligomer (Hanson and Whiteheart, 2005; Schumacher *et al.*, 2008; Chen *et al.*, 2010). In contrast to this, different proteins like apoptosomes harbouring a death domain have been reported to assemble into tetramers, heptamers or octamers (Yuan and Akey, 2013; Oroz *et al.*, 2016). The overall conformation described for a range of AAA+ ATPases, apoptosomes and inflammasomes is commonly disk-like, supporting the shape found for the envelope calculated from the SAXS data (Chen *et al.*, 2010; Yuan and Akey, 2013; Tentorey *et al.*, 2017).

For NLRP1 to become active and bind to ASC, the C-terminal cleavage fragment has been shown to be sufficient (Zhong *et al.*, 2016). In certain scenarios the N-terminal fragment has even been shown to be degraded during the activation process (Chui *et al.*, 2019; Sandstrom *et al.*, 2019). Thus, it can be speculated whether the N-terminal fragment comprised of the PYD, NACHT and LRR domain is actually required for the formation of the active oligomer. Since our study as well as the previously mentioned electron microscopy study suggest that the full-length protein forms oligomers, it can be further hypothesized that

NLRP1 might be oligomeric in its autoinhibited conformation. This could also explain, why no intramolecular interactions were found in analytical SEC experiments. PYD and LRR could contribute to autoinhibition by aiding in oligomer formation via homotypic interactions. However, purification and characterization of the PYD did not show dimer formation under the tested conditions, indicating that no homotypic interactions are present between the monomers of this domain. The LRR behaved as a dimer in solution and showed two molecules in the asymmetric unit. Nevertheless, the structure revealed that the dimer is asymmetric and did not unveil an interface that could be involved in dimer formation. These findings argue against an involvement of the PYD or LRR in forming the MBP-NLRP1 oligomer. Overall, it has to be considered that these experiments were carried out in an artificial environment not resembling physiological conditions. Homo- or heterotypic interactions of the aforementioned domains might depend on factors like the pH, the salt concentration, the temperature or the concentration of the protein itself.

Collectively, the herein presented data demonstrate that full-length NLRP1 fused to MBP forms oligomers in solution. These oligomers are potentially hexamers as determined by SEC-SAXS analysis. Further, analytical SEC experiments showed that PYD and LRR do not contribute to keeping NLRP1 autoinhibited by interacting directly with each other and are unlikely to be involved in oligomer formation. The structural basis of PYD and LRR autoinhibitory functions as well as the physiological role of the full-length NLRP1 oligomer remain to be elucidated.

4. The role of nucleotides in regulating NLRP1 activity

4.1 Introduction

As described in Chapter 3.1, NLRP1 harbours a central NACHT domain. This domain is conserved throughout the entire family of NLRs (Proell *et al.*, 2008). The NACHT domain is commonly described to be involved in nucleotide binding (Leipe *et al.*, 2004; Maharana *et al.*, 2018). The NACHT domain is commonly comprised of four subdomains, a nucleotide binding domain (NBD), a first helical domain (helical domain 1, HD1), a so-called winged helix domain (WHD), and a second helical domain (helical domain 2, HD2) (Bentham *et al.*, 2017; Maharana *et al.*, 2018). Conserved nucleotide binding motifs are located within these subdomains. These motifs are not only found in NACHT domain containing proteins but also in other members of the STAND (signal transduction ATPases with numerous domains) subfamily of the AAA+ ATPase (ATPases associated with diverse cellular activities) superfamily, to which the NLRs belong (Leipe *et al.*, 2004; Ammelburg *et al.*, 2006; Maharana *et al.*, 2018).

Commonly shared by all members of the AAA⁺ family are the Walker A motif, also referred to as the P-loop, and the Walker B motif. The Walker A motif is usually comprised of eight amino acids following the pattern GxxxxGK(T/S) (Hanson and Whiteheart, 2005; Wendler *et al.*, 2012). Here, the x denotes any of the 20 proteinogenic amino acids. In the C-terminal position either a threonine or serine residue can be found. The positively charged side chain of the lysine residue is described to form contacts with the β - and γ -phosphate of ATP (Saraste *et al.*, 1990; Wendler *et al.*, 2012). The polar residue at the end of Walker A (serine or threonine) is described to coordinate the magnesium ion with its side chain hydroxyl group (Saraste *et al.*, 1990; Miller and Enemark, 2016). Consequently, mutations of these residues result in impaired nucleotide binding and hydrolysis (Matveeva *et al.*, 1997; Babst *et al.*, 1998). The Walker B motif typically consists of four hydrophobic residues followed by an aspartic acid and glutamic acid residue (hhhhDE, h = hydrophobic residue) (Hanson and Whiteheart, 2005; Wendler *et al.*, 2012). Interestingly, for NLRs an altered Walker

B motif is found, with the glutamate of the terminal DE missing and an additional DE motif two amino acids downstream of the expected DE (hhhhDxxDE) (Proell *et al.*, 2008). This variation of the Walker B motif is also found in NOD1 and NOD2 and was termed “extended Walker B” (Zurek *et al.*, 2012). The negatively charged residues of the Walker B motif are involved in coordination of the magnesium ion and priming of a water molecule for hydrolysis via a nucleophilic attack on the γ -phosphate of ATP (Story and Steitz, 1992). Moreover, the Walker B glutamate was also termed “glutamate switch”, as it is reported to be able to switch between an active and inactive state depending on the binding of cofactors and substrates (Wendler *et al.*, 2012). Mutating the Walker B motif impairs hydrolysis but not nucleotide binding (Wendler *et al.*, 2012). Further conserved motifs include the Sensor 1 motif containing a conserved arginine residue in NLRs and the Sensor 2 motif which in NLRs contains a conserved histidine residue (Riedl *et al.*, 2005; Proell *et al.*, 2008). Sensor 1 is described to play a crucial role in coordinating the nucleotide by interacting with the γ -phosphate of ATP, thereby making it susceptible to hydrolysis (Hanson and Whiteheart, 2005; Wendler *et al.*, 2012). Sensor 2 is typically involved in nucleotide binding and mutations of this motif are known to impair nucleotide binding and hydrolysis (Ogura *et al.*, 2004).

NLRP3 is known to bind ATP and exhibit ATPase activity (Duncan *et al.*, 2007). Functionally, ATP binding but not hydrolysis activity has been demonstrated to be required for activation of the NLRP3 inflammasome. The role of nucleotide binding of NLRP3 was investigated by mutating the GKT residues of the Walker A motif to three alanine residues (Duncan *et al.*, 2007). More recent studies found that mutation of the Walker B motif results in constitutive activation of the NLRP3 inflammasome (Coll *et al.*, 2019; Tapia-Abellán *et al.*, 2019). A similar mutational approach was taken to investigate the involvement of nucleotide binding and hydrolysis in NOD1 and NOD2 activity (Zurek *et al.*, 2012). For the family of AAA⁺ ATPases it is described that the exchange of ADP for ATP and subsequent ATP hydrolysis are required to induce conformational changes to switch from the inactive to the active conformation and back (Iyer *et al.*, 2004). This is also a proposed mechanism for the transformation of NLR family proteins from the

closed, inhibited conformation to the open, active conformation (Danot *et al.*, 2009).

In contrast to NLRP3, a construct containing the NLRP1 NACHT and LRR domain has been shown to bind but not hydrolyse ATP (Liu *et al.*, 2004; Martino *et al.*, 2016). Results from early studies suggested that NLRP1 requires ATP to form an active inflammasome (Liu *et al.* 2004; Faustin *et al.* 2007; Bruey *et al.* 2007; Faustin *et al.* 2009). Interestingly, no specific inhibitory effect of ATP competitive inhibitors designed for NLRP1 was found when tested on mouse NLRP1b activated with lethal toxin (Harris *et al.*, 2015). Consistent with these results, more recent studies found that mutations within the Walker A motif of mouse NLRP1b or human NLRP1 lead to increased or constitutive inflammasome activity, respectively (Liao and Mogridge, 2013; Chavarría-Smith *et al.*, 2016). Since these mutations were shown to impair nucleotide binding, it was concluded that NLRP1 does not require ATP to form an active inflammasome.

For NLRP1, only mutations within the Walker A motif have been tested regarding their effect on inflammasome activation. Therefore, one aim of this work was to further elucidate the functional importance of the ATP binding site of NLRP1 by means of a mutagenesis study. To do so, conserved motifs and residues were identified using a sequence and structure based approach. Furthermore, a hydrolysis assay was designed and established using recombinant MBP-NLRP1 protein to test whether NLRP1 shows ATP hydrolysis activity.

4.2 Results

4.2.1 MBP-NLRP1 exhibits ATP hydrolysis activity

In previous studies, the hydrolysis activity of NLRP1 was investigated for recombinant protein containing the NACHT and LRR domains. Hydrolysis was measured as an increase in inorganic phosphate over time using a malachite-green assay (Martino *et al.*, 2016). Here, we investigated the ATPase activity of recombinant full-length MBP-NLRP1. A highly sensitive analytical assay based on the separation of different nucleotides by a Reversed-Phase High-Performance Liquid Chromatography (RP-HPLC) based technique was established in our laboratory. RP-HPLC allows the separation of ATP, ADP, and AMP. Small changes of all three nucleotides can be monitored by measuring the absorbance of the eluate at 254 nm, which is the wavelength at which the nucleotides absorb light.

For a measurement, 3 μM of the protein from the first peak described in Chapter 3.2.5 were incubated with 100 μM ATP and 5 mM MgCl_2 for 60 minutes. Samples were incubated at 25 °C and analysed by RP-HPLC at the start of the experiment and every 10 min afterwards. A representative chromatogram of an experiment with WT MBP-NLRP1 protein is shown in Figure 4.1A. In contrast to what has been reported for the NACHT-LRR construct of NLRP1, full-length MBP-NLRP1 clearly showed hydrolysis activity. This is visible in the chromatogram in form of a reduction of the level of ATP over time. Quantification of the respective peak area and subsequent normalization allowed to calculate an approximate proportion of ATP, ADP and AMP in the sample at the measured time points. By this approach, it was calculated that ATP only comprised 52 % of the total nucleotide in the sample after 60 min of the time course measurement (Figure 4.1B). Based on linear regression the rate of hydrolysis was calculated to 0.29 molecules of ATP per minute from the slope of the resulting curve. As a consequence of ATP hydrolysis, the ADP level in the sample increased over time, as ADP is a product of the hydrolysis reaction. The ADP level after 60 min was determined to be 34 % of the total amount of nucleotide in the sample.

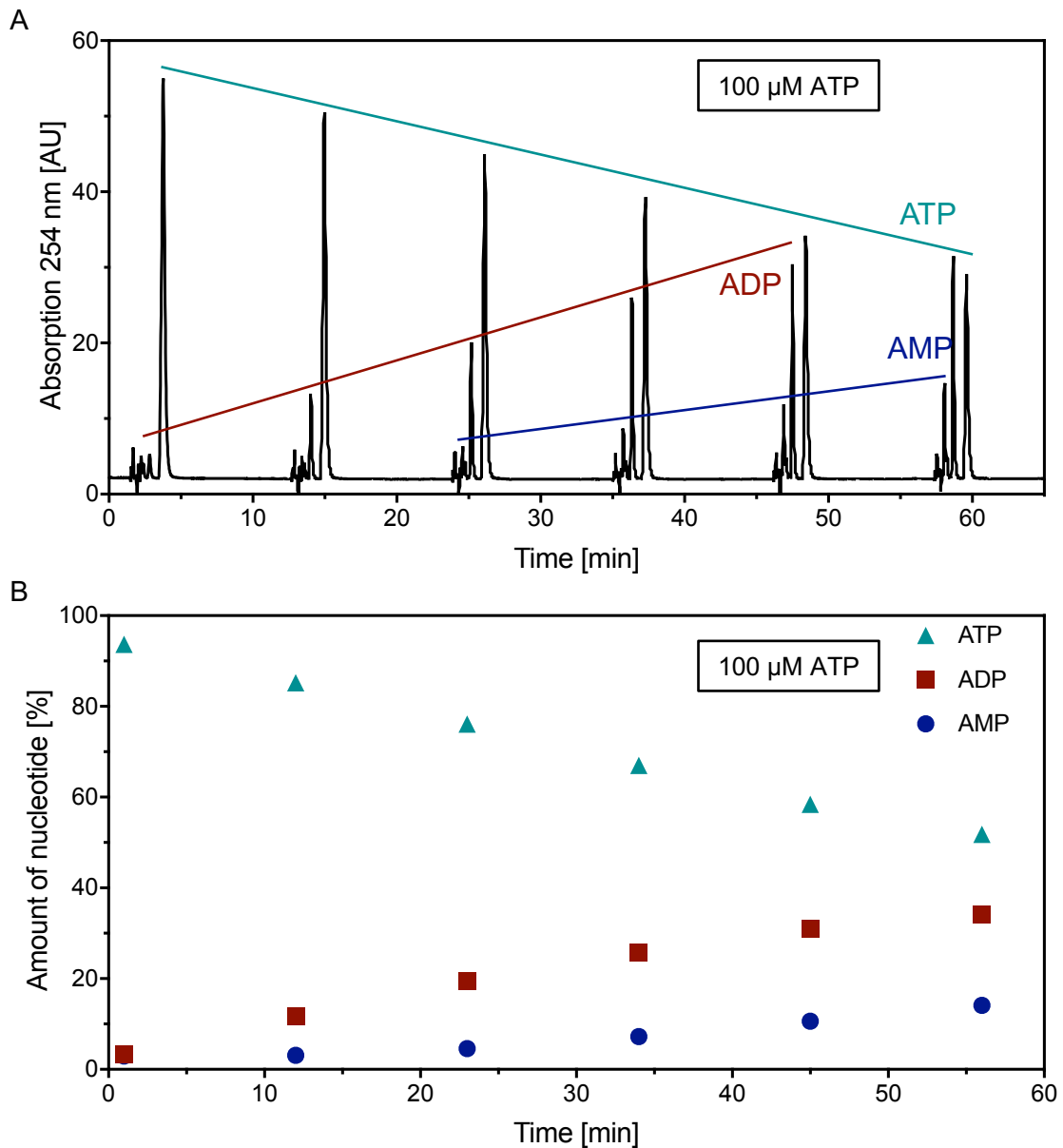


Figure 4.1: MBP-NLRP1 exhibits ATP hydrolysis activity

(A) Chromatogram of an RP-HPLC elution profile of an ATP hydrolysis measurement with MBP-NLRP1. 100 μM ATP and 5 mM MgCl_2 were incubated in the presence of 3 μM MBP-NLRP1 protein (Peak1) at 25 $^\circ\text{C}$ for 60 min. Every 10 min a sample was taken and analysed by RP-HPLC. Peaks for AMP, ADP and ATP are depicted by coloured lines and labelled accordingly. Data shown is from one experiment of two repeats. **(B)** Quantification of the data presented in A. Peak areas were integrated and normalised to 100 %.

Surprisingly, the level of AMP also increased in this measurement. After 60 min AMP made up 14 % of the entire nucleotide amount in the sample. This indicated that a second hydrolysis step is facilitated in which ADP is hydrolysed to AMP and inorganic phosphate. The observed increase in AMP did not go along with a decrease of the level of ADP, implying that the ADP hydrolysis reaction was slower than the ATP hydrolysis reaction.

To further investigate this effect, a second experiment was performed in which 100 μ M ADP instead of ATP were added to the protein (Figure 4.2). If ADP hydrolysis occurs in the sample, a decrease in ADP should be observed as well as an increase in AMP. As expected, the level of ADP decreased in this experiment as the level of AMP increased over time, again indicating hydrolysis of ADP (Figure 4.2). However, at early stages of the measurement there was also an increase in ATP levels detected. This implies that apart from AMP, ATP is generated in the sample, which initially only contained ADP. Enzymatic activity facilitating the reaction of two molecules of ADP to ATP and AMP as well as the reverse reaction is commonly described for adenylate kinases (Abele and Schulz, 1995). This class of enzymes monitors the cellular energy status by sensing nucleotide levels (Dzeja and Terzic, 2009). If required, they facilitate the alteration of nucleotide levels through the interconversion of ATP and AMP to two molecules of ADP as well as the reverse reaction. The generated nucleotides can further serve as signalling molecules to stimulate metabolic pathways (Dzeja and Terzic, 2009). To date, adenylate kinase activity has not been reported for NLR proteins.

Interestingly, ATP levels peaked after 12 min and then slowly decreased again. This might indicate that at this point of the measurement a concentration of ATP is reached at which hydrolysis of ATP is the preferred reaction. This is consistent with the observation of a drastically decreased reduction of ADP from this time point onwards. Similar to that, AMP increased at a much slower rate after this time point. To further evaluate NLRP1 ATP hydrolysis and adenylate kinase activity the amino acids involved in catalysing these reactions were identified by taking a sequence and structure based approach.

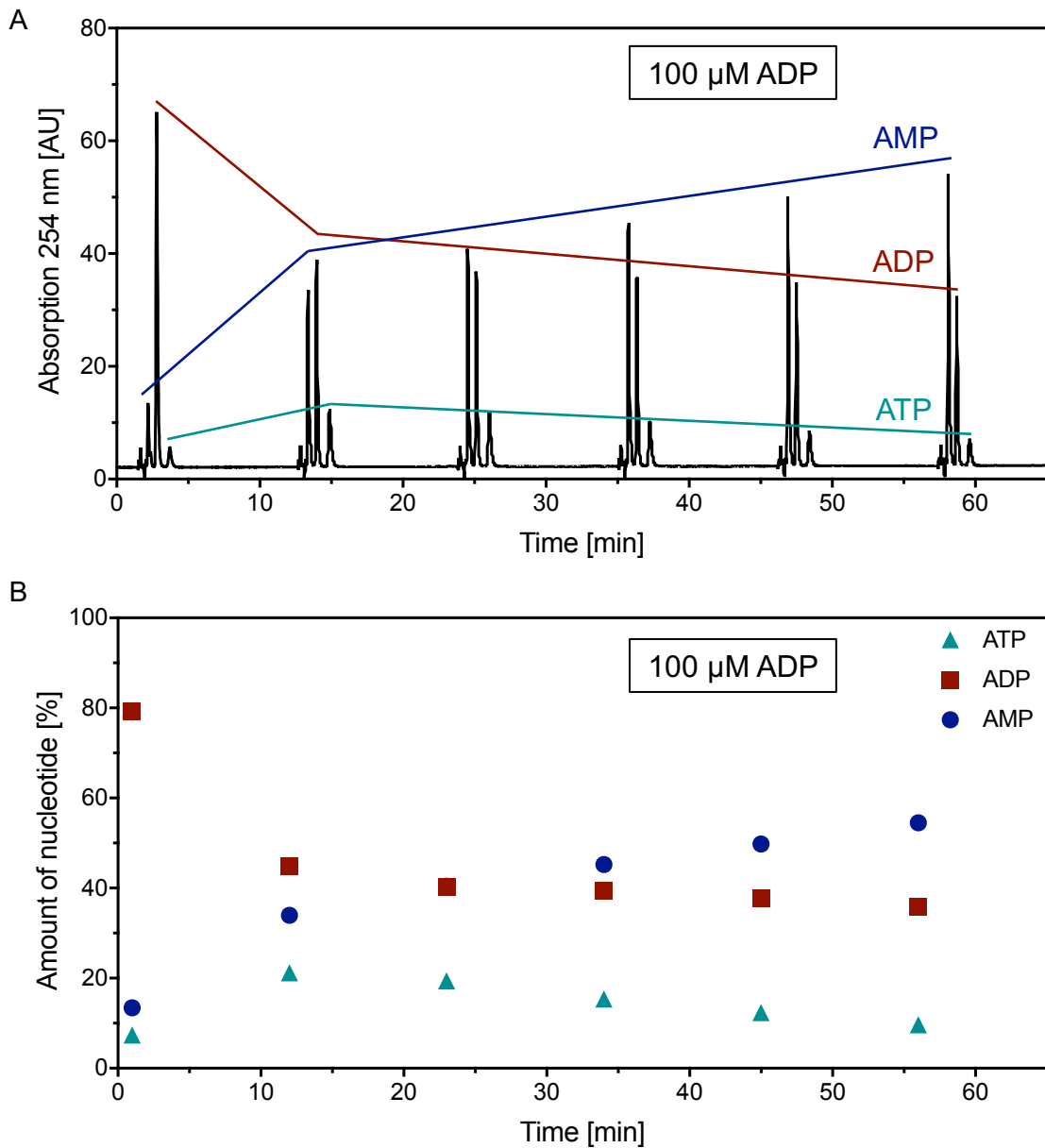


Figure 4.2: MBP-NLRP1 exhibits adenylate kinase activity

(A) Chromatogram of an RP-HPLC elution profile of an ADP hydrolysis measurement with MBP-NLRP1. 100 μM ADP and 5 mM MgCl_2 were incubated in the presence of 3 μM MBP-NLRP1 protein (Peak1) at 25 $^\circ\text{C}$ for 60 min. Every 10 min a sample was taken and analysed by RP-HPLC. Peaks for AMP, ADP and ATP are depicted by coloured lines and labelled accordingly. Data is from one experiment. **(B)** Quantification of the HPLC data presented in A. Peak areas were integrated and normalised to 100 %.

4.2.2 Identification of conserved nucleotide binding motifs in NLRP1

To identify the conserved Walker A and B motifs as well as Sensor 1 and Sensor 2 motif in NLRP1, a multiple sequence alignment of the amino acid sequences of all human NLRP proteins as well as NOD1 and NOD2 was performed (Figure 4.3A). The online multiple sequence alignment tool Clustal Omega was used with default settings to align the sequences (Madeira *et al.*, 2019). Conserved motifs were easily identified and are highlighted in a schematic of the NLRP1 NACHT domain in Figure 4.3B. The Walker A motif of NLRP1 (GAAGIGKS) follows the expected pattern of GxxxxGK(T/S). Besides NLRP5 and NLRP12, NLRP1 is one of only three members of the NLRP protein family having a serine residue instead of a threonine residue in the last position of the Walker A motif. NOD1 and NOD2 both show a serine residue in that position. Similarly, the Walker B motif is conserved within the NLRP protein family. Most NLRPs, including NLRP1, contain the extended Walker B motif with the two negatively charged residues shifted three amino acids downstream. For NLRP1, these two negatively charged residues are aspartate and glutamate. Only NLRP9 and NLRP11 have an uncharged residue in the terminal position of the extended Walker B motif. Interestingly, NLRP11 contains both the classical Walker B motif with two negatively charged residues (ED) and the extended Walker B motif with only one negatively charged residue and one polar residue (DN). Within the sensor 1 motif the last residue presents with a conserved positive charge. An arginine residue is most prominent at this position in all proteins including NOD1 and NOD2. NLRP4 and NLRP13 contain a lysine residue instead of an arginine. Only NLRP9 contains an uncharged but polar residue in sensor 1 (Q). The conserved histidine residue, shown to replace sensor 2, can be found in most NLRPs inclusive of NLRP1. NLRP8 shows a hydrophobic residue (L), whereas NLRP6 contains a negatively charged residue (D).

In summary, NLRP1 contains all motifs known to be involved in nucleotide binding and hydrolysis. Since adenylate kinase activity is a newly discovered activity of NLRP1, identification of residues involved in catalysing the according reactions can simply be achieved by aligning the amino acid sequences of NLR

proteins. It would either require a structure of a NACHT domain with bound nucleotide(s) or could be achieved by a mutagenesis approach elucidating the activity of different nucleotide binding site variants. In the next step, structural modelling of the nucleotide binding site of human NLRP1 was performed to confirm the residues identified from the sequence analysis to be directly involved in nucleotide binding and potentially hydrolysis.

A	Walker A	Walker B
NOD1	GETIFIL GDAGVGK SMLLQRLQSLW	LLRFPHVAL FTFDGL DELH
NOD2	ADTVLVV GEAGSGK STLLQRLHLLW	LLDHPDRV LLTFDGF DEFK
NLRP2	SYTVVLY GPAGLGKT TTLAQKMLDW	ILAQAARKI LFVIDGF DELG
NLRP7	PYTVVLH GPAGVGKT TTLAKKMLDW	ILAQAQRI LFVVDGL DELK
NLRP11	NLNVFLM GERASGKT IVINLAVLRW	ILSDPKKL LFILEDLD NIR
NLRP5	PRTVVVLH GKSGIGK SALARRIVLCW	IMSRPERLL LFIIDGF FDDL
NLRP13	AQTIVLV GRAGVGKT TTLAMQAMLHW	FMSQPEKLL LFIIDGF EELI
NLRP8	PKTVAIQ GAPGIGKT ILAKKVMFEW	IMSKPDQL LLLLDGF EELT
NLRP14	PQIVVLQ GAAGVGKT TTLVRKMLDW	IMYQPSSLL LFII DSFDELN
NLRP4	PRTVIIQ GPQGIGKT TLLMKLMMAW	IVSQPERLL LFVIDS FEELO
NLRP9	RHTVVLE GPDGIGKT TLLRKVMLDW	IFSQPERI LFIMDGF EQLK
NLRP1	PRIVILQ GAAGIGK STLARQVKEAW	ILSRPERLL LFILDG VDEPG
NLRP6	PLTVVLQ GPAGIGKT TMAAKKILYDW	MLAQPQRL LFILDG ADEL
NLRP10	PSLVVLQ GSAGTGKT TTLARKMVL	ILRQPERLL LFILDG FDELQ
NLRP3	VHTVVVQ GAAGIGKT ILARKMMLDW	IVRKPSRI LFIMDGF DELQ
NLRP12	PRTVVMQ GAAGIGK SMLAHKVMLDW	LIRVPERLL LFIIDGF DELK
	: . * . ** :	: . * : . . . :

	Sensor 1	Sensor 2
NOD1	KLL TAR TGI	Y EFFH LTLQAFFTAFF
NOD2	KVV TSR PAA	LE FLH ITFQCFFAAFY
NLRP2	LLV TTR PRA	YS FIH LSFQQFLTALF
NLRP7	LLV TTR PRA	YS FIH LSFQQFLTALF
NLRP11	FLI SSR PTR	YK FIH LVNQEFCTAIA
NLRP5	LIV TVR DVG	YT FFH LSLQDFCAALY
NLRP13	LLI TIK TWF	TT FTH LSFQEFFAAMS
NLRP8	LLI MIR FTS	YV FTL VTFQEFFAALF
NLRP14	LLV TTR LTT	YV FTH LHVQEFFAAMF
NLRP4	LLI AIK PVC	YV FLH VCIQEFCAALF
NLRP9	LLI ALG KLA	FA FMH LCIQEFCAAMF
NLRP1	FLI TAR TTA	YS FIH LCFQEFFAAMS
NLRP6	LLV TTR AAA	YQ FID QSFQEFALAALS
NLRP10	LLI TTR P	YS FRH ISFQDFFHAMS
NLRP3	LLI TTR PVA	YS FIH MTFQEFFAAMY
NLRP12	LLI TTR P	YS FIH LSFQEFFAAMY
	: :	* . * * * :

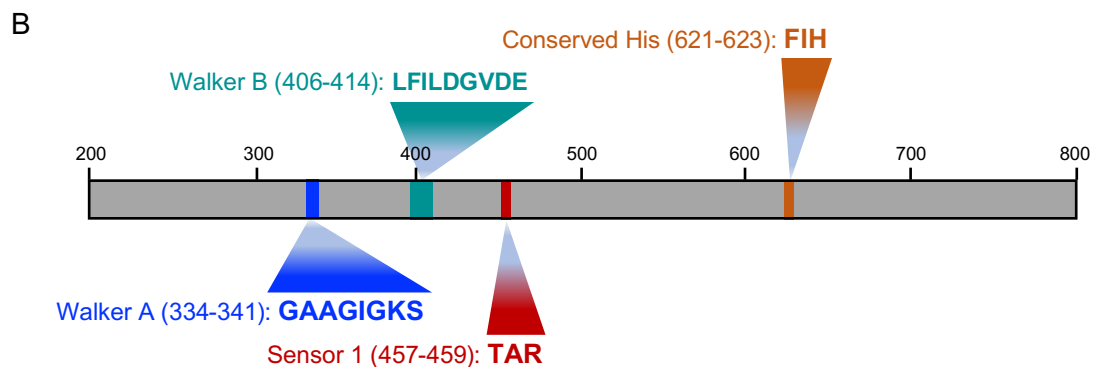


Figure 4.3: Sequence alignment of human NLRP proteins and NOD1 and NOD2 reveals conserved nucleotide binding site motifs

(A) Parts of a sequence alignment of all human NLRP proteins as well as NOD1 and NOD2. The shown parts include motifs identified to be involved in nucleotide binding or hydrolysis. The alignment was performed using the Clustal omega online tool (Madeira *et al.*, 2019). Protein sequences were obtained from the Uniprot database. Major differences in the described motifs are highlighted in cyan. Conserved motifs identified in NLRP1 are highlighted in their respective colour in the schematic in B. Stars below the sequences indicate identical residues for all sequences at the respective position. Dots indicate conserved charge, hydrophobicity or polarity of the residue at the respective position. **(B)** Schematic of NLRP1 NACHT domain with the conserved nucleotide binding and hydrolysis motifs highlighted in different colours. Numbers indicate the number of the amino acids in the sequence of NLRP1.

4.2.3 Structural model of the NLRP1 NACHT domain

As mentioned above, no high resolution structural information is available for the NLRP1 NACHT domain. Therefore, to facilitate a structural assessment of the nucleotide binding site, a homology model was generated. Among all matches identified from a sequence alignment, the crystal structure of a rabbit NOD2 NACHT-LRR construct (PDB: 5IRL) produced the best fit with 26 % sequence identity, when aligned to the NLRP1 NACHT-LRR amino acid sequence within the range 230-990. The Swiss Model Template Search was used for this alignment and to build the according model (Waterhouse *et al.*, 2018). In Figure 4.4A a superposition of the NACHT domains of the NOD2 crystal structure with bound ADP and the NLRP1 homology model is displayed. Both structures align well, allowing to identify subdomains within the NLRP1 NACHT domain (Figure 4.4B). From the homology model the NBD subdomain of NLRP1 NACHT was found to span residues 309 to 479. HD1 spans residues 480 to 544 and the WHD is located within residues 545 to 642. This is comparable with previous findings (Maharana *et al.*, 2018). HD2 was estimated to span amino acid residues 643 to 758. However, the HD2 LRR module is described to be variable among NLRs and therefore more difficult to clearly identify (Sharif *et al.*, 2019). Especially the transition between the NACHT and LRR domain is highly variable when comparing the known structures of NLRP3, NLRC4 and NOD2 (Hu *et al.*, 2013; Maekawa *et al.*, 2016; Sharif *et al.*, 2019). Thus, predicting this region in NLRP1 is particularly difficult.

Presence of the ADP molecule in the NOD2 structure in combination with the superposition of the NOD2 crystal structure and the NLRP1 NACHT homology model allowed for the identification of residues which are likely to be in proximity of the nucleotide in NLRP1. A magnified view from two different perspectives of the nucleotide binding site of the NLRP1 homology model is shown in Figure 4.4C. In the Walker A motif the conserved lysine residue and the polar serine residue are in direct vicinity of the β -phosphate of ADP, indicating an important role in coordinating the nucleotide for hydrolysis. The same holds for sensor 2 (Figure 4.4C, left panel). The glutamate of the extended Walker B motif as well

as the arginine of Sensor 1 are not forming direct contacts with the ADP molecule according to the homology model (Figure 4.4C, right panel). Noteworthy, the presented model only has an ADP molecule and not an ATP and no water molecules are included in this model. Furthermore, it is based on the structure of an NLR in the closed, inactive conformation.

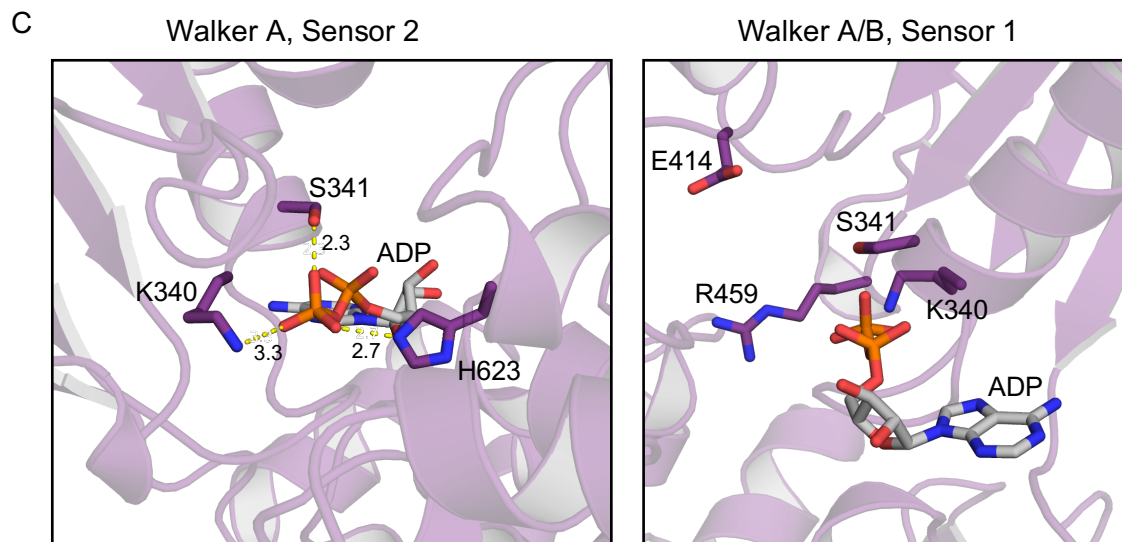
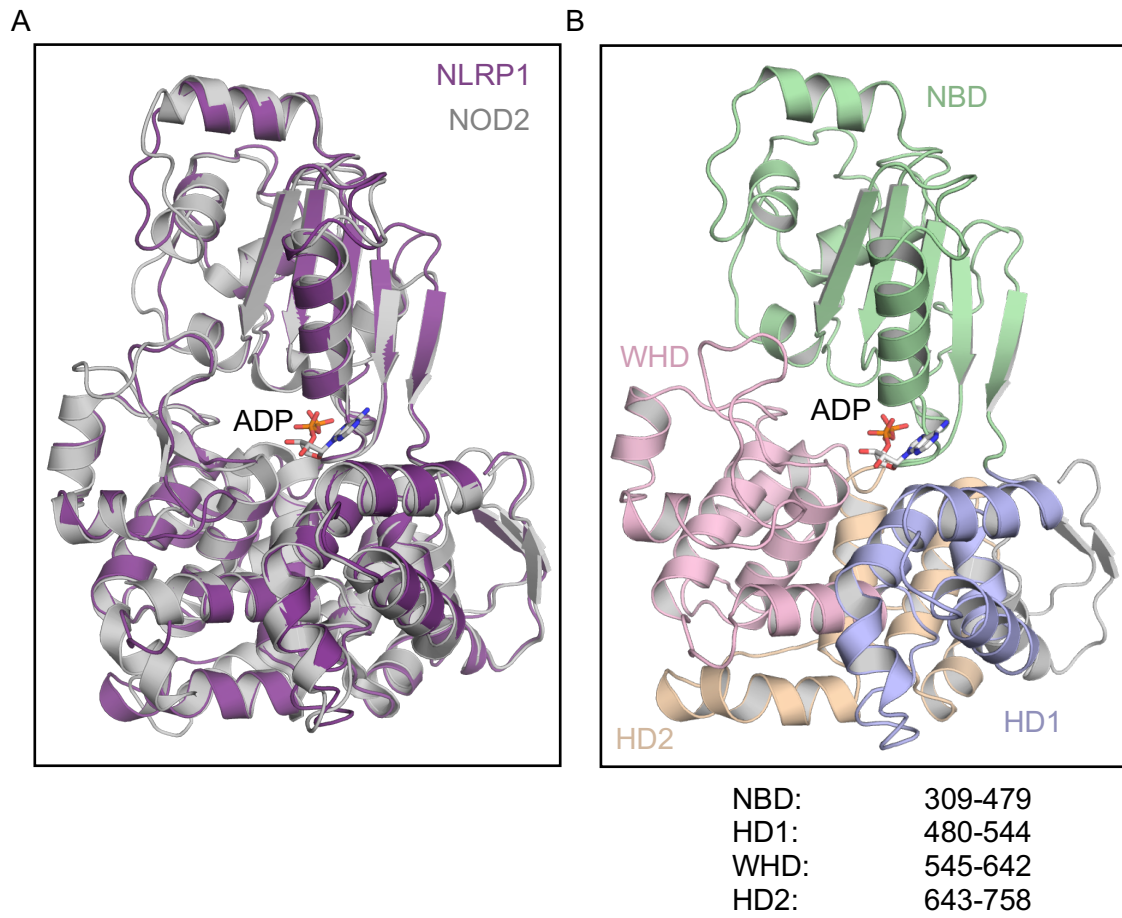


Figure 4.4: Homology model of NLRP1 NACHT domain

(A) Superposition of the NOD2 NACHT crystal structure (PDB: 5IRL) and the NLRP1 NACHT homology model generated here. The model was built using Swiss Model (Waterhouse *et al.*, 2018). Amino acids 230-990 of human NLRP1 were fed into the Swiss Model Template Finder tool. **(B)** Homology modelling of NLRP1 NACHT with the subdomains NBD, HD1, WHD and HD2 depicted in different colours. **(C)** Two different views of the NLRP1 nucleotide binding site with ADP from superposition with NOD2 crystal structure. Side chains of certain amino acids of the Walker A, Walker B, Sensor 1 and Sensor 2 are shown in stick representation. Colours of side chain atoms represent certain elements (Blue: Nitrogen, Red: Oxygen). Hydrogen atoms were excluded in these images. Residues are labelled with their respective amino acid (one letter code) and the number according to the primary sequence of human NLRP1. Numbers between residues and ADP indicate distances measured between atoms connected by dashed yellow lines. All images and distance measurements were generated in PyMOL.

4.2.4 Effect of mutations in the nucleotide binding site of MBP-NLRP1 on its hydrolysis activity

In Chapters 4.2.2 and 4.2.3 motifs and residues important for nucleotide binding and potentially hydrolysis were identified within the NACHT domain of human NLRP1. Using a mutational approach, the functional relevance of these residues for NLRP1 ATP hydrolysis activity was investigated. First, the effect of modifications of the respective residues on ATP hydrolysis was tested by introducing point mutations into the MBP-NLRP1 construct for recombinant protein production. Conserved residues of the Walker A motif (K340, S341), the Walker B motif (E414) as well as the Sensor 1 arginine (R459) and the Sensor 2 histidine (H623) of NLRP1 were analysed by mutagenesis. The following mutations were separately introduced into the WT MBP-NLRP1 expression construct: K340A, S341A, E414Q, R459A and H623A. Thus, the charge or polarity of the respective residues is replaced by a hydrophobic side chain in the case of alanine or a polar side chain in the case of glutamine. These mutations are thought to impair nucleotide binding or hydrolysis and reduce the ATP hydrolysis rate in RP-HPLC experiments. The proteins containing the mutations were purified and eluted in a single peak in the void volume and behaved similar to the WT protein described in Chapter 3.2.5 (Nucleotide binding site variants of NLRP1 purified and measured by Dr. David Fußhöller). To test ATP hydrolysis activity of the different variants designed for the nucleotide binding site, 3 μM MBP-NLRP1 Peak 1 protein harbouring one of the introduced mutations was incubated with 100 μM ATP and 5 mM MgCl_2 at 25 °C for 60 min and a sample was analysed by RP-HPLC every 10 min.

First, the consistency of the hydrolysis rate between measurements of the WT protein was tested (Figure 4.5A). The second measurement of the WT protein exhibited a slower hydrolysis rate of 0.19 molecules per min. This indicates a variability in the measurements that has to be considered when interpreting the results obtained for nucleotide binding site variants of MBP-NLRP1. The above mentioned variants were tested for their ability to hydrolyse ATP in RP-HPLC measurements as well (Figure 4.5B). When compared to the first WT

measurement all nucleotide binding site variants of MBP-NLRP1 exhibit slightly reduced hydrolysis activity. This would be consistent with the effects described for these mutations, which is to prevent nucleotide binding and impair hydrolysis (Hanson and Whiteheart, 2005). The most significant reduction in hydrolysis activity was observed for the Sensor 2 histidine variant (H623A). The Walker B mutation E414Q did not seem to impair hydrolysis as it exhibited similar activity as the WT protein. In contrast, when comparing the hydrolysis activity of the nucleotide binding site variants with the second measurement of the WT protein, most mutations show a slightly increased hydrolysis activity. Here, the Walker B mutation seemed to increase hydrolysis activity. Only the hydrolysis activity of H623A is still slightly lower compared to the second measurement of the WT protein. Taking the variation between measurements of the WT protein into account, effects seen for nucleotide binding site variants of NLRP1 might simply be due to the variability of the measurement. To make a clear statement on how these mutations affect nucleotide binding and hydrolysis of NLRP1, more experiments have to be conducted to generate statistically significant data.

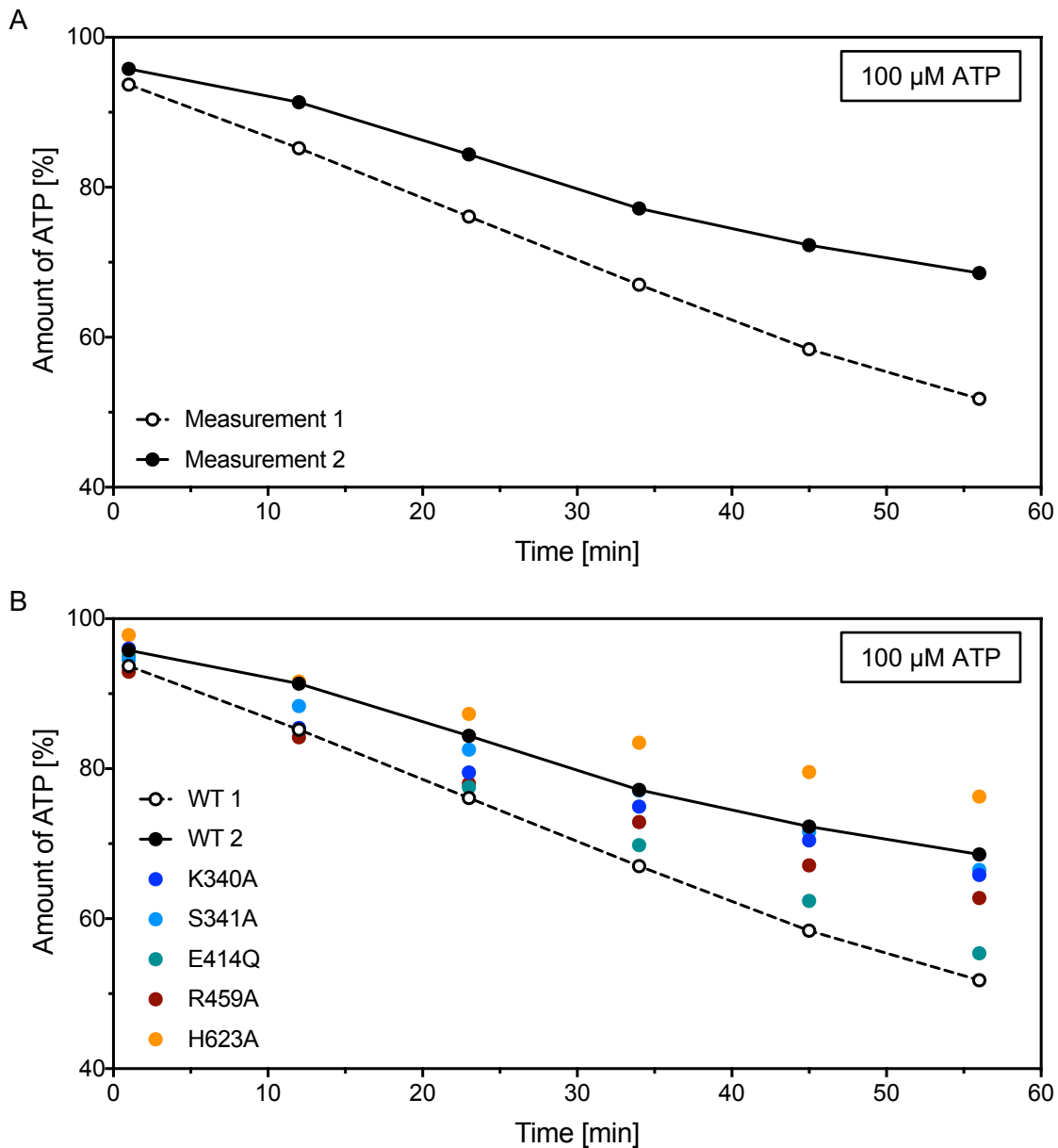


Figure 4.5: Effect of mutations in the nucleotide binding site on ATP hydrolysis

(A) Comparison of two measurements of ATP hydrolysis activity of MBP-NLRP1 Peak1 depicted by the reduction of ATP over time. Measurements were carried out with 3 μM protein, 100 μM ATP and 5 mM MgCl_2 at 25 $^\circ\text{C}$ for 60 min. Proteins for the different measurements were expressed, purified and measured separately. **(B)** Comparison of ATP hydrolysis measured for two samples of WT MBP-NLRP1 and nucleotide binding site variants (K340A, S341A, E414Q, R459A, H623A) of MBP-NLRP1. Measurements were carried out with 3 μM protein, 100 μM ATP and 5 mM MgCl_2 at 25 $^\circ\text{C}$ for 60 min. Data shown is from one experiment.

4.2.5 Nucleotide binding site variants exhibit increased NLRP1 activation

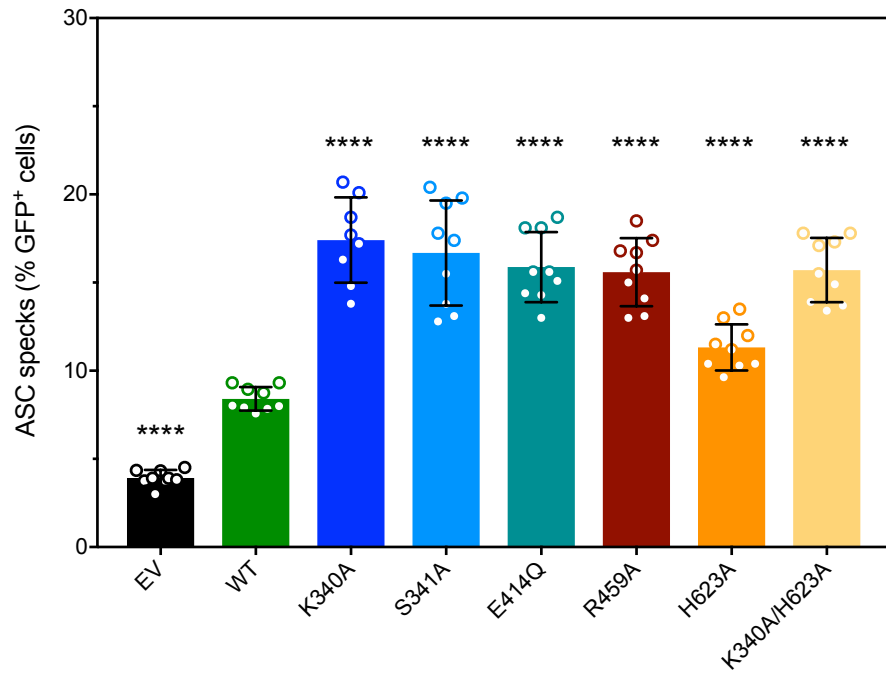
For a functional investigation of nucleotide binding site variants of NLRP1 on inflammasome activation, an *in vitro* assay was performed. In this assay, ASC speck formation is used as a measure for NLRP1 inflammasome activation. Activation of NLRP1 leads to binding of the adaptor protein ASC and induces speck formation. ASC speck formation can be quantified by flow cytometry (Sester *et al.*, 2015). Activation of NLRP1 was recorded at two time points, 24 h and 48 h post transfection.

The same mutations described in Chapter 4.2.4 were introduced into an NLRP1 construct for expression in mammalian cells. All mutations located within the nucleotide binding site led to increased activation of NLRP1 as indicated by an increased level of ASC specks when compared to the WT (Figure 4.6A and B). The frequency of ASC specks was similar for the Walker A (K340A, S341A), Walker B (E414Q) and Sensor 1 (R459A) mutations. Hence, the level of NLRP1 activation was comparable for these mutations. This was also consistent for both timepoints measured. Interestingly, mutation of the Sensor 2 histidine (H623A) exhibited only a slight increase in ASC specks compared to all other mutations. This was consistent between measurements 24 h post transfection and 42 h post transfection. Combining the Sensor 2 H623A mutation with the Walker A mutation K340A resulted in an increased amount of ASC specks, reaching a level comparable to that of the Walker A mutation by itself. This implies that either the Walker A mutation masks the effect of the Sensor 2 mutation or that NLRP1 activation by mutations of the nucleotide binding site reaches a maximum.

Altogether, nucleotide binding site variants of NLRP1 lead to hyperactivation of the protein, as determined by measuring ASC speck formation. The level of ASC specks is comparable for all variants except for the Sensor 2 variant, which showed lower hyperactivation than the other variants. Noteworthy, mutation of the conserved histidine also led to the most significant reduction in ATP hydrolysis activity (Chapter 4.2.4).

A

24 h post transfection



B

42 h post transfection

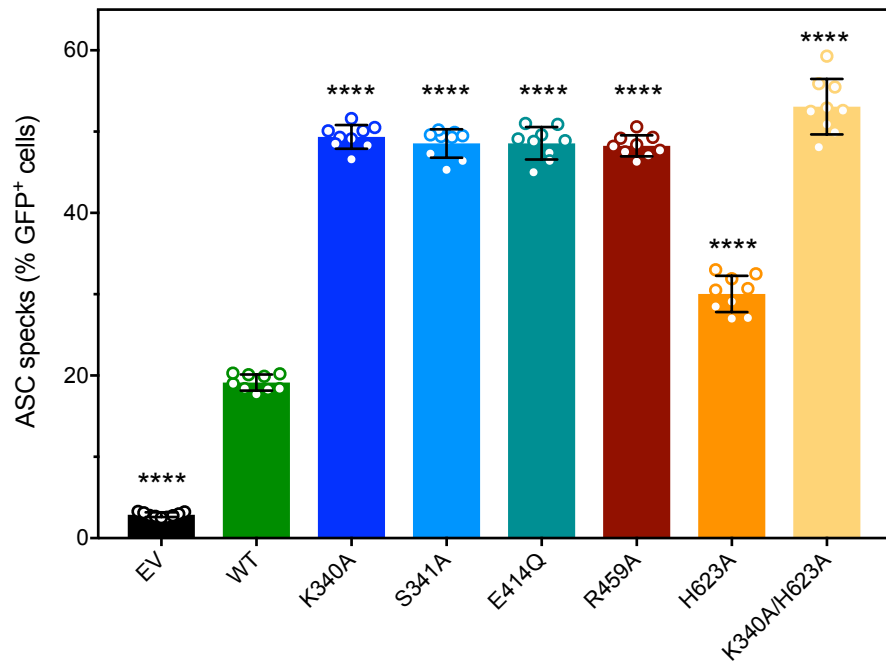


Figure 4.6: Effect of mutations in the nucleotide binding site on NLRP1 activation

ASC speck assay of WT and nucleotide binding site mutants of human NLRP1. HEK293T cells stably expressing ASC-RFP were transfected with the respective construct encoding for NLRP1 or a GFP control vector. Cells were harvested and analysed for ASC speck formation 24 h post transfection (**A**) or 42 h post transfection by flow cytometry (**B**). Graphs present pooled data of three individual experiments and are shown as mean \pm SEM. All values were compared to the WT measurement for statistical analysis using an ordinary one-way ANOVA. **** $p < 0.0001$. Representative flow cytometry plots are shown in Fig. A3.

4.2.6 Clones of THP1s harbouring the E414Q Walker B mutation show no significant spontaneous activation

To confirm the results observed in the ASC speck assay described in the previous Chapter (4.2.5), we sought to test one of the nucleotide binding site mutations in a more physiological setting. In the ASC speck assays, NLRP1 is overexpressed, therefore not mimicking a physiological cellular level of NLRP1 protein. THP1s are a human monocyte cell line that harbours endogenous NLRP1. To introduce the desired mutation a CRISPR-Cas9 based approach was taken. Single cell clones of THP1s were generated that harbour a homozygous mutation of the Walker B motif (E414Q) in their NLRP1 gene. This mutation was identified as a particularly interesting variant for two reasons. First, it is the most conservative mutation tested in this approach. Second, as mentioned above, the Walker B glutamate is described to be able to switch between an active and inactive conformation. Thus it might be directly involved in changing the overall conformation of the NLRP1 protein, affecting its activation state. As described in Chapter 4.2.5 the E414Q mutation resulted in hyperactivation of the NLRP1 protein in speck assays and is described to impair nucleotide hydrolysis but not nucleotide binding. As spontaneous activation of NLRP1 would result in activation of caspase-1 and thus in the release of mature IL-1 β and IL-18 as well as cell death, the clones were analysed for these parameters after stimulation with Pam₃CSK₄ or Talabostat. Talabostat is a DPP9 inhibitor that has been shown to induce NLRP1 activation (Zhong *et al.*, 2018). Pam₃CSK₄ directly binds TLR2 and is a known agonist, commonly used to induce expression of NLRs through activation of the NF- κ B pathway (M. S. Jin *et al.*, 2007). Treatment with DMSO served as a negative control. A combination of Pam₃CSK₄ and Nigericin served as a positive control to induce NLRP3 inflammasome activation. Nigericin is an ionophore that facilitates rapid exchange of potassium ions and protons through membranes and has been described as a potent activator of NLRP3 (Mariathasan *et al.*, 2006).

In Figure 4.7 (Experiment conducted by Pawat Laohamonthonkul) the effects of the different stimuli on NLRP1 WT, NLRP1 E414Q or NLRP1 KO clones are

summarized. For both, cell death (Figure 4.7A) and IL-18 cytokine release (Figure 4.7B), no clear trend can be observed for the E414Q clones. Clone E414Q#2 as well as clone E414Q+Pam#2 showed slightly increased levels of cell death and IL-18 when compared to the WT clones. However, the remaining two clones of the E414Q variant showed similar levels as the WT clones. This clonal variation makes a clear interpretation difficult. Furthermore, the cells did not respond to Talabostat, as all clones exhibit similar levels of cell death and IL-18 when treated with DMSO or Talabostat. The NLRP1 KO clones also show similar levels of cell death when stimulated with Pam₃CSK₄, with some clonal variation. IL-18 levels are slightly reduced for the NLRP1 KO clones compared to the WT. Taken together, the results do not indicate a role for the E414Q mutation of the Walker B motif to induce spontaneous NLRP1 activation in THP1 cells. However, clonal variation makes drawing clear conclusions from the herein presented results difficult. Additionally, supernatant IL-1 β levels were checked by ELISA. The overall results look similar to the IL-18 data and did not reveal a specific phenotype for the E414Q variant (Figure A4).

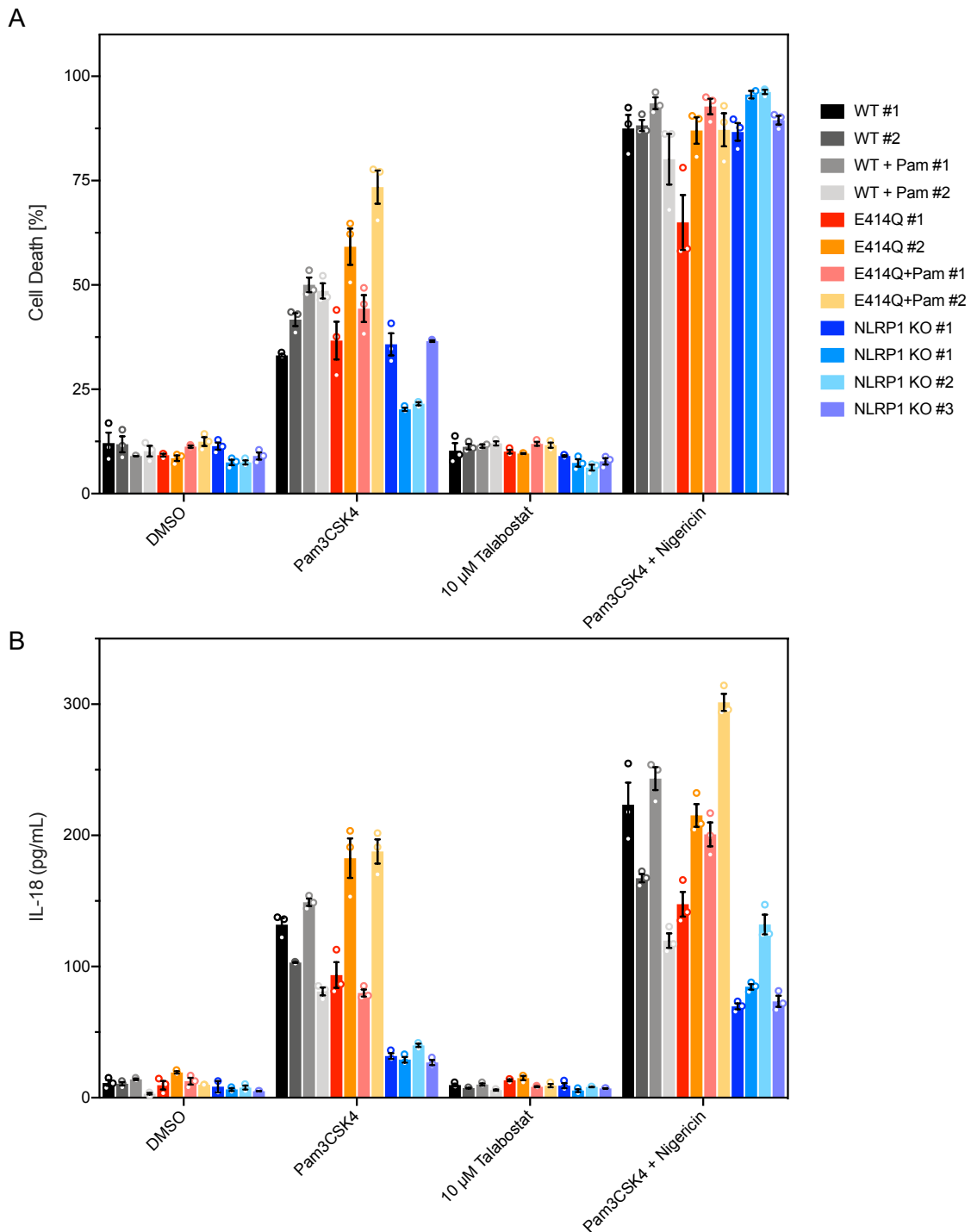


Figure 4.7: THP1 clones harbouring E414Q exhibit no spontaneous activation

(A) Clones of THP1s were treated with the indicated chemicals and analysed for cell death by PI staining. (B) The supernatant of the cells described in A was analysed for proinflammatory cytokines IL-18 by ELISA. Data is representative from two individual experiments and displayed as mean \pm SEM.

4.2.7 Mutations of the nucleotide binding site do not affect FIIND cleavage or the interaction of N- and C-terminal fragments

FIIND domain cleavage has been shown to be required for the activation of NLRP1 (Finger *et al.*, 2012). Since mutations of the nucleotide binding site led to increased activation of NLRP1 in ASC speck assays (Chapter 4.2.5), we aimed at examining whether this effect was due to a change in FIIND domain cleavage. Furthermore, the interaction of the N- and C-terminal cleavage fragments was investigated. To this end, a C-terminally FLAG-tagged NLRP1 was subjected to immunoprecipitation (IP) after overexpression in HEK293T cells (Figure 4.8A). Immunoblot of the IP samples allows both, testing the effect of mutations on FIIND domain cleavage as well as the interaction of N- and C-terminal cleavage fragments. The latter is possible as only the full-length protein or the C-terminal cleavage fragment can bind in the FLAG-IP. Therefore, the N-terminal fragment can only be detected in an immunoblot when associated with the C-terminal fragment. Using an NLRP1 antibody that binds within the N-terminal cleavage fragment, the full-length protein as well as the N-terminal fragment can be detected by immunoblotting. A FLAG antibody is used to detect the C-terminal fragment. In Figure 4.8B a representative immunoblot is shown. In this experiment a mutation identified from patients was used as a control for an activating mutation (A66V). In addition, a known variant of NLRP1, M1184V, was used as a control for a mutation inducing increased FIIND cleavage. Another mutation, S1213A, was used as a control for a mutation that abrogates FIIND cleavage. The nucleotide binding site variants of NLRP1 show similar amounts of full-length protein as well as N- and C-terminal cleavage fragments relative to the WT sample on the immunoblot. Thus, alterations of the nucleotide binding site do not affect FIIND domain cleavage or the interaction of the two cleavage fragments. Therefore, increased activity through alterations in the nucleotide binding site of NLRP1 is not caused by a change in FIIND domain cleavage or by disrupting the interaction of the cleavage fragments.

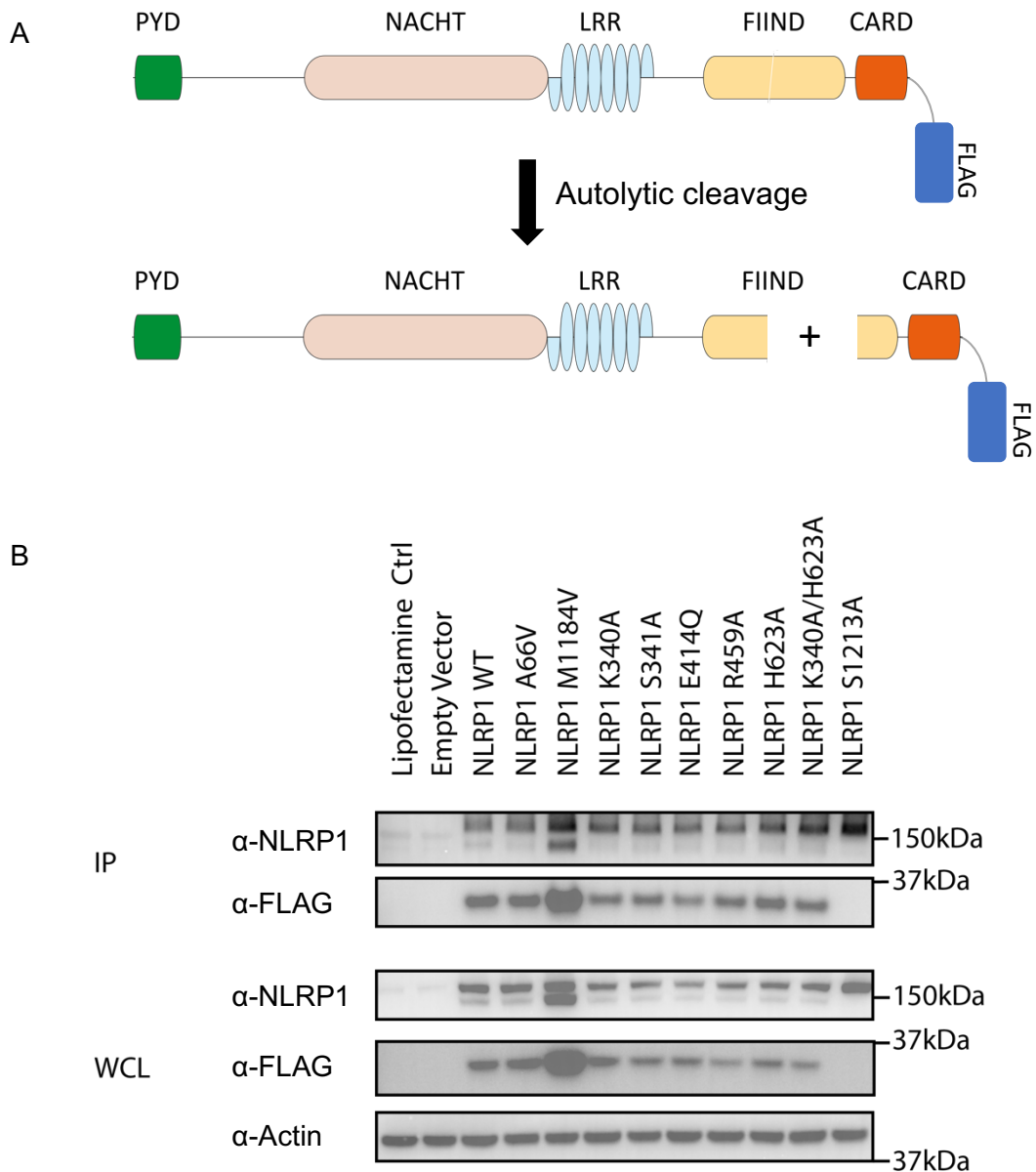


Figure 4.8: Effect of nucleotide binding site variants on FIIND cleavage

(A) Schematic of autolytic cleavage within the FIIND domain and the resulting N-terminal fragment and C-terminal fragment with the C-terminally linked FLAG-tag for immunoprecipitation. **(B)** Immunoblot of NLRP1-FLAG IP overexpressed in HEK293T cells. Different variants of NLRP1 were transfected as indicated in the blot. Cells were harvested for immunoprecipitation 24 h after transfection. NLRP1 full-length and N-terminal cleavage fragment were detected using an anti-NLRP1 antibody. C-terminal fragment was detected using an anti-FLAG antibody. The displayed blot is a representative of two individual experiments. Uncropped blots can be found in the appendix (Figure A5)

4.3 Discussion

As all NLRs, NLRP1 harbours a central NACHT domain which is described to be involved in nucleotide binding and hydrolysis as well as oligomer formation (Proell *et al.*, 2008). To date, a construct containing the NACHT and LRR domain of NLRP1 was described to bind but not hydrolyse ATP (Martino *et al.*, 2016). Using recombinant MBP-NLRP1 we were able to show for the first time that NLRP1 exhibits ATP hydrolysis activity. To further investigate the physiological relevance of this activity we first sought to identify conserved motifs required for nucleotide binding and the hydrolysis reaction. A combination of sequence alignments and structural analysis resulted in the identification of important residues within the conserved Walker A (K340, S341), Walker B (E414) and Sensor 1 (R459) motifs as well as the Sensor 2 histidine (H623). These residues were mutated in order to investigate their functional role in ATP hydrolysis and NLRP1 activity.

Most of these mutations had only minor effects on the hydrolysis activity of NLRP1. Unfortunately though, variations between measurements make it difficult to draw conclusions, as to which of these amino acids are directly involved in binding and hydrolysing ATP. Recombinant full-length MBP-NLRP1 protein was prone to unspecific oligomerization and aggregation as described in Chapter 3.2.5. This made it difficult to keep the results reproducible between different batches of protein. Variation in the ATP hydrolysis activity measured could be a result of these differences between protein batches. Therefore, further experiments comparing the activity of WT NLRP1 and nucleotide binding site variants of NLRP1 are required, to generate statistically significant data. Additionally, a high resolution structure of the full-length NLRP1 protein or the NACHT domain bound to ADP or ATP together with water molecules and a bound magnesium ion might further improve the understanding of the hydrolysis mechanism. Residues which are involved in nucleotide binding and hydrolysis could be identified and more importantly their respective role in nucleotide binding and hydrolysis could be determined.

Apart from ATP hydrolysis, a second reaction was observed in RP-HPLC experiments with MBP-NLRP1. When incubated with ADP instead of ATP, the

generation of both, AMP and ATP was detected. The interconversion of two ADP molecules to ATP and AMP as well as the reverse reaction is described for adenylate kinases. To date, now such activity is described for NLR proteins. Thus, the functional relevance of this catalytic activity is unclear and can only be speculated about. Thus far, ATP hydrolysis was described to induce a conformational change from an active, open conformation to an inactive, closed conformation (Maharana *et al.*, 2018). For instance, it could serve as a regulatory mechanism to convert from an active to an inactive state and the reverse. Since adenylate kinase activity has not been described previously for NLR proteins, a prediction of the residues involved in catalysing this reaction is difficult.

Nevertheless, the residues identified to be involved in ATP binding and hydrolysis were investigated regarding their role in NLRP1 inflammasome activation. ATP-dependent activity has been described for multiple NLR proteins including NLRP3, NLRP7, NLRP10 and NLRP12 (Duncan *et al.*, 2007; Ye *et al.*, 2008; Su *et al.*, 2013; Radian *et al.*, 2015). Formation of the active Apaf-1 apoptosome was also shown to require ATP binding (Yuanming *et al.*, 1999). Controversial findings have been reported in the literature regarding the role of nucleotides in regulating NLRP1 inflammasome activity. While some studies found that NLRP1 activity is dependent on ATP, other more recent studies found that loss of ATP binding by mutation of the Walker A motif results in constitutive or increased inflammasome activity (Faustin *et al.* 2007; Liao and Mogridge 2013; Chavarría-Smith *et al.* 2016). Furthermore, a reduction in cytosolic ATP levels was identified as an activating trigger for the mouse variant NLRP1b (Liao and Mogridge, 2013). Consistent with the more recent studies, mutation of the conserved residues within Walker A, Walker B, Sensor 1 or Sensor 2 resulted in increased activation of NLRP1 when overexpressed in HEK293T cells. One conclusion regarding the autoactivating effect of Walker A mutations stated in the literature is that NLRP1 does not require an intact Walker A motif to be activated (Chavarría-Smith *et al.*, 2016). This conclusion could now be extended to include the Walker B and Sensor 1 motif as well as the Sensor 2 histidine (H623). Furthermore, it could be assumed that a loss of ATP hydrolysis activity by mutating the nucleotide binding site leads to an activation of NLRP1. Thus,

hydrolysis activity and conformational changes depending on hydrolysis might be required for NLRP1 to adapt an autoinhibited conformation. However, the assumed loss of ATP hydrolysis by nucleotide binding site mutations was not observed in RP-HPLC based hydrolysis assays with recombinant NLRP1 and remains to be confirmed by additional hydrolysis experiments as discussed above. Also, changes in nucleotide binding and hydrolysis might not be directly linked to functionality of the protein.

Interestingly, the mutation of the Sensor 2 histidine (H623) to alanine resulted in a significantly lower increase of NLRP1 activation compared to all other mutations. Firstly, this excludes the option that any mutation within the NACHT domain has the same effect and may therefore serve as a control. Second, this result might imply a different function of this residue compared to the other residues mutated in this approach. NLRC4 also harbours a conserved histidine at the respective position. An examination of the structure of NLRC4 in its inhibited and active conformations reveals that this histidine residue is shifted away from the nucleotide binding site, probably through conformational changes in the NACHT domain (Hu *et al.*, 2013; Tenthorey *et al.*, 2017). Such conformational changes have been described for other members of the superfamily of AAA+ ATPases as well as for NLRs (Chen *et al.*, 2010; Zhang *et al.*, 2015). All other residues investigated in the mutagenesis approach reside in the nucleotide binding site in both NLRC4 structures. Thus, the conserved histidine might form a contact with ADP after ATP hydrolysis and thereby support the integrity of the autoinhibited conformation.

Moreover, it is compelling that NLRP1 NACHT seems to have a different function compared to other NLRs. As mentioned previously, formation of the NLRP3 inflammasome is dependent on ATP binding. In contrast, for NLRP1 a loss of ATP binding induced by nucleotide binding site mutations leads to activation of the inflammasome. One possible explanation could be the different domain architecture of NLRP1 compared to other members of the NLR protein family. Most importantly, the C-terminal CARD is the effector domain in NLRP1. In all other members of the NLRP family the effector domain is located at the N-terminus (Meunier and Broz, 2017). Additionally, NLRP1 undergoes autolytic

cleavage within its FIIND domain and the resulting C-terminal cleavage fragment has been shown to be sufficient for inducing ASC speck formation and IL-1 β release (Zhong *et al.*, 2016). IP and subsequent western blot analysis revealed that mutations of the nucleotide binding site do not affect FIIND domain cleavage or the interaction of the N- and C-terminal cleavage fragments (Chapter 4.2.6). Thus, the NLRP1 NACHT domain might be primarily involved in mediating the adaptation of an autoinhibited fold through conformational changes. Loss of ATP binding would prevent the NACHT domain from mediating these conformational changes and potentially destabilise the autoinhibited conformation, ultimately resulting in activation. Consistent with the finding that mutations supposed to impair ATP hydrolysis result in autoactivation of NLRP1, recently an autoactivating effect of Walker B mutations was described for NLRP3 (Coll *et al.*, 2019; Tapia-Abellán *et al.*, 2019). A similar mechanism was proposed for the plant R protein I-2, for which mutations impairing ATP hydrolysis were shown to induce autoactivation as well (Tameling *et al.*, 2006).

In the THP1 experiments, the E414Q variant of NLRP1 did not clearly show increased cell death and cytokine levels. Surprisingly, treatment with Talabostat did also not induce an increase in cell death and cytokine levels, suggesting that the THP1 system might not be suitable for NLRP1 activation assays. It should also be noted that the increase in cell death from treatment with Pam₃CSK₄ alone cannot be explained by TLR1/TLR2 activation. Thus, this experiment might need to be optimized in regards to the concentration of Pam₃CSK₄ used or the incubation time, if it was to be repeated. Since the experiments in THP1s could not confirm the findings observed in the ASC speck assay in HEK 293T cells, additional experiments are required to confirm the above stated hypothesis. A system employing cleaved IL-1 β and cleaved IL18 would be particularly helpful for this. Although, according to the manufacturer, the IL-1 β kit has a higher specificity for the mature, bioactive protein, ELISA kits are often able to detect unprocessed, inactive IL proteins. Thus, it should also be considered to do a western blot analysis to distinguish between cleaved and total IL-1 β /IL18.

Taken together, the results presented within this chapter show that recombinant NLRP1 exhibits ATP hydrolysis activity. Mutagenesis of the Walker

A, Walker B, Sensor 1 and Sensor 2 motifs led to increased inflammasome activation. Therefore, hydrolysis activity is potentially physiologically important in mediating conformational changes required for NLRP1 to adapt an autoinhibited conformation. However, in which way these mutations affect nucleotide binding and hydrolysis activity of NLRP1 remains to be elucidated in detail.

5. NLRP1 inflammasome activity is tightly regulated through diverse molecular mechanisms

5.1 Introduction

It is well described that protein activity is regulated through a large number of molecular mechanisms, including epigenetics and post-translational modifications (PTMs). For instance, modifications of histones, also referred to as the histone code, were intensively studied and the role of PTMs like acetylation, phosphorylation, methylation and ubiquitination in histone functionality has been extensively discussed in the literature (Strahl and Allis, 2000; Jenuwein and Allis, 2001). PTMs can be grouped into reversible and irreversible modifications. The addition of a chemical group (e.g. phosphorylation, acetylation) or a more complex molecule (e.g. glycosylation) to the side chain of an amino acids are usually reversible modifications. Irreversible modifications include deamidation of amino acids or proteolytic cleavage (Seo and Lee, 2004). Phosphorylation has been reported to be the most frequent PTM and can occur on serine, threonine and tyrosine residues (Khoury *et al.*, 2011). Another common PTM not as frequent as phosphorylation is proteolytic cleavage. Many proteins, especially proteases, are known to be expressed and translated as inactive zymogens and require proteolytic cleavage by another protein to become active (Khan and James, 2008). The pro-inflammatory caspase-1 is also expressed as a zymogen, Procaspase-1 (Elliott *et al.*, 2009). As a special case of proteolytic activation, so called autolysis, has been reported for a significant number of proteins (Perler *et al.*, 1997). Here, autolysis means that the proteolytic cleavage is catalysed through residues within the molecule itself. A well-studied example for this rare case of a PTM is p53-induced protein with a death domain (PIDD). PIDD undergoes autolytic cleavage at two different sites and the occurrence of autolysis determines the outcome of its signalling activity, ultimately resulting in cell survival or apoptosis. A non-cleavable variant of PIDD has been shown to be unable to become active (Tinel *et al.*, 2007).

NLRP1 was the first NLR protein described to form an inflammasome (Martinon *et al.*, 2001). To date, autoproteolysis within the FIIND domain of NLRP1 is the only post-translational mechanism regulating NLRP1 activity (Baker *et al.*, 2017). Autolytic cleavage was identified as a major modification of the mature NLRP1 protein and is a strict requirement for activation (D’Osueldo *et al.*, 2011; Finger *et al.*, 2012). However, cleavage does not result in activation by itself but requires an additional activating stimulus. Furthermore, the N- and C-terminal fragments remain associated after processing of the FIIND domain (Finger *et al.*, 2012). Apart from the residues comprising the cleavage site (S1211, F1212 and S1213) a conserved histidine residue was identified to be essential for proteolysis (Finger *et al.*, 2012). H1186 is described to initiate cleavage by deprotonating the hydroxyl group of S1213. Substituting any of these residues individually for an alanine results in loss of autolytic cleavage and consequently loss of NLRP1 inflammasome activity (Finger *et al.*, 2012). A common polymorphism of human NLRP1, M1184V (rs11651270), has been shown to be associated with multiple diseases, like vitiligo associated autoimmunity, asthma and breast cancer (Gao *et al.*, 2012; Levandowski *et al.*, 2013; Leal *et al.*, 2018). Interestingly, this polymorphism has been described to increase proteolysis within the FIIND domain and was linked to increased NLRP1 activity (Finger *et al.*, 2012).

Another proteolytic mechanism was described to activate rodent versions of NLRP1 (Hellmich *et al.*, 2012; Levinsohn *et al.*, 2012). For instance, murine NLRP1b can be cleaved by anthrax lethal toxin within the N-terminal part of the protein leading to activation of the inflammasome (Hellmich *et al.*, 2012; Chavarría-Smith and Vance, 2013). Anthrax lethal toxin does not activate human NLRP1. However, proteolytic cleavage of a human NLRP1 variant modified to contain a TEV cleavage site between its PYD and NACHT domain was also shown to be activated by proteolytic cleavage at the inserted TEV site (Chavarría-Smith *et al.*, 2016). Consistent with that finding, several mutations identified from patients with NLRP1 associated autoimmune syndromes are located within the PYD and have been shown to destabilize the six helix bundle fold of the PYD. This conformational destabilization of the N-terminus also results in

hyperactivation of human NLRP1 (Zhong *et al.*, 2016). In accordance with this, a recent study investigated if N-terminal degradation could be a general mechanism for the activation of NLRP1 (Sandstrom *et al.*, 2019). Indeed it was reported that IpaH7.8, an E3 ubiquitin ligase of the pathogenic bacterium *Shigella flexneri*, induces activation of mouse NLRP1b by degradation of the N-terminal cleavage fragment and subsequent release of the active C-terminal fragment (Sandstrom *et al.*, 2019). A different study described that inhibition of dipeptidyl peptidase 9 (DPP9) by Talabostat resulted in degradation of NLRP1b as well. Dipeptidyl peptidases are a class of regulatory proteins that is described to cleave off dipeptides from the N-terminus of proteins. The DPP9 protein had previously been identified to negatively regulate NLRP1 activity in both humans and mice by binding to the FIIND domain. Inhibition of DPP9 with various inhibitors like Talabostat was described to induce activation of NLRP1 (Okondo *et al.*, 2018; Zhong *et al.*, 2018). Further, three N-end rule proteins, UBR2, UBR4 and UBA6 were shown to be involved in directing NLRP1b to the proteasome (Chui *et al.*, 2019). The activating effect of anthrax lethal toxin and Talabostat was successfully reversed by proteasome inhibitors (Chui *et al.*, 2019; Sandstrom *et al.*, 2019).

Apart from the two mechanisms described above, no other PTMs have been described for NLRP1. Since NLRP1 is a large multidomain protein it is likely that it is regulated by other PTMs like phosphorylation. Such regulating mechanisms have been described for other NLR proteins like NLRP3. Here a phosphorylation within the PYD was described to regulate inflammasome activity by blocking PYD-PYD interactions (Stutz *et al.*, 2017). Other phosphorylation sites (S198, S295, Y861) located in the NACHT and LRR domains of NLRP3 were shown to be involved in regulating inflammasome activity as well (Song and Li, 2018). Phosphorylation was further shown to be involved in ASC speck formation. Loss of phosphorylation at residue Y146 in the CARD domain of the human ASC protein has been described to impair speck formation and thus caspase-1 activation (Hara *et al.*, 2013; Chung *et al.*, 2016). More recently, the phosphorylation status of two other tyrosine residues (Y60, Y137) of human ASC

has been reported to play an important role for ASC function (Mambwe *et al.*, 2019).

This part of the project aimed to further investigate how autolytic cleavage in the FIIND domain as a crucial PTM regulates NLRP1 activity. To this end, the polymorphism M1184V was tested regarding its effect on different activating stimuli for NLRP1. Furthermore, a potential phosphorylation site was identified in the NLRP1 CARD domain and investigated by a mutagenesis approach. Additionally, a screening of inhibitors targeting different tyrosine kinases was performed in BMDMs to potentially identify kinases regulating NLRP1 activity.

5.2 Results

5.2.1 Computational analysis of the NLRP1 polymorphism M1184V

The polymorphism M1184V has been described to be associated with multiple autoimmune syndromes (Levandowski *et al.*, 2013). To investigate how conserved this residue is in different species, a multiple sequence alignment was performed using the Clustal Omega online tool (Madeira *et al.*, 2019). In Figure 5.1A the part of this alignment containing the residue of interest is shown. Interestingly, it was found that only in the human version of NLRP1 a methionine residue is present in position 1184. In other primates and rodents the according residue was found to be a valine. In *Ophiophagus Hannah*, a lizard species, the valine residue is also conserved. Only in *Danio rerio*, a zebrafish species, the valine is not present and instead a leucine residue is found in the corresponding position. Of note, *Danio rerio* is also the only species in this alignment in which the histidine residue shown to initiate autolytic cleavage (H1186 in human NLRP1) is not conserved (Finger *et al.*, 2012). This raises the question, why human NLRP1 has evolved to contain a methionine instead of a valine in position 1184. To further investigate this, a computational structural assessment of the FIIND cleavage site was carried out and functional assays were performed *in vitro* (Chapter 5.2.2).

The presence of a valine in position 1184 has been reported to increase the autolytic cleavage in human NLRP1 (Finger *et al.*, 2012). To investigate the molecular basis for that increase in cleavage, a structural assessment of the cleavage site was performed. Since there is no structure available of the FIIND domain, a homology model was generated using a SWISS Model approach (Waterhouse *et al.*, 2018). In the according alignment the best match was found with the structure of the cytoplasmic domain of Unc5b, which showed 15 % sequence identity with NLRP1 (residues 1081-1380). The cytoplasmic domain of Unc5b consists of a ZU5-UPA domain tandem similar to the NLRP1 FIIND domain and was therefore an appropriate candidate for the generation of a homology model. The resulting structural model contains the entire ZU5 domain

including the cleavage site and only part of the UPA domain. The ZU5 domain forms a β -sheet sandwich with the cleavage site located in a loop between two β -sheets. The side chain of histidine 1186 is only 4.6 Å away from the reactive oxygen of serine 1213 (Figure 5.1B, bottom panel). This could support the proposed involvement of this histidine residue in deprotonating serine 1213 to initiate the cleavage. Furthermore, the side chain of methionine 1184 is located in close proximity to histidine 1186. However, it is not obstructing the interaction of histidine 1186 and serine 1213 structurally, as it is located on the opposite side of H1186. An exchange of methionine for valine in position 1184 would not introduce a significant change in electrostatics, since the side chain of both amino acids is aliphatic. Nevertheless, such an exchange would remove the S-methyl thioether present in the side chain of methionine and not in valine. The S-methyl thioether of methionine has been reported to be involved in cation- π interactions (Imai *et al.*, 2007). If such an interaction occurs between M1184 and H1186 it could affect the potential of the histidine to deprotonate S1213 and thereby inhibit autolytic cleavage in the FIIND domain. Moreover, a change from methionine to valine could open up space for water molecules potentially involved in catalysing autoproteolysis. However, these hypotheses are solely based on a homology model and the exact mechanism by which M1184 reduces cleavage of the FIIND domain remains to be clarified.

A

Lizard	{	Ophiophagus hannah	HTLCLNDQLSE--KAFK V FHFKKNCPFEFEGS	183
Zebrafish	{	Danio rerio	HYMCLAESDPALTNAVK L LSVEDEGISLESV	1095
		Rattus norvegicus	HFVSLQEGKVD-SSLF H VAHFQDHGMVLETP	953
Rodents	{	Mus musculus (a)	HFVALQEGIVD-SSLF H VAHFQEHGMVLETP	917
		Mus musculus (b1)	HFVSLKDTKAS-TDFDK V AHFQEHGMVLETP	968
		Microcebus murinus	HFVDLQGGHVD-ISLF Q VAHFKKEGMLLEKP	1147
		Aotus nancymae	HFVALQGGHMD-TSLF Q VAHFKEEGMLLEKP	1276
		Cebus capucinus im.	HFVALQGGHID-TSLF Q VAHFKEEGMLLEKP	1174
		Theropithecus gelada	HFVALQGGHVD-TSLF Q VAHFKEEGMLLEKP	1208
		Papio anubis	HFVALQGGHVD-TSLF Q VAHFKEEGMLLEKP	1260
Primates		Macaca nemestrina	HFVALQGGHVD-TSLF Q VAHFKEEGMLLEKP	1213
		Macaca mulatta	HFVALQGGHVD-TSLF Q VAHFKEEGMLLEKP	1199
		Pongo abelii	HFVALQGGHVD-TSLF Q VAHFKEEGMLLEKP	1196
		Homo sapiens	HFVALQGGHVD-TSLF Q MAHFKEEGMLLEKP	1197
		Pan troglodytes	HFVALQGGHVD-TSLF Q VAHFKEEGMLLEKP	1214
		Pan paniscus	HFVALQGGHVD-TSLF Q VAHFKEEGMLLEKP	1199
			* : * . . . : : *	

B

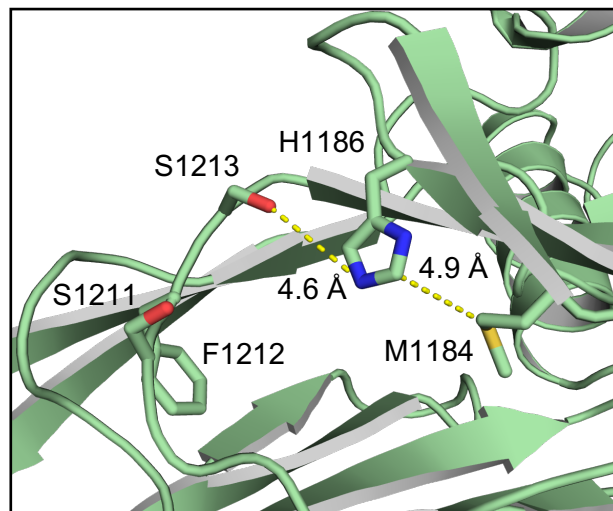
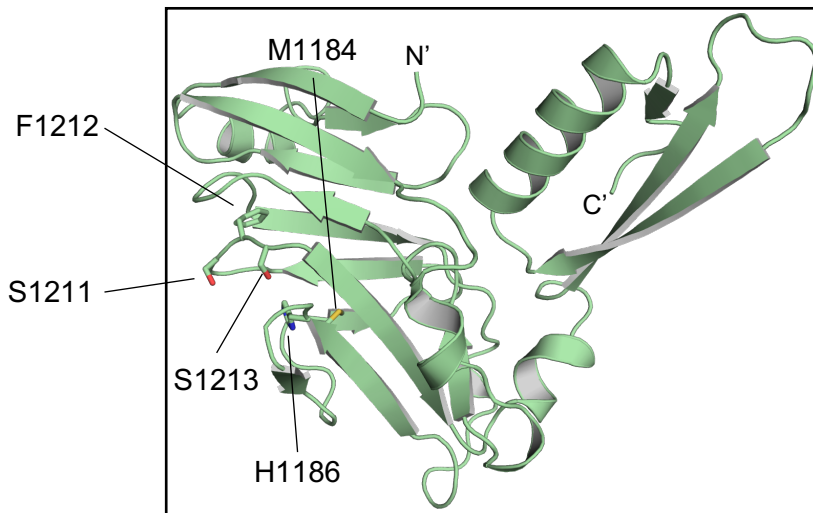


Figure 5.1: Computational analysis of the human NLRP1 FIIND domain

(A) Sequence alignment of the amino acid sequence of NLRP1 from different organisms. Sequences were taken from NCBI. Multiple sequence alignment was performed using the Clustal Omega online tool with default settings (Madeira *et al.*, 2019). Only part of the alignment is shown. Methionine 1184 in human NLRP1 and corresponding residues in other species are highlighted. **(B)** Homology modelling of the NLRP1 FIIND domain (residues 1084-1278). The homology model was generated using Swiss Model (Waterhouse *et al.*, 2018). Images and distance measurements were generated using PyMOL.

5.2.2 Effect of increased FIIND cleavage on NLRP1 activation

To investigate the effect of the M1184V polymorphism and the resulting increase in FIIND domain cleavage on NLRP1 activation, the *in vitro* ASC speck assay in HEK293T cells was utilised. First, the effect of the polymorphism was investigated in the context of NLRP1 activation by destabilization of the N-terminus. This stimulus for activation was mimicked by introducing the A66V mutation, which was found in patients presenting with NLRP1-associated autoimmunity and which has been described to induce spontaneous activation of NLRP1 (Zhong *et al.*, 2016).

ASC speck formation was measured 24 h and 42 h post transfection by flow cytometry. Consistent with previous findings, the A66V patient mutation induced increased activation of NLRP1, as reflected in the increased frequency of ASC specks (Figure 5.2). In contrast, the M1184V polymorphism does not induce spontaneous activation of NLRP1. Instead, it displays a similar frequency of ASC specks as WT NLRP1 after 24 h (Figure 5.2A). For the 42 h timepoint, a slightly lower frequency of ASC specks can be observed for M1184V compared to WT NLRP1 (Figure 5.2B). This might indicate an inhibitory effect of M1184V on spontaneous activation of NLRP1. Of note, this is in conflict with a study that described M1184V to not only induce increased cleavage in the FIIND domain but also increased NLRP1 activity, as determined by measuring IL-1 β levels in a reconstituted overexpression system in HEK293T cells (Finger *et al.*, 2012). Interestingly, when NLRP1 was activated by a destabilised N-terminus (A66V), the polymorphism significantly increased the amount of ASC specks. This suggested a synergistic effect for the combination of a destabilised N-terminus and an increase in FIIND domain cleavage (M1184V). Although significantly less pronounced, this effect was still observed after 42 h (Figure 5.2B).

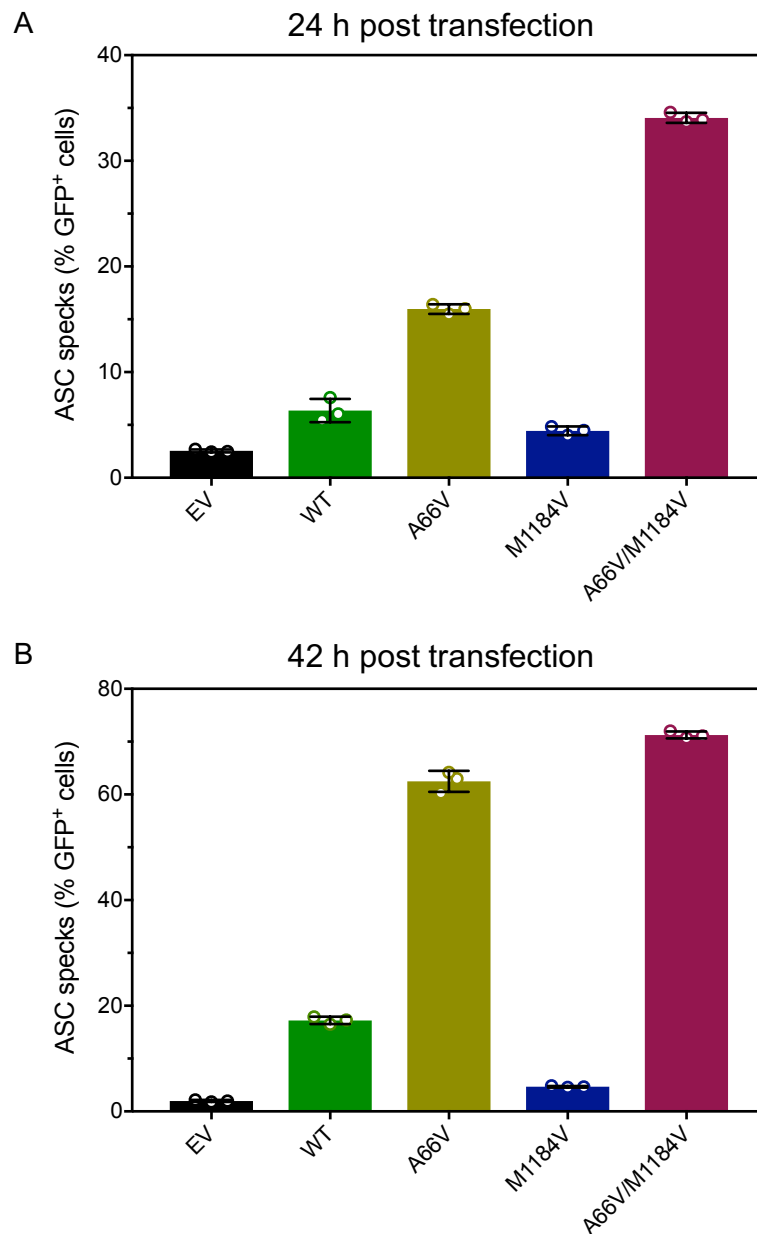


Figure 5.2: Effect of M1184V on NLRP1 activation by destabilization of the N-terminus

HEK293T cells stably expressing ASC-RFP were transfected with WT or mutant NLRP1 or a vector control (EV) and analysed for ASC formation 24 h (**A**) and 42 h (**B**) post transfection by flow cytometry. Samples were recorded in triplicates. Data was analysed in FlowJo and graphed in Prism. Data shown is a representative of two individual experiments and is graphed as mean \pm SEM. Representative flow cytometry plots are shown in Fig. A6.

To further investigate whether M1184V leads to increased speck formation upon activation of NLRP1 in the context of other activating stimuli, activation of NLRP1 by Talabostat was also investigated (Figure 5.3). Talabostat leads to activation of NLRP1 by inhibiting the negative regulator DPP9. DPP9 has been described to bind NLRP1 within its FIIND domain, assisting in keeping it in an autoinhibited conformation (Zhong *et al.*, 2018). Therefore, it was assumed that activation through Talabostat is a different mechanism than activation through destabilizing the N-terminus. This was also reflected in the results of the according ASC speck assay. Incubation of NLRP1 WT with Talabostat for 6 h (Figure 5.3A) or 24 h (Figure 5.3B) lead to a significant increase in the frequency of ASC specks recorded. Compellingly, M1184V seemed to have an inhibitory effect on NLRP1 activity, when stimulated only with Talabostat, as this variant shows a lower frequency of ASC specks compared to WT NLRP1 stimulated with Talabostat (Figure 5.3A). These results further supported the hypothesis that a destabilisation of the N-terminus (A66V) and loss of DPP9 binding (Talabostat) are two different mechanisms of NLRP1 activation. Destabilising the N-terminus synergises with increased FIIND cleavage induced by the M1184V polymorphism, while a loss of DPP9 binding does not. This effect was also observed for the later timepoint although being significantly less pronounced (Figure 5.3B). Even though the difference between the two samples is only marginal, it was consistent between experiments for the 24 h timepoint.

The S1213A mutation is located within the FIIND domain cleavage site. This variant served as a control for a non-cleavable and thus non-activatable variant of NLRP1. Indeed, this variant was not activated when stimulated with Talabostat for 6 h or 24 h (Figure 5.3A and B).

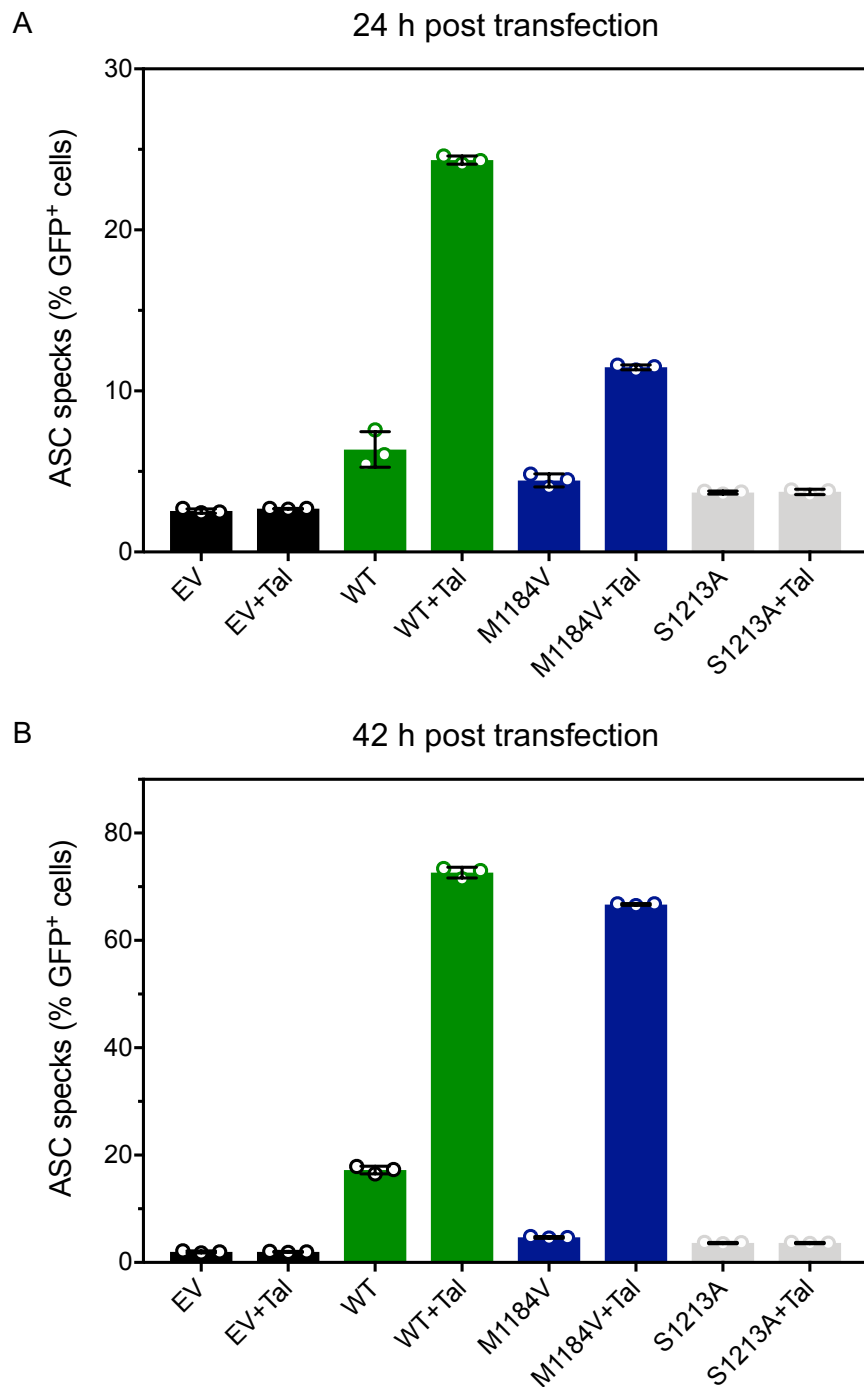
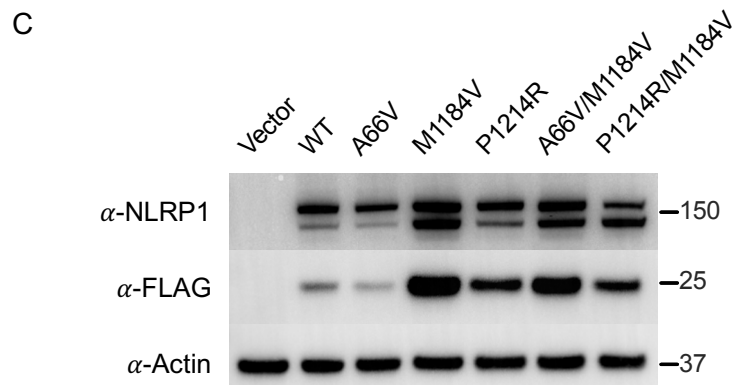
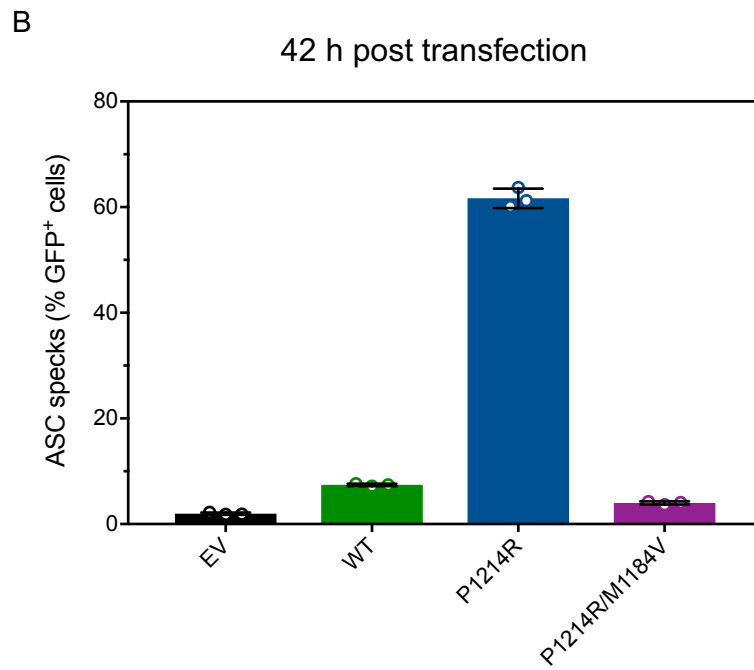
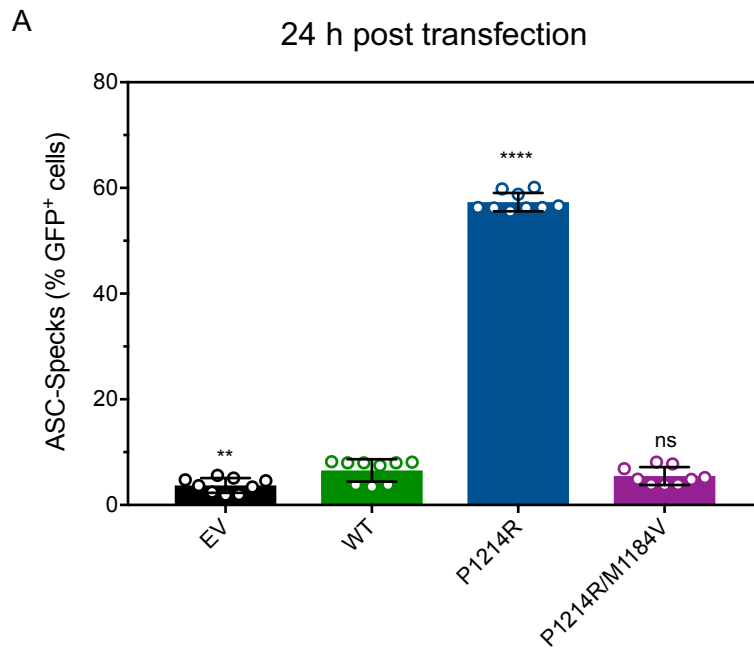


Figure 5.3: Activation of NLRP1 by Talabostat is delayed by M1184V

HEK293T cells stably expressing ASC-RFP were transfected with WT or mutant NLRP1 or a vector control (EV) and analysed for ASC formation 24 h (**A**) and 42 h (**B**) post transfection by flow cytometry. Cells were treated with 2 μ M Talabostat 18 h post transfection. Samples were recorded in triplicates. Data was analysed in FlowJo and graphed in Prism. Data shown is a representative of two individual experiments and is graphed as mean \pm SEM. Representative flow cytometry plots are shown in Fig. A7.

To confirm the inhibitory effect that M1184V had on NLRP1 activation in the context of DPP9 inhibition, a different NLRP1 variant, the P1214R patient mutation, was introduced into the NLRP1 expression vector. The mutation P1214R was reported to trigger spontaneous activation of NLRP1 by inhibiting DPP9 binding (Grandemange *et al.*, 2017; Zhong *et al.*, 2018). Thus, we hypothesized that P1214R activates NLRP1 by a mechanism comparable to Talabostat.

Again, the effect of P1214R on NLRP1 activation in the context of increased FIIND cleavage was investigated in regards to ASC speck formation 24 h and 42 h post transfection (Figure 5.4). As expected, P1214R mutation of NLRP1 led to strong spontaneous activation as reflected in the increased frequency of ASC specks. Strikingly, activation of NLRP1 by P1214R was inhibited when combined with the M1184V polymorphism, reflected in a reduced frequency of ASC specks compared to P1214R alone. In contrast to activation with Talabostat (Figure 5.3B), the inhibitory effect of M1184V on NLRP1 activation by P1214R was still clearly observable for the later timepoint (Figure 5.4B). Furthermore, treating cells transiently expressing the P1214R variant with Talabostat did not lead to an additional increase in the level of ASC specks. In contrast, treatment of cells expressing the A66V variant with Talabostat resulted in an additional significant increase in ASC specks (Appendix, Figure A8). This further supports the hypothesis that destabilization of the N-terminus (A66V mutation) and inhibition of DPP9 (Talabostat, P1214R) are two different mechanisms of NLRP1 activation.



Results

Figure 5.4: P1214R induces NLRP1 activation similar to Talabostat

HEK293T cells stably expressing ASC-RFP were transfected with WT or mutant NLRP1 or a vector control (EV) and analysed for ASC formation 24 h **(A)** and 42 h **(B)** post transfection by flow cytometry. Cells were treated with 2 μ M Talabostat 18 h post transfection. Samples were recorded in triplicate. Data was analysed in FlowJo and graphed in Prism. Data shown is pooled from three individual experiments (24 h) or from one individual experiment (42h). Graphs show the mean \pm SEM. All values were compared to the WT measurement for statistical analysis using an ordinary one-way ANOVA. ns: non-significant; * $p < 0.05$; *** $p < 0.001$; **** $p < 0.0001$ **(C)** Expression levels of different NLRP1 variants were monitored by immunoblot. The full-length protein as well as N-terminal cleavage fragment were probed by using an NLRP1 antibody specifically binding to the N-terminal part of the protein. The C-terminal fragment was probed for with a FLAG antibody. (Experiments were carried out by Pawat Laohamonthonkul)

Similar expression levels were confirmed by western blot of the different variants of NLRP1, as reported in Figure 5.4C. Only expression of the M1184V variant was slightly increased compared to WT NLRP1. Although baseline levels were increased, the western blot indicated increased FIIND cleavage for the M1184V variant. Interestingly, P1214R showed higher levels of the C-terminal cleavage fragment compared to the WT protein even without M1184V. Increased FIIND processing was observed for the M1184V/P1214R variant when probing for the full-length and N-terminal cleavage fragment. However, the level of C-terminal fragment remained unchanged when combining M1184V and P1214R. For the A66V/M1184V double mutation both, the N- and C-terminal fragment is increased compared to A66V alone.

5.2.3 Investigation of a potential phosphorylation site in NLRP1 CARD

As described above, thus far FIIND domain cleavage is the only PTM described to regulate NLRP1 activity. However, in a manuscript uploaded to the preprint server BioRxiv (<https://biorxiv.org/>) a conserved tyrosine residue within the NLRP1 CARD was described to be potentially phosphorylated (Boyle and Monie, 2016). The conserved amino acid motif follows the pattern EQYE in the NLRP1 CARD. Similar motifs with a tyrosine residue were identified in the inflammasome adaptor ASC and the receptor-interacting protein kinase 2 (RIPK2). Of note, tyrosine phosphorylation in this position was described to be essential for the effector function of both ASC and RIPK2 (Tigno-Aranjuez *et al.*, 2010; Chung *et al.*, 2016). To investigate whether the respective tyrosine residue, Y1413, is of importance for NLRP1 activity, an ASC speck assay was carried out. The activity of NLRP1 WT upon activation by Talabostat or an autoactivating mutation (E414Q, Chapter 4.2.5) was compared to NLRP1 with tyrosine 1413 substituted for phenylalanine (Y1413F). Tyrosine and phenylalanine have very similar side chains, with the latter only lacking the hydroxyl group compared to tyrosine, which is why this substitution was considered the most conservative alternative. Compellingly, a substitution of Y1413 resulted in a complete loss of NLRP1 activity, as determined by the frequency of ASC specks (Figure 5.5A and B).

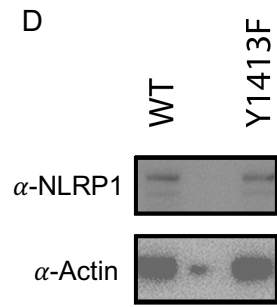
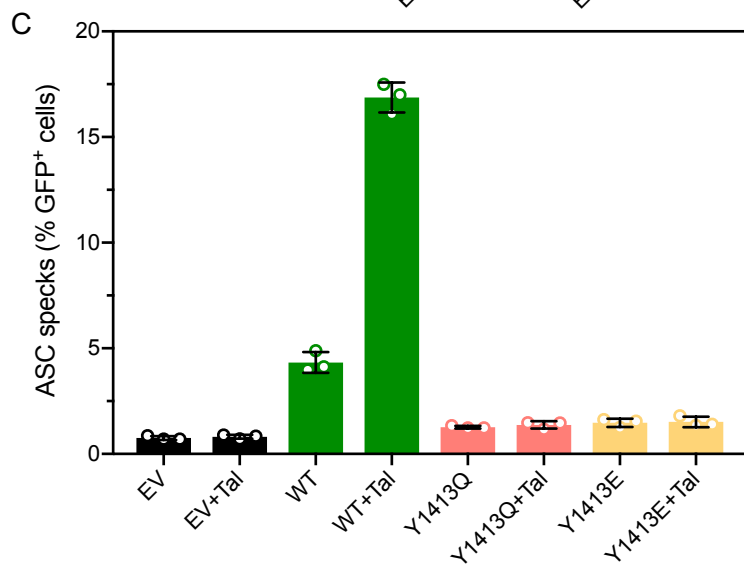
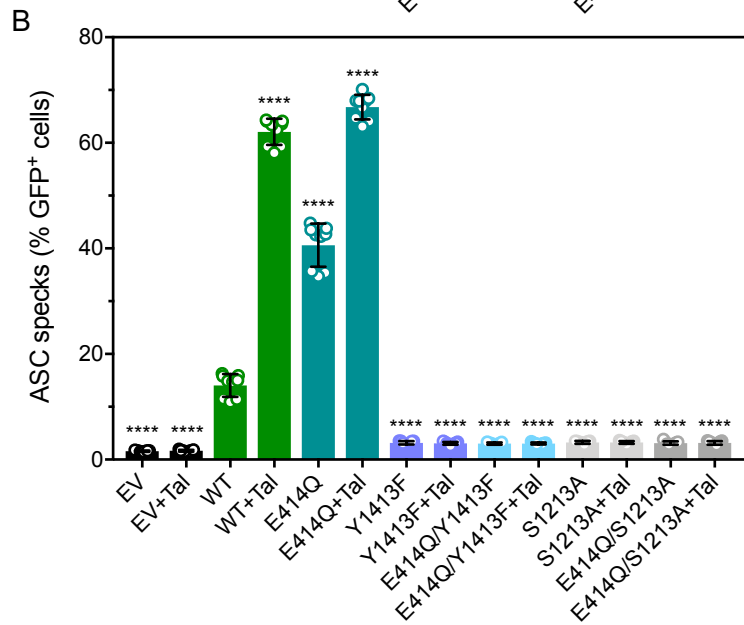
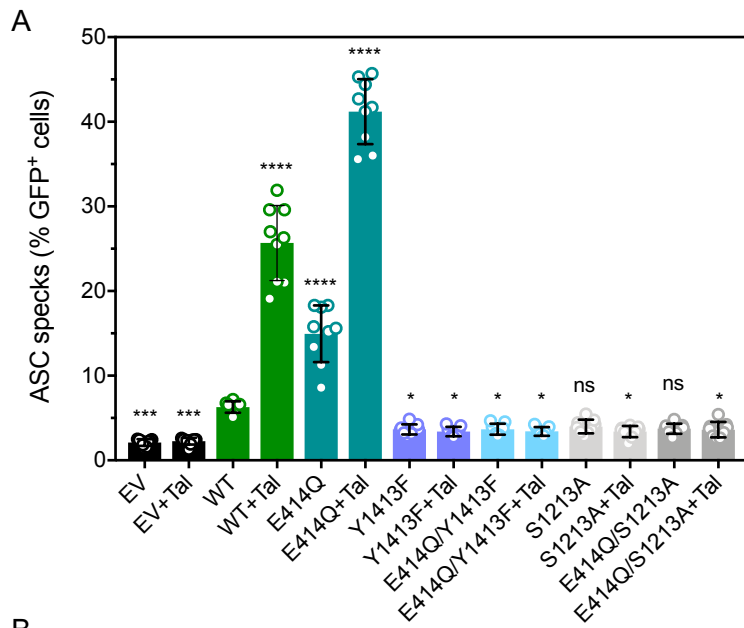


Figure 5.5: Substitution of Y1413 impairs NLRP1 activity

HEK293T cells stably expressing ASC-RFP were transfected with WT or mutant NLRP1 or a vector control (EV) and analysed for ASC speck formation 24 h (**A**, **C**) and 42 h (**B**) post transfection by flow cytometry. Cells were treated with 2 μ M Talabostat 18 h post transfection. Samples were recorded in triplicate. Data was analysed in FlowJo and graphed in Prism. For A and B graphs present pooled data of three individual experiments and are shown as mean \pm SEM. All values were compared to the WT measurement for statistical analysis using an ordinary one-way ANOVA. ns: non-significant; * $p < 0.05$; *** $p < 0.001$; **** $p < 0.0001$. Data shown in C is from one experiment. (**D**) Expression of NLRP1 WT and NLRP1 Y1413F was monitored by immunoblot. The full-length protein as well as N-terminal cleavage fragment were probed by using an NLRP1 antibody specifically binding to the N-terminal part of the protein. Samples were taken from lysates prepared from cells treated similar to cells used in the ASC speck assay. Representative flow cytometry plots and uncropped blots can be found in the appendix (Fig. A9 and A10).

Similar expression of the NLRP1 WT and NLRP1 Y1413F was confirmed by western blot (Figure 5.5D). Even when combining both activating stimuli the amount of ASC specks did not increase. This was consistent for both timepoints measured. The S1213A mutation abrogating FIIND domain processing served as a negative control for NLRP1 activation. As expected this variant was also not activated by Talabostat, the E414Q autoactivating mutation or the combination of both.

To ensure that the impairment of the NLRP1-ASC interaction is not just due to the hydrophobicity of the phenylalanine, Y1413 was also substituted for glutamate (Y1413E) or glutamine (Y1413Q). Y1413E was chosen as a substitution to potentially mimic phosphorylation by adding a negative charge. Y1413Q was chosen as the equivalent substitution to Y1413E but without the negative charge. Interestingly, both variants could not be activated with Talabostat.

Assuming that NLRP1 activation is directly dependent on Y1413 phosphorylation and that the Y1413E mutation is effectively mimicking this phosphorylation, increased ASC speck formation would be expected for this variant. To further investigate this, the structure of the NLRP1 CARD (PDB: 3KAT, Figure 5.6A) was analysed by implementing Y1413 phosphorylation and Y1413E substitution using PyMOL (Figure 5.6B and C). The structure itself reveals that Y1413 is surrounded by residues forming a negatively charged surface (E1397, D1401, E1414). When comparing the unphosphorylated with the phosphorylated state, it became evident that by phosphorylation not only two negative charges were added to the surface of the CARD domain, but also that the surface of the CARD domain was expanded (Figure 5.6A and B). This illustrates how a phosphorylation of Y1413 could be involved in facilitating an interaction with ASC. Furthermore, the insertion of Y1413E substitution into the NLRP1 CARD structure revealed that the glutamate cannot effectively mimic phosphorylation (Figure 5.6C). Although it introduced a negative charge similar to a phosphorylation, it does not reach out and expand the surface of the CARD as phosphorylation of the tyrosine would (Figure 5.6B and C). Implementing all the above mentioned substitutions also revealed that these amino acids should

not impair the conformation of NLRP1 CARD. Mutagenesis in PyMOL resulted in well suited rotamers without any steric hindrance. Still, this modelling is no evidence for the NLRP1 CARD folding correctly when containing either of the three different substitutions (F, E, Q) at position 1413.

Overall, the data herein suggest that Y1413 is important in mediating the interaction of NLRP1 CARD and ASC CARD. Further structural assessment of recombinant NLRP1 CARD harbouring the aforementioned substitutions is required to reveal, whether the structural integrity of the domain is compromised by introducing different amino acids in this position.

Since phosphorylation of NLRP1 cannot be effectively mimicked by an amino acid substitution, a different approach was taken to investigate the hypothesis of Y1413 phosphorylation. In this approach, an array of tyrosine protein kinase inhibitors was tested in combination with Talabostat on BMDMs. If phosphorylation of tyrosine 1413 is required for the interaction with ASC and therefore NLRP1 activity, inhibition of the kinase responsible for phosphorylating this residue should also inhibit NLRP1 activity. As a readout, IL-1 β release into the cell culture supernatant was measured by ELISA 24 h after LPS stimulation and subsequent treatment with Talabostat and a tyrosine protein kinase inhibitor. The results are visualized in Figure 5.7. For some of the inhibitors measured, large error bars indicate a strong variation in the duplicates measured in this experiment. However, it is still clear that most of them have either no effect or even increase cytokine levels. Only one of the tested inhibitors significantly decreased the amount of IL-1 β to the level of the LPS and DMSO control. Inhibitor number 15 (TAK165 or Mubritinib) is an inhibitor for the protein kinase human epidermal growth factor receptor 2 (HER2).

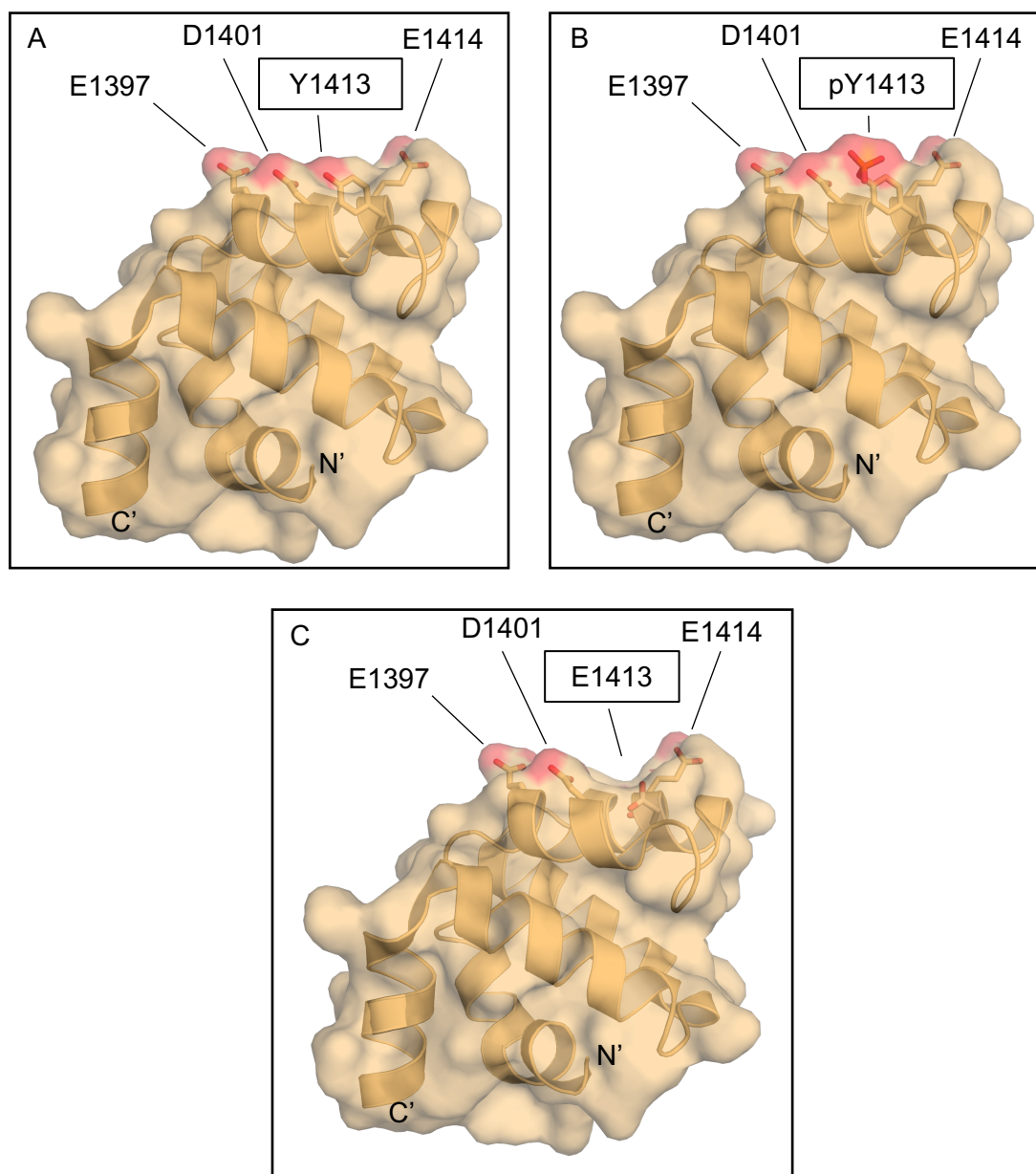


Figure 5.6: Structural analysis of Y1413 in NLRP1 CARD

Structure of the NLRP1 CARD in cartoon and surface representation. Side chains of residues E1397, D1401, E1414 and Y1413 **(A)** phospho-Y1413 **(B)** or E1413 **(C)** are shown in stick representation. The PTM was added using the Pytms plugin of PyMOL. The Y1413E substitution was generated using the mutagenesis wizard in PyMOL. Red colour in stick representation indicates oxygen atoms and orange colour represents phosphorus atoms.

To confirm that this protein tyrosine kinase is involved in regulating NLRP1 activity, another ASC speck assay was carried out. NLRP1 was activated by treatment with 2 μ M Talabostat or destabilisation of the N-terminus (A66V). Additionally, the medium was supplemented with different concentrations of TAK165 to inhibit HER2. Unfortunately, no inhibitory effect of the HER2 inhibitor was observed in this experiment (Figure 5.7B), indicating that this kinase might not directly phosphorylate the NLRP1 CARD domain. Thus, the question whether NLRP1 Y1413 is directly phosphorylated remains yet to be elucidated. Still, the herein presented data demonstrate that Y1413 is of importance for the interaction with ASC, since substitution of this residue for phenylalanine, glutamine or glutamate resulted in a complete loss of ASC speck formation.

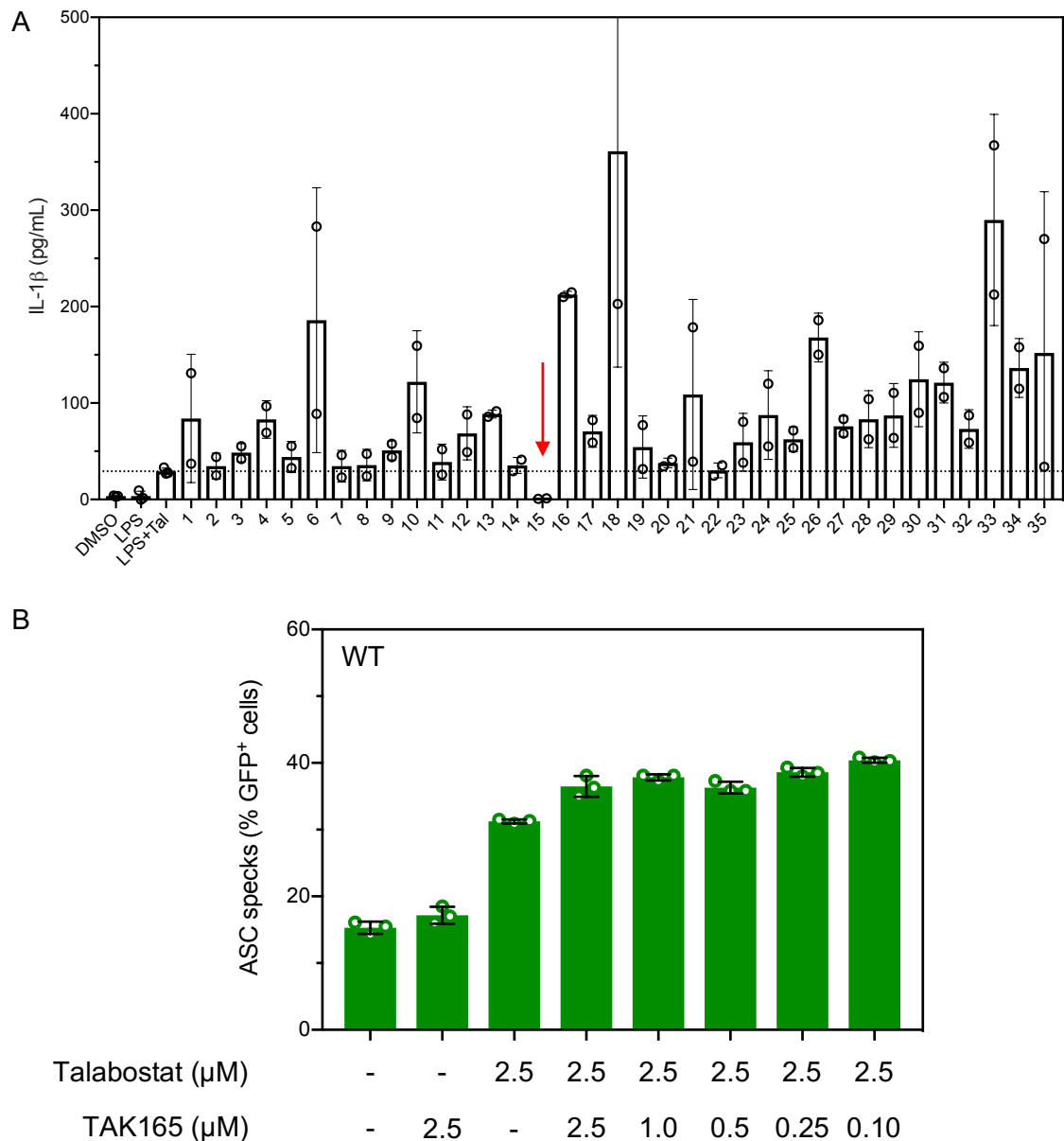


Figure 5.7: Screening for tyrosine kinase inhibitors of NLRP1 activity

(A) Screening of tyrosine protein kinase inhibitors and their effect on IL-1 β production upon activation of NLRP1. BMDMs were stimulated with LPS (200 ng/ μL) for 3 h. Afterwards BMDMs were treated with Talabostat (2.5 μM) and different inhibitors (5 μM) for 24 h before analysing the supernatant for IL-1 β . Dashed line indicates level of activation in positive control. Data shown is from one experiment. **(B):** ASC speck assay with NLRP1 WT. Cells were treated 18 h post transfection with Talabostat (2 μM) for 1 h before supplementation with TAK165 at different concentrations. Cells were incubated for 6 h before analysis for ASC speck formation by flow cytometry. Data shown is representative from two individual experiments (repeat performed by Pawat Laohamonthonkul). Representative flow cytometry plots are shown in Fig. A11.

5.3 Discussion

The activity of several inflammasomal proteins such as NLRP3, NLRC4 and ASC is regulated by a multitude of PTMs (Yang *et al.*, 2017). For instance, the activity of NLRP3 depends on both phosphorylation and deubiquitination (Py *et al.*, 2013; Stutz *et al.*, 2017). Therefore, it is likely that the activity of NLRP1 is regulated through multiple PTMs as well.

The first PTM reported for NLRP1 was proteolytic cleavage within the FIIND domain (Finger *et al.*, 2012). This processing was described to be essential for NLRP1 to be activated and allow downstream signalling through ASC and Caspase-1 (Finger *et al.*, 2012). However, other additional signals are required to trigger NLRP1 activation. To further investigate how NLRP1 activity is regulated by cleavage within the FIIND domain, we utilised the common polymorphism M1184V. This SNP was reported to increase cleavage in the FIIND domain and is reportedly involved in multiple autoimmune syndromes such as asthma and vitiligo-associated autoimmunity (Finger *et al.*, 2012; Levandowski *et al.*, 2013; Leal *et al.*, 2018). We were able to show by western blot that the M1184V polymorphism indeed increases FIIND cleavage. However, an additional densitometry approach might be useful to confirm this, since baseline expression of this variant was also slightly increased. Surprisingly, aligning the amino acid sequence of NLRP1 from different primates, rodents and a lizard species, we found that all sequences except human NLRP1 harbour a valine in position 1184. This raised the question why human NLRP1 has evolved to contain a methionine in this position and how it might be related to NLRP1-associated infection and autoimmunity. In the case of NLRP1 activation through a destabilisation of the N-terminus (A66V), NLRP1 with a valine in position 1184 showed increased ASC specks compared to NLRP1 containing methionine at this position. In contrast, a reduced frequency of ASC specks was measured for the M1184V variant when NLRP1 was activated by impairing DPP9 binding (Talabostat, P1214R). When activated with Talabostat, the M1184V variant showed lower levels of ASC specks after 6 h of treatment. This effect was significantly less pronounced for the later timepoint after 24 h of treatment. In contrast, inhibition of DPP9 binding by introduction of the P1214R mutation resulted in significantly lower ASC speck

levels for both timepoints when combined with the M1184V polymorphism. A possible explanation for this difference could be the nature of the delivery of the activating stimulus. Talabostat has to cross the plasma membrane to reach the cytoplasm and fulfil its inhibitory function. Introducing a mutation is an intrinsic stimulus, that is constantly affecting the activity of every molecule of NLRP1 that is expressed in the cell. Furthermore, Talabostat is likely to induce cell stress by off-target effects.

Given the different effects observed depending on the activating stimulus, it is conceivable that humans have adopted a methionine at position 1184 as protection against certain pathogens. However, this variant might in turn predispose to other types of infection or have a pleiotropic impact on autoimmunity, depending on the way in which NLRP1 is activated.

To compare the role of M1184V (SNP rs11651270) in different diseases it is associated with, a table was generated listing the Odds Ratio, the respective p value and whether M1184V and IL-1 β /IL-18 contribute to or protect from the according disease (Table 5.1). Interestingly, this comparison revealed that M1184V indeed protects from some diseases and contributes or predisposes to developing others. For instance, individuals carrying the rs11651270 polymorphism are more protected from developing Type I diabetes, but more susceptible to acquiring asthma (Leal *et al.*, 2018; Sun *et al.*, 2019). This supports the above stated hypothesis of the M1184V variant having evolutionary emerged in humans as a protection from some disease. However, the role of inflammasome activation in the development of the respective disease, here reviewed as the involvement of IL-1 β /IL-18, is not always clear. In some cases these proinflammatory cytokines play a protective role and in others they contribute to the severity of the disease. In some diseases the role of one or both cytokines is not entirely clear. Thus, conclusions regarding the mechanism of activation of NLRP1 in the disease based on the presence of M1184V remains speculative. Moreover, it is very likely that other factors play a role in development and outcome of each of the diseases associated with the M1184V polymorphism. It is furthermore difficult, to transfer the results observed in this analysis to

protection from pathogenic stimuli, due to the lack of data on pathogenic ligands for human NLRP1.

Finally, additional repeats of experiments with less than three repeats would have been preferable, since this would allow for statistical analysis and thus strengthen the findings described in this chapter.

Table 5.1: Disease associated with the M1184V polymorphism

Disease	Odds Ratio	P value	M1184V (rs11651270) contributes/protects to/from disease (Reference) + (PMID)	Inflammasome contributes/protects to/from disease (Reference) + (PMID)
Vitiligo and associated autoimmunity	1.6	n/a	Contributes together with L155H/V1059M ¹ (23382179)	IL-1 β contributes ^{2,3} (28082234, 25221996)
Asthma	3.4	0.013	Contributes ⁴ (29154202)	IL-1 β contributes ^{5,6,7} (16210060, 23837489, 8527954) IL-18 protects ^{8,9,10} (12006423, 10629451, 11972614)
Breast Cancer	n/a	0.013	Potentially contributes ¹¹ (23107584)	IL-1 β contributes ¹² (30545915) IL-18 protects ¹³ (29725393)
HPV infection and associated cervical cancer	0.43	0.003	Protects ¹⁴ (26945813)	IL-1 β contributes to cancer ¹⁵ (19904560) IL-18 protects from infection ¹⁶ (11470273)
Crohn's disease	1.35	0.02	Contributes to inflammatory phenotype ¹⁷ (20403135)	IL-1 β contributes ^{18,19} (22891275, 7817982) IL-18 contributes ^{20,21} (10352304, 10384110)
Chagas cardiomyopathy	n/a	0.036	Contributes ²² (29438387)	IL-1 β involvement unclear ²³ (30354432) IL-18 involvement unclear ²⁴ (25743241)

Type 1 Diabetes	0.643	0.002	Protects ²⁵ (31396539)	IL-1 β unclear ^{26,27} (23562090, 21518168) IL-18 contributes ^{28,29} (25576800, 18359638)
Diabetic Kidney Disease	0.36	0.01	Protects ³⁰ (29031829)	IL-1 β contributes ^{31,32} (27516236, 31191559) IL-18 contributes ^{33,34,35} (12759891, 16306550, 17425653)
Malaria (<i>Plasmodium vivax</i>)	n/a	n/a	Potentially contributes ³⁶ (26946405)	IL-1 β potentially contributes to severity ³⁷ (29602073) IL-18 reduces severity (with IL-12) ³⁸ (28615061)
Bacterial meningitis	2.32	0.023	Potentially contributes ³⁹ (23053059)	IL-1 β protects ⁴⁰ (12707352) IL-18 contributes to inflammation ⁴¹ (12742650)

List of references:

Vitiligo: 1: (Levandowski *et al.*, 2013); 2: (Bhardwaj *et al.*, 2017); 3: (Laddha *et al.*, 2014); **Asthma:** 4: (Leal *et al.*, 2018); 5: (Johnson *et al.*, 2005); 6: (Johnson *et al.*, 2005); 7: (Konno *et al.*, 1996); 8: (Ho *et al.*, 2002); 9: (Kodama *et al.*, 2000); 10: (Kuribayashi *et al.*, 2002); **Breast cancer:** 11: (Gao *et al.*, 2012); 12: (Kaplanov *et al.*, 2019); 13: (Liu *et al.*, 2018); **HPV infection/cervical cancer:** 14: (Pontillo *et al.*, 2016); 15: (Qian *et al.*, 2010); 16: (Cho *et al.*, 2001); **Crohn's disease:** 17: (Cummings *et al.*, 2010); 18: (Coccia *et al.*, 2012); 19: (Sher *et al.*, 1995); 20: (Monteleone *et al.*, 1999); 21: (Pizarro *et al.*, 1998); **Chagas cardiomyopathy:** 22: (Clipman *et al.*, 2018); 23: (Nunes *et al.*, 2018); 24: (Nogueira *et al.*, 2015); **Type I Diabetes:** 25: (Sun *et al.*, 2019); 26: (Moran *et al.*, 2013); 27: (Sumpter *et al.*, 2011); 28: (Altinova *et al.*, 2008); 29: (Harms *et al.*, 2015); **Diabetic kidney disease:** 30: (Soares *et al.*, 2018); 31: (Anders, 2016); 32: (Lei *et al.*, 2019); 33: (Moriwaki *et al.*, 2003); 34: (Nakamura *et al.*, 2005); 35: (Wong *et al.*, 2007); **Malaria (*Plasmodium vivax*):** 36: (Santos *et al.*, 2016); 37: (Singh *et al.*, 2018); 38: (Schofield *et al.*, 2017); **Bacterial meningitis:** 39: (Geldhoff *et al.*, 2013); 40: (Petra J. G. Zwijnenburg *et al.*, 2003); 41: (Petra J.G. Zwijnenburg *et al.*, 2003)

n/a: not available/not stated

Apart from autolytic cleavage in the FIIND domain, proteolytic degradation of the N-terminus was described to be involved in activating NLRP1 (Chui *et al.*, 2019; Sandstrom *et al.*, 2019). However, no PTMs like phosphorylation have been described to be involved in NLRP1 regulation. We investigated the role of a previously identified conserved tyrosine within the NLRP1 CARD, which is potentially phosphorylated (Boyle and Monie, 2016). NLRP1, in contrast to other NLRP proteins, interacts with the adaptor protein ASC via its CARD domain (Zhong *et al.*, 2016). Thus, we hypothesized that the interaction of NLRP1 and ASC is regulated by phosphorylation of the NLRP1 CARD. Indeed, we found that substituting tyrosine 1413 for phenylalanine, glutamine or glutamate results in a complete loss of NLRP1 activity, as determined by ASC speck formation. This implies, that this residue has a crucial role for the interaction with ASC.

Phosphorylation of amino acid side chains is well described to add two negative (net) charges to the protein surface. Interestingly, other negatively charged residues are found in this part of the CARD (E1397, D1401, E1414). Hence, an additional negative charge might increase the affinity to a positively charged interface of an interacting protein. More importantly, comparison of the phosphorylated and unphosphorylated structure revealed that phosphorylation also expanded the surface of the NLRP1 CARD. Phosphorylation of Y1413 was achieved by *in silico* modification of the available structure of NLRP1 CARD (PDB: 3KAT) using the Pytms plugin for PyMOL. Computational modelling of the Y1413E substitution further revealed that the negative charge of the glutamate cannot effectively mimic the phosphorylation of Y1413, since the side chain of glutamate is not large enough. This problem of mimicking tyrosine phosphorylation is also well documented in the literature (Anthis *et al.*, 2009).

The surface area of NLRP1 CARD harbouring the respective tyrosine residue has been discussed to form an interface for the interaction with procaspase-1 (Jin *et al.*, 2013). A comparison of the Apaf-1/Procaspase-9 complex revealed similar interfaces, which could be involved in mediating the interaction (Jin *et al.*, 2013). However, phosphorylation of Y1413 was not taken into account and the interface in this model was comprised of only three negative charges without phosphorylation. Additional negative charges in this surface might contribute to

the interaction with procaspase-1. Alternatively, phosphorylation might be involved in regulating specific binding of either NLRP1 CARD ASC or procaspase-1 directly.

As mentioned previously, phosphorylation of conserved tyrosine residues in CARD domains has been reported to be essential for protein activity by mediating protein-protein interactions. For the human and murine version of the inflammasome adaptor protein ASC, phosphorylation of Y146 (Y144 in mice) was described to be crucial for speck formation (Hara *et al.*, 2013; Chung *et al.*, 2016). Furthermore, RIPK2 was reported to auto-phosphorylate tyrosine residues within its CARD, which was shown to be a crucial event for the interaction of RIPK2 with NOD2 (Tigno-Aranjuez *et al.*, 2010). These findings support the hypothesis of NLRP1 activity being dependent on phosphorylation of Y1413.

From an initial screening of protein tyrosine kinase inhibitors we identified Mubritinib (TAK165) as a potential inhibitor of NLRP1 activity in BMDMs when activated with Talabostat. Mubritinib specifically inhibits HER2, a member of the epidermal growth factor receptor family of receptor tyrosine kinases. HER2 was described to be involved in multiple regulatory pathways, such as the mitogen-activated protein kinase (MAPK) pathway (Roy and Perez, 2009). Interestingly, NLRP1 expression was shown to be induced by activation of the MAPK pathway in neurons (Fann *et al.*, 2018). However, the inhibiting effect of Mubritinib on NLRP1 activity could not be confirmed for human NLRP1 in ASC speck assays. Since the initial screening was performed in mouse macrophages and the following experiment was performed in a human cell line (HEK293T), it has to be considered that differences in these cells are the reason for the different results obtained. Moreover, HER2 might not be the proximal kinase responsible for phosphorylation of Y1413 in the NLRP1 CARD, or the Mubritinib could have off-target effects. These alternate pathways could operate differently in the two systems used for studying the effect of Mubritinib. Finally, only IL-1 β and not IL-18 was used as a readout, since a stronger response in the IL-1 β signal was expected. An ELISA looking at IL-18 levels might reveal additional compounds that act on the NLRP1 activation pathway.

Altogether, the data presented herein demonstrate that different molecular mechanisms play a role in regulating NLRP1 inflammasome activity. As shown by utilising the M1184V polymorphism, regulation of autolytic cleavage is a major determinant of NLRP1 activity depending on the activating stimulus. Further, a potential phosphorylation site in NLRP1 CARD was described to be essential for the interaction with the inflammasome adaptor ASC. For now, phosphorylation of this residue remains to be confirmed. However, if confirmed, identification of the kinase responsible for phosphorylation might pose a new target for the treatment of NLRP1-associated autoinflammatory disease. The same holds for the identification and characterisation of other PTMs involved in regulating NLRP1 activity.

6. Overall Discussion

6.1 Key findings

NLRP1 is well-known to form an inflammasome and to potently induce an inflammatory immune response by activating caspase-1, ultimately leading to the release of mature IL-1 β /IL-18 and pyroptosis. It is often highlighted as the first inflammasome forming NLR described in the literature (Martinon *et al.*, 2002). As sensor component of the NLRP1 inflammasome, NLRP1 is described to respond to different pathogenic and non-pathogenic stimuli, like *Toxoplasma gondii* infection or inhibition of the negative regulator DPP9, respectively (Ewald *et al.*, 2014; Gorfou *et al.*, 2014; Okondo *et al.*, 2018; Zhong *et al.*, 2018). Several missense mutations were found to cause autoinflammatory diseases in patients presenting with different skin and systemic inflammatory symptoms. Identification and functional characterization of these mutations improved the understanding of the physiological role of NLRP1 and the molecular mechanisms regulating the activity of this inflammasome (Zhong *et al.*, 2016; Grandemange *et al.*, 2017). Functional degradation of the N-terminal cleavage fragment was recently identified as the molecular basis of different activating stimuli for mouse NLRP1b and could pose a unified mechanism for NLRP1 activation (Chui *et al.*, 2019; Sandstrom *et al.*, 2019).

Despite these advances in the understanding of NLRP1 biology, many questions regarding the molecular mechanisms regulating the activity of the NLRP1 inflammasome as well as its physiological role remain unclear. Work presented in this thesis therefore aimed at advancing the understanding of the molecular basis of molecular mechanisms regulating NLRP1 activity. To clarify how NLRP1 is maintained in an autoinhibited conformation, recombinant protein was produced and analysed biochemically and structurally. Results of the biochemical analysis of separate domains of NLRP1 revealed that the PYD and LRR domains do not contribute to autoinhibition by direct intramolecular interaction. NLRP1 PYD also showed no significant interaction with recombinant MBP fusion proteins containing the NACHT, FIIND or CARD domains.

Furthermore, recombinant full-length NLRP1 fused to MBP was shown to form oligomers in solution. SAXS analysis of the NLRP1 oligomer further allowed for the calculation of a low resolution molecular envelope of the oligomer. The oligomeric state was estimated to be hexameric, based on a particle volume approximation.

Moreover, the requirement of ATP as a cofactor for NLRP1 activity was explored by biochemical and functional means. Using an RP-HPLC based approach, the herein presented results demonstrated for the first time that recombinant NLRP1 exhibits ATP hydrolysis activity. Conserved motifs involved in nucleotide binding and hydrolysis previously described for NLRs were identified for NLRP1 by computational sequence and structure analysis. The identified residues were mutated to investigate how ATP hydrolysis regulates NLRP1 activity. An *in vitro* overexpression assay utilising ASC speck formation as a measure for NLRP1 activation unveiled a potential involvement in autoinhibitory mechanisms for ATP hydrolysis.

Apart from the role of ATP as a cofactor for NLRP1 activity, the involvement of direct modifications of the NLRP1 protein was examined as well. Differential FIIND domain cleavage and its effect on NLRP1 activity was investigated by applying the common NLRP1 polymorphism M1184V in functional assays. Differential FIIND domain cleavage was thereby shown to either increase or decrease inflammasome activation, depending on the activating stimulus. Destabilising the N-terminus by introducing a patient mutation in the PYD of NLRP1 synergised with increased FIIND domain cleavage in regards to inflammasome activation. In contrast, increased cleavage led to retarded NLRP1 activation when stimulated by inhibition of DPP9.

A potential phosphorylation of a conserved tyrosine motif within the NLRP1 CARD domain was identified as another mechanism regulating NLRP1 activity by direct modification of the protein. Substitution of the respective tyrosine residue completely abrogated NLRP1 activation in the ASC speck assay.

6.2 Physiological implications of NLRP1 self-assembly

Structural information on inflammasome sensor proteins has greatly improved the understanding of regulatory mechanisms underlying the activation of the respective inflammasome (Diebolder *et al.*, 2015; Zhang *et al.*, 2015; Maekawa *et al.*, 2016; Tenthorey *et al.*, 2017; Sharif *et al.*, 2019). So far, only separate domains of NLRP1 have been structurally characterised including the calculation of high resolution structures of the PYD (Solution NMR), LRR and CARD (both X-ray crystallography) domains, and a low resolution SAXS-derived envelope for a NACHT-LRR construct (Hiller *et al.*, 2003; Jin *et al.*, 2013; Reubold *et al.*, 2014; Martino *et al.*, 2016). However, this data does not give any insight into the overall fold of the NLRP1 protein.

The SAXS data presented in this work suggests that the full-length MBP-NLRP1 protein self assembles into a hexamer. The majority of purified recombinant MBP-NLRP1 protein sample contained the uncleaved full-length protein, as shown by SDS-PAGE. Thus, the protein particle analysed by SAXS is likely to contain uncleaved MBP-NLRP1 as well. Cleavage in the FIIND domain has been described to be essential for NLRP1 activation (Finger *et al.*, 2012). This result was also confirmed in the ASC speck assays with the uncleavable NLRP1 variant S1213A presented in Chapter 5. Therefore, the protein in the oligomer analysed by SAXS was most likely inactive. Consequently, it can be concluded that the full-length MBP-NLRP1 oligomer represents the inactive form of NLRP1. Oligomeric conformations in both the inactive and active state have been described for different members of the AAA+ ATPase superfamily, like NtrC1 and p97 (Chen *et al.*, 2010; Hänzelmann and Schindelin, 2016). Moreover, all NLRs are described to form functional oligomers upon activation (Danot *et al.*, 2009; Maharana *et al.*, 2018). Structures of the active NLRC4 inflammasome provided direct evidence for this model (Diebolder *et al.*, 2015; Zhang *et al.*, 2015; Tenthorey *et al.*, 2017). However there is no experimental evidence for NLRs forming oligomers in their inactive state.

In the above described model, FIIND domain cleavage would occur in the oligomer for two reasons. First, the protein particle characterized in SAXS

contained the full-length protein. Second, the cleavage within the FIIND domain is not sufficient for activation of NLRP1, meaning that the protein remains autoinhibited even after the autoproteolysis event in the FIIND domain. Interaction of the N- and C-terminal cleavage fragments has been reported for NLRP1 (Finger *et al.*, 2012). In the case of an oligomeric conformation in the autoinhibited state, the N- and C-terminal cleavage fragments of NLRP1 could be retained in the oligomer by intermolecular interactions. Additionally, the negative regulator DPP9 could be involved in maintaining an oligomeric conformation. Regulation of protein activity by autoproteolytic cleavage has been reported for other proteins, like the nuclear pore protein Nup98 (nucleoporin 98) and the apoptosis inducing protein PIDD (p53-induced protein with a death domain) (Hodel *et al.*, 2002; Hänzelmann and Schindelin, 2016). PIDD has further been described to form oligomers upon activation to form a signalling platform termed the PIDDosome (Park, Logette, *et al.*, 2007). However, there is no evidence that autoproteolysis occurs in the oligomeric state of PIDD. In contrast, the C-terminal PIDD death domain was shown to form an oligomer together with the death domain of the adapter protein RAIDD, without the need for N-terminal domains, including two ZU-5 domains and an LRR domain (Park, Logette, *et al.*, 2007). In the context of NLRP1, this would argue more for the ability of the C-terminal cleavage fragment to oligomerize together with ASC without need for the NACHT or any other domain of the N-terminal fragment. However, this does not completely exclude the possibility of an oligomeric conformation in the autoinhibited state. It should be mentioned that the above described model is only a speculation about the potential physiological role of the MBP-NLRP1 oligomer characterized in Chapter 3.2.

6.3 The role of ATP hydrolysis in NLRP1 oligomerisation

Different members of the family of STAND proteins, like Apaf-1 or MalT, have also been reported to form functional oligomers upon activation. Both proteins were described to require a ligand and ATP as a cofactor for activation and oligomer formation (Larquet *et al.*, 2004; Zhou *et al.*, 2015). While Apaf-1 requires

ATP hydrolysis for binding of its ligand Cytochrome C and subsequent oligomerisation, MalT only binds ATP together with its ligand maltotriose to oligomerise. MalT does not require hydrolysis of ATP for oligomerisation (Yuanming *et al.*, 1999; Larquet *et al.*, 2004). For NLRP1 no activating ligand, as Cytochrome C for Apaf-1 or maltotriose for MalT, is known. An overarching hypothesis for NLRs is that ATP binding and hydrolysis is involved in mediating conformational changes that allow oligomer formation (Danot *et al.*, 2009; Maharana *et al.*, 2018).

The herein presented data showed that NLRP1 has ATP hydrolysis activity. Substitution of residues located in the conserved ATP binding and hydrolysis site of NLRP1 resulted in constitutive activation, indicating that ATP hydrolysis might have autoinhibitory functions in the regulation of NLRP1. This is consistent with the constitutively active Walker B mutants found for NLRP3 and the plant R protein I-2 (Tameling *et al.*, 2006; Coll *et al.*, 2019; Tapia-Abellán *et al.*, 2019). ATP hydrolysis might thus be required to adapt the oligomeric autoinhibited conformation (Chapter 6.2) upon translation of the NLRP1 protein. For NLRP1, the oligomeric conformation could provide protection from N-terminal degradation, which would result in activation of the NLRP1 inflammasome. It would further pose a possible explanation for how the PYD and LRR contribute to maintaining NLRP1 in an autoinhibited conformation - they are involved in oligomer formation. Although no homotypic interactions were found for both domains, they could still support the oligomeric state by binding to another domain or a linker region between domains.

Assuming that NLRP1 does require ATP hydrolysis for oligomer formation and to adapt an inhibited conformation, impairing ATP hydrolysis by substituting residues involved in nucleotide binding or hydrolysis would consequently inhibit oligomer formation and result in constitutive activation of NLRP1. Monomeric NLRP1 could be more prone to N-terminal degradation, resulting in the liberation of the C-terminal cleavage fragment and formation of the NLRP1 inflammasome. The C-terminal fragment of NLRP1 has been described to be sufficient to form an active inflammasome (Zhong *et al.*, 2016). An autoinhibitory or at least regulatory function of the NACHT domain and the nucleotide binding site within

this domain is further indicated by the N-terminal degradation model of activation. This model implies that all domains located N-terminal of the FIIND cleavage site, including the NACHT domain, are dispensable for inflammasome activity. In turn, this would also mean that ATP hydrolysis is not required for the activity of NLRP1, as previously concluded in the literature (Chavarría-Smith *et al.*, 2016).

6.4 The mechanisms and role of PTMs and DPP9 in NLRP1 regulation

As discussed previously (Chapter 5.3), PTMs are directly involved in regulating NLRP1 activity. Oligomer formation of NLRP1 in an autoinhibited state as discussed above could serve as an explanation for the differential effects observed in experiments with the M1184V variant of NLRP1. Cleavage within the oligomeric form of NLRP1 would likely induce conformational changes in the oligomer. These could expose the PYD and thus make it more susceptible to interaction with a protein able to induce N-terminal degradation, ultimately resulting in activation of NLRP1. In contrast to predisposition to N-terminal degradation, DPP9 binding and its function could become redundant in this conformation. Consequently, more cleavage would lead to increased activation of NLRP1 by N-terminal destabilisation (A66V). However, loss of DPP9 binding (Talabostat, P1214R) would not result in activation, since the oligomer would remain autoinhibited even without DPP9 directly bound.

Conformational changes induced by FIIND cleavage could also occur in the case of NLRP1 being monomeric in its autoinhibited state. Thus, the differential effects of increased FIIND domain cleavage induced by the variant M1184V could be explained by an autoinhibitory interaction between the PYD and the cleaved FIIND domain. A similar mechanism of the PYD folding back onto another domain to mediate an inhibitory conformation has been proposed previously (Zhong *et al.*, 2016). However, intramolecular binding of the PYD was never discussed in the context of FIIND domain cleavage. Disturbing the fold of the PYD, as induced by the A66V disease mutation, would abrogate the interaction with the FIIND domain. Thus, increased cleavage would induce increased binding between the two domains in the WT protein. For the A66V variant however, increased

cleavage would consequently result in increased cleavage, since the PYD cannot mediate autoinhibition through FIIND domain interaction. An interaction was not observed in experiments with recombinant protein of the PYD and MBP-FIIND domains. As discussed earlier, this does not exclude the possibility of an interaction between these two domains. Particularly since the MBP-tag could block interaction surfaces as shown for the MBP-CARD protein and a CARD-specific nanobody. Furthermore, the MBP-FIIND fusion did not appear as two cleavage products in SDS-PAGE analysis.

Considering the role of DPP9, the evaluation of the role of PTMs in regulating NLRP1 activity becomes more complex. It is possible that DPP9 directly modifies NLRP1 by cleaving a dipeptide off the N-terminus of the C-terminal cleavage fragment. Thereby it could regulate protein turnover of this fragment and consequently NLRP1 activity. A similar model has been discussed previously in the literature (Zhong *et al.*, 2018). It poses a logical explanation for the molecular mechanism underlying hyperactivation of the NLRP1 disease mutation P1214R. In the context of an interaction of the PYD and FIIND domains, DPP9 could regulate turnover of the C-terminal cleavage fragment upon release of the C-terminal fragment from the N-terminal fragment. Since DPP9 cleavage requires a proline or an alanine residue in position 2, the P1214R disease variant could not be recognized by DPP9 and would thus accumulate and induce inflammasome formation. This is consistent with the finding that the activity of the A66V disease variant can be further increased by DPP9 inhibition. The contrary is the case for the P1214R mutation. However, a substrate screening of peptidases showed that DPP8/9 does not directly cleave mouse NLRP1b (Griswold *et al.*, 2019). As for the others models described above, the reason for the differential effects seen for increased FIIND cleavage on NLRP1 activity induced by diverse activating stimuli remains a matter of speculation.

As described above, NLRP1b was not found to be a direct target of DPP9. This suggests that this peptidase is indirectly involved in regulating NLRP1 activity. A possible way of indirectly regulating NLRP1 could be the regulation of phosphorylation of the NLRP1 CARD domain. DPP9 has been reported to directly cleave off a dipeptide of the N-terminus of spleen tyrosine kinase (SYK) and

thereby regulate the protein turnover of SYK. Cleavage of SYK at its N-terminus directs it to the N-terminal degradation pathway (Justa-Schuch *et al.*, 2016). Assuming DPP9 has a similar function in regulating protein turnover of the kinase phosphorylating Y1413 in the NLRP1 CARD domain, inhibition of DPP9 would increase the level of intracellular kinase and likely result in increased phosphorylation of NLRP1 CARD. This way, phosphorylation could be a control mechanism regulating NLRP1 activity. However, this would be in conflict with DPP9 being required to directly bind to NLRP1 to maintain NLRP1 autoinhibition (Zhong *et al.*, 2018).

Taken together, FIIND domain cleavage, DPP9 binding and CARD phosphorylation all regulate NLRP1 activity. However, the exact mechanisms and the order in which they occur remain elusive. In the context of an autoinhibited NLRP1 oligomer all three regulatory events would likely occur post self-assembly of the protein. In contrast, for a monomeric autoinhibited NLRP1, DPP9 binding and FIIND domain cleavage would precede oligomerisation of the C-terminal cleavage fragment. Phosphorylation could serve as a check-point mechanism independent of self-assembly and could thus occur before and after oligomerisation.

The different mechanisms regulating NLRP1 activity arising from the results presented in this work will be summarised in Chapter 6.5 together with existing models of NLRP1 activation.

6.5 Model of NLRP1 activation

The current model of inflammasome activation includes two steps. In a first priming step, expression of the inflammasome sensor molecules is induced through NF- κ B upon activation by TLR signalling (Bauernfeind *et al.*, 2010; Schroder and Tschopp, 2010; Walsh *et al.*, 2014). The second step is the direct activation of the inflammasome sensor protein, for example the binding of bacterial flagellin to NAIP5 (Tenthorey *et al.*, 2017).

Although multiple pathogens and disease mutations are described to activate NLRP1, no direct ligand has been reported. This makes the investigation of the

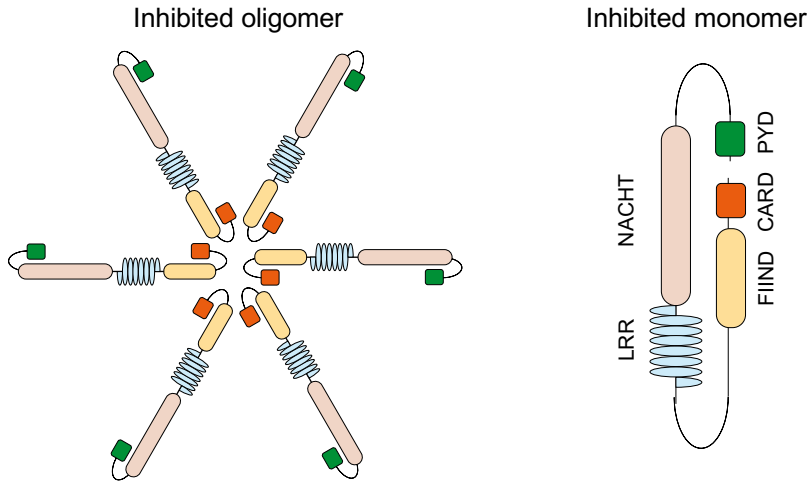
sequence in which molecular events required for NLRP1 activity occur difficult. However, taking recent advances in the understanding of NLRP1 activation into account, I will try to summarise and order the molecular mechanisms underlying NLRP1 regulation and activation. A graphical summary can be found in Figure 6.1.

A first step after transcription and translation would be the adaptation of an autoinhibited conformation. To this end, NLRP1 could oligomerize in an ATP hydrolysis dependent manner. Subsequently, autolytic cleavage and DPP9 binding would occur successively or simultaneously. DPP9 binding is unlikely to precede autolytic cleavage, since uncleavable variants of NLRP1 were shown to be unable to bind DPP9 (Zhong *et al.*, 2018). Activation of NLRP1 by inhibition of DPP9 or a destabilized N-terminus result in impaired oligomer formation and consequently activation of the NLRP1 inflammasome by degradation of the N-terminal cleavage fragment. Finally, tyrosine 1413 in the NLRP1 CARD domain is phosphorylated to allow interaction with ASC and full activation of the NLRP1 inflammasome.

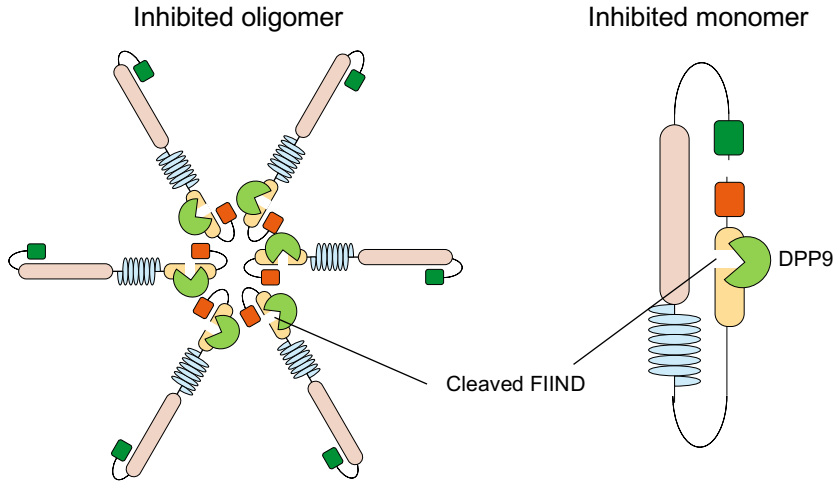
The inhibitory role of nucleotide binding and hydrolysis could also be to facilitate conformational changes or the stabilization of a monomeric NLRP1 in its autoinhibited conformation. The sequence of events in this monomeric model would be similar to the above described model of an oligomeric inhibited conformation. An exception would be that oligomerisation occurs after activation, N-terminal degradation and release of the C-terminal fragment of NLRP1.

These models and the sequence of events are still speculative. For instance, phosphorylation could also occur earlier in the sequence and the interaction surface for the CARD could simply be blocked sterically. More research is required to completely reveal the molecular mechanisms regulating NLRP1 activity and the order in which they occur.

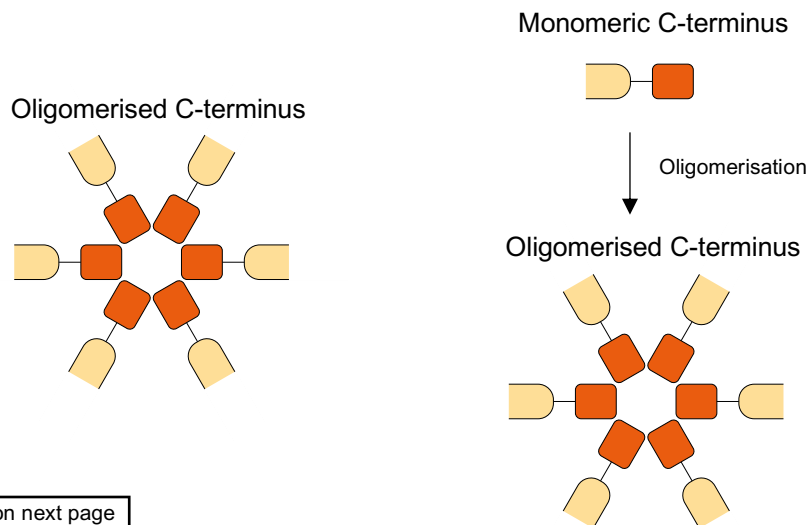
1. ATP hydrolysis and adaptation of an inhibited conformation



2. Autoproteolysis and DPP9 binding



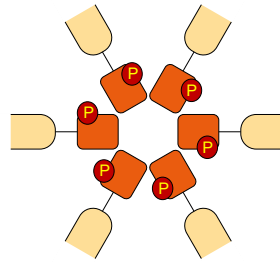
3. Activation (e.g. LeTx, T. gondii, DPP9 inhibition), N-terminal degradation, release (and oligomerization) of C-terminal fragment



Continued on next page

4. Phosphorylation of NLRP1 CARD (Y1413)

Phosphorylated oligomer



5. Inflammasome formation

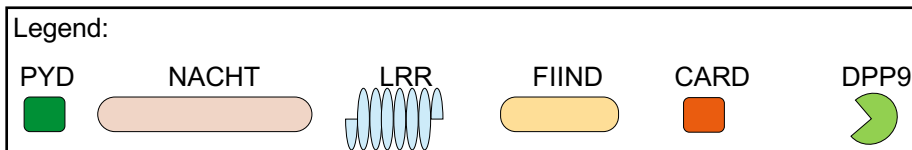
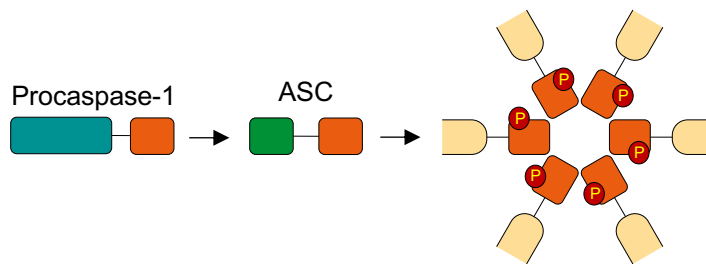


Figure 6.1: Sequence of molecular events required for NLRP1 activation

(1) Upon transcription and translation NLRP1 adapts an inhibited conformation in an ATP hydrolysis dependent manner. The inhibited conformation might be oligomeric or monomeric, but definitely requires the N-terminus of NLRP1. (2) After adapting its correct conformation, the cleavage event in the FIIND domain occurs. This allows the negative regulator DPP9 to bind to the inhibited NLRP1 protein. (3) Activation of NLRP1 by different mechanisms exposes the N-terminus for degradation. This results in liberation of the C-terminal fragment, (4) which can be phosphorylated. (5) The phosphorylated oligomeric C-terminus provides a platform for the recruitment of ASC and procaspase-1 to form an active inflammasome.

6.3 Future directions

As mentioned in previous chapters, many of the conclusions described above are speculative. To further improve the understanding of how NLRP1 is regulated, generation of a high resolution structure of the MBP-NLRP1 oligomer would provide valuable information. Cryo-EM is probably the most feasible approach to obtain that information. Since it was not possible to keep the full-length NLRP1 protein in solution at high concentrations, X-ray crystallography analysis is restricted to separate domains of NLRP1. Additionally, a screening of other expression and solubility tags could improve the stability of the protein, to make structural analysis more achievable. Expressing full-length NLRP1 only with a His₆-tag resulted in an extremely low protein yield, emphasizing the requirement for a tag that improves expression of the protein. Alternatively, a change of the expression system might improve solubility of the protein. Insect cells are able to perform posttranslational modifications like phosphorylation and glycosylation. However, the respective pattern is usually different between mammalian cells and insect cells (Owczarek *et al.*, 2019). Thus, a mammalian cell line would be more likely to modify human NLRP1 in a native way, ensuring biological activity of the recombinant protein.

A high resolution structure could also provide insight into the nucleotide binding site of NLRP1 and confirm the residues important for ATP binding and hydrolysis identified in this work. Additional hydrolysis assays could further confirm the involvement of these residues in ATP hydrolysis.

Moreover, testing the nucleotide binding site variants of NLRP1 in a different assay measuring inflammasome activation at the level of IL-1 β and IL-18 secretion as well as cell deaths is required to support the findings from the ASC speck assay. The THP-1 monocyte cell line proved to be unsuitable, since no specific activation of NLRP1 was achieved in viral transduction experiments (not shown) as well as in a CRISPR-Cas9 based approach (Chapter 4.3.6). Immortalized keratinocytes have been shown to be a suitable system for the investigation of NLRP1 biology (Zhong *et al.*, 2016; Zhong *et al.*, 2018). Basic transfection experiments could already reveal, if the effects seen in the ASC

speck assay can be reproduced in a different system in regards to IL-1 β and IL-18 secretion as well as cell death. However, the ELISA kit used to detect IL-18 in this work can potentially detect unprocessed (inactive) IL-18. Thus, a western blot analysis of cell culture supernatants looking at total and cleaved IL-18 should be considered to additionally support the findings from ELISA experiments. The kit used to detect IL-1 β has a high specificity for the processed (active) protein. An additional analysis by western blot would still be beneficial, as it could support the findings found in the ELISA analysis.

A system employing release of cleaved IL-1 β and IL-18 as a measure for inflammasome activation could also be useful to support the results described on the effects of differential FIIND domain cleavage. As for the nucleotide binding site variants, immortalized keratinocytes might be a suitable system to test this. Additionally, other activating stimuli could be tested, like UV-B irradiation or depletion of intracellular ATP, to further explore the effects of differential FIIND cleavage on NLRP1 inflammasome activation. Infection with different strains of *Toxoplasma gondii* was attempted to be employed as an activating stimulus in the ASC speck assay. However, no specific activation of NLRP1 could be observed in these experiments (not shown). Again, using a different cell line or an alternative readout for inflammasome activation might resolve this problem.

To confirm phosphorylation of Y1413 in the NLRP1 CARD, different approaches could be taken. Transiently expressed protein could be purified by immunoprecipitation and subsequently analysed by SDS-PAGE and mass spectrometry. Alternatively, the protein could be analysed by immunoblotting using a phospho-tyrosine antibody. NLRP1 WT and Y1413F could be compared in the immunoblot-based approach, to specifically show Y1413 phosphorylation.

If phosphorylation of this residue can be confirmed, identification of the kinase would be the next step. However, this would be more difficult to achieve. The inhibitor screen described in Chapter 5.3 did not reveal a kinase. A problem of this approach is of course, that inhibition of a kinase will inevitably result in the alteration of multiple pathways, since kinases usually have more than one target. Thus, a screening of tyrosine kinase inhibitors would always require follow-up experiments to confirm direct phosphorylation of NLRP1 by the identified kinase.

This could for example be achieved using recombinant protein and radiolabelled ATP in an *in vitro* kinase assay (Hastie *et al.*, 2006). Assuming that CARD phosphorylation proves to be essential for NLRP1 activity, identification of the respective kinase might pose a possible target for the treatment of NLRP1-associated autoinflammatory diseases.

Research on NLRP1 is still emerging and becoming more and more of a focus in inflammasome biology. Together with recently published studies, the data presented herein highlight the complexity of NLRP1 biology and challenges arising when investigating regulatory mechanisms underlying NLRP1 activity. Collectively, the results of this work contribute to improving our current understanding of molecular mechanisms governing the regulation of the NLRP1 inflammasome.

Bibliography

Abele, U. and Schulz, G.E. (1995) 'High-resolution Structures of Adenylate Kinase from Yeast Ligated with Inhibitor Ap5A, Showing the Pathway of Phosphoryl Transfer'. *Protein Science*, 4(7), pp. 1262–1271.

Acehan, D., Jiang, X., Morgan, D.G., Heuser, J.E., Wang, X. and Akey, C.W. (2004) 'Three-Dimensional Structure of the Apoptosome'. *Molecular Cell*, 9(2), pp. 423–432.

Akira, S. and Hemmi, H. (2003) 'Recognition of Pathogen-Associated Molecular Patterns by TLR Family'. *Immunology Letters*, 85(2), pp. 85–95.

Alghamdi, M. (2017) 'Familial Mediterranean Fever, Review of the Literature.' *Clinical Rheumatology*, 36(8), pp. 1707–1713.

Altinova, A.E., Yetkin, I., Akbay, E., Bukan, N. and Arslan, M. (2008) 'Serum IL-18 Levels in Patients with Type 1 Diabetes: Relations to Metabolic Control and Microvascular Complications.' *Cytokine*, 42(2), pp. 217–221.

Ammelburg, M., Frickey, T. and Lupas, A.N. (2006) 'Classification of AAA+ Proteins'. *Journal of Structural Biology*, 156(1), pp. 2–11.

Anders, H.-J. (2016) 'Of Inflammasomes and Alarmins: IL-1 β and IL-1 α in Kidney Disease'. *Journal of the American Society of Nephrology*, 27(9), pp. 2564–2575.

Anthis, N.J., Haling, J.R., Oxley, C.L., Memo, M., Wegener, K.L., Lim, C.J., Ginsberg, M.H. and Campbell, I.D. (2009) 'B Integrin Tyrosine Phosphorylation Is a Conserved Mechanism for Regulating Talin-Induced Integrin Activation'. *Journal of Biological Chemistry*, 284(52), pp. 36700–36710.

Babst, M., Wendland, B., Estepa, E.J. and Emr, S.D. (1998) 'The Vps4p AAA ATPase Regulates Membrane Association of a Vps Protein Complex Required for Normal Endosome Function'. *EMBO Journal*, 17(11), pp. 2982–2993.

Baek, Y.M., Yoon, S., Hwang, Y.E. and Kim, D.-E. (2016) 'Dependence of RIG-I Nucleic Acid-Binding and ATP Hydrolysis on Activation of Type I Interferon Response'. *Immune Network*, 16(4), p. 249.

Baker, P.J., De Nardo, D., Moghaddas, F., Tran, L.S., Bachem, A., Nguyen, T., Hayman, T., Tye, H., Vince, J.E., Bedoui, S., Ferrero, R.L. and Masters, S.L. (2017) 'Posttranslational Modification as a Critical Determinant of Cytoplasmic Innate Immune Recognition'. *Physiological Reviews*, 97(3), pp. 1165–1209.

Barber, G.N. (2015) 'STING: Infection, Inflammation and Cancer'. *Nature Reviews Immunology*, 15(12), pp. 760–770.

Bardoel, B.W. and Van Strijp, J.A.G. (2011) 'Molecular Battle between Host and Bacterium: Recognition in Innate Immunity'. *Journal of Molecular Recognition*, 24(6), pp. 1077–1086.

Bauernfeind, F., Horvath, G., Stutz, A., Alnemri, E.S., Speert, D., Fernandes-alnemri, T., Wu, J., Brian, G., Fitzgerald, K.A., Hornung, V. and Latz, E. (2010) 'NF- κ B Activating Pattern Recognition and Cytokine Receptors License NLRP3 Inflammasome Activation by Regulating NLRP3 Expression'. *Journal of Immunology (Baltimore, Md. : 1950)*, 183(2), pp. 787–791.

Bentham, A., Burdett, H., Anderson, P.A., Williams, S.J. and Kobe, B. (2017) 'Animal NLRs Provide Structural Insights into Plant NLR Function'. *Annals of Botany*, 119(5), pp. 689–702.

Beutler, B. (2004) 'Innate Immunity: An Overview'. *Molecular Immunology*, 40(12), pp. 845–859.

Bhardwaj, S., Rani, S., Srivastava, N., Kumar, R. and Parsad, D. (2017) 'Increased Systemic and Epidermal Levels of IL-17A and IL-1 β Promotes Progression of Non-Segmental Vitiligo.' *Cytokine*, 91, pp. 153–161.

Bottazzi, B., Doni, A., Garlanda, C. and Mantovani, A. (2010) 'An Integrated View of Humoral Innate Immunity: Pentraxins as a Paradigm'. *Annual Review of Immunology*, 28(1), pp. 157–183.

Boyden, E.D. and Dietrich, W.F. (2006) 'Nalp1b Controls Mouse Macrophage Susceptibility to Anthrax Lethal Toxin'. *Nature Genetics*, 38(2), pp. 240–244.

Boyle, J.P. and Monie, T.P. (2016) 'Structure-based Alignment of Human Caspase Recruitment Domains Provides a Framework for Understanding Their Function'. *BioRxIV*.

Brown, G.D., Taylor, P.R., Reid, D.M., Willment, J.A., Williams, D.L., Martinez-Pomares, L., Wong, S.Y.C. and Gordon, S. (2002) 'Dectin-1 Is A Major β -Glucan Receptor On Macrophages'. *The Journal of Experimental Medicine*, 196(3), pp. 407–412.

Brown, G.D. and Gordon, S. (2001) 'A New Receptor for β -Glucans'. *Nature*, 413(6851), pp. 36–37.

Broz, P. and Dixit, V.M. (2016) 'Inflammasomes: Mechanism of Assembly, Regulation and Signalling'. *Nature Reviews Immunology*, 16(7), pp. 407–420.

Bruey, J.-M., Bruey-Sedano, N., Luciano, F., Zhai, D., Balpai, R., Xu, C., Kress, C.L., Bailly-Maitre, B., Li, X., Osterman, A., Matsuzawa, S., Terskikh, A. V., Faustin, B. and Reed, J.C. (2007) 'Bcl-2 and Bcl-XL Regulate Proinflammatory Caspase-1 Activation by Interaction with NALP1.' *Cell*, 129(1), pp. 45–56.

Cao, W., Zhang, L., Rosen, D.B., Bover, L., Watanabe, G., Bao, M., Lanier, L.L. and Liu, Y.J. (2007) 'BDCA2/FcεR1y Complex Signals through a Novel BCR-like Pathway in Human Plasmacytoid Dendritic Cells'. *PLoS Biology*, 5(10), pp. 2190–2200.

Carrillo, J.L.M., Rodríguez, F.P.C., Coronado, O.G., García, M.A.M. and Cordero, J.F.C. (2017) 'Physiology and Pathology of Innate Immune Response Against Pathogens'. In *Physiology and Pathology of Immunology*. InTech, p. 13.

Cavaillès, P., Flori, P., Papapietro, O., Bisanz, C., Lagrange, D., Pilloux, L., Massera, C., Cristinelli, S., Jublot, D., Bastien, O., Loeuillet, C., Aldebert, D., Touquet, B., Fournié, G.J. and Cesbron-Delauw, M.F. (2014) 'A Highly Conserved Toxo1 Haplotype Directs Resistance to Toxoplasmosis and Its Associated Caspase-1 Dependent Killing of Parasite and Host Macrophage' Sasseti, C.M. (ed.). *PLoS Pathogens*, 10(4), p. e1004005.

Cavaillès, P., Sergent, V., Bisanz, C., Papapietro, O., Colacios, C., Mas, M., Subra, J.-F., Lagrange, D., Calise, M., Appolinaire, S., Faraut, T., Druet, P., Saoudi, A., Bessières, M.-H., Pipy, B., Cesbron-Delauw, M.-F. and Fournie, G.J. (2006) 'The Rat Toxo1 Locus Directs Toxoplasmosis Outcome and Controls Parasite Proliferation and Spreading by Macrophage-Dependent Mechanisms'. *Proceedings of the National Academy of Sciences*, 103(3), pp. 744–749.

Chavarría-Smith, J., Mitchell, P.S., Ho, A.M., Daugherty, M.D. and Vance, R.E. (2016) 'Functional and Evolutionary Analyses Identify Proteolysis as a General Mechanism for NLRP1 Inflammasome Activation' Lewinsohn, D.M. (ed.). *PLoS Pathogens*, 12(12), p. e1006052.

Chavarria-Smith, J. and Vance, R.E. (2015) 'The NLRP1 Inflammasomes'. *Immunological Reviews*, 265(1), pp. 22–34.

Chavarría-Smith, J. and Vance, R.E. (2013) 'Direct Proteolytic Cleavage of NLRP1B Is Necessary and Sufficient for Inflammasome Activation by Anthrax Lethal Factor.' *PLoS Pathogens*, 9(6), p. e1003452.

Chen, B., Sysoeva, T.A., Chowdhury, S., Guo, L., De Carlo, S., Hanson, J.A., Yang, H. and Nixon, B.T. (2010) 'Engagement of Arginine Finger to ATP Triggers Large Conformational Changes in NtrC1 AAA+ ATPase for Remodeling Bacterial RNA Polymerase'. *Structure*, 18(11), pp. 1420–1430.

Chen, G., Shaw, M.H., Kim, Y.-G. and Nuñez, G. (2009) 'NOD-like Receptors: Role in Innate Immunity and Inflammatory Disease'. *Annual Review of Pathology*, 4, pp. 365–398.

Cho, Y.-S., Kang, J.-W., Cho, M., Cho, C.-W., Lee, S., Choe, Y.-K., Kim, Y., Choi, I., Park, S.-N., Kim, S., Dinarello, C.A. and Yoon, D.-Y. (2001) 'Down Modulation of IL-18 Expression by Human Papillomavirus Type 16 E6 Oncogene via Binding to IL-18'. *FEBS Letters*, 501(2–3), pp. 139–145.

Chu, L.H., Gangopadhyay, A., Dorfleutner, A. and Stehlik, C. (2015) 'An Updated View on the Structure and Function of PYRIN Domains'. *Apoptosis*, 20(2), pp. 157–173.

Chui, A.J., Okondo, M.C., Rao, S.D., Gai, K., Griswold, A.R., Johnson, D.C., Ball, D.P., Taabazuing, C.Y., Orth, E.L., Vitimberga, B.A. and Bachovchin, D.A. (2019) 'N-Terminal Degradation Activates the NLRP1B Inflammasome'. *Science*, 364(6435), pp. 82–85.

Chung, I.C., OuYang, C.N., Yuan, S.N., Li, H.P., Chen, J.T., Shieh, H.R., Chen, Y.J., Ojcius, D.M., Chu, C.L., Yu, J.S., Chang, Y.S. and Chen, L.C. (2016) 'Pyk2 Activates the NLRP3 Inflammasome by Directly Phosphorylating ASC and Contributes to Inflammasome-Dependent Peritonitis'. *Scientific Reports*, 6(June), pp. 1–13.

Ciechanover, A. (1994) 'The Ubiquitin-Proteasome Proteolytic Pathway'. *Cell*, 79(1), pp. 13–21.

Cirelli, K.M., Gorfou, G., Hassan, M.A., Printz, M., Crown, D., Leppla, S.H., Grigg, M.E., Saeij, J.P.J. and Moayeri, M. (2014) 'Inflammasome Sensor NLRP1 Controls Rat Macrophage Susceptibility to *Toxoplasma Gondii*' Sasseti, C.M. (ed.). *PLoS Pathogens*, 10(3), p. e1003927.

Clipman, S.J., Henderson-Frost, J., Fu, K.Y., Bern, C., Flores, J. and Gilman, R.H. (2018) 'Genetic Association Study of NLRP1, CARD, and CASP1 Inflammasome Genes with Chronic Chagas Cardiomyopathy among *Trypanosoma Cruzi* Seropositive Patients in Bolivia'. *PLoS ONE*, 13(2), pp. 1–9.

Coccia, M., Harrison, O.J., Schiering, C., Asquith, M.J., Becher, B., Powrie, F. and Maloy, K.J. (2012) 'IL-1 β Mediates Chronic Intestinal Inflammation by Promoting the Accumulation of IL-17A Secreting Innate Lymphoid Cells and CD4 + Th17 Cells'. *The Journal of Experimental Medicine*, 209(9), pp. 1595–1609.

Coll, R.C., Hill, J.R., Day, C.J., Zamoshnikova, A., Boucher, D., Massey, N.L., Chitty, J.L., Fraser, J.A., Jennings, M.P., Robertson, A.A.B. and Schroder, K. (2019) 'MCC950 Directly Targets the NLRP3 ATP-Hydrolysis Motif for Inflammasome Inhibition'. *Nature Chemical Biology*, 15(6), pp. 556–559.

Corpet, F. (1988) 'Multiple Sequence Alignment with Hierarchical Clustering'. *Nucleic Acids Research*, 16(22), pp. 10881–10890.

Cummings, J.R.F., Cooney, R.M., Clarke, G., Beckly, J., Geremia, A., Pathan, S., Hancock, L., Guo, C., Cardon, L.R. and Jewell, D.P. (2010) 'The Genetics of NOD-like Receptors in Crohn's Disease.' *Tissue Antigens*, 76(1), pp. 48–56.

Curran, M.P. and McKeage, K. (2009) 'Bortezomib: A Review of Its Use in Patients with Multiple Myeloma'. *Drugs*, 69(7), pp. 859–888.

D'Oswaldo, A., Weichenberger, C.X., Wagner, R.N., Godzik, A., Wooley, J. and Reed, J.C. (2011) 'CARD8 and NLRP1 Undergo Autoproteolytic Processing through a ZU5-like Domain.' *PloS One*, 6(11), p. e27396.

Dambuza, I.M. and Brown, G.D. (2015) 'C-Type Lectins in Immunity: Recent Developments'. *Current Opinion in Immunology*, 32, pp. 21–27.

Danot, O., Marquenet, E., Vidal-Ingigliardi, D. and Richet, E. (2009) 'Wheel of Life, Wheel of Death: A Mechanistic Insight into Signaling by STAND Proteins'. *Structure*, 17(2), pp. 172–182.

Dick, M.S., Sborgi, L., Rühl, S., Hiller, S. and Broz, P. (2016) 'ASC Filament Formation Serves as a Signal Amplification Mechanism for Inflammasomes'. *Nature Communications*, 7(May), p. 11929.

Diebolder, C.A., Halff, E.F., Koster, A.J., Huizinga, E.G. and Koning, R.I. (2015) 'Cryoelectron Tomography of the NAIP5/NLRC4 Inflammasome: Implications for NLR Activation'. *Structure*, 23(12), pp. 2349–2357.

Dinarello, C.A. (1999) 'IL-18: A TH1-Inducing, Proinflammatory Cytokine and New Member of the IL-1 Family.' *The Journal of Allergy and Clinical Immunology*, 103(1 Pt 1), pp. 11–24.

Dinarello, C.A. (2009) 'Immunological and Inflammatory Functions of the Interleukin-1 Family'. *Annual Review of Immunology*, 27(1), pp. 519–550.

Dinarello, C.A., Novick, D., Kim, S. and Kaplanski, G. (2013) 'Interleukin-18 and IL-18 Binding Protein'. *Frontiers in Immunology*, 4(OCT), pp. 1–10.

Dinarello, C.A. (2018) 'Overview of the IL-1 Family in Innate Inflammation and Acquired Immunity'. *Immunological Reviews*, 281(1), pp. 8–27.

Ding, J., Wang, K., Liu, W., She, Y., Sun, Q., Shi, J., Sun, H., Wang, D.-C. and Shao, F. (2016) 'Pore-Forming Activity and Structural Autoinhibition of the Gasdermin Family'. *Nature*, 535(7610), pp. 111–116.

Dong, C., Davis, R.J. and Flavell, R.A. (2002) 'MAP Kinases in the Immune Response.' *Annual Review of Immunology*, 20(1), pp. 55–72.

Drickamer, K. and Taylor, M.E. (2015) 'Recent Insights into Structures and Functions of C-Type Lectins in the Immune System'. *Current Opinion in Structural Biology*, 34, pp. 26–34.

Duncan, J.A., Bergstralh, D.T., Wang, Y., Willingham, S.B., Ye, Z., Zimmermann, A.G. and Ting, J.P.-Y. (2007) 'Cryopyrin/NALP3 Binds ATP/DATP, Is an ATPase, and Requires ATP Binding to Mediate Inflammatory Signaling'. *Proceedings of the National Academy of Sciences*, 104(19), pp. 8041–8046.

Dzeja, P. and Terzic, A. (2009) 'Adenylate Kinase and AMP Signaling Networks: Metabolic Monitoring, Signal Communication and Body Energy Sensing'. *International Journal of Molecular Sciences*, 10(4), pp. 1729–1772.

Elliott, J.M., Rouge, L., Wiesmann, C. and Scheer, J.M. (2009) 'Crystal Structure of Procaspase-1 Zymogen Domain Reveals Insight into Inflammatory Caspase Autoactivation'. *Journal of Biological Chemistry*, 284(10), pp. 6546–6553.

Ewald, S.E., Chavarria-Smith, J. and Boothroyd, J.C. (2014) 'NLRP1 Is an Inflammasome Sensor for *Toxoplasma Gondii*'. *Infection and Immunity*.

Fann, D.Y.W., Lim, Y.A., Cheng, Y.L., Lok, K.Z., Chunduri, P., Baik, S.H., Drummond, G.R., Dheen, S.T., Sobey, C.G., Jo, D.G., Chen, C.L.H. and Arumugam, T. V. (2018) 'Evidence That NF-KB and MAPK Signaling Promotes NLRP Inflammasome Activation in Neurons Following Ischemic Stroke'. *Molecular Neurobiology*, 55(2), pp. 1082–1096.

Faustin, B., Chen, Y., Zhai, D., Le Negrate, G., Lartigue, L., Satterthwait, A. and Reed, J.C. (2009) 'Mechanism of Bcl-2 and Bcl-X(L) Inhibition of NLRP1 Inflammasome: Loop Domain-Dependent Suppression of ATP Binding and Oligomerization'. *Proc Natl Acad Sci U S A*, 106(10), pp. 3935–3940.

Faustin, B., Lartigue, L., Bruey, J.-M., Luciano, F., Sergienko, E., Bailly-Maitre, B., Volkmann, N., Hanein, D., Rouiller, I. and Reed, J.C. (2007) 'Reconstituted NALP1 Inflammasome Reveals Two-Step Mechanism of Caspase-1 Activation'. *Molecular Cell*, 25(5), pp. 713–724.

Feng, S., Fox, D. and Man, S.M. (2018) 'Mechanisms of Gasdermin Family Members in Inflammasome Signaling and Cell Death'. *Journal of Molecular Biology*, 430(18), pp. 3068–3080.

Fernandes-Alnemri, T., Yu, J.-W., Datta, P., Wu, J. and Alnemri, E.S. (2009) 'AIM2 Activates the Inflammasome and Cell Death in Response to Cytoplasmic DNA'. *Nature*, 458(7237), pp. 509–513.

Finger, J.N., Lich, J.D., Dare, L.C., Cook, M.N., Brown, K.K., Duraiswamis, C., Bertin, J.J. and Gough, P.J. (2012) 'Autolytic Proteolysis within the Function to Find Domain (FIIND) Is Required for NLRP1 Inflammasome Activity'. *Journal of Biological Chemistry*, 287(30), pp. 25030–25037.

Fink, S.L. and Cookson, B.T. (2006) 'Caspase-1-Dependent Pore Formation during Pyroptosis Leads to Osmotic Lysis of Infected Host Macrophages'. *Cellular Microbiology*, 8(11), pp. 1812–1825.

Fischer, H., de Oliveira Neto, M., Napolitano, H.B., Polikarpov, I. and Craievich, A.F. (2010) 'Determination of the Molecular Weight of Proteins in Solution from a Single Small-Angle X-Ray Scattering Measurement on a Relative Scale'. *Journal of Applied Crystallography*, 43(1), pp. 101–109.

Franchi, L., Warner, N., Viani, K. and Nuñez, G. (2009) 'Function of Nod-like Receptors in Microbial Recognition and Host Defense'. *Immunological Reviews*, 227(1), pp. 106–128.

Gai, K., Okondo, M.C., Rao, S.D., Chui, A.J., Ball, D.P., Johnson, D.C. and Bachovchin, D.A. (2019) 'DPP8/9 Inhibitors Are Universal Activators of Functional NLRP1 Alleles'. *Cell Death & Disease*, 10(8), p. 587.

Galluzzi, L. *et al.* (2018) 'Molecular Mechanisms of Cell Death: Recommendations of the Nomenclature Committee on Cell Death 2018.' *Cell Death and Differentiation*, 25(3), pp. 486–541.

Gantner, B.N., Simmons, R.M., Canavera, S.J., Akira, S. and Underhill, D.M. (2003) 'Collaborative Induction of Inflammatory Responses by Dectin-1 and Toll-like Receptor 2'. *The Journal of Experimental Medicine*, 197(9), pp. 1107–1117.

Gao, C., Devarajan, K., Zhou, Y., Slater, C.M., Daly, M.B. and Chen, X. (2012) 'Identifying Breast Cancer Risk Loci by Global Differential Allele-Specific Expression (DASE) Analysis in Mammary Epithelial Transcriptome.' *BMC Genomics*, 13(1), p. 570.

Gao, P., Zillinger, T., Wang, W., Ascano, M., Dai, P., Hartmann, G., Tuschl, T., Deng, L., Barchet, W. and Patel, D.J. (2014) 'Binding-Pocket and Lid-Region Substitutions Render Human STING Sensitive to the Species-Specific Drug DMXAA'. *Cell Reports*, 8(6), pp. 1668–1676.

Gao, P., Ascano, M., Zillinger, T., Wang, W., Dai, P., Serganov, A.A., Gaffney, B.L., Shuman, S., Jones, R.A., Deng, L., Hartmann, G., Barchet, W., Tuschl, T. and Patel, D.J. (2013) 'Structure-Function Analysis of STING Activation by c[G(2',5')PA(3',5')p] and Targeting by Antiviral DMXAA.' *Cell*, 154(4), pp. 748–62.

Garlanda, C., Dinarello, C.A. and Mantovani, A. (2013) 'The Interleukin-1 Family: Back to the Future'. *Immunity*, 39(6), pp. 1003–1018.

Gay, N.J. and Gangloff, M. (2007) 'Structure and Function of Toll Receptors and Their Ligands'. *Annual Review of Biochemistry*, 76(1), pp. 141–165.

Geldhoff, M., Mook-Kanamori, B.B., Brouwer, M.C., Valls Seron, M., Baas, F., van der Ende, A. and van de Beek, D. (2013) 'Genetic Variation in Inflammasome Genes Is Associated with Outcome in Bacterial Meningitis.' *Immunogenetics*, 65(1), pp. 9–16.

Giacomelli, R., Ruscitti, P., Alvaro, S., Ciccia, F., Liakouli, V., Di Benedetto, P., Guggino, G., Berardicurti, O., Carubbi, F., Triolo, G. and Cipriani, P. (2016) 'IL-1 β at the Crossroad between Rheumatoid Arthritis and Type 2 Diabetes: May We Kill Two Birds with One Stone?' *Expert Review of Clinical Immunology*, 12(8), pp. 849–855.

Girardin, S.E., Boneca, I.G., Viala, J., Chamaillard, M., Labigne, A., Thomas, G., Philpott, D.J. and Sansonetti, P.J. (2003) 'Nod2 Is a General Sensor of Peptidoglycan through Muramyl Dipeptide (MDP) Detection'. *Journal of Biological Chemistry*, 278(11), pp. 8869–8872.

Gloria, Y.C., Latz, E. and De Nardo, D. (2018) 'Generation of Innate Immune Reporter Cells Using Retroviral Transduction'. *Methods in Molecular Biology*, 1714, pp. 97–117.

Van Goethem, S., Matheussen, V., Joossens, J., Lambeir, A.-M., Chen, X., De Meester, I., Haemers, A., Augustyns, K. and Van der Veken, P. (2011) 'Structure–Activity Relationship Studies on Isoindoline Inhibitors of Dipeptidyl Peptidases 8 and 9 (DPP8, DPP9): Is DPP8-Selectivity an Attainable Goal?' *Journal of Medicinal Chemistry*, 54(16), pp. 5737–5746.

Gorfu, G., Cirelli, K.M., Melo, M.B., Mayer-Barber, K., Crown, D., Koller, B.H., Masters, S., Sher, A., Leppla, S.H., Moayeri, M., Saeij, J.P.J. and Grigg, M.E. (2014) 'Dual Role for Inflammasome Sensors NLRP1 and NLRP3 in Murine Resistance to Toxoplasma Gondii' Weiss, L.M. (ed.). *MBio*, 5(1), pp. e01117-13.

Gov, L., Karimzadeh, A., Ueno, N. and Lodoen, M.B. (2013) 'Human Innate Immunity to Toxoplasma Gondii Is Mediated by Host Caspase-1 and ASC and Parasite GRA15.' *MBio*, 4(4), pp. 1–11.

Graham, L.M. and Brown, G.D. (2009) 'The Dectin-2 Family of C-Type Lectins in Immunity and Homeostasis'. *Cytokine*, 48(1–2), pp. 148–155.

Grandemange, S. et al. (2017) 'A New Autoinflammatory and Autoimmune Syndrome Associated with NLRP1 Mutations: NAIAD (NLRP1- Associated Autoinflammation with Arthritis and Dyskeratosis)'. *Annals of the Rheumatic Diseases*, 76(7), pp. 1191–1198.

Griswold, A.R., Cifani, P., Rao, S.D., Axelrod, A.J., Miele, M.M., Hendrickson, R.C., Kentsis, A. and Bachovchin, D.A. (2019) 'A Chemical Strategy for Protease Substrate Profiling'. *Cell Chemical Biology*, pp. 1–7.

Gundacker, D., Leys, S.P., Schröder, H.C., Müller, I.M. and Müller, W.E.G. (2001) 'Isolation and Cloning of a C-Type Lectin from the Hexactinellid Sponge *Aphrocallistes Vastus*: A Putative Aggregation Factor'. *Glycobiology*, 11(1), pp. 21–29.

Guo, H., Callaway, J.B. and Ting, J.P.-Y. (2015) 'Inflammasomes: Mechanism of Action, Role in Disease, and Therapeutics.' *Nature Medicine*, 21(7), pp. 677–687.

Hanson, P.I. and Whiteheart, S.W. (2005) 'AAA+ Proteins: Have Engine, Will Work'. *Nature Reviews Molecular Cell Biology*, 6(7), pp. 519–529.

Hansson, G.K. and Edfeldt, K. (2005) 'Toll to Be Paid at the Gateway to the Vessel Wall'. *Arteriosclerosis, Thrombosis, and Vascular Biology*, 25(6), pp. 1085–1087.

Hänzelmann, P. and Schindelin, H. (2016) 'Structural Basis of ATP Hydrolysis and Intersubunit Signaling in the AAA+ ATPase P97.' *Structure (London, England: 1993)*, 24(1), pp. 127–139.

Hara, H., Tsuchiya, K., Kawamura, I., Fang, R., Hernandez-Cuellar, E., Shen, Y., Mizuguchi, J., Schweighoffer, E., Tybulewicz, V. and Mitsuyama, M. (2013) 'Phosphorylation of the Adaptor ASC Acts as a Molecular Switch That Controls the Formation of Speck-like Aggregates and Inflammasome Activity'. *Nature Immunology*, 14(12), pp. 1247–1255.

Harms, R.Z., Yarde, D.N., Guinn, Z., Lorenzo-Arteaga, K.M., Corley, K.P., Cabrera, M.S. and Sarvetnick, N.E. (2015) 'Increased Expression of IL-18 in the Serum and Islets of Type 1 Diabetics.' *Molecular Immunology*, 64(2), pp. 306–312.

Harris, P.A., Duraiswami, C., Fisher, D.T., Fornwald, J., Hoffman, S.J., Hofmann, G., Jiang, M., Lehr, R., McCormick, P.M., Nickels, L., Schwartz, B., Wu, Z., Zhang, G., Marquis, R.W., Bertin, J. and Gough, P.J. (2015) 'High Throughput Screening Identifies ATP-Competitive Inhibitors of the NLRP1 Inflammasome'. *Bioorganic & Medicinal Chemistry Letters*, 25(14), pp. 2739–2743.

Hastie, C.J., McLauchlan, H.J. and Cohen, P. (2006) 'Assay of Protein Kinases Using Radiolabeled ATP: A Protocol'. *Nature Protocols*, 1(2), pp. 968–971.

He, W.T., Wan, H., Hu, L., Chen, P., Wang, X., Huang, Z., Yang, Z.H., Zhong, C.Q. and Han, J. (2015) 'Gasdermin D Is an Executor of Pyroptosis and Required for Interleukin-1 β Secretion'. *Cell Research*, 25(12), pp. 1285–1298.

Heilig, R. and Broz, P. (2018) 'Function and Mechanism of the Pysin Inflammasome'. *European Journal of Immunology*, 48(2), pp. 230–238.

Hellmich, K.A., Levinsohn, J.L., Fattah, R., Newman, Z.L., Maier, N., Sastalla, I., Liu, S., Leppla, S.H. and Moayeri, M. (2012) 'Anthrax Lethal Factor Cleaves Mouse Nlrp1b in Both Toxin-Sensitive and Toxin-Resistant Macrophages'. *PLoS ONE*, 7(11), pp. 1–5.

Hiller, S., Kohl, A., Fiorito, F., Herrmann, T., Wider, G., Tschopp, J., Grütter, M.G. and Wüthrich, K. (2003) 'NMR Structure of the Apoptosis- and Inflammation-Related NALP1 Pysin Domain'. *Structure*, 11(10), pp. 1199–1205.

Ho, L.-P., Davis, M., Denison, A., Wood, F.T. and Greening, A.P. (2002) 'Reduced Interleukin-18 Levels in BAL Specimens From Patients With Asthma Compared to Patients With Sarcoidosis and Healthy Control Subjects'. *Chest*, 121(5), pp. 1421–1426.

Hodel, A.E., Hodel, M.R., Griffis, E.R., Hennig, K.A., Ratner, G.A., Xu, S. and Powers, M.A. (2002) 'The Three-Dimensional Structure of the Autoproteolytic, Nuclear Pore-Targeting Domain of the Human Nucleoporin Nup98'. *Molecular Cell*, 10(2), pp. 347–358.

Hoffmann, J.A., Lemaitre, B., Nicolas, E., Michaut, L. and Reichhart, J.-M. (1996) 'The Dorsoventral Regulatory Gene Cassette Spätzle/Toll/Cactus Controls the Potent Antifungal Response in *Drosophila* Adults'. *Cell*, 86(6), pp. 973–983.

Hornung, V., Ablasser, A., Charrel-Dennis, M., Bauernfeind, F., Horvath, G., Caffrey, D.R., Latz, E. and Fitzgerald, K.A. (2009) 'AIM2 Recognizes Cytosolic DsDNA and Forms a Caspase-1-Activating Inflammasome with ASC'. *Nature*, 458(7237), pp. 514–518.

Hoving, J.C., Wilson, G.J. and Brown, G.D. (2014) 'Signalling C-Type Lectin Receptors, Microbial Recognition and Immunity'. *Cellular Microbiology*, 16(2), pp. 185–194.

Hu, J., Liu, X., Zhao, J., Xia, S., Ruan, J., Luo, X., Kim, J., Lieberman, J. and Wu, H. (2018) 'Identification of Pyroptosis Inhibitors That Target a Reactive Cysteine in Gasdermin D'. *BioRxiv*, unpublishe.

Hu, Z., Yan, C., Liu, P., Huang, Z., Ma, R., Zhang, C., Wang, R., Zhang, Y., Martinon, F., Miao, D., Deng, H., Wang, J., Chang, J. and Chai, J. (2013) 'Crystal Structure of NLRC4 Reveals Its Autoinhibition Mechanism'. *Science*, 341(6142), pp. 172–175.

Hu, Z. and Chai, J. (2016) 'Structural Mechanisms in NLR Inflammasome Assembly and Signaling'. *Current Topics in Microbiology and Immunology*, 397, pp. 23–42.

Huysamen, C. and Brown, G.D. (2008) 'The Fungal Pattern Recognition Receptor, Dectin-1, and the Associated Cluster of C-Type Lectin-like Receptors'. *FEMS Microbiology Letters*, 290(2), pp. 121–128.

Imai, Y.N., Inoue, Y. and Yamamoto, Y. (2007) 'Propensities of Polar and Aromatic Amino Acids in Noncanonical Interactions: Nonbonded Contacts Analysis of Protein–Ligand Complexes in Crystal Structures'. *Journal of Medicinal Chemistry*, 50(6), pp. 1189–1196.

Inohara, N., Ogura, Y., Fontalba, A., Gutierrez, O., Pons, F., Crespo, J., Fukase, K., Inamura, S., Kusumoto, S., Hashimoto, M., Foster, S.J., Moran, A.P., Fernandez-Luna, J.L. and Nuñez, G. (2003) 'Host Recognition of Bacterial Muramyl Dipeptide Mediated through NOD2: Implications for Crohn's Disease'. *Journal of Biological Chemistry*, 278(8), pp. 5509–5512.

Ishikawa, H., Ma, Z. and Barber, G.N. (2009) 'STING Regulates Intracellular DNA-Mediated, Type I Interferon-Dependent Innate Immunity'. *Nature*, 461(7265), pp. 788–792.

Iyer, L.M., Leipe, D.D., Koonin, E. V. and Aravind, L. (2004) 'Evolutionary History and Higher Order Classification of AAA+ ATPases'. *Journal of Structural Biology*, 146(1–2), pp. 11–31.

Jacques, D.A. and Trewella, J. (2010) 'Small-Angle Scattering for Structural Biology - Expanding the Frontier While Avoiding the Pitfalls'. *Protein Science*, 19(4), pp. 642–657.

Jakobs, C., Perner, S. and Hornung, V. (2015) 'AIM2 Drives Joint Inflammation in a Self-DNA Triggered Model of Chronic Polyarthritis.' *PloS One*, 10(6), p. e0131702.

James Milner-White, E., Coggins, J.R. and Anton, I.A. (1991) 'Evidence for an Ancestral Core Structure in Nucleotide-Binding Proteins with the Type A Motif'. *Journal of Molecular Biology*, 221(3), pp. 751–754.

Jenuwein, T. and Allis, C.D. (2001) 'Translating the Histone Code'. *Science*, 293(5532), pp. 1074–1080.

Jin, M.S., Kim, S.E., Heo, J.Y., Lee, M.E., Kim, H.M., Paik, S.G., Lee, H. and Lee, J.O. (2007) 'Crystal Structure of the TLR1-TLR2 Heterodimer Induced by Binding of a Tri-Acylated Lipopeptide'. *Cell*, 130(6), pp. 1071–1082.

Jin, M.S. and Lee, J.-O. (2008) 'Structures of the Toll-like Receptor Family and Its Ligand Complexes'. *Immunity*, 29(2), pp. 182–191.

Jin, T., Curry, J., Smith, P., Jiang, J. and Xiao, T.S. (2013) 'Structure of the NLRP1 Caspase Recruitment Domain Suggests Potential Mechanisms for Its Association with Procaspace-1'. *Proteins: Structure, Function and Bioinformatics*, 81(7), pp. 1266–1270.

Jin, Y., Mailloux, C.M., Gowan, K., Riccardi, S.L., LaBerge, G., Bennett, D.C., Fain, P.R. and Spritz, R.A. (2007) 'NALP1 in Vitiligo-Associated Multiple Autoimmune Disease'. *N Engl J Med*, 356(12), pp. 1216–1225.

Johnson, D.C. *et al.* (2018) 'DPP8 / 9 Inhibitor-Induced Pyroptosis for Treatment of Acute Myeloid Leukemia'. *Nature Medicine*.

Johnson, V.J., Yucesoy, B. and Luster, M.I. (2005) 'Prevention of IL-1 Signaling Attenuates Airway Hyperresponsiveness and Inflammation in a Murine Model of Toluene Diisocyanate-Induced Asthma'. *Journal of Allergy and Clinical Immunology*, 116(4), pp. 851–858.

Jones, J.D.G., Vance, R.E. and Dangl, J.L. (2016) 'Intracellular Innate Immune Surveillance Devices in Plants and Animals'. *Science*, 354(6316), pp. aaf6395–aaf6395.

Jorgensen, I. and Miao, E.A. (2015) 'Pyroptotic Cell Death Defends against Intracellular Pathogens'. *Immunological Reviews*, 265(1), pp. 130–142.

Justa-Schuch, D., Silva-Garcia, M., Pilla, E., Engelke, M., Kilisch, M., Lenz, C., Möller, U., Nakamura, F., Urlaub, H. and Geiss-Friedlander, R. (2016) 'DPP9 Is a Novel Component of the N-End Rule Pathway Targeting the Tyrosine Kinase Syk'. *ELife*, 5(September), pp. 1–26.

Kale, J., Osterlund, E.J. and Andrews, D.W. (2018) 'BCL-2 Family Proteins: Changing Partners in the Dance towards Death'. *Cell Death & Differentiation*, 25(1), pp. 65–80.

Kanazawa, N. (2007) 'Dendritic Cell Immunoreceptors: C-Type Lectin Receptors for Pattern-Recognition and Signaling on Antigen-Presenting Cells.' *Journal of Dermatological Science*, 45(2), pp. 77–86.

Kanazawa, N., Tashiro, K. and Miyachi, Y. (2004) 'Signaling and Immune Regulatory Role of the Dendritic Cell Immunoreceptor (DCIR) Family Lectins: DCIR, DCAR, Dectin-2 and BDCA-2'. *Immunobiology*, 209(1–2), pp. 179–190.

Kaplanov, I., Carmi, Y., Kornetsky, R., Shemesh, A., Shurin, G. V., Shurin, M.R., Dinarello, C.A., Voronov, E. and Apte, R.N. (2019) 'Blocking IL-1 β Reverses the Immunosuppression in Mouse Breast Cancer and Synergizes with Anti-PD-1 for Tumor Abrogation.' *Proceedings of the National Academy of Sciences of the United States of America*, 116(4), pp. 1361–1369.

Kaplanski, G. (2018) 'Interleukin-18: Biological Properties and Role in Disease Pathogenesis'. *Immunological Reviews*, 281(1), pp. 138–153.

Kato, H., Takeuchi, O., Mikamo-Satoh, E., Hirai, R., Kawai, T., Matsushita, K., Hiiragi, A., Dermody, T.S., Fujita, T. and Akira, S. (2008) 'Length-Dependent Recognition of Double-Stranded Ribonucleic Acids by Retinoic Acid-Inducible Gene-1 and Melanoma Differentiation-Associated Gene 5'. *The Journal of Experimental Medicine*, 205(7), pp. 1601–1610.

Kawai, T. and Akira, S. (2007) 'TLR Signaling'. *Seminars in Immunology*, 19(1), pp. 24–32.

Kawasaki, T. and Kawai, T. (2014) 'Toll-like Receptor Signaling Pathways.' *Frontiers in Immunology*, 5(5625), p. 461.

Kayagaki, N. *et al.* (2015) 'Caspase-11 Cleaves Gasdermin D for Non-Canonical Inflammasome Signalling'. *Nature*, 526(7575), pp. 666–671.

Khan, A.R. and James, M.N.G. (2008) 'Molecular Mechanisms for the Conversion of Zymogens to Active Proteolytic Enzymes'. *Protein Science*, 7(4), pp. 815–836.

Khoury, G.A., Baliban, R.C. and Floudas, C.A. (2011) 'Proteome-Wide Post-Translational Modification Statistics: Frequency Analysis and Curation of the Swiss-Prot Database'. *Scientific Reports*, 1, pp. 1–5.

Kim, H.-E., Du, F., Fang, M. and Wang, X. (2005) 'Formation of Apoptosome Is Initiated by Cytochrome C-Induced DATP Hydrolysis and Subsequent Nucleotide Exchange on Apaf-1'. *Proceedings of the National Academy of Sciences*, 102(49), pp. 17545–17550.

Kingeter, L.M. and Lin, X. (2012) 'C-Type Lectin Receptor-Induced NF- κ B Activation in Innate Immune and Inflammatory Responses'. *Cellular and Molecular Immunology*, 9(2), pp. 105–112.

Kodama, T., Matsuyama, T., Kuribayashi, K., Nishioka, Y., Sugita, M., Akira, S., Nakanishi, K. and Okamura, H. (2000) 'IL-18 Deficiency Selectively Enhances Allergen-Induced Eosinophilia in Mice'. *Journal of Allergy and Clinical Immunology*, 105(1), pp. 45–53.

Kofoed, E.M. and Vance, R.E. (2011) 'Innate Immune Recognition of Bacterial Ligands by NALPs Determines Inflammasome Specificity'. *Nature*, 477(7366), pp. 592–595.

Kolakofsky, D., Kowalinski, E. and Cusack, S. (2012) 'A Structure-Based Model of RIG-I Activation'. *Rna*, 18(12), pp. 2118–2127.

Konno, S., Gonokami, Y., Kurokawa, M., Kawazu, K., Asano, K., Okamoto, K. and Adachi, M. (1996) 'Cytokine Concentrations in Sputum of Asthmatic Patients'. *International Archives of Allergy and Immunology*, 109(1), pp. 73–78.

Koonin, E. V., Wolf, Y.I. and Aravind, L. (2004) 'Protein Fold Recognition Using Sequence Profiles and Its Application in Structural Genomics'. 54, pp. 245–275.

Kovarova, M., Hesker, P.R., Jania, L., Nguyen, M., Snouwaert, J.N., Xiang, Z., Lommatzsch, S.E., Huang, M.T., Ting, J.P.-Y. and Koller, B.H. (2012) 'NLRP1-Dependent Pyroptosis Leads to Acute Lung Injury and Morbidity in Mice'. *The Journal of Immunology*, 189(4), pp. 2006–2016.

Kumar, H., Kawai, T. and Akira, S. (2011) 'Pathogen Recognition by the Innate Immune System'. *International Reviews of Immunology*, 30(1), pp. 16–34.

Kummer, J.A., Broekhuizen, R., Everett, H., Agostini, L., Kuijk, L., Martinon, F., Van Bruggen, R. and Tschopp, J. (2007) 'Inflammasome Components NALP 1 and 3 Show Distinct but Separate Expression Profiles in Human Tissues Suggesting a Site-Specific Role in the Inflammatory Response'. *Journal of Histochemistry and Cytochemistry*, 55(5), pp. 443–452.

Kuribayashi, K., Kodama, T., Okamura, H., Sugita, M. and Matsuyama, T. (2002) 'Effects of Post-Inhalation Treatment with Interleukin-12 on Airway Hyper-Responsiveness, Eosinophilia and Interleukin-18 Receptor Expression in a Mouse Model of Asthma.' *Clinical and Experimental Allergy: Journal of the British Society for Allergy and Clinical Immunology*, 32(4), pp. 641–649.

Lacy, P. (2015) 'Editorial: Secretion of Cytokines and Chemokines by Innate Immune Cells'. *Frontiers in Immunology*, 6(190).

Laddha, N.C., Dwivedi, M., Mansuri, M.S., Singh, M., Patel, H.H., Agarwal, N., Shah, A.M. and Begum, R. (2014) 'Association of Neuropeptide Y (NPY), Interleukin-1B (IL1B) Genetic Variants and Correlation of IL1B Transcript Levels with Vitiligo Susceptibility.' *PloS One*, 9(9), p. e107020.

Lam, E., Stein, S. and Falck-Pedersen, E. (2014) 'Adenovirus Detection by the CGAS/STING/TBK1 DNA Sensing Cascade'. *Journal of Virology*, 88(2), pp. 974–981.

Larquet, E., Schreiber, V., Boisset, N. and Richet, E. (2004) 'Oligomeric Assemblies of the Escherichia Coli MalT Transcriptional Activator Revealed by Cryo-Electron Microscopy and Image Processing'. *Journal of Molecular Biology*, 343(5), pp. 1159–1169.

Lässig, C., Matheisl, S., Sparrer, K.M.J., de Oliveira Mann, C.C., Moldt, M., Patel, J.R., Goldeck, M., Hartmann, G., García-Sastre, A., Hornung, V., Conzelmann, K.-K., Beckmann, R. and Hopfner, K.-P. (2015) 'ATP Hydrolysis by the Viral RNA Sensor RIG-I Prevents Unintentional Recognition of Self-RNA'. *ELife*, 4 (November 2015), pp. 1–20.

Leal, V.N.C., Genov, I.R., Mallozi, M.C., Solé, D. and Pontillo, A. (2018) 'Polymorphisms in Inflammasome Genes and Risk of Asthma in Brazilian Children'. *Molecular Immunology*, 93(August 2017), pp. 64–67.

Lei, Y., Devarapu, S.K., Motrapu, M., Cohen, C.D., Lindenmeyer, M.T., Moll, S., Kumar, S. V. and Anders, H.-J. (2019) 'Interleukin-1 β Inhibition for Chronic Kidney Disease in Obese Mice With Type 2 Diabetes.' *Frontiers in Immunology*, 10(MAY), p. 1223.

Leipe, D.D., Koonin, E. V. and Aravind, L. (2004) 'STAND, a Class of P-Loop NTPases Including Animal and Plant Regulators of Programmed Cell Death: Multiple, Complex Domain Architectures, Unusual Phyletic Patterns, and Evolution by Horizontal Gene Transfer'. *Journal of Molecular Biology*, 343(1), pp. 1–28.

Levandowski, C.B., Mailloux, C.M., Ferrara, T.M., Gowan, K., Ben, S., Jin, Y., McFann, K.K., Holland, P.J., Fain, P.R., Dinarello, C.A. and Spritz, R.A. (2013) 'NLRP1 Haplotypes Associated with Vitiligo and Autoimmunity Increase Interleukin-1 β Processing via the NLRP1 Inflammasome'. *Proceedings of the National Academy of Sciences*, 110(8), pp. 2952–2956.

Levinsohn, J.L., Newman, Z.L., Hellmich, K.A., Fattah, R., Getz, M.A., Liu, S., Sastalla, I., Leppla, S.H. and Moayeri, M. (2012) 'Anthrax Lethal Factor Cleavage of Nlrp1 Is Required for Activation of the Inflammasome'. *PLoS Pathogens*, 8(3).

Li, S.-C., Goto, N.K., Williams, K.A., Deber, C.M. and Fasman, G.D. (2005) 'A-Helical, but Not (β -Sheet, Propensity of Proline Is Determined by Peptide Environment'. *Biochemistry A-Helical*, 93(June), pp. 1–6.

Liao, K.-C. and Mogridge, J. (2009) 'Expression of Nlrp1b Inflammasome Components in Human Fibroblasts Confers Susceptibility to Anthrax Lethal Toxin'. *Infection and Immunity*, 77(10), pp. 4455–4462.

Liao, K.C. and Mogridge, J. (2013) 'Activation of the Nlrp1b Inflammasome by Reduction of Cytosolic ATP'. *Infection and Immunity*, 81(2), pp. 570–579.

Lim, E.-J., Lee, S.-H., Lee, J.-G., Kim, J.-R., Yun, S.-S., Baek, S.-H. and Lee, C. (2007) 'Toll-like Receptor 9 Dependent Activation of MAPK and NF-KB Is Required for the CpG ODN-Induced Matrix Metalloproteinase-9 Expression'. *Experimental & Molecular Medicine*, 39(2), pp. 239–245.

Liston, A. and Masters, S.L. (2017) 'Homeostasis-Altering Molecular Processes as Mechanisms of Inflammasome Activation'. *Nature Reviews Immunology*, 17(3), pp. 208–214.

Liu, F., Lo, C.F., Ning, X., Kajkowski, E.M., Jin, M., Chiriac, C., Gonzales, C., Naureckiene, S., Lock, Y.W., Pong, K., Zaleska, M.M., Jacobsen, J.S., Silverman, S. and Ozenberger, B.A. (2004) 'Expression of NALP1 in Cerebellar Granule Neurons Stimulates Apoptosis'. *Cellular Signalling*, 16(9), pp. 1013–1021.

Liu, X., Zhang, Z., Ruan, J., Pan, Y., Magupalli, V.G., Wu, H. and Lieberman, J. (2016) 'Inflammasome-Activated Gasdermin D Causes Pyroptosis by Forming Membrane Pores'. *Nature*, 535(7610), pp. 153–158.

Liu, X., Hu, J., Li, Y., Cao, W., Wang, Y., Ma, Z. and Li, F. (2018) 'Mesenchymal Stem Cells Expressing Interleukin-18 Inhibit Breast Cancer in a Mouse Model.' *Oncology Letters*, 15(5), pp. 6265–6274.

Liu, Y. *et al.* (2014) 'Activated STING in a Vascular and Pulmonary Syndrome'. *New England Journal of Medicine*, 371(6), pp. 507–518.

Liu, Z., Wang, C., Yang, J., Zhou, B., Yang, R., Ramachandran, R., Abbott, D.W. and Xiao, T.S. (2019) 'Crystal Structures of the Full-Length Murine and Human Gasdermin D Reveal Mechanisms of Autoinhibition, Lipid Binding, and Oligomerization.' *Immunity*, 51(1), pp. 43-49.e4.

Loo, Y.M. and Gale, M. (2011) 'Immune Signaling by RIG-I-like Receptors'. *Immunity*, 34(5), pp. 680–692.

Lugrin, J. and Martinon, F. (2018) 'The AIM2 Inflammasome: Sensor of Pathogens and Cellular Perturbations'. *Immunological Reviews*, 281(1), pp. 99–114.

Lukens, J.R., Gross, J.M. and Kanneganti, T.D. (2012) 'IL-1 Family Cytokines Trigger Sterile Inflammatory Disease'. *Frontiers in Immunology*, 3(OCT), pp. 1–12.

Luo, D., Ding, S.C., Vela, A., Kohlway, A., Lindenbach, B.D. and Pyle, A.M. (2011) 'Structural Insights into RNA Recognition by RIG-I'. *Cell*, 147(2), pp. 409–422.

Macdonald, J.A., Wijekoon, C.P., Liao, K.C. and Muruve, D.A. (2013) 'Biochemical and Structural Aspects of the ATP-Binding Domain in Inflammasome-Forming Human NLRP Proteins'. *IUBMB Life*, 65(10), pp. 851–862.

Madeira, F., Park, Y., Lee, J., Buso, N., Gur, T., Madhusoodanan, N., Basutkar, P., Tivey, A.R.N., Potter, S.C., Finn, D. and Lopez, R. (2019) 'The EMBL-EBI Search and Sequence Analysis Tools APIs in 2019'. *Nucleic Acids Research*, 47(April), pp. 636–641.

Maekawa, S., Ohto, U., Shibata, T., Miyake, K. and Shimizu, T. (2016) 'Crystal Structure of NOD2 and Its Implications in Human Disease.' *Nature Communications*, 7(May), p. 11813.

Maharana, J., Panda, D. and De, S. (2018) 'Deciphering the ATP-Binding Mechanism(s) in NLRP-NACHT 3D Models Using Structural Bioinformatics Approaches'. *PLoS ONE*, 13(12), pp. 1–17.

Mambwe, B., Neo, K., Javanmard Khameneh, H., Leong, K.W.K., Colantuoni, M., Vacca, M., Muimo, R. and Mortellaro, A. (2019) 'Tyrosine Dephosphorylation of ASC Modulates the Activation of the NLRP3 and AIM2 Inflammasomes'. *Frontiers in Immunology*, 10(July), pp. 1–9.

Man, S.M., Karki, R. and Kanneganti, T.-D. (2016) 'AIM2 Inflammasome in Infection, Cancer, and Autoimmunity: Role in DNA Sensing, Inflammation, and Innate Immunity'. *European Journal of Immunology*, 46(2), pp. 269–280.

Mariathasan, S., Weiss, D.S., Newton, K., McBride, J., O'Rourke, K., Roose-Girma, M., Lee, W.P., Weinrauch, Y., Monack, D.M. and Dixit, V.M. (2006) 'Cryopyrin Activates the Inflammasome in Response to Toxins and ATP'. *Nature*, 440(7081), pp. 228–232.

Martino, L., Holland, L., Christodoulou, E., Kunzelmann, S., Esposito, D. and Rittinger, K. (2016) 'The Biophysical Characterisation and SAXS Analysis of Human NLRP1 Uncover a New Level of Complexity of NLR Proteins'. *Plos One*, 11(10), p. e0164662.

Martinon, F., Agostini, L., Meylan, E. and Tschopp, J. (2004) 'Identification of Bacterial Muramyl Dipeptide as Activator of the NALP3/Cryopyrin Inflammasome'. *Current Biology*, 14(21), pp. 1929–1934.

Martinon, F., Burns, K. and Tschopp, J. (2002) 'The Inflammasome: A Molecular Platform Triggering Activation of Inflammatory Caspases and Processing of ProIL- β '. *Molecular Cell*, 10(2), pp. 417–426.

Martinon, F., Hofmann, K. and Tschopp, J. (2001) 'The Pysin Domain: A Possible Member of the Death Domain-Fold Family Implicated in Apoptosis and Inflammation'. *Current Biology*, 11(4), pp. 118–120.

Martinon, F. and Tschopp, J. (2005) 'NLRs Join TLRs as Innate Sensors of Pathogens'. *Trends in Immunology*, 26(8), pp. 447–454.

Masters, S.L. *et al.* (2016) 'Familial Autoinflammation with Neutrophilic Dermatitis Reveals a Regulatory Mechanism of Pysin Activation.' *Science Translational Medicine*, 8(332), p. 332ra45.

Masters, S.L. *et al.* (2012) 'NLRP1 Inflammasome Activation Induces Pyroptosis of Hematopoietic Progenitor Cells'. *Immunity*, 37(6), pp. 1009–1023.

- Matsushima, N., Tanaka, T., Enkhbayar, P., Mikami, T., Taga, M., Yamada, K. and Kuroki, Y. (2007) 'Comparative Sequence Analysis of Leucine-Rich Repeats (LRRs) within Vertebrate Toll-like Receptors'. *BMC Genomics*, 8, pp. 1–20.
- Matveeva, E.A., He, P. and Whiteheart, S.W. (1997) 'N-Ethylmaleimide Fusion Protein Contains High and Low Affinity ATP- Binding Sites That Are Functionally Distinct'. *Journal of Biological Chemistry*, 272(42), pp. 26413–26418.
- Maver, A. *et al.* (2017) 'Identification of Rare Genetic Variation of NLRP1 Gene in Familial Multiple Sclerosis'. *Scientific Reports*, 7(1), p. 3715.
- McGreal, E.P., Rosas, M., Brown, G.D., Zamze, S., Wong, S.Y.C., Gordon, S., Martinez-Pomares, L. and Taylor, P.R. (2006) 'The Carbohydrate-Recognition Domain of Dectin-2 Is a C-Type Lectin with Specificity for High Mannose'. *Glycobiology*, 16(5), pp. 422–430.
- Medzhitov, R., Preston-Hurlburt, P., Kopp, E., Stadlen, A., Chen, C., Ghosh, S. and Janeway, C.A. (1998) 'MyD88 Is an Adaptor Protein in the HToll/IL-1 Receptor Family Signaling Pathways'. *Molecular Cell*, 2(2), pp. 253–258.
- Medzhitov, R. and Janeway, C.A. (1997) 'Innate Immunity: Minireview The Virtues of a Nonclonal System of Recognition'. 91, pp. 295–298.
- Merad, M., Sathe, P., Helft, J., Miller, J. and Mortha, A. (2013) 'The Dendritic Cell Lineage: Ontogeny and Function of Dendritic Cells and Their Subsets in the Steady State and the Inflamed Setting'. *Annual Review of Immunology*, 31(1), pp. 563–604.
- Meunier, E. and Broz, P. (2017) 'Evolutionary Convergence and Divergence in NLR Function and Structure'. *Trends in Immunology*, 38(10), pp. 744–757.

Meyer, H., Bug, M. and Bremer, S. (2012) 'Emerging Functions of the VCP/P97 AAA-ATPase in the Ubiquitin System'. *Nature Cell Biology*, 14(2), pp. 117–123.

Miao, E.A. (2015) 'Pyroptotic Cell Death Defends againstPdf'. *Immunological Reviews*, 265, pp. 130–142.

Miller, J.M. and Enemark, E.J. (2016) 'Fundamental Characteristics of AAA+ Protein Family Structure and Function'. *Archaea*, 2016, pp. 1–12.

Moayeri, M., Sastalla, I. and Leppla, S.H. (2012) 'Anthrax and the Inflammasome'. *Microbes and Infection*, 14(5), pp. 392–400.

Moghaddas, F., Llamas, R., De Nardo, D., Martinez-Banaclocha, H., Martinez-Garcia, J.J., Mesa-Del-Castillo, P., Baker, P.J., Gargallo, V., Mensa-Vilaro, A., Canna, S., Wicks, I.P., Pelegrin, P., Arostegui, J.I. and Masters, S.L. (2017) 'A Novel Pyrin-Associated Autoinflammation with Neutrophilic Dermatitis Mutation Further Defines 14-3-3 Binding of Pyrin and Distinction to Familial Mediterranean Fever.' *Annals of the Rheumatic Diseases*, 76(12), pp. 2085–2094.

Moghaddas, F. *et al.* (2018) 'Autoinflammatory Mutation in NLRC4 Reveals an LRR-LRR Oligomerization Interface'. *Journal of Allergy and Clinical Immunology*.
Monteleone, G., Trapasso, F., Parrello, T., Biancone, L., Stella, A., Iuliano, R., Lizza, F., Fusco, A. and Pallone, F. (1999) 'Bioactive IL-18 Expression Is up-Regulated in Crohn's Disease.' *Journal of Immunology (Baltimore, Md. : 1950)*, 163, pp. 143–147.

Moran, A. *et al.* (2013) 'Interleukin-1 Antagonism in Type 1 Diabetes of Recent Onset: Two Multicentre, Randomised, Double-Blind, Placebo-Controlled Trials'. *The Lancet*, 381(9881), pp. 1905–1915.

Moriwaki, Y., Yamamoto, T., Shibutani, Y., Aoki, E., Tsutsumi, Z., Takahashi, S., Okamura, H., Koga, M., Fukuchi, M. and Hada, T. (2003) 'Elevated Levels of Interleukin-18 and Tumor Necrosis Factor- α in Serum of Patients with Type 2 Diabetes Mellitus: Relationship with Diabetic Nephropathy'. *Metabolism*, 52(5), pp. 605–608.

Nakamura, A., Shikata, K., Hiramatsu, M., Nakatou, T., Kitamura, T., Wada, J., Itoshima, T. and Makino, H. (2005) 'Serum Interleukin-18 Levels Are Associated With Nephropathy and Atherosclerosis in Japanese Patients With Type 2 Diabetes'. *Diabetes Care*, 28(12), pp. 2890–2895.

Nakanishi, K., Yoshimoto, T., Tsutsui, H. and Okamura, H. (2001) 'Interleukin-18 Regulates Both Th1 and Th2 Responses.' *Annual Review of Immunology*, 19(1), pp. 423–74.

Neiman-Zenevich, J., Stuart, S., Abdel-Nour, M., Girardin, S.E. and Mogridge, J. (2017) 'Listeria Monocytogenes and Shigella Flexneri Activate the NLRP1B Inflammasome.' *Infection and Immunity*, 85(11), pp. 1–10.

Nie, L., Cai, S.-Y., Shao, J.-Z. and Chen, J. (2018) 'Toll-Like Receptors, Associated Biological Roles, and Signaling Networks in Non-Mammals'. *Frontiers in Immunology*, 9(1523), pp. 1–19.

Nogueira, L.G. *et al.* (2015) 'Functional IL18 Polymorphism and Susceptibility to Chronic Chagas Disease.' *Cytokine*, 73(1), pp. 79–83.

Nunes, M.C.P., Beaton, A., Acquatella, H., Bern, C., Bolger, A.F., Echeverría, L.E., Dutra, W.O., Gascon, J., Morillo, C.A., Oliveira-Filho, J., Ribeiro, A.L.P. and Marin-Neto, J.A. (2018) 'Chagas Cardiomyopathy: An Update of Current Clinical Knowledge and Management: A Scientific Statement From the American Heart Association'. *Circulation*, 138(12), pp. e169–e209.

Ogura, T., Whiteheart, S.W. and Wilkinson, A.J. (2004) 'Conserved Arginine Residues Implicated in ATP Hydrolysis, Nucleotide-Sensing, and Inter-Subunit Interactions in AAA and AAA+ ATPases'. *Journal of Structural Biology*, 146(1–2), pp. 106–112.

Ogura, T. and Wilkinson, A.J. (2001) 'AAA+ Superfamily ATPases: Common Structure - Diverse Function.' *Genes to Cells: Devoted to Molecular & Cellular Mechanisms*, 6(7), pp. 575–597.

Ogura, Y., Inohara, N., Benito, A., Chen, F.F., Yamaoka, S. and Nunez, G. (2001) 'Nod2, a Nod1/Apaf-1 Family Member That Is Restricted to Monocytes and Activates NF-KappaB.' *The Journal of Biological Chemistry*, 276(7), pp. 4812–8.

Okamura, H., Tsutsi, H., Komatsu, T., Yutsudo, M., Hakura, A., Tanimoto, T., Torigoe, K., Okura, T., Nukada, Y. and Hattori, K. (1995) 'Cloning of a New Cytokine That Induces IFN-Gamma Production by T Cells.' *Nature*, 378(6552), pp. 88–91.

Okondo, M.C., Rao, S.D., Taabazuing, C.Y., Chui, A.J., Poplawski, S.E., Johnson, D.C. and Bachovchin, D.A. (2018) 'Inhibition of Dpp8/9 Activates the Nlrp1b Inflammasome'. *Cell Chemical Biology*, pp. 1–6.

Van Opendenbosch, N., Gurung, P., Vande Walle, L., Fossoul, A., Kanneganti, T.D. and Lamkanfi, M. (2014) 'Activation of the NLRP1b Inflammasome Independently of ASC-Mediated Caspase-1 Autoproteolysis and Speck Formation'. *Nature Communications*, 5, pp. 1–14.

Oroz, J., Barrera-Vilarmau, S., Alfonso, C., Rivas, G. and De Alba, E. (2016) 'ASC Pyrin Domain Self-Associates and Binds NLRP3 Protein Using Equivalent Binding Interfaces*'. *Journal of Biological Chemistry*, 291(37), pp. 19487–19501.

Owczarek, B., Gerszberg, A. and Hnatuszko-Konka, K. (2019) 'A Brief Reminder of Systems of Production and Chromatography-Based Recovery of Recombinant Protein Biopharmaceuticals'. *BioMed Research International*, 2019, pp. 1–13.

Pandeya, A., Li, L., Li, Z. and Wei, Y. (2019) 'Gasdermin D (GSDMD) as a New Target for the Treatment of Infection'. *MedChemComm*, 10(5), pp. 660–667.

Park, H.H., Logette, E., Raunser, S., Cuenin, S., Walz, T., Tschopp, J. and Wu, H. (2007) 'Death Domain Assembly Mechanism Revealed by Crystal Structure of the Oligomeric PIDDosome Core Complex'. *Cell*, 128(3), pp. 533–546.

Park, H.H., Lo, Y.-C., Lin, S.-C., Wang, L., Yang, J.K. and Wu, H. (2007) 'The Death Domain Superfamily in Intracellular Signaling of Apoptosis and Inflammation'. *Annual Review of Immunology*, 25(1), pp. 561–586.

Park, K., Shen, B.W., Parmeggiani, F., Huang, P.-S., Stoddard, B.L. and Baker, D. (2015) 'Control of Repeat-Protein Curvature by Computational Protein Design'. *Nature Structural & Molecular Biology*, 22(2), pp. 167–174.

Park, Y.H., Wood, G., Kastner, D.L. and Chae, J.J. (2016) 'Pyrin Inflammasome Activation and RhoA Signaling in the Autoinflammatory Diseases FMF and HIDS'. *Nat Immunol*, 17(8), pp. 914–921.

Perler, F.B., Xu, M.Q. and Paulus, H. (1997) 'Protein Splicing and Autoproteolysis Mechanisms'. *Current Opinion in Chemical Biology*, 1(3), pp. 292–299.

Petoukhov, M. V., Franke, D., Shkumatov, A. V., Tria, G., Kikhney, A.G., Gajda, M., Gorba, C., Mertens, H.D.T., Konarev, P. V. and Svergun, D.I. (2012) 'New Developments in the ATSAS Program Package for Small-Angle Scattering Data Analysis'. *Journal of Applied Crystallography*, 45(2), pp. 342–350.

Pettersen, E.F., Goddard, T.D., Huang, C.C., Couch, G.S., Greenblatt, D.M., Meng, E.C. and Ferrin, T.E. (2004) 'UCSF Chimera?A Visualization System for Exploratory Research and Analysis'. *Journal of Computational Chemistry*, 25(13), pp. 1605–1612.

Piiaodov, V., Ares de Araújo, E., Oliveira Neto, M., Craievich, A.F. and Polikarpov, I. (2019) 'SAXSMoW 2.0: Online Calculator of the Molecular Weight of Proteins in Dilute Solution from Experimental SAXS Data Measured on a Relative Scale'. *Protein Science*, 28(2), pp. 454–463.

Pizarro, T.T., Huybrechts, M., Bentz, M., Foley, E., Moskaluk, C.A., Bickston, S.J. and Cominelli, F. (1998) 'IL-18, a Novel Immunoregulatory Cytokine, Is Upregulated in Crohn's Disease: Expression and Localization in Intestinal Mucosal Cells'. *Gastroenterology*, 114(11), pp. 6829–6835.

Place, D.E. and Kanneganti, T.D. (2018) 'Recent Advances in Inflammasome Biology'. *Current Opinion in Immunology*, 50, pp. 32–38.

Polly Matzinger. (2002) 'The Danger Model: A Renewed Sense of Self'. *Science*, 296(5566), pp. 301–306.

Pontillo, A., Bricher, P., Leal, V.N.C., Lima, S., Souza, P.R.E. and Crovella, S. (2016) 'Role of Inflammasome Genetics in Susceptibility to HPV Infection and Cervical Cancer Development.' *Journal of Medical Virology*, 88(9), pp. 1646–51.

Proell, M., Riedl, S.J., Fritz, J.H., Rojas, A.M. and Schwarzenbacher, R. (2008) 'The Nod-Like Receptor (NLR) Family: A Tale of Similarities and Differences'. *PLoS ONE*, 3(4), pp. 1–11.

Py, B.F., Kim, M.S., Vakifahmetoglu-Norberg, H. and Yuan, J. (2013) 'Deubiquitination of NLRP3 by BRCC3 Critically Regulates Inflammasome Activity'. *Molecular Cell*, 49(2), pp. 331–338.

Qian, N., Chen, X., Han, S., Qiang, F., Jin, G., Zhou, X., Dong, J., Wang, X., Shen, H. and Hu, Z. (2010) 'Circulating IL-1 β Levels, Polymorphisms of IL-1B, and Risk of Cervical Cancer in Chinese Women'. *Journal of Cancer Research and Clinical Oncology*, 136(5), pp. 709–716.

Radian, A.D., Khare, S., Chu, L.H., Dorfleutner, A. and Stehlik, C. (2015) 'ATP Binding by NLRP7 Is Required for Inflammasome Activation in Response to Bacterial Lipopeptides'. *Molecular Immunology*, 67(2), pp. 294–302.

Rathinam, V.A.K., Vanaja, S.K. and Fitzgerald, K.A. (2012) 'Regulation of Inflammasome Signaling'. *Nature Immunology*, 13(4), pp. 333–342.

Reubold, T.F., Hahne, G., Wohlgemuth, S. and Eschenburg, S. (2014) 'Crystal Structure of the Leucine-Rich Repeat Domain of the NOD-like Receptor NLRP1: Implications for Binding of Muramyl Dipeptide'. *FEBS Letters*, 588(18), pp. 3327–3332.

Ricklin, D., Hajishengallis, G., Yang, K. and Lambris, J.D. (2010) 'Complement: A Key System for Immune Surveillance and Homeostasis'. *Nature Immunology*, 11(9), pp. 785–797.

Riedl, S.J., Li, W., Chao, Y., Schwarzenbacher, R. and Shi, Y. (2005) 'Structure of the Apoptotic Protease-Activating Factor 1 Bound to ADP'. *Nature*, 434(7035), pp. 926–933.

Robert, X. and Gouet, P. (2014) 'Deciphering Key Features in Protein Structures with the New ENDscript Server'. *Nucleic Acids Research*, 42(W1), pp. 320–324.

Ross, B., Krapp, S., Augustin, M., Kierfersauer, R., Arciniega, M., Geiss-Friedlander, R. and Huber, R. (2018) 'Structures and Mechanism of Dipeptidyl Peptidases 8 and 9, Important Players in Cellular Homeostasis and Cancer'. *Proceedings of the National Academy of Sciences*, 115(7), pp. E1437–E1445.

Roy, V. and Perez, E.A. (2009) 'Beyond Trastuzumab: Small Molecule Tyrosine Kinase Inhibitors in HER-2-Positive Breast Cancer'. *The Oncologist*, 14(11), pp. 1061–1069.

Russo, A.J., Behl, B., Banerjee, I. and Rathinam, V.A.K. (2018) 'Emerging Insights into Noncanonical Inflammasome Recognition of Microbes'. *Journal of Molecular Biology*, 430(2), pp. 207–216.

Sandstrom, A., Mitchell, P.S., Goers, L., Mu, E.W., Lesser, C.F. and Vance, R.E. (2019) 'Functional Degradation: A Mechanism of NLRP1 Inflammasome Activation by Diverse Pathogen Enzymes.' *Science (New York, N.Y.)*, 364(6435), p. eaau1330.

Santos, M.L.S., Reis, E.C., Bricher, P.N., Sousa, T.N., Brito, C.F.A., Lacerda, M.V.G., Fontes, C.J.F., Carvalho, L.H. and Pontillo, A. (2016) 'Contribution of Inflammasome Genetics in Plasmodium Vivax Malaria.' *Infection, Genetics and Evolution: Journal of Molecular Epidemiology and Evolutionary Genetics in Infectious Diseases*, 40, pp. 162–166.

Saraste, M., Sibbald, P.R. and Wittinghofer, A. (1990) 'The P-Loop - a Common Motif in ATP- and GTP- Binding Proteins'. *Molecular Biology of the Cell*, 15(11), pp. 430–434.

Schindler, R., Ghezzi, P. and Dinarello, C.A. (1990) 'IL-1 Induces IL-1. IV. IFN-Gamma Suppresses IL-1 but Not Lipopolysaccharide-Induced Transcription of IL-1.' *Journal of Immunology (Baltimore, Md. : 1950)*, 144(6), pp. 2216–2222.

Schofield, L., Ioannidis, L.J., Karl, S., Robinson, L.J., Tan, Q.Y., Poole, D.P., Betuela, I., Hill, D.L., Siba, P.M., Hansen, D.S., Mueller, I. and Eriksson, E.M. (2017) 'Synergistic Effect of IL-12 and IL-18 Induces TIM3 Regulation of $\Gamma\delta$ T Cell Function and Decreases the Risk of Clinical Malaria in Children Living in Papua New Guinea.' *BMC Medicine*, 15(1), p. 114.

Schroder, K. and Tschopp, J. (2010) 'The Inflammasomes'. *Cell*, 140(6), pp. 821–832.

Schumacher, J., Joly, N., Claeys-Bouuaert, I.L., Aziz, S.A., Rappas, M., Zhang, X. and Buck, M. (2008) 'Mechanism of Homotropic Control to Coordinate Hydrolysis in a Hexameric AAA+ Ring ATPase'. *Journal of Molecular Biology*, 381(1), pp. 1–12.

Seo, J.-W. and Lee, K.-J. (2004) 'Post-Translational Modifications and Their Biological Functions: Proteomic Analysis and Systematic Approaches'. *BMB Reports*, 37(1), pp. 35–44.

Sester, D.P., Thygesen, S.J., Sagulenko, V., Vajjhala, P.R., Cridland, J.A., Vitak, N., Chen, K.W., Osborne, G.W., Schroder, K. and Stacey, K.J. (2015) 'A Novel Flow Cytometric Method To Assess Inflammasome Formation'. *The Journal of Immunology*, 194(1), pp. 455–462.

Sharif, H., Wang, L., Wang, W.L., Magupalli, V.G., Andreeva, L., Qiao, Q., Hauenstein, A. V., Wu, Z., Núñez, G., Mao, Y. and Wu, H. (2019) 'Structural Mechanism for NEK7-Licensed Activation of NLRP3 Inflammasome'. *Nature*, 570(7761), pp. 338–343.

Shaw, M.H., Reimer, T., Kim, Y.G. and Nuñez, G. (2008) 'NOD-like Receptors (NLRs): Bona Fide Intracellular Microbial Sensors'. *Current Opinion in Immunology*, 20(4), pp. 377–382.

Sher, M.E., D'Angelo, A.J., Stein, T.A., Bailey, B., Burns, G. and Wise, L. (1995) 'Cytokines in Crohn's Colitis'. *The American Journal of Surgery*, 169(1), pp. 133–136.

Shi, J., Zhao, Y., Wang, K., Shi, X., Wang, Y., Huang, H., Zhuang, Y., Cai, T., Wang, F. and Shao, F. (2015) 'Cleavage of GSDMD by Inflammatory Caspases Determines Pyroptotic Cell Death'. *Nature*, 526(7575), pp. 660–665.

Shi, J., Zhao, Y., Wang, Y., Gao, W., Ding, J., Li, P., Hu, L. and Shao, F. (2014) 'Inflammatory Caspases Are Innate Immune Receptors for Intracellular LPS'. *Nature*, 514(7521), pp. 187–192.

Shu, C., Li, X. and Li, P. (2014) 'The Mechanism of Double-Stranded DNA Sensing through the CGAS-STING Pathway'. *Cytokine and Growth Factor Reviews*, 25(6), pp. 641–648.

Singh, K.P. *et al.* (2018) 'Role of IL-1 β , IL-6 and TNF- α Cytokines and TNF- α Promoter Variability in Plasmodium Vivax Infection during Pregnancy in Endemic Population of Jharkhand, India.' *Molecular Immunology*, 97(March), pp. 82–93.

Smith, H. and Keppie, J. (1954) 'Observations on Experimental Anthrax: Demonstration of a Specific Lethal Factor Produced in Vivo by Bacillus Anthracis'. *Nature*, 173(4410), pp. 869–870.

Snider, J. and Houry, W.A. (2008) 'AAA+ Proteins: Diversity in Function, Similarity in Structure'. *Biochemical Society Transactions*, 36(1), pp. 72–77.

Snider, J., Thibault, G. and Houry, W.A. (2008) 'The AAA+ Superfamily of Functionally Diverse Proteins'. *Genome Biology*, 9(4), pp. 1–8.

Soares, J.L.S., Fernandes, F.P., Patente, T.A., Monteiro, M.B., Parisi, M.C., Giannella-Neto, D., Corrêa-Giannella, M.L. and Pontillo, A. (2018) 'Gain-of-Function Variants in NLRP1 Protect against the Development of Diabetic Kidney Disease: NLRP1 Inflammasome Role in Metabolic Stress Sensing?' *Clinical Immunology*, 187, pp. 46–49.

Soler, V.J. *et al.* (2013) 'Whole Exome Sequencing Identifies a Mutation for a Novel Form of Corneal Intraepithelial Dyskeratosis'. *Journal of Medical Genetics*, 50(4), pp. 246–254.

Sollberger, G., Strittmatter, G.E., Garstkiewicz, M., Sand, J. and Beer, H.-D. (2014) 'Caspase-1: The Inflammasome and Beyond'. *Innate Immunity*, 20(2), pp. 115–125.

Song, N. and Li, T. (2018) 'Regulation of NLRP3 Inflammasome by Phosphorylation'. *Frontiers in Immunology*, 9(OCT), pp. 1–9.

Story, R.M. and Steitz, T.A. (1992) 'Structure of the RecA Protein–ADP Complex'. *Nature*, 355(6358), pp. 374–376.

Strahl, B.D. and Allis, C.D. (2000) 'The Language of Covalent Histone Modifications'. *Nature*, 403(6765), pp. 41–45.

Stutz, A., Kolbe, C.-C., Stahl, R., Horvath, G.L., Franklin, B.S., van Ray, O., Brinkschulte, R., Geyer, M., Meissner, F. and Latz, E. (2017) 'NLRP3 Inflammasome Assembly Is Regulated by Phosphorylation of the Pyrin Domain'. *The Journal of Experimental Medicine*, 214(6), pp. 1725–1736.

Su, M.Y., Kuo, C.I., Chang, C.F. and Chang, C.I. (2013) 'Three-Dimensional Structure of Human NLRP10/PYNOD Pyrin Domain Reveals a Homotypic Interaction Site Distinct from Its Mouse Homologue'. *PLoS ONE*, 8(7), pp. 1–9.

Sumpter, K.M., Adhikari, S., Grishman, E.K. and White, P.C. (2011) 'Preliminary Studies Related to Anti-Interleukin-1 β Therapy in Children with Newly Diagnosed Type 1 Diabetes'. *Pediatric Diabetes*, 12(7), pp. 656–667.

Sun, X., Xia, Y., Liu, Y., Wang, Y., Luo, S., Lin, J., Huang, G., Li, X., Xie, Z. and Zhou, Z. (2019) 'Polymorphisms in NLRP1 Gene Are Associated with Type 1 Diabetes'. *Journal of Diabetes Research*, 2019, pp. 1–9.

Swanson, K. V., Deng, M. and Ting, J.P.Y. (2019) 'The NLRP3 Inflammasome: Molecular Activation and Regulation to Therapeutics'. *Nature Reviews Immunology*, 19(8), pp. 477–489.

Sysoeva, T.A. (2017) 'Assessing Heterogeneity in Oligomeric AAA+ Machines.' *Cellular and Molecular Life Sciences : CMLS*, 74(6), pp. 1001–1018.

Takeuchi, O. and Akira, S. (2010) 'Pattern Recognition Receptors and Inflammation'. *Cell*, 140(6), pp. 805–820.

Tameling, W.I.L., Vossen, J.H., Albrecht, M., Lengauer, T., Berden, J.A., Haring, M.A., Cornelissen, B.J.C. and Takken, F.L.W. (2006) 'Mutations in the NB-ARC Domain of I-2 That Impair ATP Hydrolysis Cause Autoactivation'. *Plant Physiology*, 140(4), pp. 1233–1245.

Tapia-Abellán, A., Angosto-Bazarra, D., Martínez-Banaclocha, H., de Torre-Minguela, C., Cerón-Carrasco, J.P., Pérez-Sánchez, H., Arostegui, J.I. and Pelegrin, P. (2019) 'MCC950 Closes the Active Conformation of NLRP3 to an Inactive State'. *Nature Chemical Biology*, 15(6), pp. 560–564.

Tenthorey, J.L., Haloupek, N., López-Blanco, J.R., Grob, P., Adamson, E., Hartenian, E., Lind, N.A., Bourgeois, N.M., Chacón, P., Nogales, E. and Vance, R.E. (2017) 'The Structural Basis of Flagellin Detection by NAIP5: A Strategy to Limit Pathogen Immune Evasion'. *Science*, 358(6365), pp. 888–893.

Tigno-Aranjuez, J.T., Asara, J.M. and Abbott, D.W. (2010) 'Inhibition of RIP2's Tyrosine Kinase Activity Limits NOD2-Driven Cytokine Responses'. *Genes & Development*, 24(23), pp. 2666–2677.

Tinel, A., Janssens, S., Lippens, S., Cuenin, S., Logette, E., Jaccard, B., Quadroni, M. and Tschopp, J. (2007) 'Autoproteolysis of PIDD Marks the Bifurcation between Pro-Death Caspase-2 and pro-Survival NF-KappaB Pathway.' *The EMBO Journal*, 26(1), pp. 197–208.

Tosi, M.F. (2005) 'Innate Immune Responses to Infection'. *Journal of Allergy and Clinical Immunology*, 116(2), pp. 241–249.

Tschopp, J., Martinon, F. and Burns, K. (2003) 'NALPs: A Novel Protein Family Involved in Inflammation.' *Nature Reviews. Molecular Cell Biology*, 4(2), pp. 95–104.

Turk, B.E. (2007) 'Manipulation of Host Signalling Pathways by Anthrax Toxins'. *Biochemical Journal*, 402(3), pp. 405–417.

Vajjhala, P.R., Mirams, R.E. and Hill, J.M. (2012) 'Multiple Binding Sites on the Pyrin Domain of ASC Protein Allow Self-Association and Interaction with NLRP3 Protein'. *Journal of Biological Chemistry*, 287(50), pp. 41732–41743.

de Vasconcelos, N.M., Vliegen, G., Gonçalves, A., De Hert, E., Martín-Pérez, R., Van Opdenbosch, N., Jallapally, A., Geiss-Friedlander, R., Lambeir, A.-M., Augustyns, K., Van Der Veken, P., De Meester, I. and Lamkanfi, M. (2019) 'DPP8/DPP9 Inhibition Elicits Canonical Nlrp1b Inflammasome Hallmarks in Murine Macrophages'. *Life Science Alliance*, 2(1), p. e201900313.

Volin, M. V. and Koch, A.E. (2011) 'Interleukin-18: A Mediator of Inflammation and Angiogenesis in Rheumatoid Arthritis'. *Journal of Interferon & Cytokine Research*, 31(10), pp. 745–751.

Walker, J.E., Saraste, M., Runswick, M.J. and Gay, N.J. (1982) 'Distantly Related Sequences in the Alpha- and Beta-Subunits of ATP Synthase, Myosin, Kinases and Other ATP-Requiring Enzymes and a Common Nucleotide Binding Fold.' *The EMBO Journal*, 1(8), pp. 945–951.

Walsh, J.G., Muruve, D.A. and Power, C. (2014) 'Inflammasomes in the CNS'. *Nature Publishing Group*, 15(February), pp. 1–14.

Wang, H., Wang, S., Peng, J., Wang, Z., Lu, H. and Xu, J. (2016) 'Template-Based Protein Structure Modeling Using the RaptorX Web Server'. *Nat Protoc.*, 7(8), pp. 1511–1522.

Wang, R., Wei, Z., Jin, H., Wu, H., Yu, C., Wen, W., Chan, L.N., Wen, Z. and Zhang, M. (2009) 'Autoinhibition of UNC5b Revealed by the Cytoplasmic Domain Structure of the Receptor'. *Molecular Cell*, 33(6), pp. 692–703.

Wang, Y., Cirelli, K.M., Barros, P.D.C., Sangaré, L.O., Butty, V., Hassan, M.A., Pesavento, P., Mete, A. and Saeij, J.P.J. (2019) 'Three Toxoplasma Gondii Dense Granule Proteins Are Required for Induction of Lewis Rat Macrophage Pyroptosis.' *MBio*, 10(1), p. e1003927.

Waterhouse, A., Bertoni, M., Bienert, S., Studer, G., Tauriello, G., Gumienny, R., Heer, F.T., De Beer, T.A.P., Rempfer, C., Bordoli, L., Lepore, R. and Schwede, T. (2018) 'SWISS-MODEL: Homology Modelling of Protein Structures and Complexes'. *Nucleic Acids Research*, 46(W1), pp. W296–W303.

Waumans, Y., Baerts, L., Kehoe, K., Lambeir, A.-M. and De Meester, I. (2015) 'The Dipeptidyl Peptidase Family, Prolyl Oligopeptidase, and Prolyl Carboxypeptidase in the Immune System and Inflammatory Disease, Including Atherosclerosis.' *Frontiers in Immunology*, 6(12), p. 387.

Weber, C.H. and Vincenz, C. (2001) 'The Death Domain Superfamily: A Tale of Two Interfaces?' *Trends in Biochemical Sciences*, 26(8), pp. 475–481.

Wendler, P., Ciniawsky, S., Kock, M. and Kube, S. (2012) 'Structure and Function of the AAA+ Nucleotide Binding Pocket'. *Biochimica et Biophysica Acta - Molecular Cell Research*, 1823(1), pp. 2–14.

Witola, W.H., Mui, E., Hargrave, A., Liu, S., Hypolite, M., Montpetit, A., Cavailles, P., Bisanz, C., Cesbron-Delauw, M.F., Fournié, G.J. and McLeod, R. (2011) 'NALP1 Influences Susceptibility to Human Congenital Toxoplasmosis, Proinflammatory Cytokine Response, and Fate of Toxoplasma Gondii-Infected Monocytic Cells'. *Infection and Immunity*, 79(2), pp. 756–766.

Wong, C.K., Ho, A.W.Y., Tong, P.C.Y., Yeung, C.Y., Kong, A.P.S., Lun, S.W.M., Chan, J.C.N. and Lam, C.W.K. (2007) 'Aberrant Activation Profile of Cytokines and Mitogen-Activated Protein Kinases in Type 2 Diabetic Patients with Nephropathy'. *Clinical & Experimental Immunology*, 149(1), pp. 123–131.

Woodward, J.J., Iavarone, A.T. and Portnoy, D.A. (2010) 'C-Di-AMP Secreted by Intracellular *Listeria Monocytogenes* Activates a Host Type I Interferon Response'. *Science*, 328(5986), pp. 1703–1705.

Wu, X., Wu, F.H., Wang, X., Wang, L., Siedow, J.N., Zhang, W. and Pei, Z.M. (2014) 'Molecular Evolutionary and Structural Analysis of the Cytosolic DNA Sensor CGAS and STING'. *Nucleic Acids Research*, 42(13), pp. 8243–8257.

Yamasaki, S., Ishikawa, E., Sakuma, M., Hara, H., Ogata, K. and Saito, T. (2008) 'Mincle Is an ITAM-Coupled Activating Receptor That Senses Damaged Cells'. *Nature Immunology*, 9(10), pp. 1179–1188.

Yang, J., Liu, Z. and Xiao, T.S. (2017) 'Post-Translational Regulation of Inflammasomes'. *Cellular and Molecular Immunology*, 14(1), pp. 65–79.

Ye, Z., Lich, J.D., Moore, C.B., Duncan, J.A., Williams, K.L. and Ting, J.P.-Y. (2008) 'ATP Binding by Monarch-1/NLRP12 Is Critical for Its Inhibitory Function'. *Molecular and Cellular Biology*, 28(5), pp. 1841–1850.

Yoneyama, M., Kikuchi, M., Natsukawa, T., Shinobu, N., Imaizumi, T., Miyagishi, M., Taira, K., Akira, S. and Fujita, T. (2004) 'The RNA Helicase RIG-I Has an Essential Function in Double-Stranded RNA-Induced Innate Antiviral Responses'. *Nature Immunology*, 5(7), pp. 730–737.

Yoneyama, M., Onomoto, K., Jogi, M., Akaboshi, T. and Fujita, T. (2015) 'Viral RNA Detection by RIG-I-like Receptors'. *Current Opinion in Immunology*, 32, pp. 48–53.

Yu, C.-H., Moecking, J., Geyer, M. and Masters, S.L. (2018) 'Mechanisms of NLRP1-Mediated Autoinflammatory Disease in Humans and Mice.' *Journal of Molecular Biology*, 430(2), pp. 142–152.

Yuan, S. and Akey, C.W. (2013) 'Apoptosome Structure, Assembly, and Procaspase Activation'. *Structure*, 21(4), pp. 501–515.

Yuanming, H., Benedict, M.A., Ding, L. and Núñez, G. (1999) 'Role of Cytochrome c and DATP/ATP Hydrolysis in Apaf-1-Mediated Caspase-9 Activation and Apoptosis'. *EMBO Journal*, 18(13), pp. 3586–3595.

Zelensky, A.N. and Gready, J.E. (2005) 'The C-Type Lectin-like Domain Superfamily'. *FEBS Journal*, 272(24), pp. 6179–6217.

Zhang, H., Chen, Y., Keane, F.M. and Gorrell, M.D. (2013) 'Advances in Understanding the Expression and Function of Dipeptidyl Peptidase 8 and 9'. *Molecular Cancer Research*, 11(12), pp. 1487–1496.

Zhang, L., Chen, S., Ruan, J., Wu, J., Tong, A.B., Yin, Q., Li, Y., David, L., Lu, A., Wang, W.L., Marks, C., Ouyang, Q., Zhang, X., Mao, Y. and Wu, H. (2015) 'Cryo-EM Structure of the Activated NAIP2-NLRC4 Inflammasome Reveals Nucleated Polymerization'. *Science*, 350(6259), pp. 404–409.

Zhong, F.L. et al. (2016) 'Germline NLRP1 Mutations Cause Skin Inflammatory and Cancer Susceptibility Syndromes via Inflammasome Activation'. *Cell*, 167(1), pp. 187-202.e17.

Zhong, F.L., Robinson, K., Teo, D.E.T., Tan, K.-Y., Lim, C., Harapas, C.R., Yu, C.-H., Xie, W.H., Sobota, R.M., Au, V.B., Hopkins, R., D'Oswaldo, A., Reed, J.C., Connolly, J.E., Masters, S.L. and Reversade, B. (2018) 'Human DPP9 Represses NLRP1 Inflammasome and Protects against Autoinflammatory Diseases via Both Peptidase Activity and FIIND Domain Binding.' *The Journal of Biological Chemistry*, 293(49), pp. 18864–18878.

Zhou, M., Li, Y., Hu, Q., Bai, X.-C., Huang, W., Yan, C., Scheres, S.H.W. and Shi, Y. (2015) 'Atomic Structure of the Apoptosome: Mechanism of Cytochrome c - and DATP-Mediated Activation of Apaf-1'. *Genes & Development*, 29(22), pp. 2349–2361.

Zurek, B., Proell, M., Wagner, R.N., Schwarzenbacher, R. and Kufer, T.A. (2012) 'Mutational Analysis of Human NOD1 and NOD2 NACHT Domains Reveals Different Modes of Activation'. *Innate Immunity*, 18(1), pp. 100–111.

Zwijnenburg, Petra J. G., van der Poll, T., Florquin, S., Roord, J.J. and van Furth, A.M. (2003) 'IL-1 Receptor Type 1 Gene-Deficient Mice Demonstrate an Impaired Host Defense Against Pneumococcal Meningitis'. *The Journal of Immunology*, 170(9), pp. 4724–4730.

Zwijnenburg, Petra J.G., van der Poll, T., Florquin, S., Akira, S., Takeda, K., Roord, J.J. and van Furth, A.M. (2003) 'Interleukin-18 Gene-Deficient Mice Show Enhanced Defense and Reduced Inflammation during Pneumococcal Meningitis'. *Journal of Neuroimmunology*, 138(1–2), pp. 31–37.

Curriculum Vitae

Jonas Möcking

Education

Since April 2016	PhD student Prof. Dr. Matthias Geyer, Institute of Structural Biology, University of Bonn, Germany Prof. Seth L. Masters, The Walter and Eliza Hall Institute, The University of Melbourne, Australia
Oct 2012 – Jan 2016	Molecular and Applied Biotechnology Master of Science RWTH Aachen
Oct 2008 – Aug 2012	Biotechnology/Molecular Biotechnology Bachelor of Science RWTH Aachen
2005 – 2008	High School Vera Beckers Berufskolleg Krefeld
1999 – 2005	High School Liebfrauenschule Mülhausen Grefrath

Work experience

Jul 2014 – Oct 2015	Research Assistant Clinic of occupational medicine, University Hospital RWTH Aachen
Sep 2014 – Feb 2015	Technical Assistant

Health & Safety Department, School of Biotechnology
and Biomolecular Sciences
University of New South Wales, Sydney

May – Aug 2014 Research Intern
Professor Marc Wilkins, Systems Biology, School of
Biotechnology and Biomolecular Sciences
University of New South Wales, Sydney

Apr 2012 – Mar 2014 Research Assistant
Prof. Dr. Ing. Jochen Büchs, Institute of Biochemical
Engineering
RWTH Aachen

Appendix

		$\alpha 3$	
NLRP8	----ENGVMLYMRNVSHEELQRFKQLLLTEL-----	STGTMPITWDQVETASWAEVV	85
NLRP2	M---GFNLQALLEQLSQDELKSKFKYLITTFSL-----	AHELQKIPHKEVDKADGKQLV	56
NLRP7	L---EWTLQTLLEQLNEDELKSFKSLWAFPL-----	EDVLQKTPWSEVEEADGKKLA	55
NLRP5	LTFSSYGLQWCLYELDKEEFQTFKELLKKKSS-----	ESTTCSIPQFEIENANVECLA	110
NLRP3	-ASTRCKLARYLEDLEDVDLKKFKMHLEDYPP-----	QGCIPLPARGQTEKADHVDLA	55
NLRP10	ARKPREALLWALSDEENDFKKLKFYLRDMTL-----	SEGQPPLARGELEGLIPVDLA	58
ASC	MGRARDAILDALENLTAEELKFKLKLSSVPL-----	REGYGRIPRGALLSMDALDLT	53
NLRP13	----NQGLLPYLMALDQYQLEEFKLCLEPQQLMDFWSAPQGHFPRIPWANLRAADPLNLS		69
NLRP6	LAVARELLLALEELSQEQLKRFHRHLRDV-----	GPDGRSIPWGRLEERADAVDLA	65
NLRP1	-AWG--RLACYLEFLKKEELKEFQLLLANKAH-----	SRSSSGETPAQPEKTSGMEVA	54
NLRP12	-RDGLCRSLSTYLEEAEVLELKKFKLYLGTAT-----	ELGEGKIPWGSMEKAGPLEMA	57
NLRP11	-DSTDFDLLWYLENLSKKEFQSFKKYLARKIL-----	DFKLPQFPLIQ--MTKEELA	53
NLRP14	-FFPDFGLLLYLEELNKEELNTFKLFLKETM-----	EPEHGLTPWNEVKKARREDLA	59
NLRP4	-FFSDFGLMWYLEELKKEEFRKFEHLKQMTL-----	QLELKQIPWTEVKKASREELA	56
NLRP9	-FFSDFGLLWYLKELRKEEFWKFKELLKQPLE-----	KFELKPTPWAELEKASKEDVA	56
	: : : : : :		

Figure A1: Sequence alignment of PYDs of all NLRPs and ASC

Sequence alignment of the first 120 amino acids of all human NLRP proteins as well as human ASC. Only part of the sequence alignment is shown, to highlight the presence of a proline only in NLRP1 within the sequence expected to form α -helix 3 in the PYD. The alignment was performed using the Clustal Omega sequence alignment tool (Madeira *et al.*, 2019). Amino acid sequences were obtained from the UniProt database. The sequence described as canonical isoform 1 of all proteins was used in the alignment.

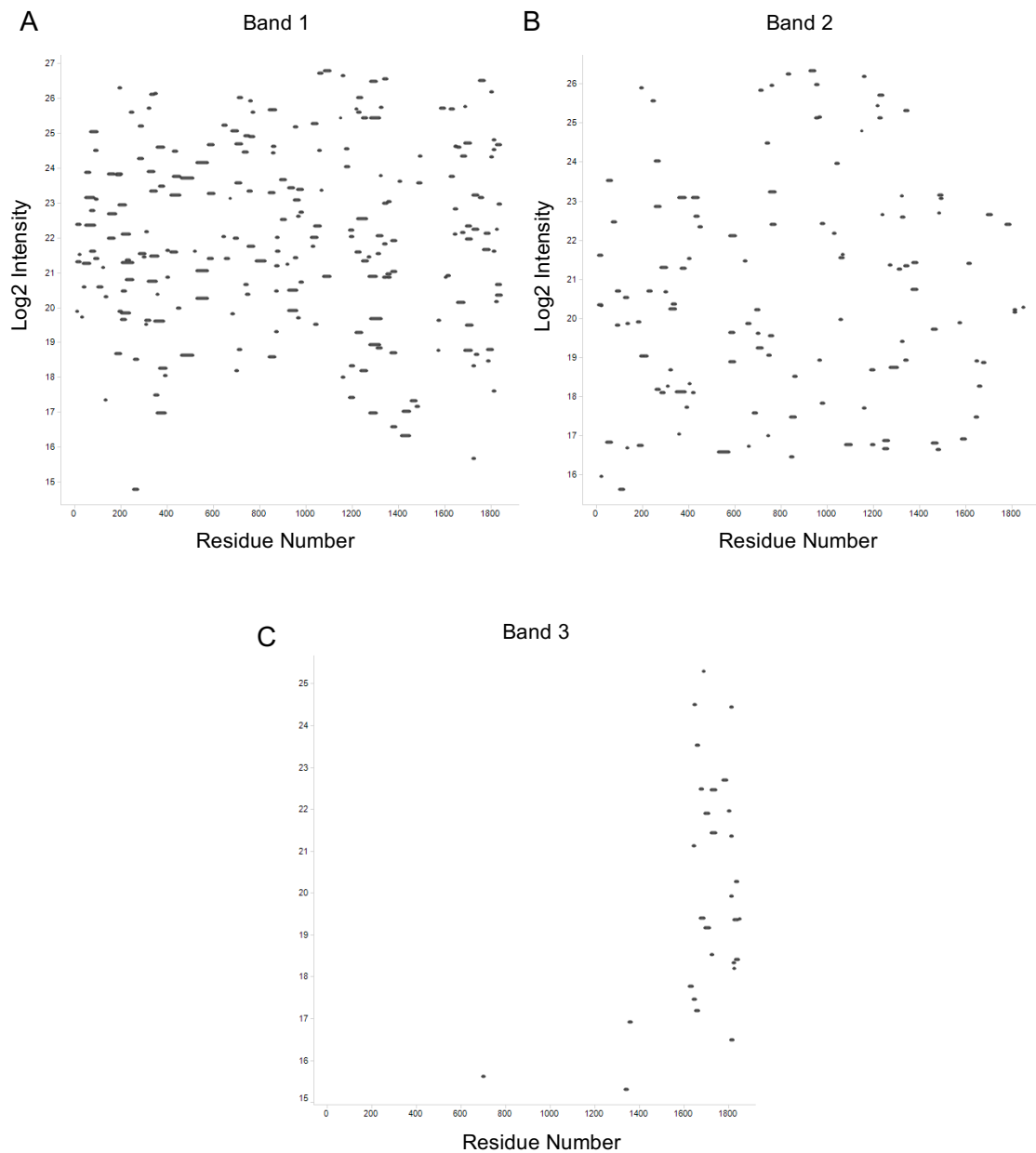


Figure A2: Mass spectrometry analysis of MBP-NLRP1

Peptide coverage as determined by mass spectrometry of band 1 (A) band 2 (B) and band 3 (C) observed from SDS-PAGE analysis of MBP-NLRP1 Peak 2 (Figure 3.7). The Log₂ intensity measured for the different peptides is plotted on the y-axis. The x-axis represents the primary sequence of the MBP-NLRP1 protein, which is comprised of 1851 amino acids. MS analysis was performed at the WEHI mass spectrometry facility.

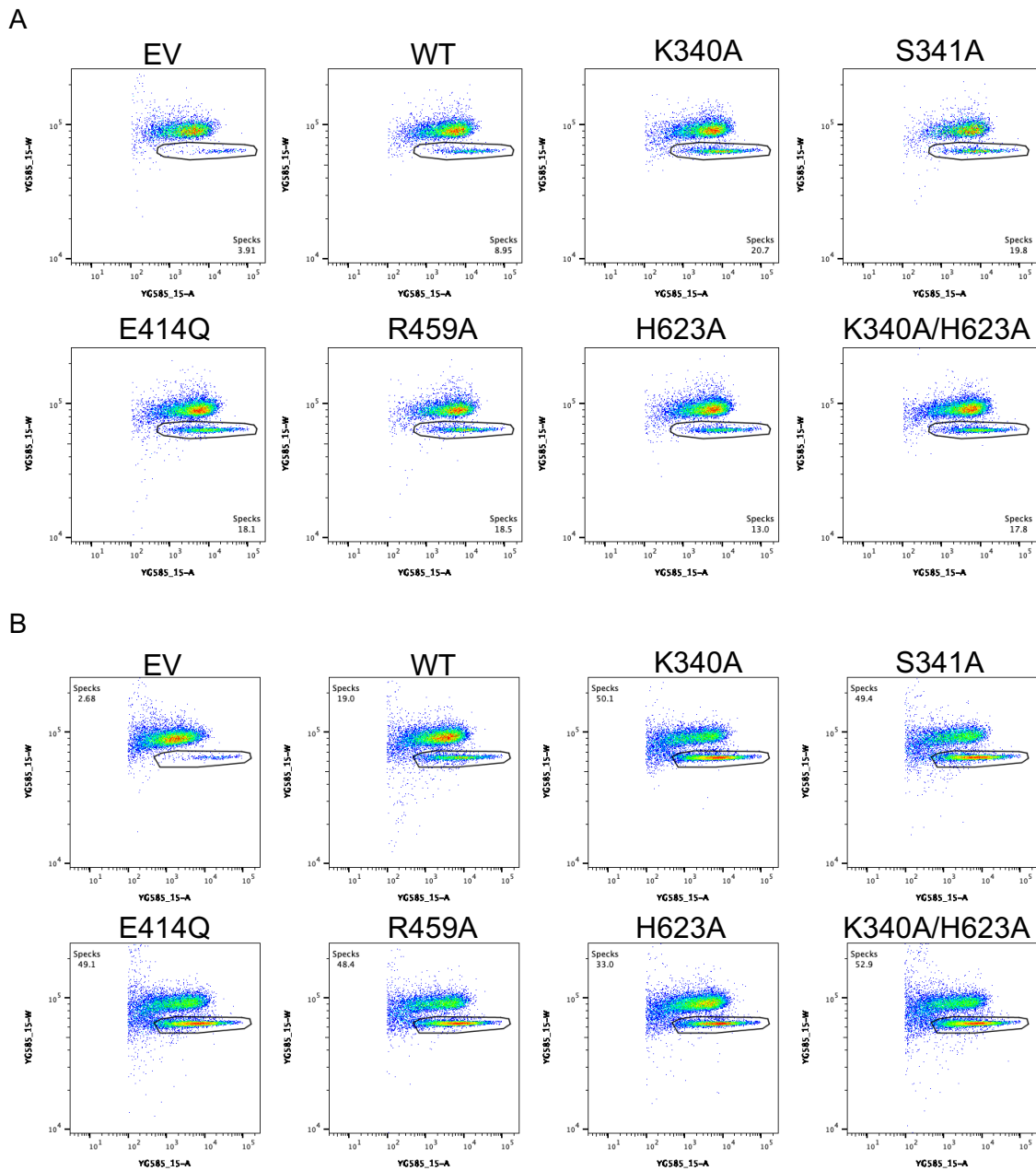


Figure A3: Representative FACS plots of ASC speck assay (Fig 4.6)

Shown are dot plots of each variant tested in the respective ASC speck assay displayed in Figure 4.6. **A** and **B** correspond with panel A and B in Figure 4.6. The width of the RFP signal (YG585-15) is plotted over the area of the RFP signal.

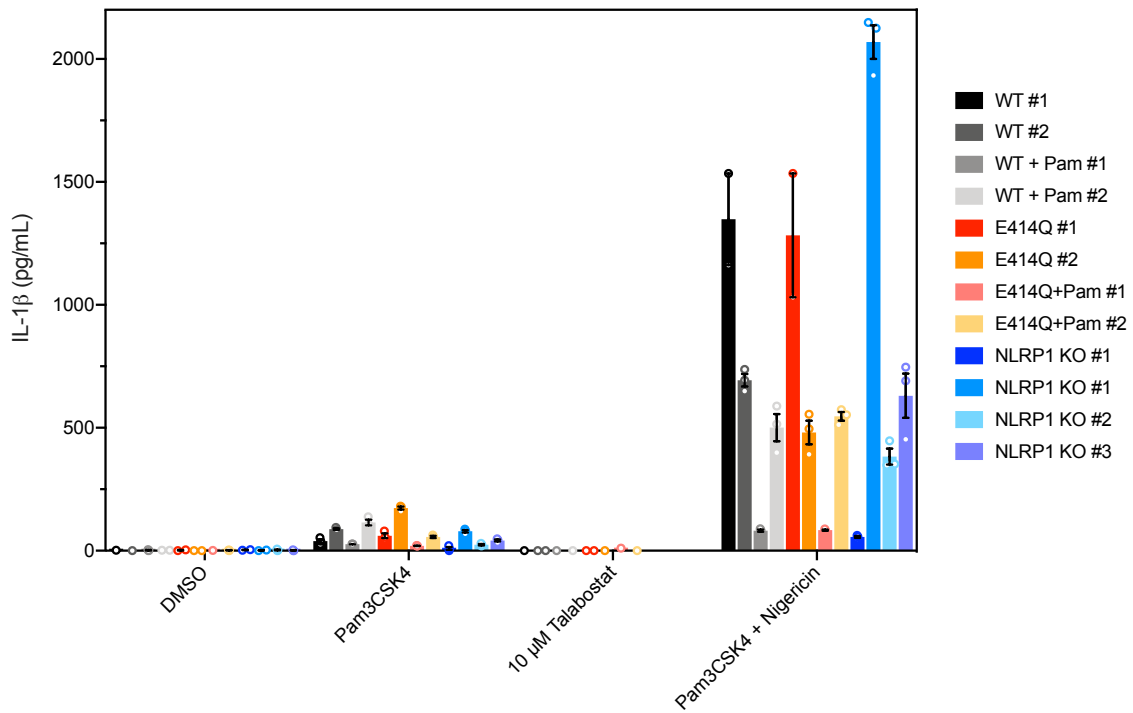


Figure A4: Effect of Talabostat on NLRP1 A66V and P1214R variants

The supernatant of the cells described in A was analysed for the proinflammatory cytokine IL-1 β by ELISA. Data is pooled from two experiments and displayed as mean \pm SEM.

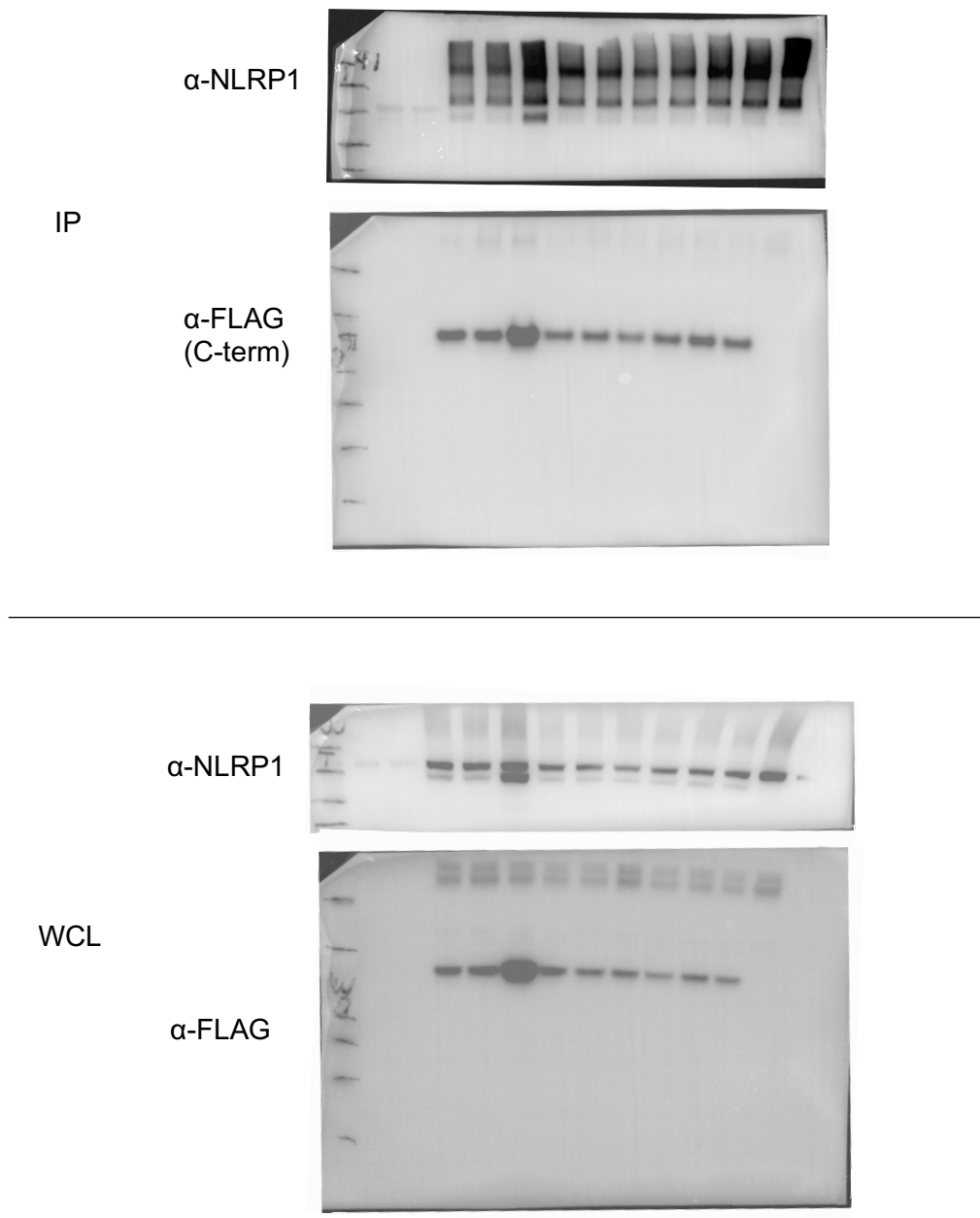


Figure A5: Uncropped blots (Fig. 4.8)

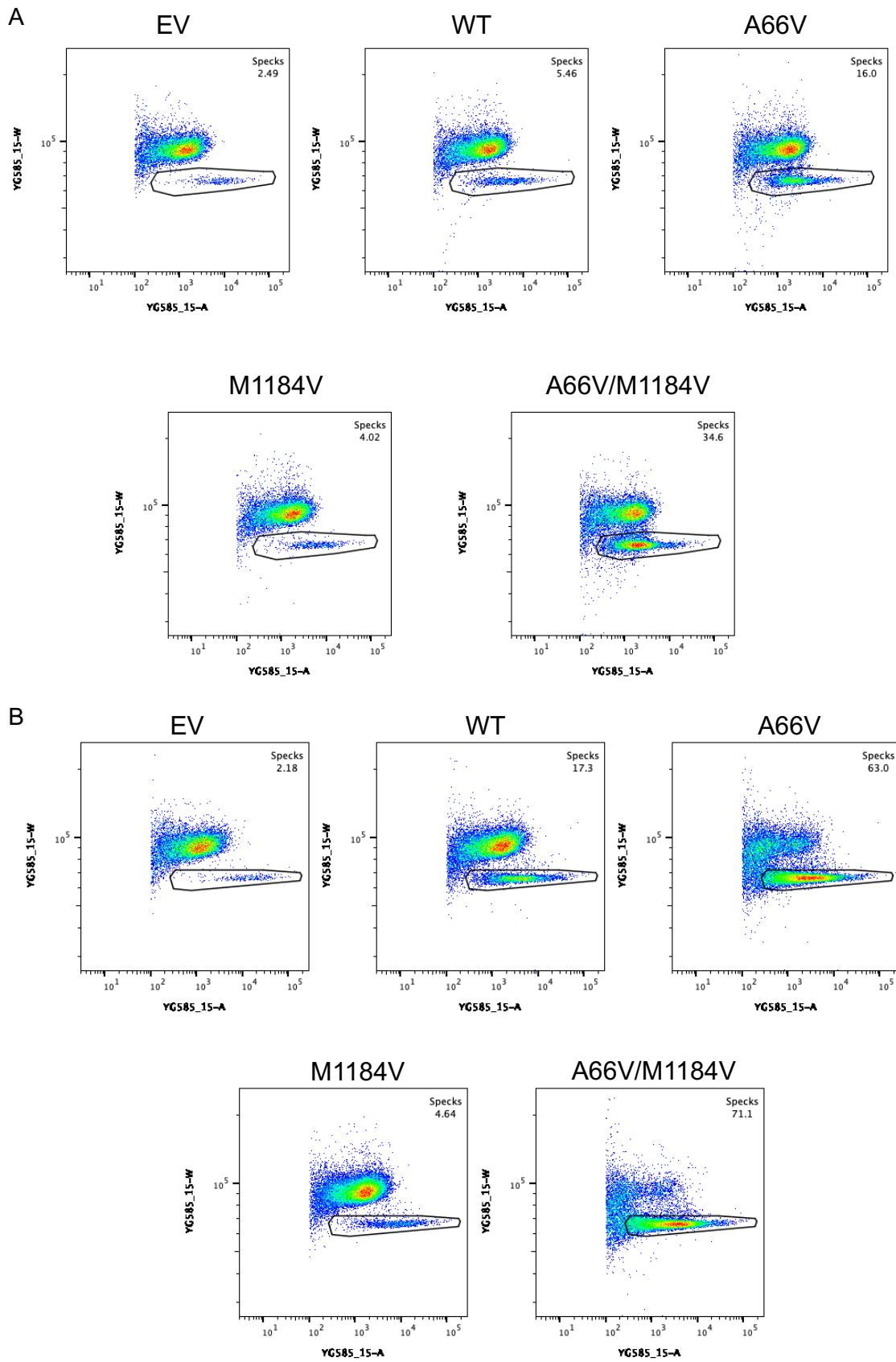


Figure A6: Representative FACS plots of ASC speck assay (Fig 5.2)

Shown are dot plots of each variant tested in the respective ASC speck assay displayed in Figure 5.2. **A** and **B** correspond with panel A and B in Figure 4.6. The width of the RFP signal (YG585-15) is plotted over the area of the RFP signal.

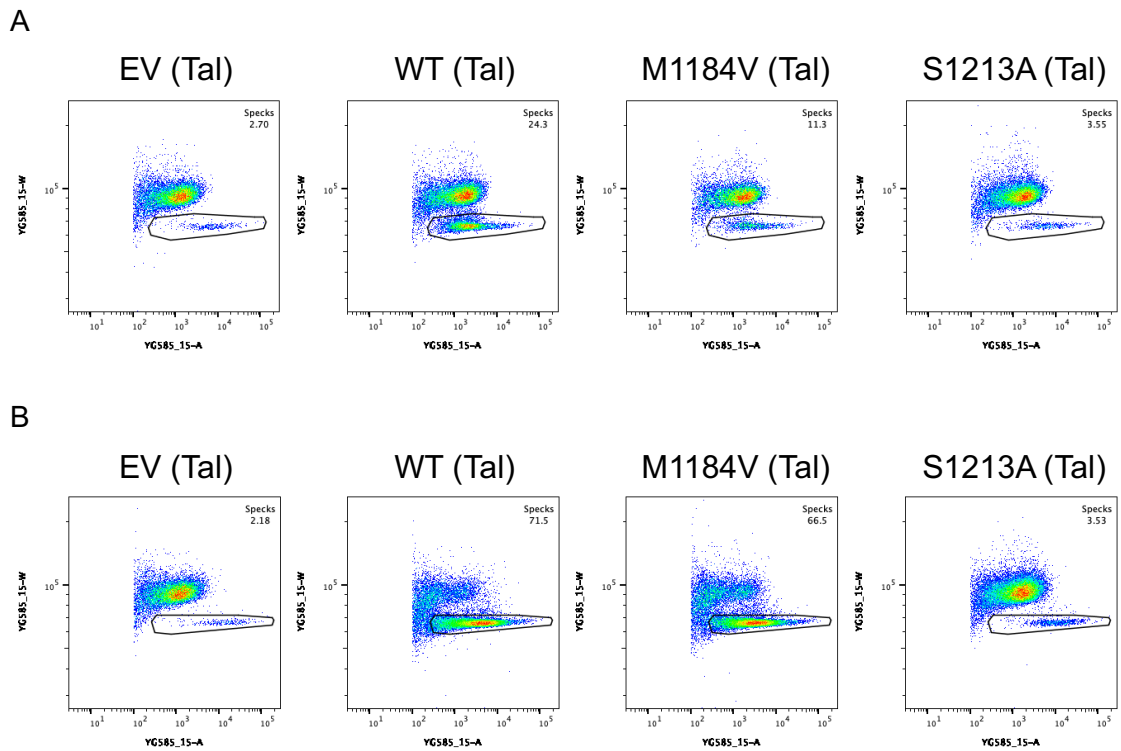


Figure A7: Representative FACS plots of ASC speck assay (Fig 5.3)

Shown are dot plots of each variant tested in the respective ASC speck assay displayed in Figure 5.3. **A** and **B** correspond with panel A and B in Figure 5.3. The width of the RFP signal (YG585-15) is plotted over the area of the RFP signal.

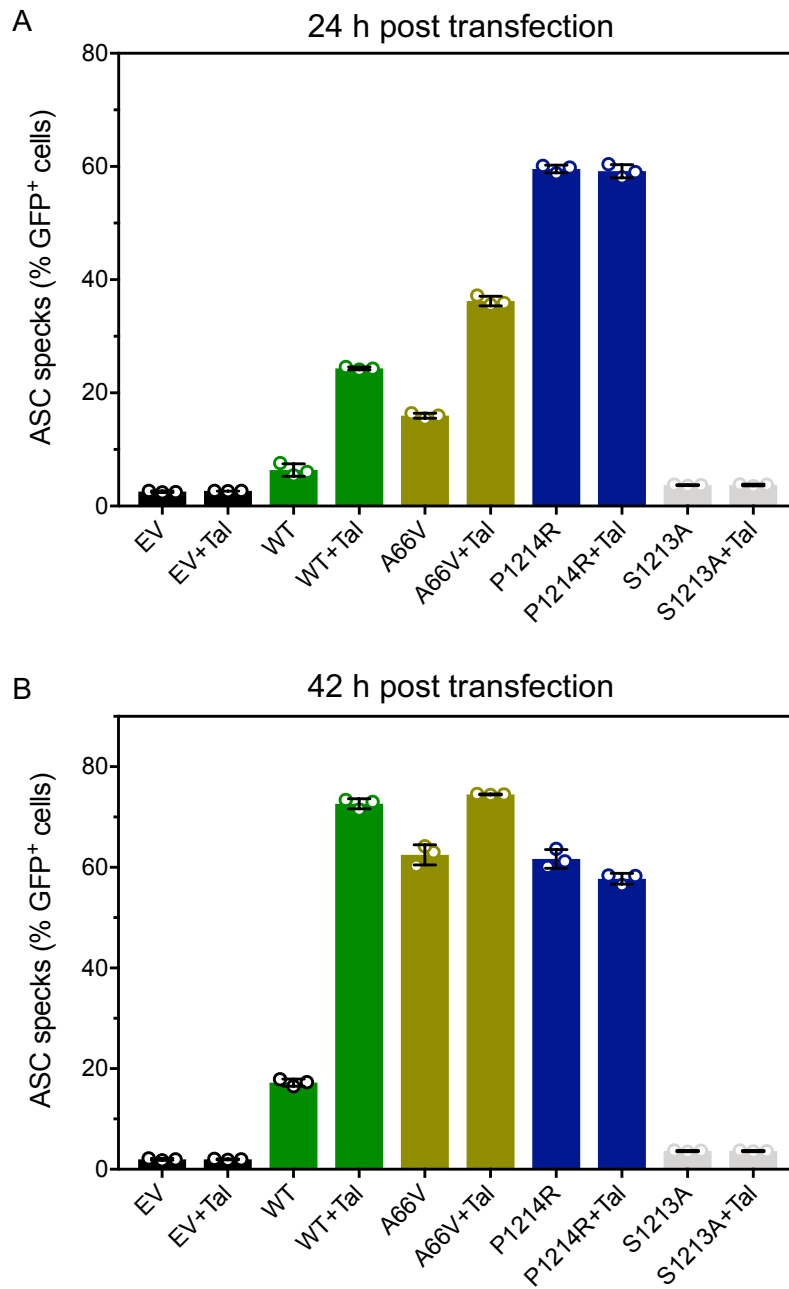


Figure A8: Effect of Talabostat on NLRP1 A66V and P1214R variants

HEK293T cells stably expressing ASC-RFP were transfected with WT or mutant NLRP1 or a vector control (EV) and analysed for ASC formation 24 h (**A**) and 42 h (**B**) post transfection by flow cytometry. Cells were treated with 2 μ M Talabostat 18 h post transfection. Samples were recorded in triplicates. Data was analysed in FlowJo and graphed in Prism. Data shown is a representative of two individual experiments and is graphed as mean \pm SEM.

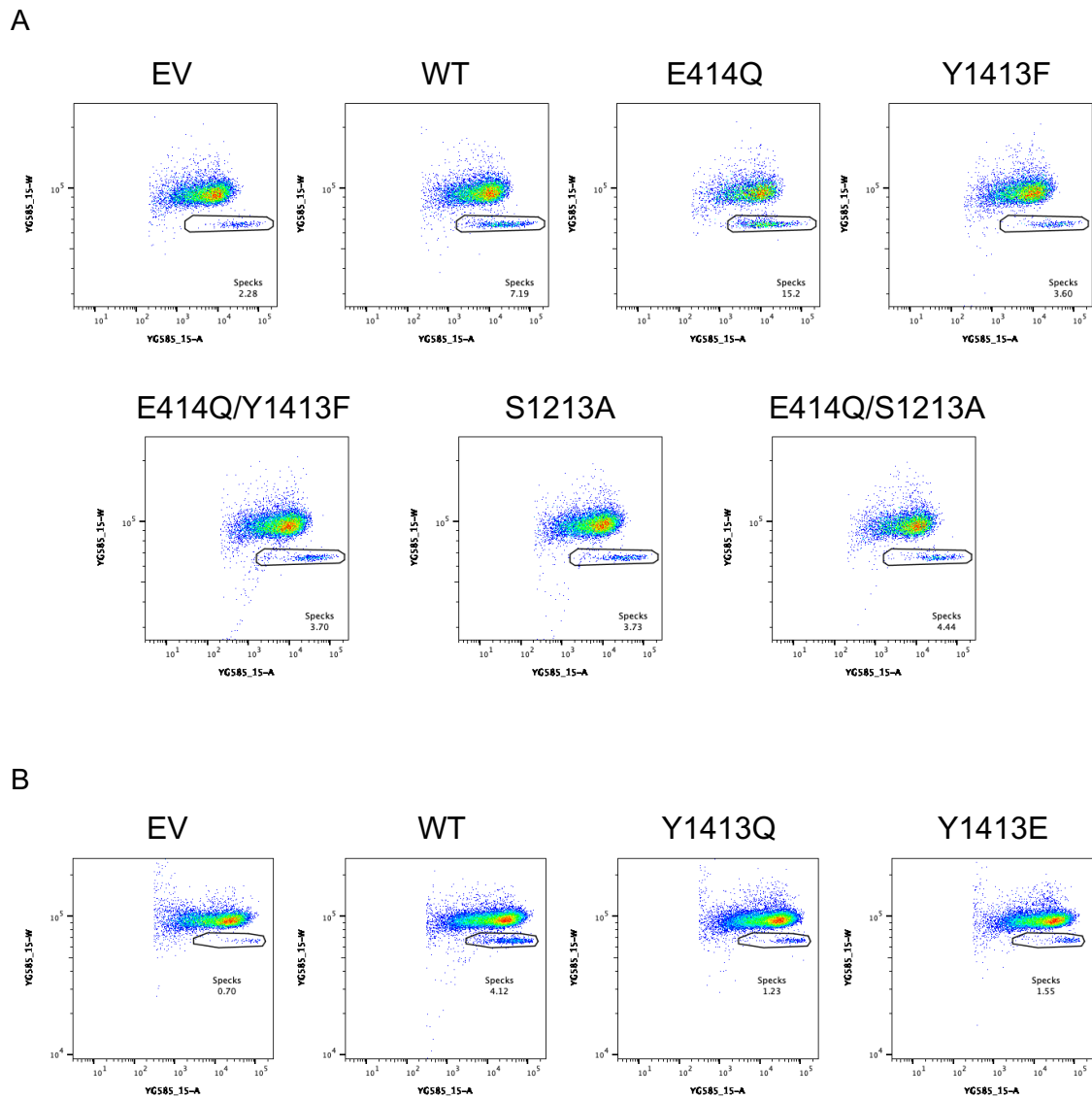


Figure A9: Representative FACS plots of ASC speck assay (Fig 5.5)

Shown are dot plots of each variant tested in the respective ASC speck assay displayed in Figure 5.5. **A** and **B** correspond with panel A and B in Figure 5.5. The width of the RFP signal (YG585-15) is plotted over the area of the RFP signal.

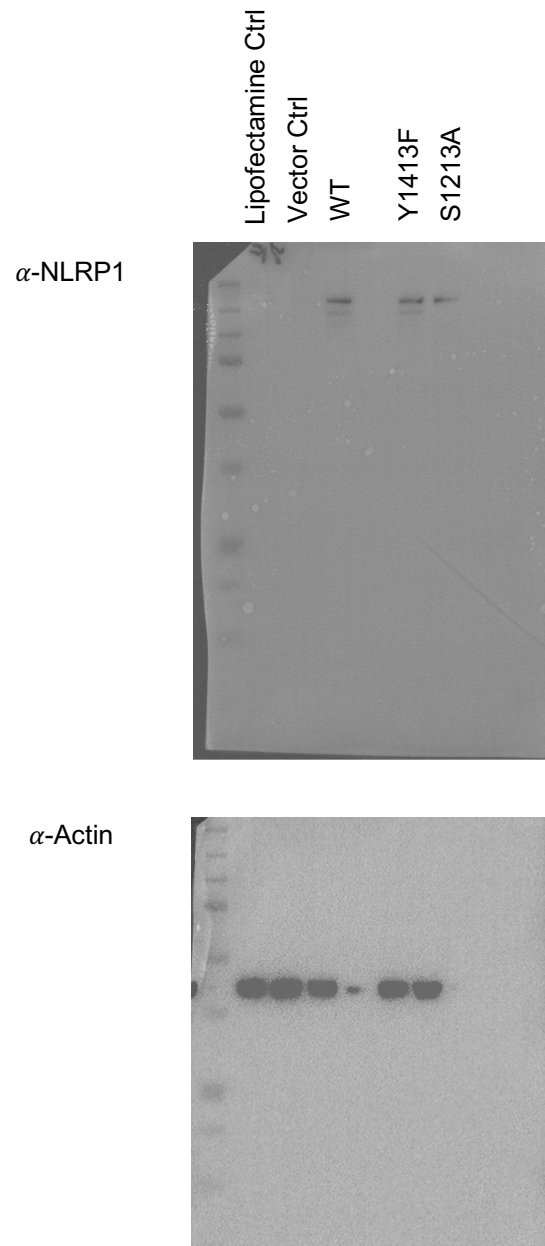


Figure A10: Uncropped blots (Fig. 5.5)

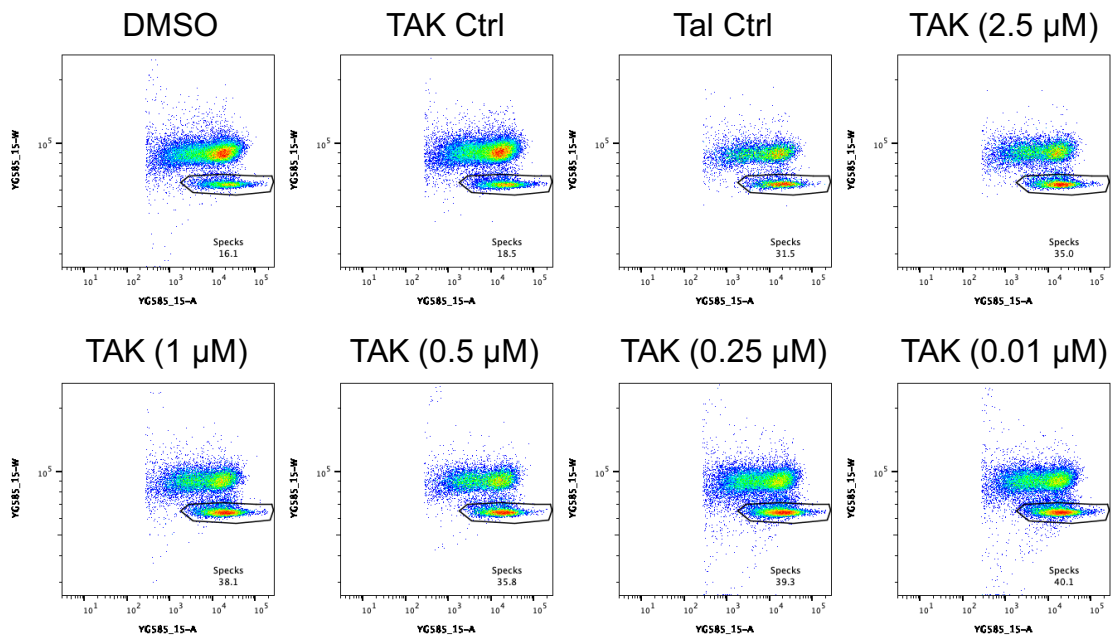


Figure A11: Representative FACS plots of ASC speck assay (Fig. 5.7)

Shown are dot plots of each variant tested in the respective ASC speck assay displayed in Figure 5.7. **A** and **B** correspond with panel A and B in Figure 5.7. The width of the RFP signal (YG585-15) is plotted over the area of the RFP signal.